U.PORTO
INSTITUTO DE CIÊNCIAS BIOMÉDICAS ABEL SALAZAR
UNIVERSIDADE DO PORTO

U.PORTO
FMUP FACULDADE DE MEDICINA
UNIVERSIDADE DO PORTO

U.PORTO
FACULDADE DE CIÊNCIAS
UNIVERSIDADE DO PORTO

STUDIES ON THE MECHANISMS OF MATURATION AND MEMBRANE DISASSEMBLY OF VACUOLES CONTAINING INVASIVE BACTERIA

JOSÉ CARLOS VIEIRA DOS SANTOS

Tese de doutoramento em Biologia Básica e Aplicada

2015

JOSÉ CARLOS VIEIRA DOS SANTOS

STUDIES ON THE MECHANISMS OF MATURATION AND MEMBRANE DISASSEMBLY OF VACUOLES CONTAINING INVASIVE BACTERIA

Tese de Candidatura ao grau de Doutor em Biologia Básica e Aplicada submetida ao Instituto de Ciências Biomédicas Abel Salazar da Universidade do Porto.

Orientador – Jost Enninga

Categoria – Director de Investigação

Afiliação – Institut Pasteur, Paris, França

Co-orientador – Sandra Sousa

Categoria – Investigador auxiliar

Afiliação – Instituto de Biologia Molecular e Celular da Universidade do Porto, Porto, Portugal

“Ó mar salgado, quanto do teu sal
São lágrimas de Portugal!
Por te cruzarmos, quantas mães choraram,
Quantos filhos em vão rezaram!
Quantas noivas ficaram por casar
Para que fosses nosso, ó mar!

Valeu a pena? Tudo vale a pena
Se a alma não é pequena.
Quem quer passar além do Bojador
Tem que passar além da dor.
Deus ao mar o perigo e o abismo deu,
Mas nele é que espelhou o céu.”

– Fernando Pessoa; in Mensagem

Acknowledgments

Serendipity often plays an important role in science. One of my most fortunate contacts with serendipity was meeting Jost for the first time. I am extremely grateful for that event and now, after making the balance of these last years, I could not be happier about choosing Jost as my PhD mentor. I had the chance to work in a fantastic and vibrant environment, for which Jost always was (and still is) the driving force. Our scientific project was difficult, bold, some people even told us we were a bit crazy, but Jost always trusted me and gave me the motivation to move forward and not to give up or give in. No words will ever suffice or convey how thankful I am. Anyway, I really want to thank Jost for teaching me so many important things. Things that I believe will help me during my scientific career; things that made me a better scientist; things that helped me in so many circumstances… Jost have always given me intellectual freedom to follow my scientific instincts, not to be afraid of failing, and to take the risk. All this with a perfect balance of proximity and independence, which I think was crucial to make these last years a personal and scientific success. In the end, it was fun, a lot of fun. I would also like to thank Jost for all the support in any kind of other situations: for helping me settling down in Paris, for all the personal advices, and for all the support in the preparation of my next scientific steps. I will always be grateful to Jost, who was an excellent mentor and a good friend.

Over these last years at Pasteur, I met fantastic people in the DIHP lab. First I would like to acknowledge the ones that have already left. To the Portuguese crew, Cristina and Mónica: they helped me a lot when I arrived at the lab. It was great to have them around and to keep in mind that, as a Portuguese, we really love our country. I would also like to thank Ricardo: even if he was not from our lab, he was as part of the family (also because he is Cristina's husband). It was great to be around him: a great friend always with a funny story, and with whom I learned a lot as well. Many thanks to Alex, whose help was precious when I needed to change apartment, and with whom was great to share conversations about football. I would like to thank Soudeh, with whom I worked closely together, and also Juliane, for all their important advices. It was great to have met and shared the lab with Marianne, Charlotte and Geneviève, and to have Andrew around, for his one-year sabbatical experience.

Many thanks to Anne-Marie and to Laurence for all the help taking care of the bureaucracies: without you, the lab would be a total chaos. I am also thankful to all the current members of the DIHP family. To Patricia, Célia and Laura for their feedback. To Camille and Virginie, for being so friendly and for sharing your knowledge with me. I would like to thank Laurent for all his support with everything: the lab would not be the same without his “MacGyverisms”. To Nora, many thanks. It was great to share many moments with her, to be desk neighbors (for the first years) and also lab bench neighbors. I would like to thank Jennifer for all the help during my project, for teaching me a lot of things and for all the linguistic help with English. She is a great friend with whom I really learned a lot. Last but not least, special thanks to Allon: a great friend, with whom I had the pleasure to share not only the office, but also cultural and scientific knowledge. I really learned a lot with Allon. I learned how to be a better scientist and also to appreciate the potential and the beauty of three-dimensional electron microscopy. I can say that meeting Allon changed my scientific career. All these people are fantastic, and my words are not enough.

I would like to thank Paul Lazarow for sharing crucial knowledge about subcellular fractionation, and Genèvieve Milon and Javier Pizarro-Cerdá for the support during my last year of PhD. I want to thank Magalie, Mariette, Véronique and Julia for the amazing collaboration: I learned a lot from all of them, and proteomics can be really fun. Many thanks to Adeline, Perrine and Christine Schmitt for the help with electron microscopy. I would also like to thank to all the people that I met at Pasteur and to everyone that shared reagents with me.

Nothing of this would be possible without the GABBA doctoral program, a very special setting for young scientists that gave me my PhD fellowship through the FCT. In particular, thanks to my co-supervisor Sandra Sousa, one of the persons that showed me for the first time the amazing world of cellular microbiology. And, of course, thanks to GABBA13 (Bruno, Clara, João, “Mega John”, Joana, Mariana, Sara, Susana and Olga) for all the great moments during my first year of PhD.

Very importantly, I would like to thank my mother, my father and my brother, for all the support and good advices. It’s not easy to be away from them. Finally, I am extremely grateful to my girlfriend Mariana, with whom I shared amazing experiences during our time together in Paris. My PhD would not be possible without her, whose contribution goes far beyond what I can acknowledge here.

Table of contents

i. List of abbreviations

2DGE	Two-dimensional gel electrophoresis
AP2	Adaptor protein complex 2
Arp2/3	Actin-related protein-2/3
ADP	Adenosine diphosphate
ATP	Adenosine triphosphate
Arf	ADP-ribosylation factor
BCG	Bacillus Calmette-Guérin
CALM	Clathrin assembly lymphoid myeloid leukemia
CD-M6PR	Cation-dependent mannose-6-phosphate receptor
cER	Cortical endoplasmic reticulum
C-FIB/SEM	Correlative focused ion beam/scanning electron tomography
CFU	Colony forming unit
CI-M6PR	Cation-independent mannose-6-phosphate receptor
CLEM	Correlative light and electron microscopy
COP	Coat protein complex
DRF	Diaphanous-related formin
EEA-1	Early endosomal antigen-1
EGF	Epidermal growth factor
ELISA	Enzyme-linked immunosorbent assay
ELMO	Engulfment and cell motility
EM	Electron microscopy
ER	Endoplasmic reticulum
ERC	Endocytic recycling compartment
ERES	ER exit sites
ERGIC	ER-Golgi intermediate compartment
ESCRT	Endosomal sorting complex required for transport
F-actin	Filamentous actin
FIB	Focused ion beam
FRET	Fluorescence resonance energy transfer
G-actin	Globular actin
GAPs	GTPase activating proteins
GDFs	GDI displacement factors
GDIs	Guanine dissociation inhibitors
GDP	Guanosine-5’-diphosphate

GEFs	Guanine nucleotide exchange factors
GILT	γ-interferon-inducible lysosomal thiol reductase
GTP	Guanosine-5'-triphosphate
HIP1R	HIP1-related protein
HOPS	Homotypic fusion and protein sorting
Hrs	Hepatocyte growth factor-regulated tyrosine kinase substrate
ILVs	Intraluminal vesicles
InlA	Internalin A
InlB	Internalin B
IRSp53	Insulin-receptor substrate p53
iTRAQ	Isobaric tag for relative and absolute quantitation
kDa	kilodalton
Lamp-1	Lysosomal associated membrane protein-1
LBP	Latex bead-containing phagosome
LC3	Microtubule-associated protein light chain 3
LC-MS/MS	Liquid chromatography-tandem mass spectrometry
LCV	*Legionella*-containing vacuole
LLO	Listeriolysin O
LNTs	Lamp-1-negative tubules
M6PR	Mannose-6-phosphate receptor
MALDI-TOF	Matrix-assisted laser desorption/ionization-time of flight
MAPs	Microtubule-associated proteins
MCS	Membrane contact site
MLC	Myosin light chain
MS	Mass spectrometry
MS/MS	Tandem mass spectrometry
MT	Microtubule
MTOC	Microtubule-organizing center
MVBs	Multivesicular bodies
NDP52	Nuclear dot protein 52
NLRs	Nod-like receptors
NPFs	Nucleation-promoting factors
NTS	Non-typhoidal *Salmonella*
P	Phosphate
PAGE	Polyacrylamide gel electrophoresis
PAK	p21-activated kinase
PC-PLC	Phosphatidylinositol-phospholipase C

p.i.	Post-invasion
PI-PLC	Phosphatidylcholine-phospholipase C
PI(3)K	Phosphatidylinositol-3-kinase
PtdIns	Phosphatidylinositol
PM	Plasma membrane
RILP	Rab-interacting lysosomal protein
ROCK	Rho-associated protein kinase
SCAMP3	Secretory carrier membrane protein 3
SCV	*Salmonella*-containing vacuole
SDS	Sodium dodecyl sulfate
SEM	Scanning electron tomography
SIFs	*Salmonella*-induced filaments
SILAC	Stable isotope labeling by amino acids in cell culture
SISTs	*Salmonella*-induced SCAMP3 tubules
SKIP	SifA and kinesin-interacting protein
siRNA	Small interfering RNA
SNAP	Synaptosome-associated protein
SNARE	Soluble *N*-ethylmaleimide-sensitive factor attachment protein receptor
SNX	Sorting nexin
SPI	*Salmonella* pathogenicity island
TEM	Transmission electron microscopy
TOF	Time of flight
TGN	*trans*-Golgi network
TRAPPI	Transport protein particle I
T3SS	Type III secretion system
T4SS	Type IV secretion system
VAMP	Vesicle-associated membrane protein
VAP	VAMP-associated protein
vATPase	Vacuolar ATPase
WASP	Wiskott-Aldrich syndrome protein
WAVE	WASP-family verprolin homologue
WH2	WASP homology 2
WRC	WAVE regulatory complex

ii. List of figures

iii. List of tables

iv. Abstract

Eukaryotic cells receive diverse extracellular stimuli that lead to the generation of intracellular responses. To regulate this, cells have evolved ways to partition off different functions to various intracellular compartments, called organelles. This compartmentalization requires the existence of communication routes between organelles, which is mostly done via vesicular trafficking that transfer biological content and information in a precise and regulated manner. Invasive bacterial pathogens, such as *Salmonella* and *Shigella*, are able to manipulate many of these communication routes, in order to invade and survive inside eukaryotic epithelial cells. Within the host cell, *Salmonella* resides inside a membrane-bound vacuole, called *Salmonella*-containing vacuole (SCV), which undergoes several steps of maturation that can either result in the establishment of a bacterial replicative niche or in vacuolar membrane rupture. Similarly, *Shigella* is engulfed within a membrane-bound vacuole, but this is rapidly ruptured, with subsequent bacterial escape into the host cytosol. In both cases, the formation, maturation and rupture of the bacteria-containing vacuoles are crucial steps for bacterial survival. In order to obtain a better understanding of these steps, at a molecular level, we investigated the dynamic association of several host factors with the bacteria-containing vacuoles, through the use of real time fluorescence microscopy. Our results show that several host small GTPases and kinases are dynamically recruited to the sites of *Shigella* entry and vacuolar rupture, and that these processes follow precise kinetics. Moreover, we isolated and determined the protein composition of bacteria-containing vacuoles, namely the SCV, which revealed hundreds of proteins associated with this compartment. By combining three-dimensional fluorescence and electron microscopies, we demonstrated that the SCV interacts with several host cell organelles, namely with endoplasmic reticulum-derived COPII vesicles and VAMP7-positive lysosome-like vesicles. The dynamic communication between the SCV and different host organelles modulates vacuolar maturation and rupture, affecting intracellular *Salmonella* localization and growth. Together, our results provide new insights into the mechanisms of maturation and membrane rupture of vacuoles containing invasive bacteria.

v. Resumo

Células eucarióticas recebem diversos estímulos extracelulares que despoletam repostas intracelulares. Para regular estes processos, as células evoluíram de forma a dividir diferentes funções por vários compartimentos intracelulares, denominados organelos. Esta compartimentalização requer a existência de vias de comunicação entre organelos, o que é feito sobretudo através do tráfego de vesículas que transferem conteúdos biológicos de uma maneira precisa e regulada. Bactérias patogénicas intracelulares, como *Salmonella* e *Shigella*, têm a capacidade de manipular muitas destas vias de comunicação, de forma a invadirem e sobreviverem no interior de células epiteliais eucarióticas. Dentro da célula hospedeira, *Salmonella* reside no interior de um vacúolo membranar, designado SCV, que é sujeito a diversos passos de maturação que tanto podem resultar no estabelecimento de um nicho bacteriano replicativo como na ruptura da membrana do vacúolo. De forma semelhante, *Shigella* é internalizada num vacúolo membranar, mas este rapidamente sofre lise, com subsequente passagem da bactéria para o citosol do hospedeiro. Em ambos os casos, a formação, maturação e ruptura de vacúolos que contêm bactérias são passos cruciais para a sobrevivência bacteriana. De modo a melhor compreender estes passos, a um nível molecular, investigámos a presença de proteínas da célula hospedeira em vacúolos que contêm bactérias, através do uso de microscopia de fluorescência em tempo real. Os resultados aqui apresentados mostram que, durante infecção por *Shigella*, GTPases e proteínas cinases são recrutadas de forma dinâmica para os locais de entrada da bactéria e para locais de ruptura do vacúolo, e que estes processos seguem cinéticas precisas. Para além disto, isolámos e determinámos a composição proteica de vacúolos que contêm bactérias, nomeadamente do SCV, o que evidenciou a presença de centenas de proteínas neste compartimento. Através da combinação entre microscopias de fluorescência e electrónica tridimensionais, demonstrámos também que o SCV interage com vários organelos da célula hospedeira, particularmente com vesículas COPII derivadas do retículo endoplasmático e com vesículas lisossomais positivas para VAMP7. Esta comunicação dinâmica entre o SCV e diferentes organelos celulares controla a maturação e lise do vacúolo,

afectando a localização intracelular de *Salmonella* e o crescimento bacteriano. Na sua globalidade, estes resultados fornecem novas pistas acerca dos mecanismos de maturação e ruptura membranares de vacúolos que contêm bactérias intracelulares.

"… the cell is not just an inert playground for a few almighty masterminding molecules, but is a system, a hierarchically ordered system, of mutually interdependent species of molecules, molecular groupings, and supramolecular entities; and that life, through cell life, depends on the order of their interactions."

– Paul Alfred Weiss

PART I

INTRODUCTION

Chapter 1

Small GTPases as Master Regulators of Cellular Functions

Eukaryotic cells, individually or as part of multicellular organisms, receive a multitude of extracellular stimuli and respond to their environment through the generation of intracellular responses. The extracellular stimuli alter the affected cell, both by inducing changes at the cell surface and by modifying the communication between intracellular organelles. Communication relies on the compartmentalization within eukaryotic cells and is dependent on several steps, such as budding of vesicles from donor membranes that are transported to specific acceptor membranes, followed by their docking and fusion, which leads to content mixing. These dynamic processes in the cell are regulated by several proteins, of which small GTPases play a crucial role in ensuring the correct crosstalk between the different cellular compartments.

A. The Ras superfamily of small GTPases: activity and regulation

The Ras superfamily of small GTPases is a group of low molecular weight (20-30 kDa) proteins composed of more than 150 members with highly conserved structural and biochemical properties. Due to their capacity to hydrolyze guanosine-5'-triphosphate (GTP) to guanosine-5'-diphosphate (GDP), Ras GTPases can act as molecular switches that convert extracellular cues to intracellular signaling pathways, thus regulating numerous basic cellular processes, such as actin cytoskeleton regulation, adhesion, migration, phagocytosis, endocytosis, differentiation, polarization, morphogenesis and cell survival (Cherfils and Zeghouf, 2013; Goitre et al., 2014; Jaffe and Hall, 2005; Stenmark, 2009). Depending on the sequence and functional similarities, the Ras superfamily can be divided into five major families (Ras, Rho, Rab, Arf and Ran) and subfamilies (***Table 1***). Small GTPases are localized to distinct membrane microdomains, alternating cyclically between a GDP-bound "off" and a GTP-bound

"on" form, in response to different stimuli. Generally, GDP is tightly bound to the GTPases (Bos et al., 2007; Wittinghofer et al., 1997), therefore these proteins require the catalytic helping of guanine nucleotide exchange factors (GEFs), which facilitate GDP-to-GTP exchange (Cherfils and Zeghouf, 2013; Jaffe and Hall, 2005). Since GTP is highly abundant in the cytosol (~1 mM), it quickly binds as soon as GDP has been released. On the other hand, GTP-to-GDP conversion, and signaling termination, is driven by GTPase activating proteins (GAPs) given that GTP hydrolysis is very slow (Bos et al., 2007). Thus, the entire molecular switch is composed of a small GTPase, a GEF and GAP, altogether (***Figure 1***).

Table 1 – List of human proteins of the Ras superfamily of small GTPases. Adapted from Goitre et al., 2014.

Family	Subfamily	Function	Members
Ras	- Ras	Cell proliferation, differentiation, survival, and apoptosis. Gene expression	E-Ras; N-Ras; H-Ras; K-Ras; R-Ras; R-Ras-2; Di-Ras-1; Di-Ras-2; Di-Ras-3; NKIRas-1; NKIRas-2; Ras-D1; Ras-D2; Ras-L10A; Ras-L10B; Ras-L11A; Ras-L11B; Ras-L12, Rerg
	- Ral	GTP-dependent exocytosis	Ral-A; Ral-B
	- Rap	Cell adhesion	Rap-1A; Rap-1B; Rap-2A; Rap-2B; Rap-2C
	- Rad	Cell shape. Cell cycle checkpoint	Rad; Gem; Kir; Rem-1; Rem-2
	- Rheb	mTOR pathway. Cell growth and cell-cycle progression	Rheb; Rheb-L1
	- Rit	Neuronal differentiation and survival	Rit-1; Rit-2; Rin; Ric
Rho		Cytoskeletal dynamics. Cell shape, polarity, adhesion and movement. Cell cycle progression. Gene expression.	RhoA; RhoB; RhoBTB1; RhoBTB2; RhoBTB3; RhoC; RhoD; RhoF; RhoG; RhoH; RhoJ; RhoQ; RhoU; RhoV; Rnd1; Rnd2; Rnd3; Rac1; Rac2; Rac3; Cdc42
Rab		Protein and membrane vesicle trafficking in the endocytic and secretory pathways.	Rab1a; Rab1b; Rab2; Rab3a; Rab3b; Rab3c; Rab3d; Rab4a; Rab4b; Rab5a; Rab5b; Rab5c; Rab6a; Rab6b; Rab6c; Rab7a; Rab7b; Rab7L1; Rab8a; Rab8b; Rab9a; Rab9b; Rab10; Rab11a; Rab11b; Rab12; Rab13; Rab14; Rab15; Rab17; Rab18; Rab19; Rab20; Rab21; Rab22a; Rab23; Rab24; Rab25; Rab26; Rab27a; Rab27b; Rab28; Rab30; Rab31; Rab32; Rab33a; Rab33b; Rab34; Rab35, Rab36; Rab37
Arf		Vesicle trafficking. Endocytosis and exocytosis.	Arf1; Arf3; Arf4; Arf5; Arf6; Arl1; Arl2; Arl3; Arl4; Arl5; Arl5C; Arl6; Arl7; Arl8; Arl9; Arl10A; Arl10B; Arl10C; Arl11; Arl13A; Arl13B; Arl14; Arl15; Arl16; Arl17; TRIM23, Arl4D; ArfRP1; Arl13B
Ran		Nuclear transport. Mitotic spindle organization.	Ran

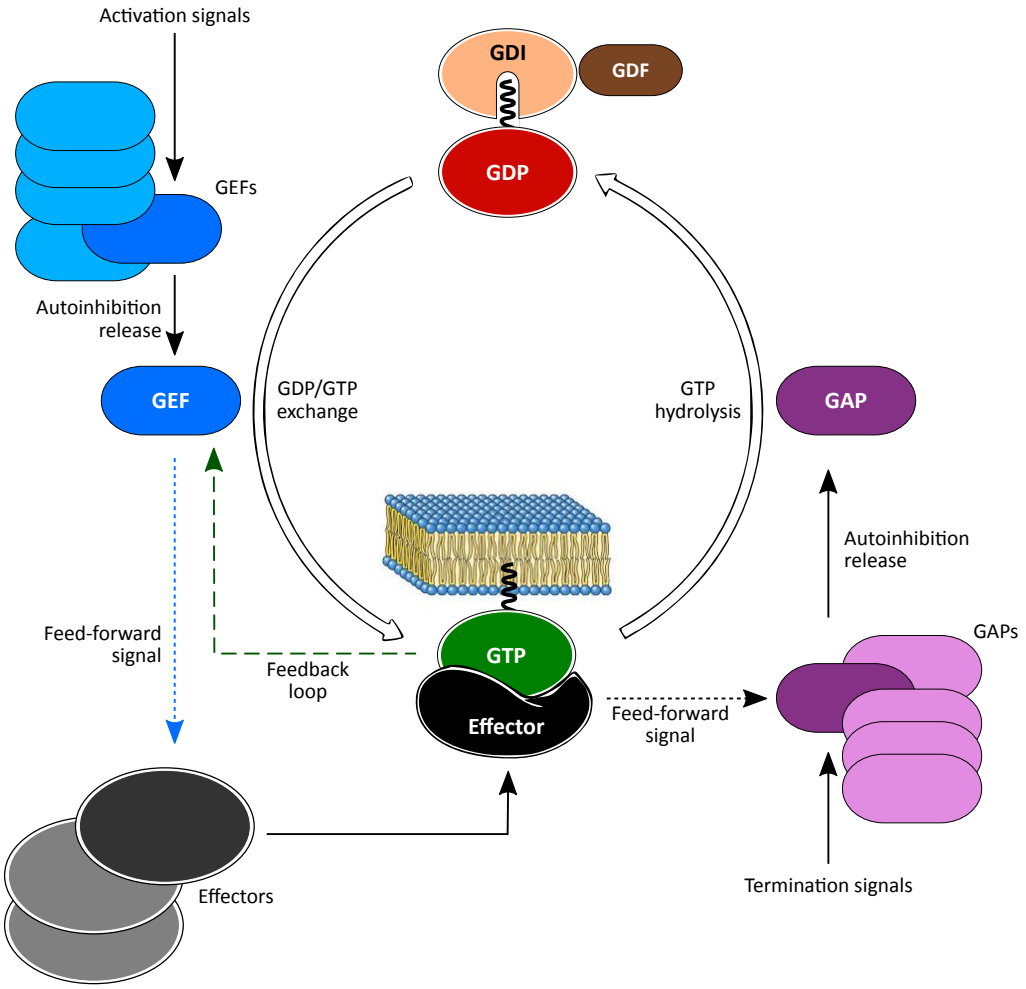

Figure 1 – The small GTPase switch and its complex regulation. All small GTPases are activated by GDP/GTP exchange stimulated by GEFs (blue) and inactivated by GTP hydrolysis by GAPs (magenta). The individual GAP and GEF proteins acting in the regulatory switch (among several possible GAPs and GEFs) are depicted in dark colors. In addition, many GTPase families combine their GDP/GTP switch with a cytosol/membrane alternation, which is regulated by GDIs (beige). Targeting of the GTPase-GDI complex to specific membranes is mediated by interaction with a membrane-bound GDF (brown). Activation or termination signals act over a specific GEF or GAP, promoting conformational changes that result in their activation. Moreover, feedback loops (green broken arrow) from the active GTPase can control the GEF efficiency, and feed-forward signaling (blue broken arrow) emanating from the GEF contributes to the selection of the specific effector that will be recruited by the active GTPase. Feed-forward signaling from the selected effector (black broken arrow) can also provide an additional level of regulation over a specific GAP. Adapted from Cherfils and Zeghouf, 2013.

Most small GTPases are modified at their C-terminus by the addition of a farnesyl or geranylgeranyl group, which act as lipid tails that anchor and localize these proteins to membranes. Guanine dissociation inhibitors (GDIs) play an important role in the regulation of GTPase activity and GTP-to-GDP conversion. GDIs remove certain small GTPases (mostly Rho and Rab proteins) from membranes and, by masking their lipid tails, establish cytosolic soluble complexes (***Figure 1***). In this way, GDIs prevent small GTPases from associating with membranes and thus inhibit interaction with regulators or effectors (Bos et al.,

2007; Cherfils and Zeghouf, 2011; 2013). Since active (GTP-bound) Rho and Rab GTPases are localized to cellular membranes, they need to be targeted in a specific manner. Even though this mechanism is not completely understood, recent data show that membrane-bound GDI displacement factors (GDFs) play an important role. These recognize the small GTPase-GDI complex and promote GDI release, thus targeting the small GTPase to the correct membrane (Cherfils and Zeghouf, 2013; Sivars et al., 2003; Stenmark, 2009). In this way, active GTP-bound GTPases can then be targeted to specific membranes, where they initiate cellular responses.

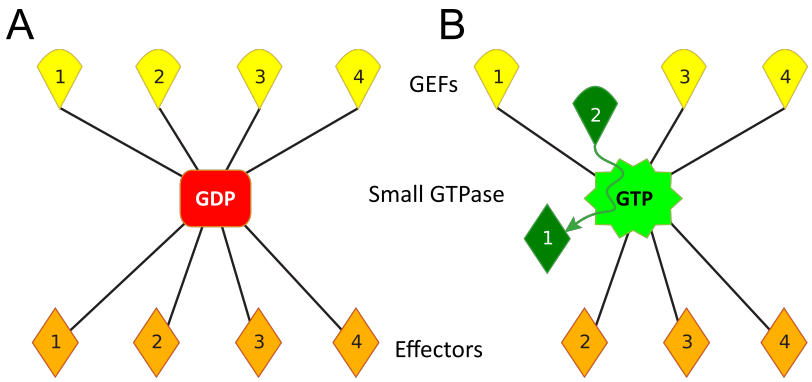

Figure 2 – The orchestration of GTPase and effector activation. An individual GEF (among several possible GEFs) activates a small GTPase, propagating input information into an output pathway that selects a specific effector (among several possible effectors). **A.** In the absence of a signal, GEFs (yellow) remain autoinhibited and do not activate the GDP-bound small GTPase (red), which in turn cannot interact with any of its effectors (orange). **B.** In the presence of an upstream signal, a specific GEF (GEF 2 in this case) activates the small GTPase (light green), and this selects and interacts with a particular downstream effector (effector 1 in this figure). Adapted from Cherfils and Zeghouf, 2011.

So far more than 70 GEFs and more than 80 GAPs have been identified. This diversity allows that a wide range of cellular receptors can control the activity of different Ras GTPases, which in turn interact with a myriad of target molecules (including protein and lipid kinases, phospholipases, adaptor molecules and cell-surface receptors), consequently functioning as strategic nodes for signaling coordination and propagation (Etienne-Manneville and Hall, 2002; Marinissen and Gutkind, 2005). Therefore, within the cell many different molecules can converge to regulate the activity of several Ras GTPases, which in turn can act over diverse effectors, establishing a complex ensemble of interconnected factors. However, it is surprising that there is a high functional specialization and specificity among the different Ras superfamily members, which results in a precise orchestration of the

appropriate cellular response to a specific cellular cue (***Figure 2***). How the cell is "able to choose" the downstream targets for a certain small GTPase to provide signal specificity and reliability is fascinating and largely unknown (Cherfils and Zeghouf, 2011). GDP-to-GTP nucleotide exchange, stimulated by GEFs, is a complex reaction that involves different steps, but its kinetic is understood only for a few small GTPases (Klebe et al., 1995; Lenzen et al., 1998). The initial formation of a low affinity complex between the GDP-bound GTPase and the GEF initiates the exchange reaction. After GDP dissociation, there is the conversion to a high affinity nucleotide-free GTPase/GEF complex. GTP binding then displaces the GEF and leads to the formation of the active form of the GTPase, bound to GTP (Cherfils and Zeghouf, 2013). Additionally, it is now also clear that the nucleotide exchange activity of most GEFs is autoregulated by intramolecular interactions, which generally induce large conformational changes around the catalytic domain that result in autoinhibition mechanisms. This mechanism ensures that upstream signals are filtered so that only the appropriate GEF and its associated downstream pathway are properly selected. Moreover, feedback loop signals from the active GTPase control GEF activity, together with feed-forward mechanisms, in which GEFs induce small GTPases to bind to specific effectors (***Figure 1***). Similarly, GAP-stimulated GTP-to-GDP exchange is also tightly regulated, by either protein-protein or protein-lipid interactions, binding of second messengers or post-translational modifications (Bos et al., 2007). This exchange can release GAPs from their autoinhibited state, resulting in conformational changes in the active small GTPase that favor GTP hydrolysis and generation of GDP, thus switching off the circuitry more quickly (Cherfils and Zeghouf, 2013). Spatiotemporal fine-tuning of GAPs can also be controlled by negative regulatory mechanisms coming from downstream targets of small GTPases, which can both inhibit or activate GAPs (Cherfils and Zeghouf, 2011; Xie and Palmer, 2007).

B. Rho GTPases

Mammalian Rho GTPases comprise a family of 23 intracellular molecules that are involved in signaling networks regulating the actin cytoskeleton organization

and microtubules dynamics, cell adhesion, vesicle trafficking, polarity and motility, cell-cycle progression, and gene expression (Goitre et al., 2014; Heasman and Ridley, 2008). The best characterized members of this family are the highly conserved Cdc42, Rac1 and RhoA, all located to cellular membranes when activated. They transform signals on plasma membrane receptors into cytoskeletal rearrangements (***Figure 3A***). Impressively, for these Rho GTPases more that 60 molecular targets have been identified so far, highlighting their complexity and importance in the cell (Etienne-Manneville and Hall, 2002).

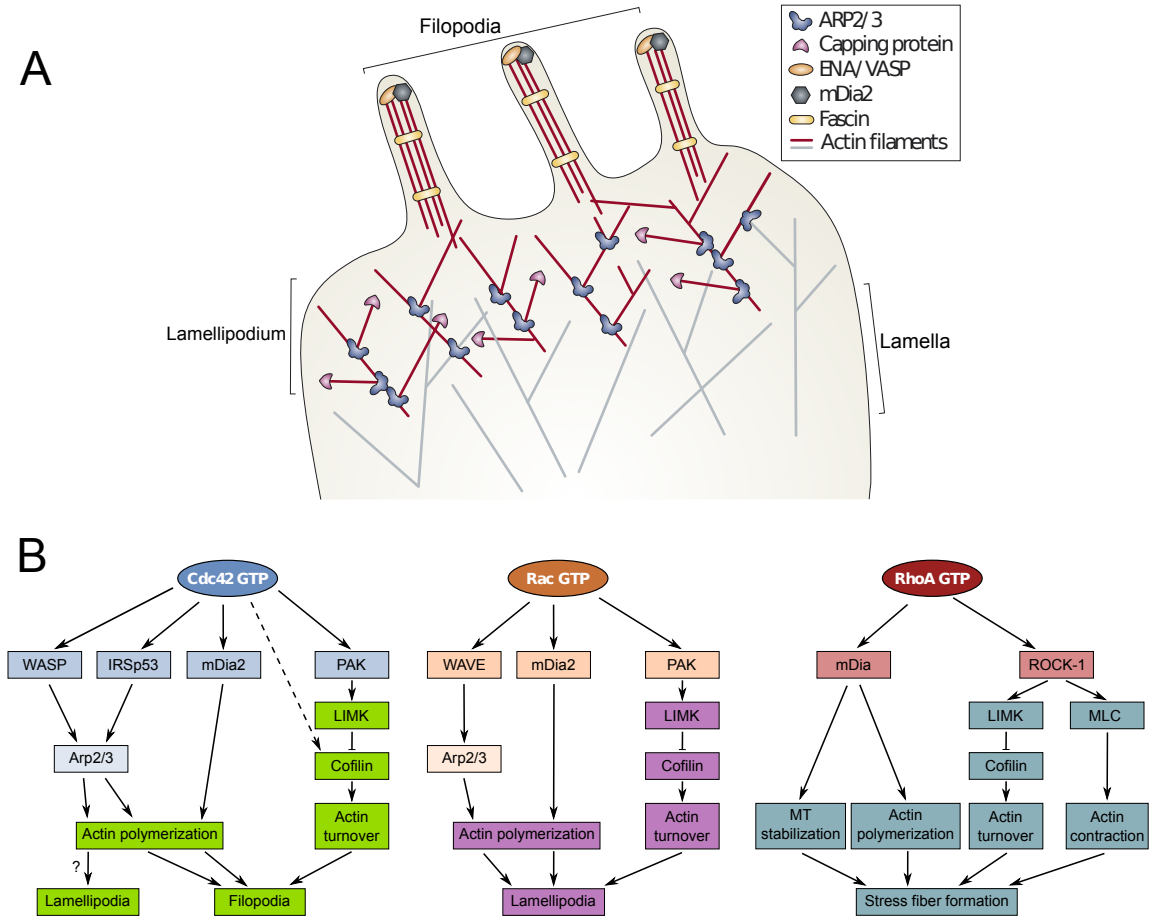

Figure 3 – Signaling pathways involved in the formation of filopodia, lamellipodia and stress fibers. A. Filopodia are thin cell membrane protrusions that extend beyond the leading edge of lamellipodia in many migratory cells and probably function as sensory probes for the establishing of cell-cell contacts. They contain parallel bundles of actin filaments crosslinked into bundles by actin-binding proteins, such as fascin. At the leading edge of the cell, lamellipodia are extended by Arp2/3 complex-mediated formation of new actin filaments, which leads to the assembly of a network of branched actin filaments. Other proteins, such as WAVE and mDia2, also regulate lamellipodia formation. Capping proteins that bind to the barbed ends terminate actin filament elongation. The lamella is located behind the lamellipodium. In the lamella, the actin filaments are longer and less branched. (ENA/VASP: enabled/vasodilator-stimulated phosphoprotein) **B.** Downstream effector targets of Cdc42, Rac and RhoA GTPases that are involved in the regulation of actin polymerization. Adapted from Heasman et al. 2008 and Spiering et al. 2011.

Cdc42

Cdc42 is involved in the formation of highly dynamic finger-like actin-rich protrusions known as filopodia, which contain parallel bundles of filamentous (F)-actin (Gupton and Gertler, 2007). The active GTP-bound Cdc42 directly binds to the ubiquitously expressed neuronal Wiskott-Aldrich syndrome protein (N-WASP) (or to the closely related hemopoietic-specific WASP), which subsequently can act as a scaffold that recruits and activates the actin-related protein-2/3 (Arp2/3) complex, leading to actin polymerization (***Figure 3B***). Additionally, Cdc42 can target the insulin-receptor substrate p53 (IRSp53), which also results in Arp2/3 complex activation and filopodia formation, by actin filament bundling and by inducing membrane curvature. Another target of Cdc42 is the diaphanous-related formin (DRF) mDia2, which when activated can directly stimulate polymerization of unbranched actin filaments and mediate filopodia formation. A different subset of protein targets of Cdc42, which negatively regulate filopodia formation, are the Ser/Thr p21-activated kinases (PAK) -1, -2 and -4. PAK phosphorylates and activates LIM kinase (LIMK), which in turn phosphorylates and inhibits cofilin thereby stabilizing actin filaments. Differently, in neurons, Cdc42 is able to stimulate cofilin, by reducing its phosphorylation level, leading to actin polymerization and filopodium formation (Bishop and Hall, 2000; Heasman and Ridley, 2008).

Rac proteins

Rac proteins (such as Rac1 and Rac2) are known to stimulate lamellipodia and membrane ruffle formation, as well as induce membrane extension during phagocytosis (Jaffe and Hall, 2005). Rac-dependent lamellipodia extension, membrane ruffling and cell migration has been observed in multiple cell types, such as epithelial cells, macrophages, T cells and fibroblasts (Ridley, 2001). These small GTPases can activate mDia2 or the Arp2/3 complex (via WASP-family verprolin homologue (WAVE) proteins), both of which induce actin polymerization and lamellipodia extension (***Figure 3B***). Moreover, Rac proteins activate PAK-1, -2 and -3, which, by negatively regulating cofilin via LIMK phosphorylation, leads to actin filaments stabilization and affect actin turnover (Bishop and Hall, 2000; Heasman and Ridley, 2008; Jaffe and Hall, 2005). Finally,

is has been shown that Rac2 activity is involved in the formation of the phagocytic cup in neutrophils (Koh et al., 2005).

RhoA

RhoA, together with its RhoB and RhoC isoforms, induces actin stress fiber formation (Fujita et al., 2000; Heasman and Ridley, 2008). RhoA directly stimulates actin polymerization through mDia1 and mDia2. When the active RhoA directly binds to mDia1, the latter gets activated and then binds to the barbed end of actin filaments, thus promoting linear actin elongation (Jaffe and Hall, 2005). In this way, RhoA plays a crucial role in the regulation of cell shape, polarity and locomotion (***Figure 3B***). Furthermore, RhoA has been described to interact with Rho-associated protein kinase (ROCK) -1, which in turn phosphorylates myosin light chain (MLC) phosphatase and promotes actomyosin contractility due to increased actin filament cross-linking activity of myosin-II (Amano et al., 2010; Jaffe and Hall, 2005). Activated ROCK-1 also interacts and phosphorylates LIMK that, by inhibiting cofilin activity, prevents actin depolymerization and results in stabilization of actin filaments and decreased branching (Amano et al., 2010; Bishop and Hall, 2000).

C. Rab GTPases

The Rab GTPases constitute the largest family of small GTPases (with over 60 members in humans) and are localized to distinct intracellular membrane compartments, such as the endoplasmic reticulum (ER), the Golgi apparatus, and the early, late, or recycling endosomes (***Figure 4***). Subcellular localization specificity and function is dictated by geranylgeranyl groups attached to the C-terminal sequences, which ensures that Rab GTPases coordinate different steps of membrane trafficking, such as vesicle formation, vesicle and organelle motility, and fusion of vesicles to their target compartment (Stenmark, 2009; Wennerberg et al., 2005; Zerial and McBride, 2001). The role of Rab GTPases in vesicle trafficking will be addressed in chapter 3A.

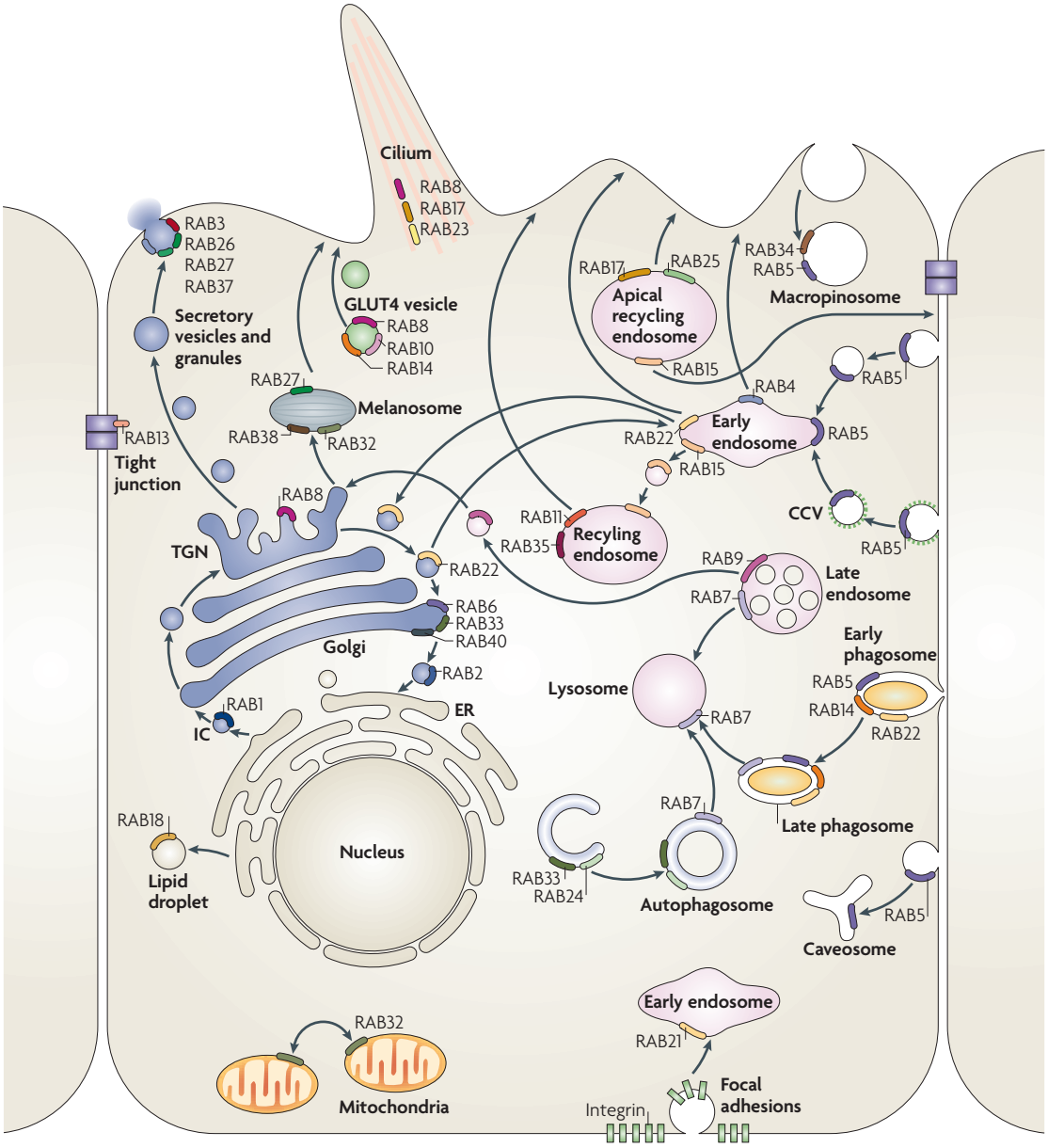

Figure 4 – Localization and function of small Rab GTPases. An epithelial cell is depicted with its vesicle transport pathways and the localizations of several Rab GTPases. Rab1 can be localized at the endoplasmic reticulum (ER) exit sites and at the ER-Golgi intermediate compartment (IC, or ERGIC), mediating ER-Golgi trafficking. Rab2, located at the IC might also control this mechanism. Rab6, Rab33 and Rab40, all localized to the Golgi, regulate intra-Golgi trafficking. Together with Rab24, Rab33 is also implicated in the formation of autophagosomes. Rab8 mediates constitutive biosynthetic trafficking from the *trans*-Golgi network (TGN) to the plasma membrane and, together with Rab10 and Rab14, participates in GLUT4 vesicle translocation. Additionally, Rab8 is involved in cilium formation (together with Rab17 and Rab23). Rab13 controls the assembly of tight junctions between epithelial cells and Rab18 is involved in the formation of lipid droplets. Rab3, Rab26, Rab27 and Rab37 are involved in different types of exocytosis events. Rab27 also mediates the translocation of melanosomes to the cell periphery. Moreover, Rab32 and Rab38 regulate melanosome biogenesis. Rab32 is also involved in mitochondrial fission. Rab22 mediates bidirectional trafficking between the TGN and early endosomes. Rab5, which is localized at the plasma membrane, early endosomes, phagosomes and caveosomes, mediates endocytosis and endosome fusion of clathrin-coated vesicles (CCVs), macropinocytosis (with Rab34) and phagosome maturation (with Rab14 and Rab22). Integrin endocytosis is regulated by Rab21. Rab11 and Rab35 mediate slow endocytic recycling through recycling endosomes, whereas Rab4 is involved in fast recycling directly from endosomes. Rab15 is involved in the trafficking from early endosomes to recycling endosomes and in the trafficking from apical recycling endosomes to the basolateral plasma membrane. Rab17 and Rab25 mediate trafficking through the apical recycling endosomes to the apical plasma membrane. Late endosome-associated Rab7 controls late endosome and phagosome maturation, and their fusion with lysosomes. Rab9, another late endosomal GTPase, is involved in the trafficking from late endosomes to the TGN. Adapted from Stenmark, 2009.

Chapter 2

Cellular Communication With the Outside Environment

The various environmental signals acting over eukaryotic cells induce the generation of selective cellular responses. These are governed by the activation of different proteins embedded in the plasma membrane, which induce dynamic remodeling of the cell cytoskeleton and generation of an intracellular signal transduction.

A. Plasma membrane and the cytoskeleton as interface

The plasma membrane of eukaryotic cells, together with all associated protein receptors, acts as an interface that separates the intracellular contents from its outside environment, and regulates what enters and exits the cell. Additionally, is also serves as a base of attachment for the cytoskeleton, thus helping in the maintenance of the cell shape. Despite etymological similarities with the body skeleton, the cytoskeleton is functionally very different, displaying a highly dynamic structure that is continuously reorganized in response to cellular requirements. Thus, the cytoskeleton plays major cellular functions such as spatial organization of the intracellular contents, physical and biochemical connection of the cell to the extracellular milieu and generation of coordinated forces that enable the cell to move and change shape. Most of these processes are accompanied by deformation of the cell membrane, such as the formation of filopodia and lamellipodia, endocytosis, phagocytosis, membrane trafficking events and intracellular movement of pathogenic bacteria.

There are three main cytoskeletal building blocks (***Figure 5***): actin microfilaments, microtubules (MTs) and intermediate filaments. However, recently it has been proposed that septins constitute an additional component of the cytoskeleton (Chang and Goldman, 2004; Fletcher and Mullins, 2010; Mostowy and Cossart, 2012).

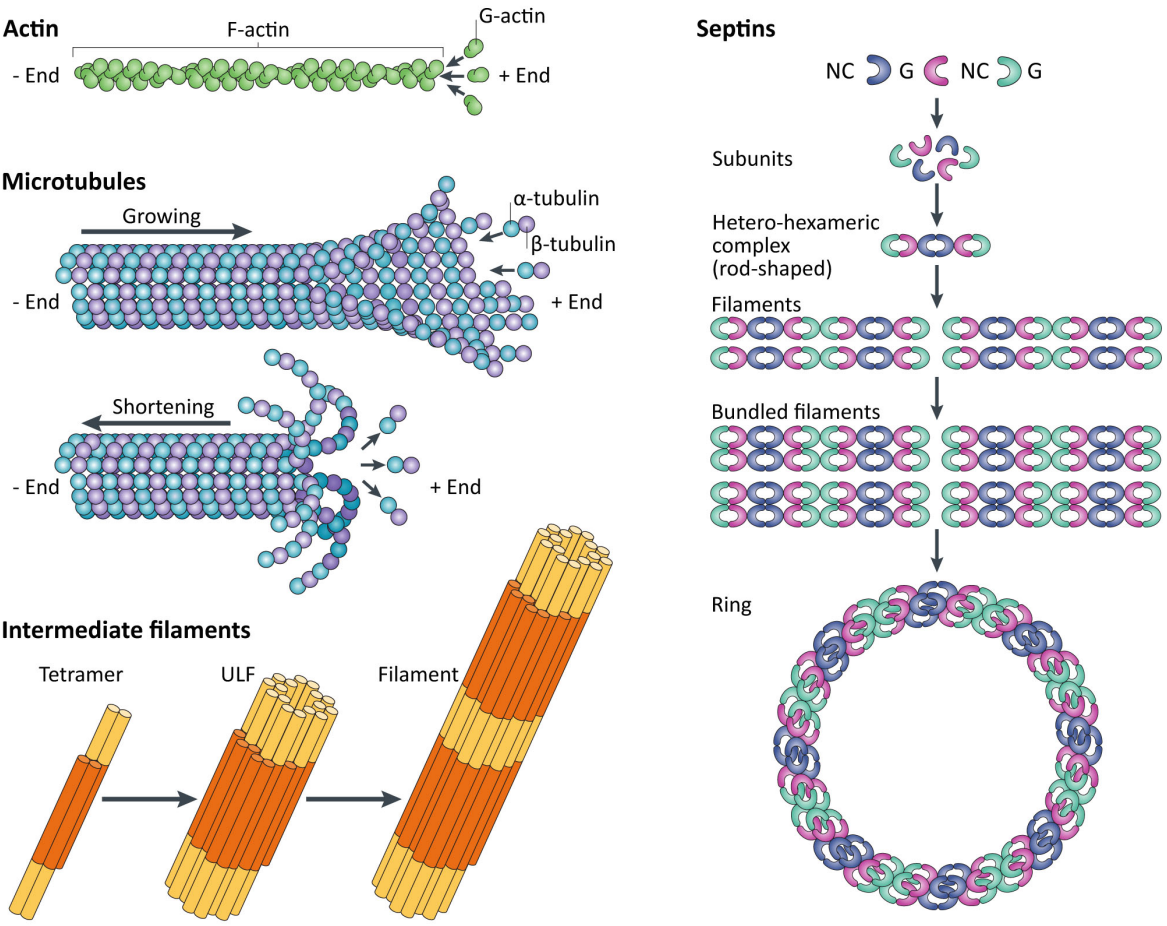

Figure 5 – Schematic representation of the main cellular cytoskeletal components: actin, microtubules, intermediate filaments and septins. Septins from different groups are depicted in different colors, and they interact through their GTP-binding domain (the G interface) and their N-terminal and C-terminal regions (the NC interface). Adapted from Mostowy and Cossart, 2012.

Actin filaments

Actin is one of the most abundant and highly conserved proteins in eukaryotic cells. This 42 kDa protein is able to bind ATP (adenosine triphosphate), and in its monomeric form is known as globular actin (G-actin), which can undergo cycles of self-polymerization into filamentous actin (F-actin), a process that is accompanied by ATP hydrolysis. Long polymerized chains of actin filaments are organized in a helix structure with a diameter of ~7 nm, and are highly dynamic branched networks. These can regulate a wide variety of cellular processes requiring generation of forces, such as phagocytosis, endocytosis, cell junction assembly, membrane ruffling and lamellipodia dynamics, and filopodia and stress fiber formation. F-actin filaments are polar, containing dynamic barbed plus ends (where monomers preferentially assemble), and less active pointed minus ends (where monomers preferentially disassemble). Moreover, filament turnover is

controlled by different actin-binding proteins, which can sequester or deliver actin monomers, or promote filament nucleation, capping, elongation, severing or depolymerization. Actin assembly is initiated by the generation of free plus ends that act as templates for polymerization. Nevertheless, spontaneous assembly of actin monomers into polymers (known as nucleation) is kinetically unfavorable and inefficient. Therefore, cells utilize several actin-binding proteins that directly nucleate actin filament formation (***Figure 6***), such as the Arp2/3 complex, formins and WASP homology 2 (WH2) domain-containing nucleators (Campellone and Welch, 2010; Mostowy and Cossart, 2012; Rottner et al., 2010; Rotty et al., 2012).

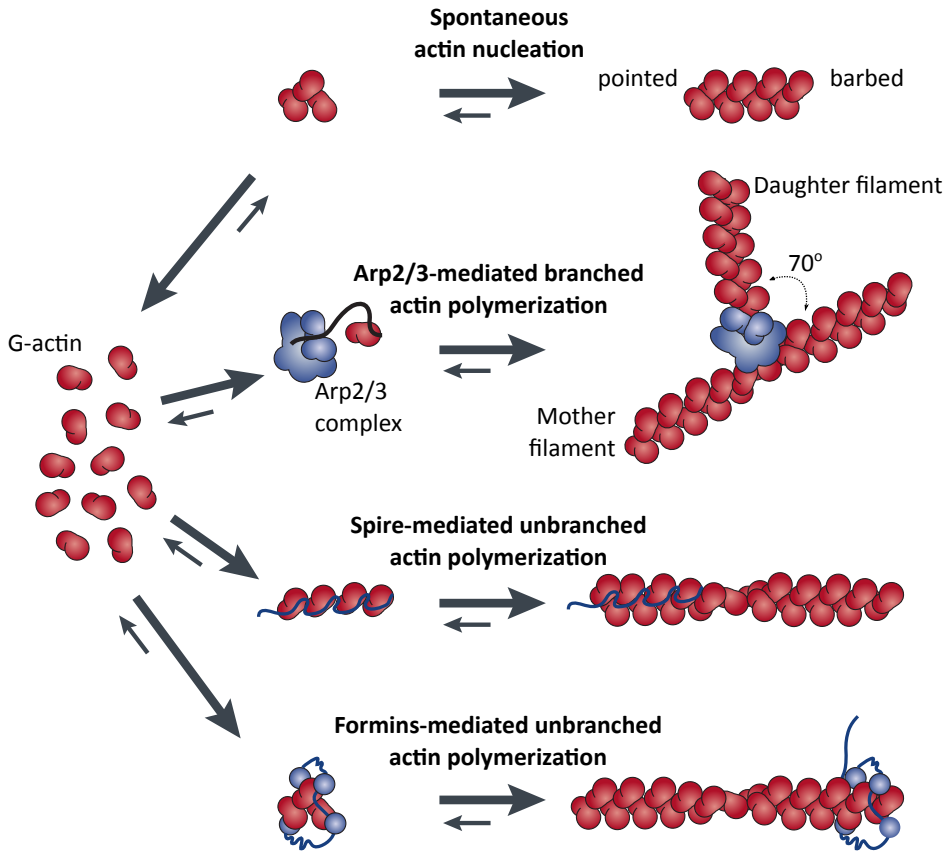

Figure 6 – Schematic representation of different paths of actin polymerization. Adapted from Goley and Welch, 2006.

The Arp2/3 complex is one the most important actin nucleators. This is a 220 kDa protein complex composed of seven stably associated polypeptides that include Arp2, Arp3 and five additional subunits, ArpC1-ArpC5. The Arp2/3 complex binds to the side of existing acting filaments and initiates the branching off and elongation of new filaments at a ~70º Y-branch angle (***Figure 6***). By itself,

the Arp2/3 complex is not an efficient actin nucleator, but when bound to actin filaments its activity increases. Other factors contribute to increased nucleation and branching activity, such as Arp2 phosphorylation and the binding of nucleation-promoting factors (NPFs), such as the N-WASP factor (Campellone and Welch, 2010; Rotty et al., 2012). Signal transduction pathways initiated at the plasma membrane that include Cdc42 activation can result in activation of N-WASP, through a conformational change, then leading to Arp2/3-mediated actin polymerization (Tomasevic et al., 2007). Interestingly, N-WASP function seems to be important for several processes such as plasma membrane ruffling and invagination, and endocytosis, a process in which F-actin facilitates membrane fission (Legg et al., 2007; Tsujita et al., 2006). Another group of NPFs are the WAVE proteins that, when activated by Rac GTPases, can activate the Arp2/3 complex and induce lamellipodia formation (Takenawa and Suetsugu, 2007). Other NPFs include the WASH (WASP and SCAR homologue), WHAMM (WASP homolog associated with actin, membranes and microtubules) and JMY (junction-mediating and regulatory protein) proteins, as well as cortactin, each exerting specific functions that extend the repertoire of Arp2/3 complex activation (Campellone and Welch, 2010; Rottner et al., 2010).

Other actin nucleators, unlike Arp2/3, induce formation of unbranched actin filaments. One of the best characterized examples are the formins, such as DRF proteins. Formins bind to barbed ends and enable actin filament elongation by preventing other capping proteins from terminating this process (***Figure 6***). Additionally, formins help determining the length of F-actin filaments. More specifically, DRFs are activated by different Rho GTPases and participate in the formation of stress fibers, filopodia, lamellipodia and phagocytic cups (Campellone and Welch, 2010). Finally, a new class of actin nucleating proteins has been described: the WH2 domain-containing nucleators. Factors from this family include Spire, cordon-bleu and leiomodin proteins. These proteins induce the tethering of three or more G-actin monomers in either a single linear F-actin multimeric strand or a short trimer, thereby promoting actin nucleation at the barbed ends (Baum and Kunda, 2005; Qualmann and Kessels, 2009).

Dissociation of Y-branches can be regulated by coronins and cofilin, which inhibit the Arp2/3 complex and promote actin depolymerization and recycling (Rotty et al., 2012; Sit and Manser, 2011). The tightly orchestrated equilibrium

between nucleation, branching and turnover allows the efficient formation of actin networks in the eukaryotic cell.

Microtubules

MTs are long, filamentous, tube-shaped protein polymers with a diameter of ~25 nm and that can be many micrometers long, composed of α-tubulin and β-tubulin heterodimers. MTs are essential in all eukaryotic cells and play crucial roles in the development and maintenance of cell shape, in the transport of vesicles within the cell, in cell signaling, and in cell division and mitosis. Like actin filaments, MTs are polarized polymers, with a structurally asymmetrical molecular organization comprised of a plus end and a minus end. The polymerization of MTs is driven by a nucleation-elongation mechanism, is highly dynamic and is regulated both spatially and temporally (Jordan and Wilson, 2004; Mostowy and Cossart, 2012). These filaments are in a constant state of non-equilibrium dynamics that can occur via two different mechanisms. One kind of dynamic behavior is known as dynamic instability and involves the addition and loss of tubulin subunits at the plus end of MTs, which is driven mainly by GTP hydrolysis. GTP-bound tubulin subunits are incorporated into a MT plus end, creating a stable GTP cap that prevent filament depolymerization. However, GTP is rapidly hydrolyzed in the β-tubulin subunit, the MT becomes unstable and depolymerizes due to the adoption of a outward curved conformation, leading to further destabilization of the filament. When GDP is substituted by GTP in the disassembled tubulin subunits, the cycle can restart. Thus, MTs constantly switch between phases of growth (known as rescue) and shortening (known as catastrophe), which happens more rapidly and more extensively in the plus end than in the minus end. The other mechanism of MT dynamic behavior, known as treadmilling, occurs through the gain of tubulin at the plus end of MTs (growing) and loss of tubulin at the minus end of the filaments (shortening), together with an intrinsic flow of tubulin subunits (Ferreira et al., 2014; Jordan and Wilson, 2004).

Among other factors, MT behavior is controlled through the binding of regulatory proteins that include MT-associated proteins (MAPs), such as the dynein and kinesis motor proteins, and dynactin-1. Many of these MAPs are able to recognize only the MT plus end, and are involved in the regulation of dynamic

instability parameters, therefore controlling MT activity (Akhmanova and Hoogenraad, 2005; Jordan and Wilson, 2004).

Intermediate filaments

Intermediate filaments are a group of around 70 proteins that, unlike actin and tubulin, do not form seeds to which individual subunits grow. Instead, intermediate filaments are built by the assembly of individual proteins that form a tetrameric subunit composed of two antiparallel coiled-coil dimers. Then, eight tetrameric subunits associate with each other laterally, forming a unit length filament (ULF), which then joins end-to-end with other ULFs to form short filaments, in a process that only takes a few seconds. Short filaments then grow into longer filaments through the longitudinal annealing with other ULFs (Herrmann et al., 2007; Mostowy and Cossart, 2012). Intermediate filaments have a diameter of ~ 11 nm and are not polarized. They are the least stiff of all the types of cytoskeletal polymers, so they are able to resist tensile forces much more effectively than compressive forces. Moreover, intermediate filaments can crosslink to actin filaments and MTs, through the action of plectin proteins, which regulates several cellular functions (Fletcher and Mullins, 2010).

Within the cell, there is a system of cytoplasmic intermediate filaments that connects intercellular junctional complexes at the plasma membrane with the outer nuclear membrane, thus helping in the stabilization of the cell shape. One example is intermediate filament protein vimentin. Additionally, there is another intermediate filament system that is attached to the inner nuclear membrane, inside the nucleus, and that consists of lamins (Herrmann et al., 2007).

Septins

Septins comprise a family of highly conserved proteins in eukaryotes and were only recently recognized as a novel component of the cytoskeleton. Human cells have 13 septin genes that encode for over 30 protein isoforms (Hall et al., 2005; Mostowy and Cossart, 2012; Spiliotis, 2010). These are 30-65 kDa proteins structurally composed of a central core domain that can directly bind to phosphoinositides on the plasma membrane, a GTP-binding domain and 53 highly conserved amino acids of unknown function (Pan et al., 2007). All septins bind to GTP and most hydrolyze it to GDP, which appears to induce stable conformational

changes and therefore enable or prevent septin-septin interactions (Estey et al., 2011; Sirajuddin et al., 2007; 2009). In human cells, septins generally interact as hetero-oligomeric complexes of three different septin proteins, each of which is present in duplicate, therefore generating a hexameric structure. An example is the structure of the septin-2, -6 and -7 complex, which displays a linear non-polar hexamer with two copies of each septin symmetrically arranged in the order 7-6-2-2-6-7 (Mostowy and Cossart, 2012; Sirajuddin et al., 2007). Furthermore, recent work showed that both ends of this hexamer also bind septin-9, therefore forming an octamer (Kim et al., 2011). All septin complexes are able to form non-polar filaments as a result of end-to-end protein assembly, which results in structures that are more stable and less dynamic than other cytoskeletal elements such as actin microfilaments or MTs. Additionally, septin filaments can associate laterally, forming bundled filaments that ultimately tend to self-assemble into higher-ordered structures such as rings, both of which are considered to be the biological active forms of septins (Estey et al., 2011; Mostowy and Cossart, 2012). This plasticity results in a notable combinatorial diversity of septin complexes, which might provide them multiple roles that cannot be carried out by other cytoskeleton components.

Septins have also been shown to interact with other components of the cytoskeleton such as actin, and seem to be involved in several cellular processes such as actin bundle formation and phagocytosis (Huang et al., 2008; Kinoshita et al., 2002). This suggests that septins could also associate with the Arp2/3 complex or with members of the WASP family to control actin polymerization (Mostowy and Cossart, 2012). Moreover, septins associate with MTs in different mammalian cells, where colocalization was observed with septin-2 and -9 (Nagata et al., 2003; Spiliotis et al., 2008). Therefore septins might contribute to MT-dependent movement of membranes, as well to the spatial coordination of cell motility and MT-actin crosstalk (Spiliotis, 2010).

Functionally, septin filaments appear to act as macromolecular scaffolds that accumulate proteins and promote their interaction. Given that septins can interact with phospholipids on the plasma membrane (Bertin et al., 2010), they can regulate the distribution of membrane-bound proteins at this site, such as the receptor tyrosine kinase Met. Moreover, septins seem to have a role in clathrin-mediated endocytosis (Mostowy and Cossart, 2009; Mostowy et al., 2011). It is

even possible that septin filaments might function as crosslinkers between the plasma membrane and actin (Saarikangas and Barral, 2011). Additionally, these septins scaffolds localize to sites of exocytosis, where they participate and regulate events of vesicle docking and fusion with the plasma membrane (Amin et al., 2008; Estey et al., 2011). The association of septin filaments with the plasma membrane is also involved in generating membrane diffusion barriers that compartmentalize membrane proteins to specific membrane domains. In such a way, septins can create barricades that isolate specific cellular domains thus preventing free diffusion of molecules in the membranes (Caudron and Barral, 2009; Estey et al., 2011).

B. Endocytosis and phagocytosis

Eukaryotic cells are able to take up macromolecules and particles from the surrounding medium through a process called endocytosis, coined for the first time in 1963, by Christian de Duve. In this process, signals at the plasma membrane trigger actin filaments to assemble locally, inducing membrane internalization and particle ingestion into an endocytic vesicle that pinches off into the cytoplasm. Given that the plasma membrane defines the boundary by which the cell communicates with the environment, its composition has to be tightly regulated by the cell in order to allow effective cellular response mechanisms. During endocytosis there is production of new intracellular membranous structures deriving from the plasma membrane. These structures contain membrane lipids, proteins and extracellular fluid. In this way, cells efficiently regulate the levels of surface receptors, as well as their interaction with the environment, which is crucial for the control of diverse intracellular cascades. Moreover, many pathogens exploit endocytosis to force their internalization into the host cell (described in more detail in chapter 4). Interestingly, there are different mechanisms and routes of endocytic uptake into the cell (***Figure 7***) (Doherty and McMahon, 2009).

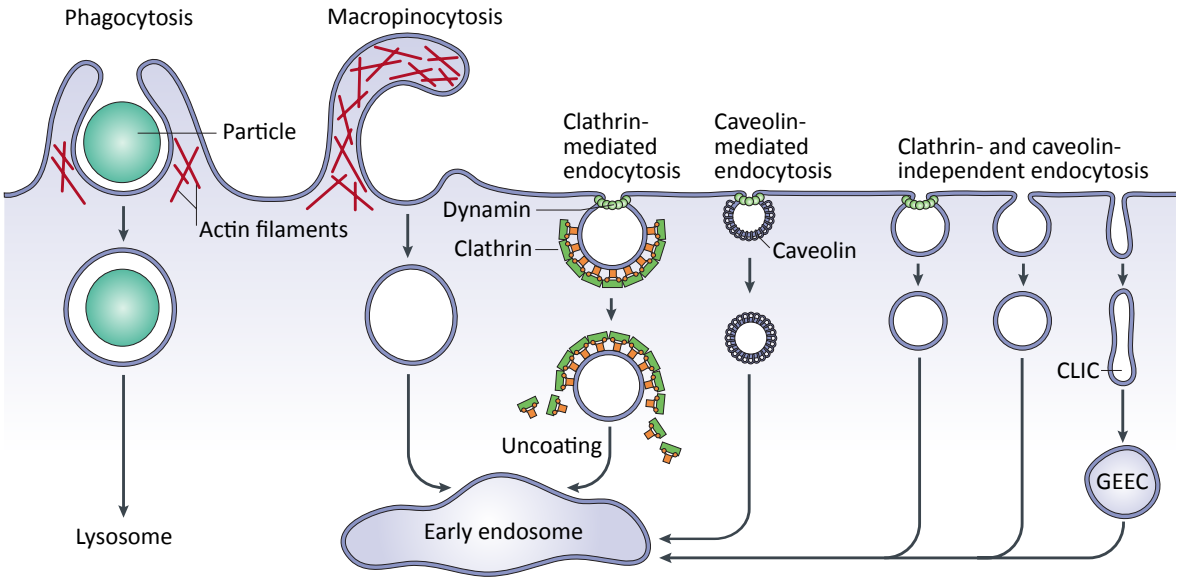

Figure 7 – Schematic representation of different cellular endocytic pathways. Large particles are internalized by phagocytosis, whereas fluid internalization occurs by macropinocytosis. In both cases, there is the formation of considerably large intracellular vesicles. The majority of the endocytosed cargo is internalized to the early endosome, via clathrin- or caveolin-coated vesicles that are derived from the plasma membrane. Cdc42-regulated endocytosis may lead to the internalization of cargoes that are delivered via clathrin- and dynamin-independent carriers (CLICs) into a glycosyl phosphatidylinositol-anchored protein-enriched early endosomal compartment (GEEC), on the way to the early endosome. Adapted from Johannes et al., 2015 and Mayor and Pagano, 2007.

Clathrin-mediated endocytosis

Clathrin-mediated endocytosis is the most extensively studied and best understood process of endocytosis. As in any other endocytic pathway, it requires a budding structure from the plasma membrane, through a well-defined sequence of events. In mammalian cells, clathrin-mediated endocytosis involves the packaging of transmembrane receptors and their ligands into vesicles, called clathrin-coated vesicles (~80-100 nm in diameter), with the aid of adaptor proteins. This mechanism involves sequential steps of nucleation, cargo selection, coat assembly and invagination, and ultimately scission of the vesicle from the plasma membrane. The coat of the inward-budding clathrin-coated pit is formed by a triskelion shape composed of three clathrin heavy chains and three light chains, which confers structural support to the vesicle. Since clathrin does not bind directly to lipids or cargo, it requires additional accessory proteins and cargo adaptors that promote triskelion assembly, cargo sequestration and vesicle formation. One of the most abundant clathrin adaptors is the adaptor protein complex 2 (AP2), which acts as a bridge that links transmembrane cargo to the nucleating clathrin coat (Doherty and McMahon, 2009). Another important adaptor is the clathrin assembly

lymphoid myeloid leukemia (CAML) protein. It is known that these two adaptor proteins are crucial for endocytosis. Additionally, CALM is a major factor that regulates the size of clathrin-coated pits and clathrin-coated vesicles, by directly sensing and driving membrane curvature (Miller et al., 2015). An additional step for vesicle formation depends on the rim complex, which consists of several proteins such as epsin and intersectin, and localizes to the edge of the growing vesicle. This promotes further clathrin nucleation and the formation of clathrin curved lattices that stabilize the curvature of the attached membrane and induce invagination (***Figure 8***). Interestingly, membrane curvature generation depends on other factors than clathrin polymerization alone (Doherty and McMahon, 2009; Humphries and Way, 2013). Indeed, it was recently shown that epsin accumulation and high local protein crowding, on one side of the membrane, drives membrane bending by creating steric pressure (Stachowiak et al., 2012).

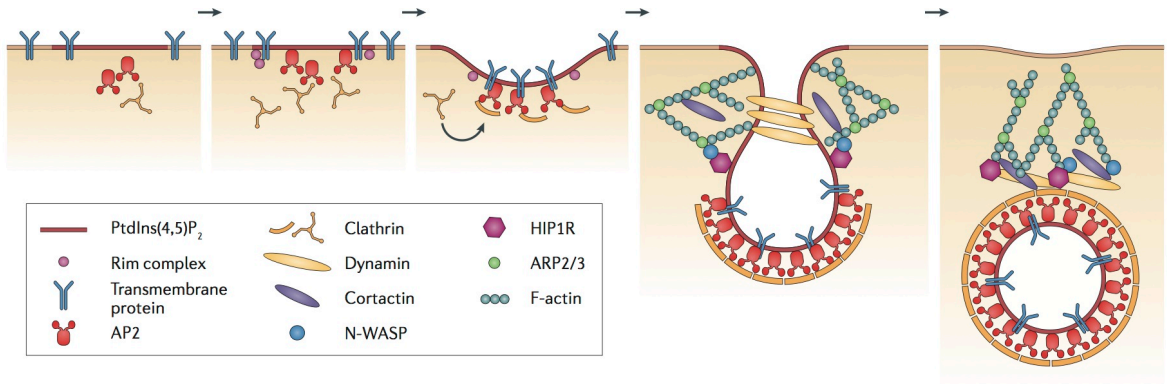

Figure 8 – Different steps of clathrin-mediated endocytosis. The process starts at plasma membrane sites that are enriched in phosphatidylinositol-4,5-bisphosphate (PtdIns(4,5)P_2), with the recruitment of AP2 and clathrin. AP2 then selectively sequesters cargo and recruits other accessory proteins. The rim complex promotes further clathrin lattice formation, resulting in membrane invagination and vesicle formation. Scission depends on the action of the GTPase dynamin, allowing full internalization of the vesicle and cargo into the cell. At the final stages, Arp2/3-dependent actin nucleation leads to the formation of branched actin filaments that help vesicle scission. HIP1R is thought to tether the actin cytoskeleton to clathrin. Additionally, HIP1R interacts with cortactin and inhibits the interaction of this protein with N-WASP, dynamin and the Arp2/3 complex. This seems to regulate both the location and extent of actin polymerization and thus ensures that actin nucleation is restricted to the site of vesicle neck formation. Adapted from Humphries and Way, 2013.

Membrane scission from the plasma membrane requires dynamin, a large GTPase that forms a helical polymer around the constricted vesicle neck. Upon GTP hydrolysis, dynamin mediates vesicle fission from the plasma membrane, irreversibly releasing the clathrin-coated vesicle into the cell (Praefcke and McMahon, 2004). During the step of vesicle scission, recruitment of actin to the

invaginating pit also takes place. The formation of a branched actin network around the endocytic pit is regulated by the Arp2/3 complex that, together with N-WASP, dynamin, cortactin and HIP1-related protein (HIP1R), regulate endocytosis. In addition to its role in vesicle scission, dynamin could also coordinate actin nucleation at the site of clathrin-mediated endocytosis. Furthermore, during endocytosis, actin filament barbed ends are directed towards the neck of the vesicle, thus providing force and promoting elongation of the growing vesicle neck and its scission. Subsequently, actin also promotes inward propulsion and movement of the vesicle away from the plasma membrane and into the cell (***Figure 8***). The basket of clathrin coating the vesicle is then released and the naked vesicle subsequently undergoes further trafficking within the cell (Doherty and McMahon, 2009; Humphries and Way, 2013).

It has become increasingly likely that different accessory and adaptor proteins are able to control the internalization of distinct cargoes. Then different subtypes of clathrin-coated vesicles may be formed, each containing a specific population of proteins.

Clathrin-independent endocytosis

Additional endocytic pathways, that are independent of clathrin and can be either dynamin-dependent or -independent, exist in the cell (***Figure 7***). Caveolae-mediated endocytosis is one of the best characterized dynamin-dependent clathrin-independent pathways. Caveolae are 50-80 nm flask-shaped plasma membrane invaginations that are enriched in caveolins, cavins, sphingolipids and cholesterol, signaling proteins and clustered glycosyl phosphatidylinositol-anchored proteins. These micro-domains are present on the surface of different cell types, and they can play an important role in the trafficking of lipids, proteins and pathogens (Mayor and Pagano, 2007). The caveolar coat is composed of two major protein layers. In non-muscle cells, the inner layer is composed of caveolin-1 and caveolin-2, which are integral membrane proteins that form an interconnected scaffold that determines the size of the micro-domain, as well as other properties. Additionally, there is an outer cytosolic protein layer, formed at least by cavins, which cover the highly curved membrane of caveolae and are thought to promote membrane curvature and regulate caveolae budding (Hayer et al., 2010a; McMahon et al., 2009). At the plasma membrane, caveolae are stable

structures. Nevertheless, they can be disassembled, which involves the release of cavin-1 from intact caveolae, followed by caveolae endocytosis and subsequent delivery and degradation in the endocytic pathway (Hayer et al., 2010b). This study was particularly interesting, since it showed that the previously described “caveosome” is most likely a modified late endosome or lysosome, and therefore is not an independent organelle (Parton and Howes, 2010). Moreover, dynamin was shown to localize to the neck of caveolae, where it has a role in caveolar budding (Henley et al., 1998; Oh et al., 1998). A distinct dynamin-dependent clathrin-independent endocytosis mechanism relies on the small GTPase RhoA, and leads to the internalization of the β-chain of the interleukin-2 receptor (IL-2R-β), as well as other proteins. Given that RhoA plays a crucial role in the regulation of actin cytoskeleton dynamics, it could also be important for recruiting the actin polymerization machinery to regulate this endocytic pathway (Mayor and Pagano, 2007).

Additionally, there are clathrin-independent and dynamin-independent endocytic pathways. Nevertheless, a common player in these pathways are flotillin proteins, which oligomerize in distinct membrane microdomains and might play a role in the ordering of lipids, similarly to caveolae (Doherty and McMahon, 2009). These endocytic processes can be either regulated by Cdc42 (which can lead to the uptake of cholera toxin B or fluid-phase markers) or by the ADP-ribosylation factor (Arf) family GTPase Arf6 (which can lead to the internalization of E-cadherin, β1 integrin, among others) (Mayor and Pagano, 2007).

Macropinocytosis

Macropinocytosis is an actin-dependent endocytic pathway that leads to the internalization of fluid and relatively large portions of the plasma membrane into large vacuoles. This process is usually initiated by external stimuli (commonly growth factors) that trigger plasma membrane ruffling induced by the activation of actin and microfilaments connected to the plasma membrane. These membrane ruffles protrude to the external milieu and take the form of lamellipodia, circular ruffles and in some cases large blebs, depending on the cell type and stimuli. When the membrane ruffle folds back to the plasma membrane it can also be internalized by the cell, forming fluid-phase cavities that can undergo membrane fission. This then results in the formation of closed vesicles, called

macropinosomes, which lack protein coats to guide their formation and thus can vary in shape and size, and have a diameter of 0.2 to 10 µm (Jones, 2007; Swanson, 2008). Several intracellular pathogens are also able to induce ruffle formation in the host cell, independently of growth factors, resulting in their internalization together with fluid in macropinosomes. This will be described in detail in chapter 4.

Macropinocytosis is generally triggered by activation of receptor tyrosine kinases, which then activate a signaling pathway resulting in changes in the dynamics of actin filaments. For this process, the GTPase Rac1 plays an important role, inducing the formation of membrane ruffles through the activation of actin polymerization, stability and turnover. Rab5 and its effector Rabankyrin-5 also promote macropinocytosis and fluid phase uptake, through a mechanism that remains largely unknown (Doherty and McMahon, 2009; Schnatwinkel et al., 2004). Additionally, plasma membrane-localized Arf6 promotes small GTPase-mediated ruffling and macropinocytosis by recycling Rac1 to the plasma membrane. Macropinocytosis also depends on kinases, such as phosphatidylinositol-3-kinase (PI(3)K), PAK1 or c-Src. When activated, c-Src, a non-receptor tyrosine Src-family kinase, shuttles from the cytoplasm to the sites of ruffling where it enhances receptor activity and activates Arp2/3, Rac1 and PI(3)K (Doherty and McMahon, 2009; Jones, 2007; Mercer and Helenius, 2009).

Membrane fission and macropinosome closure is regulated by different factors, such as kinases, myosins, fusion/fission factors and GTPases. Rab34 and activated PI(3)K might be required for macropinosome formation and closure. Moreover, myosins that are present in the membrane ruffles provide contractile activity for the closure of macropinosomes (Mercer and Helenius, 2009). Once formed, macropinosomes undergo dynamic processes of maturation, which might be cell specific. In macrophages, for example, macropinosomes follow a conventional route to lysosomes, acquiring Rab7 and fusing with lysosomes. In other cell types, macropinosome fate is largely unknown (Jones, 2007).

Phagocytosis

Phagocytosis is the process that enables some cells, particularly professional phagocytes such as macrophage and dendritic cells, to engulf large opsonized particles (> 0.5 µm) and then eliminate them. Thus, phagocytosis plays a central

role in innate and adaptive immunity. When antibody-opsonized particles, like bacteria, are recognized by Fc receptors on the phagocyte plasma membrane, the cell forms filopodia-like extensions around the particle. This process requires Cdc42 activation and then leads to particle internalization, which is Rac1-dependent. These small GTPases recruit N-WASP and Arp2/3 complex to the phagocytic membranes, resulting in actin polymerization and phagocytosis. On the contrary, when a particle is opsonized with the complement effector fragment C3b, it binds to the complement receptor CR3 (a modified integrin) that then is internalized in a RhoA-dependent manner. In this process, Arp2/3 complex is also recruited but membrane protrusions are usually not observed (Doherty and McMahon, 2009; Fairn and Grinstein, 2012).

Particle internalization occurs through membrane invagination and formation of an intracellular membrane-bound vacuole called phagosome. Newly formed phagosomes present a composition similar to that of the plasma membrane from which they originate. Even though the plasma membrane is thought to be the major source of membrane for early phagosome formation, other cellular endomembranes have been suggested to also contribute to the process, such as the endoplasmic reticulum (ER). Despite controversy in the field, it is thought that the ER might be recruited to the site of phagocytosis, contributing with membrane to the formation of plasma membrane extensions (Gagnon et al., 2002; Guermonprez et al., 2003; Houde et al., 2003). Nascent phagosomes lack the microbicidal and degradative capacity to eliminate pathogens. These capabilities are acquired subsequently, through a series of signaling events that lead to phagosome maturation. This involves sequential fusion with other organelles in the cell cytoplasm, which will be explained in detail in chapter 3B.

Chapter 3

Intracellular Organelle Communication

Compartimentalization within eukaryotic cells is of crucial importance since it allows the establishment of physical boundaries, in which each compartment or organelle is associated with a specific biological process. Additionally, cellular compartmentalization creates specific cellular microenvironments that spatially and temporally regulate different functions. This implies that there is the need to transfer biological content and information between different organelles in a precise and tightly regulated manner (Palade, 1982). The mechanism of intracellular transport can occur via membrane-bound vesicular transport carriers, and is regulated by multiple trafficking proteins, such as coat proteins (for budding), motor proteins (for motility), tethering factors (for docking), SNAREs (soluble *N*-ethylmaleimide-sensitive factor attachment proteins receptors, for fusion) and Rab GTPases (for multiple steps of vesicular trafficking).

A. Regulators of vesicular membrane trafficking

Vesicular membrane trafficking, or the flow of membrane material between different endomembrane compartments, is crucial for the transport of proteins and other macromolecules to various destinations inside and outside of the cell. This process is also essential to enable the maintenance of cellular homeostasis, as well as to meet specific demands during signal transduction. Membrane trafficking from a donor compartment to a target compartment is tightly controlled, through a sophisticated coordination between different factors. In this section, the role of Rab GTPases and SNAREs during vesicle trafficking will be addressed.

Rab GTPases regulate vesicle budding and uncoating

Due to the high level of intracellular vesicle flow between various organelles, there is the need to guarantee that specific cargoes are transported in the correct

vesicles. This is ensured by several factors such as the cargo itself, the lipid composition of a membrane and its curvature, and Rab GTPases. It was shown that Rab1 is involved in vesicle budding from the ER (Nuoffer et al., 1994) and that the late endosomal Rab9 facilitates sorting and recycle of mannose-6-phosphate receptors (M6PRs) from late endosomal recycling buds to the *trans*-Golgi network (TGN) (Carroll et al., 2001; Riederer et al., 1994). Rab5 was also described to have a role in cargo sequestration and vesicle formation, and it associates with early endosomes. This GTPase is a crucial factor for the assembly of clathrin-coated pits at the plasma membrane and for clathrin-mediated endocytosis of transferrin receptors (McLauchlan et al., 1998). Thus it seems that at least some Rab GTPases influence vesicle budding from donor membranes, and they might also aid incorporation of cargo molecules into the nascent vesicles. Moreover, active Rab GTPase could act as a checkpoint that guarantees vesicle delivery to the correct target organelle (Stenmark, 2009).

After their budding, vesicles are coated with molecular complexes that need to be shed to allow correct membrane engagement and fusion with the acceptor membrane. On clathrin-coated pits, for example, Rab5 activity helps in the uncoating of the adaptor protein complex AP2 from endocytic vesicles, which is important for proper membrane trafficking in epithelial cells (Semerdjieva et al., 2008).

Rab GTPases regulate vesicle motility

Actin filaments and MTs can function as tracks for molecular motors that carry vesicles between intracellular compartments. Rab proteins also regulate vesicle motility within the cell along the cytoskeletal filaments, which requires a high specificity in the binding of motor proteins to vesicles. In general, two main protein families associate with MTs to mediate trafficking: kinesins, which move intracellular material to the MT plus-end; and dyneins, which act as minus-end-directed MT motors (Chang and Goldman, 2004). It has been shown that active Rab6a (localized to the Golgi) associates with kinesin-1, kinesin-3 and kinesin-6, but also with the cytoplasmic dynein-1, thus regulating different trafficking steps in separate cellular contexts (Horgan and McCaffrey, 2011; Stenmark, 2009). Rab5 regulates both the attachment of early endosomes to, and the motility along, MTs (Nielsen et al., 1999). Rab11a regulates endosomal trafficking by associating with

kinesin-2, and can also control additional trafficking from sorting endosomes to recycling endosomes by binding to dynein-1. Rab27a and Rab27b associate with kinesin-1 to regulate axonal transport of certain vesicles. Moreover, Rab27a is able to mediate association of cargo vesicles to the actin motor myosin-Va, which is crucial to transport Rab27-positive vesicles to the cell periphery, in melanocytes (Stenmark, 2009). Finally, it was shown that the Rab7 effector Rab-interacting lysosomal protein (RILP) facilitates the dynein-mediated transport of late endosomes along MTs (Jordens et al., 2001).

Rab GTPases regulate vesicle fusion

Rab GTPases also cooperate with components of the vesicle docking and fusion machinery, such as the SNARE complexes. For example, the active GTP-bound form of Rab5 (localized to early endosomes) is vital for homotypic early endosome fusion thus regulating endosome maturation (Stenmark et al., 1994). The abovementioned Rab27a also plays a role in vesicle fusion, since it controls docking of exocytic vesicles to the plasma membrane (Stenmark, 2009).

SNAREs

Membrane fusion is a fundamental process within eukaryotic cells. At a molecular level it is mostly regulated by SNARE proteins. In mammalian cells, at least 35 different SNAREs have been found, which act in the final step of docking of donor vesicles and their fusion with target compartments (Hong, 2005). Functionally, SNAREs were originally classified into v-SNAREs and t-SNAREs according to their donor vesicle (v) or target (t) membrane localization. Though, to avoid ambiguity in the case of homotypic membrane fusion, SNAREs have been reclassified as R-SNAREs (generally act as v-SNAREs) or Q-SNAREs (often act as t-SNAREs) (Chen and Scheller, 2001). Interaction between R- and Q-SNAREs leads to the formation of the *trans*-SNARE complex (or SNAREpin), in which one SNARE helix wraps around similar helixes on three other SNAREs (***Figure 9A***). In the center of the SNAREpin, one R-SNARE contributes with an arginine (R) residue, whereas three Q-SNAREs contribute with a glutamine (Q) residue each (Hong, 2005; Luzio et al., 2007). Many of the VAMP (vesicle-associated membrane protein) proteins belong to the group of R-SNAREs, whereas syntaxins and SNAPs (synaptosome-associated proteins) belong to the group of Q-

SNAREs. Most of these are found in specific subcellular compartments, indicating that they are selectively involved in particular intracellular trafficking steps (Chen and Scheller, 2001). For example syntaxin-1, syntaxin-2, syntaxin-4 and SNAP25 are found at the plasma membrane. Syntaxin-5 and VAMP4 localize to the Golgi, VAMP8 localizes to early and late endosomes, and VAMP7 localized to late endosomes and lysosomes (Jahn and Scheller, 2006).

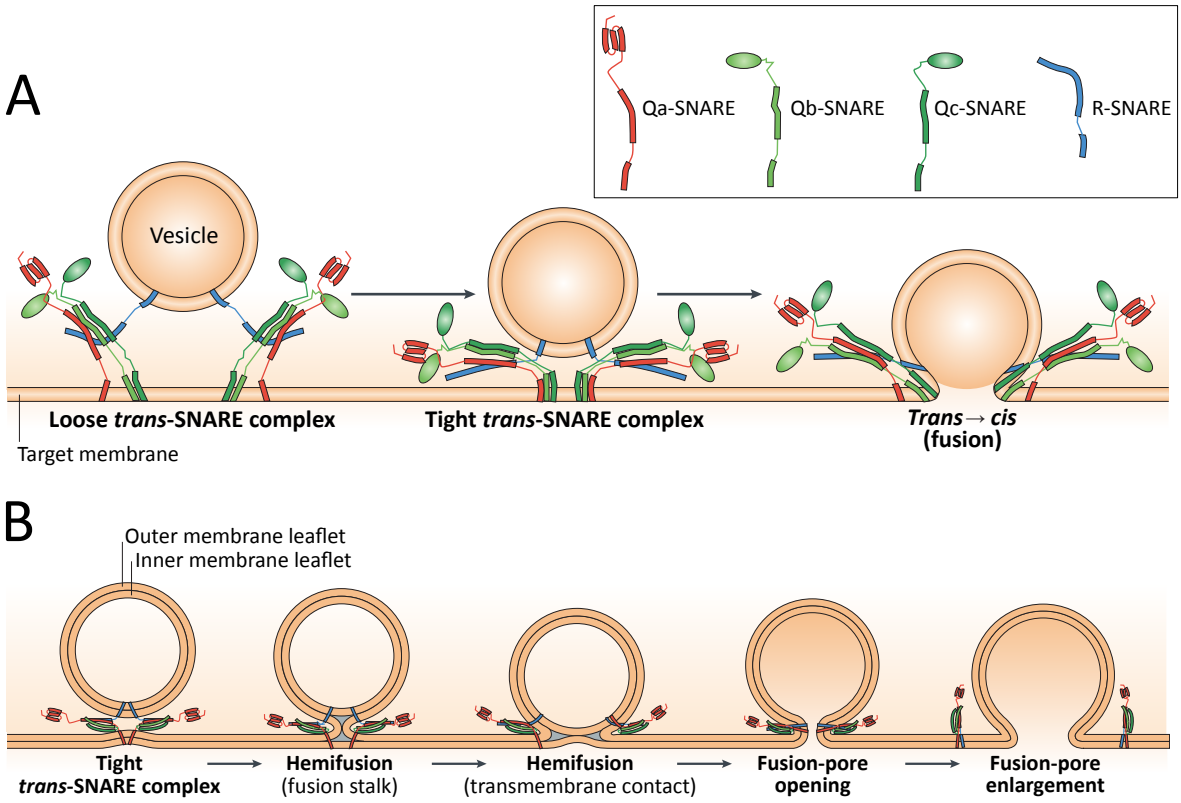

Figure 9 – Schematic representation of SNARE-mediated vesicle membrane fusion. Adapted from Jahn and Scheller, 2006.

Mechanistically, it is not energetically favorable to fuse two membranes in an aqueous environment. The formation of the *trans*-SNARE complex exerts a mechanical force on membranes, which direct two membranes towards each other and creates membrane curvature and tension, directly causing fusion. After the formation of a tight *trans*-SNARE complex, apposing membranes start hemifusing, followed by distal leaflet membrane breakdown and opening of a fusion pore (***Figure 9B***). Subsequently, the fusion pore expands, resulting in content mixing and membrane relaxation (Chen and Scheller, 2001; Jahn and Scheller, 2006).

B. Endosome and phagosome maturation

The early endosome network

Endocytosis and endosome maturation have been extensively studied, mostly by using mammalian tissue culture cells. Endosomes play a major role in controlling the reutilization or degradation of membrane components, thus regulating basic cellular processes, such as nutrient uptake, immunity, signaling, adhesion, and membrane turnover. Extracellular material that is endocytosed by several pathways (as described on chapter 2B) is delivered to a common organelle, the early endosome. From there, many cell membrane receptors and other proteins are recycled back to the plasma membrane (via recycling endosomes), whereas other molecules are directed towards the TGN or the lysosomes for degradation (***Figure 10***). In this way, the early endosomes functions as a key sorting station in the cell, ensuring that components that need to be reutilized are separated from the ones that need to be degraded (Huotari and Helenius, 2011; Scott et al., 2014).

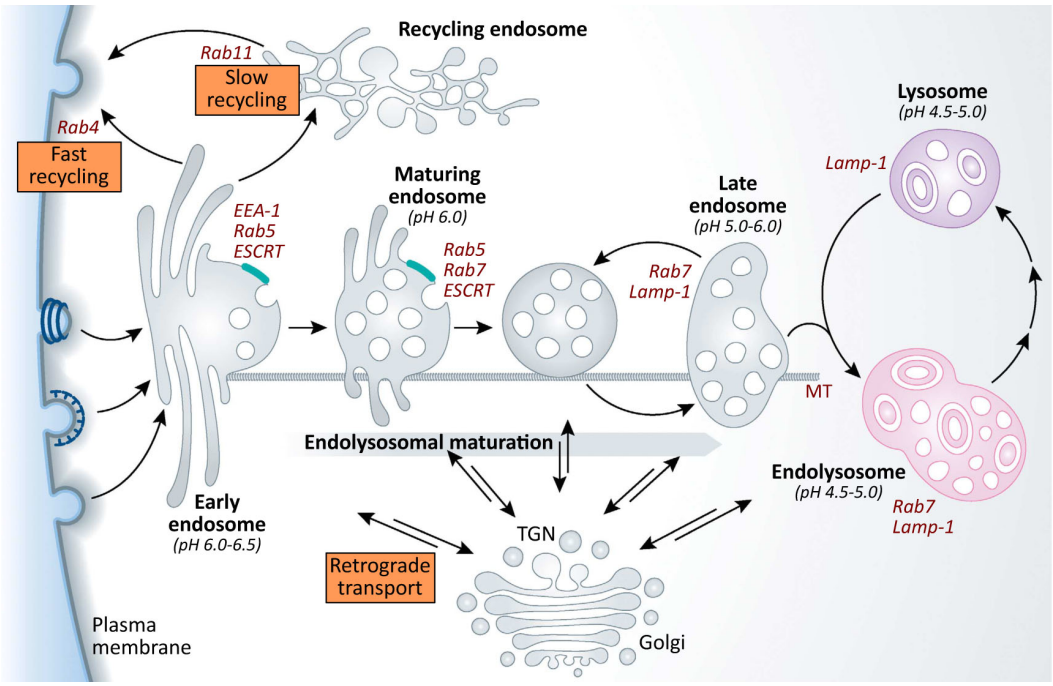

Figure 10 – The endosomal/lysosomal network. The early endosomes accumulate cargo and support recycling back to the plasma membrane, through fast and slow pathways, or retrograde transport to the TGN. The early endosome can also mature, by successive steps that result in the conversion into maturing endosomes and late endosomes. At the same time, the endosomes move to the perinuclear space along microtubules (MT). Endosomes undergo homotypic fusion reactions and grow in size, with the formation of intraluminal vesicles. Late endosomes fuse with lysosomes, generating a transient acidic hybrid organelle, the endolysosome, in which active degradative reactions take place. The endolysosome is then converted into a dense lysosome. Adapted from Huotari and Helenius, 2011.

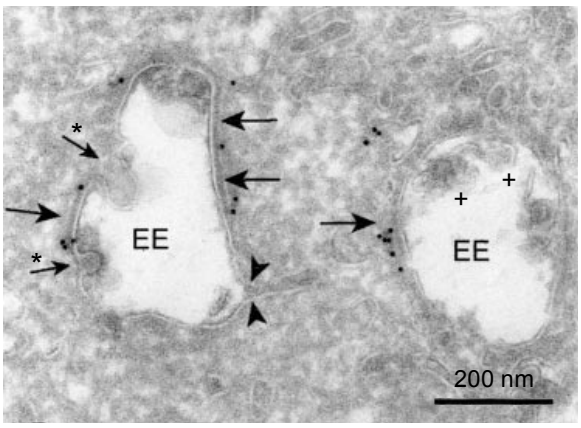

Figure 11 – The early endosome ultrastructure. Early endosomes (EE) display inward budding invaginations (arrows with an asterisk) and recycling membrane tubules (arrowheads). Additionally, the early endosome on the right side of the figure contains intraluminal vesicles (ILVs, shown with the + signal). Data from chinese hamster ovary cells is depicted (Sachse et al. 2002).

The early endosome is the first endocytic membrane-bound vesicle to accept incoming cargo. This organelle is a highly dynamic structure, composed of regions of thin tubular extensions (~60 nm) and large vesicles (~ 400 nm) that have membrane invaginations and present a multi-vesicular appearance (***Figure 11***) (Gruenberg, 2001; Sachse et al., 2002). It is thought that the morphologically distinct early endosome sub-domains are important for different functions: the tubular membranes might be involved in recycling pathways, whereas the multi-vesicular sub-domain may be involved in sorting of cargo to the degradative pathways (Jovic et al., 2010). Typically, within minutes (~10 minutes) after endocytosis and early endosome formation, there is the separation of the different cargo molecules. The majority of plasma membrane proteins and lipids are actively and accurately recycled back to the cell surface for additional rounds of internalization (***Figure 10***). Many receptors are uncoupled from their ligands at the early endosome mildly acidic pH (pH ~ 6.2) and then returned to the plasma membrane either through a direct and rapid recycling pathway (fast recycling route) or via the recycling endosomes (slow recycling route) (Goldstein et al., 1985; Huotari and Helenius, 2011; Scott et al., 2014). The fast recycling route ($t_{1/2}$ = 2-5 minutes) is regulated by the small GTPases Rab4 and Rab35. The slow recycling route ($t_{1/2}$ = 15-30 minutes) involves the transport of cargo proteins in vesicles, along MTs, to the perinuclear endocytic recycling compartment (ERC), which is localized near the microtubule-organizing center (MTOC) and Golgi complex in many of the tissue culture cells. Subsequently, recycling endosomes detach from the ERC and are transported to the plasma membrane. This pathway is coordinated by Rab11, which associates with recycling endosomes and the ERC (Grant and Donaldson, 2009; Jovic et al., 2010).

In addition to its role as a divergent point between the recycling and degradative pathways, the early endosome is also the intersection point between

the endocytic and biosynthetic routes. Some lipids and proteins, such as the cation-independent mannose-6-phosphate receptor (CI-M6PR), are trafficked to the TGN (***Figure 10***), a process called retrograde transport (Bonifacino and Rojas, 2006; Scott et al., 2014). This trafficking pathway is mediated by the retromer complex, which consists of a core of at least three cargo selection proteins (Vps26, Vps29 and Vps35) and members of the sorting nexin (SNX) family (SNX1, SNX2, and possibly SNX5 and SNX6) (Seaman, 2012).

Formation and maturation of late endosomes

The early endosome is also the starting point in the degradative endolysosomal pathway. Since the majority of the endocytosed cargo is actively recycled back to the plasma membrane, the transport to lysosomes can be considered as a side pathway that is limited to a relatively small fraction of the internalized components. Furthermore, cargo that is directed to the degradative pathway needs to undergo stringent selective selection (***Figure 10***). Different proteins associate with the early endosome membrane thus orchestrating its maturation and function. Rab5 is a key component of the early endosome and, together with its effector hVPS34, a PI(3)K, regulates generation of phosphatidylinositol-3-phosphate (PtdIns(3)P), which is the most abundant phosphoinositide on this organelle membrane. Generation of PtdIns(3)P recruits other Rab5 effectors that bind to this phosphoinositide via a FYVE domain, such as early endosomal antigen-1 (EEA-1) or hepatocyte growth factor-regulated tyrosine kinase substrate (Hrs), which in turn mediate homotypic fusion of early endosomes (Huotari and Helenius, 2011; Jovic et al., 2010). Additionally, several SNAREs associate with the early endosome, mediating events of membrane fusion during its maturation. Rab5 is also a crucial protein in endosome maturation, as it is the main regulator of the conversion to late endosomes at later stages.

As described before, early endosomes have a complex structure with tubular and vacuolar domains (***Figure 11***), and the latter are important for gradual maturation into late endosomes. The presence of the Hrs protein on the early endosome allows recruitment of the endosomal sorting complex required for transport (ESCRT) -I, through interaction with its Tsg101 subunit. Subsequently, ESCRT-II and ESCRT-III complexes are recruited to the early endosome, leading

to membrane invagination and formation of intraluminal vesicles (ILVs). Furthermore, homotypic fusion leads to the accumulation of additional ILVs and formation of multivesicular bodies (MVBs), which are enriched in PtdIns(3)P and PtdIns(3,5)P_2 (Jovic et al., 2010; Scott et al., 2014; Wollert and Hurley, 2010). Once formed, MVBs quickly acidify to a pH ~ 5.5, and move along MT towards the cell center for further maturation into late endosomes (***Figure 10***). The switch from early-to-late endosomes involves the conversion from Rab5 to Rab7, and this change in membrane identity ensures that different functions in the endosomal pathway remain spatially, temporally and functionally separated (Huotari and Helenius, 2011).

Initial Rab5 activation, promoted by the GEF Rabex-5 and Rabaptin-5, establishes a feedback loop in which Rab5-GTP promotes further Rab5 binding, thus defining the identity of the early endosome (Horiuchi et al., 1997; Lippé et al., 2001). At later stages of endosome maturation, Rab5 recruits and activates Rab7, which in turn inactivates Rab5 and promotes its dissociation through a negative feedback loop (Del Conte-Zerial et al., 2008). In this way, there is the formation of the late endosome, an hybrid compartment that is typically round or oval and has a diameter of 250-1000 nm. Rab7-GTP then recruits several downstream effectors, including RILP (a protein that connects late endosomes to dynein motors), components of the homotypic fusion and protein sorting (HOPS) complex (function as a tether of late endosome fusion), and machinery for heterotypic vesicle fusion (Zhang et al., 2009). This leads to the formation of an organelle containing multiple ILVs. One of the crucial roles of the Rab5/Rab7 conversion is to exchange the fusion machinery on the endosomal membrane, guarantying that late endosomes can only fuse with other late endosomes, lysosomes, and possibly autophagosomes (Huotari and Helenius, 2011). Importantly, late endosomes also interact with vesicles deriving from the TGN, thereby acquiring protein markers such as the lysosomal associated membrane protein-1 (Lamp-1), M6PR and lysosomal hydrolase precursors (Scott et al., 2014).

Endosomal motility is crucial for its maturation. Is has been suggested that the distance to the nucleus is a key parameter that influences intracellular position, number, size, and cargo contents of endosomes during endosomal maturation (Collinet et al., 2010). Movement of endosomes depends on both dynein and kinesin motors, which provide opposing forces that move endosomes in opposite

directions. Additionally, these motor proteins play a role in fusion of endosomes with each other during different steps of maturation (Driskell et al., 2007; Soppina et al., 2009). Whereas kinesins are implicated in the movement of early endosomes and late endosomes, dynein-dependent transport seems to be the major factor involved in the motility of late endosomes. This compartment binds dynein either directly or through the adaptor protein dynactin, which is dependent on Rab7-mediated recruitment of RILP (Huotari and Helenius, 2011). Moreover, members of the annexin family of proteins, such as annexins A2 and A8, link the actin cytoskeleton the endosome membranes, which might regulate early endosome fission and contribute to late endosome biogenesis (Goebeler et al., 2008; Morel et al., 2009).

Endosome fusion with lysosomes

Late endosomes that are formed continue to undergo maturation mechanisms and eventually fuse with lysosomes. Lysosomes are acidic membrane-bound organelles (luminal pH can drop to 4.5) containing proton-pumping vacuolar ATPases (vATPases) and acid hydrolases (Mellman et al., 1986). They were discovered 60 years ago by Christian de Duve, as a result of studies using subcellular fractionation (DE DUVE et al., 1955), and were then visualized by electron microscopy (NOVIKOFF et al., 1956), which showed that lysosomes appear heterogeneous in size and morphology (***Figure 12***). More recently, time-lapse confocal microscopy studies have contributed to the understanding of how lysosomes dynamically interact with endosomes.

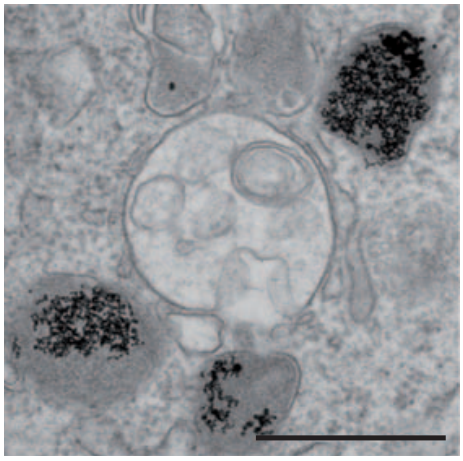

Figure 12 – Electron microscopy of late endosomes and lysosomes. Dense-core lysosomes (dark grey) are structurally different from a less-dense late endosome seen in the center of the image. Scale bar is 500 nm (Luzio et al. 2007).

Electron microscopy data, together with cell-free content-mixing assays, provided evidence that late endosomes and MVBs fuse directly with lysosomes (reviewed in (Luzio et al., 2007)). The majority of these fusions events happen in the perinuclear region, since late endosomes and lysosomes are concentrated near the MTOC. The usage of correlative live-cell and electron microscopy has allowed the understanding of the successive steps during endosome-lysosome

fusion (Bright et al., 2005). There is initial physical contact between the organelles, that then transiently fuse (kissing events) or undergo permanent fusion. Additionally, live-cell imaging studies have helped to establish the protein machinery involved in the fusion of late endosomes with lysosomes, which requires small GTPases, SNAREs, among others (Luzio et al., 2007).

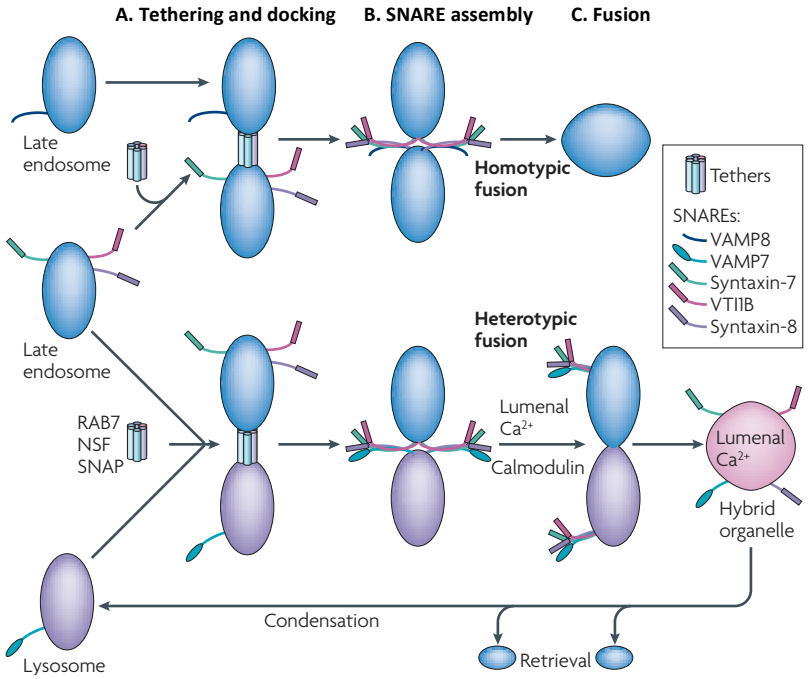

Figure 13 – Schematic representation of homotypic late endosome fusion and heterotypic late endosome-lysosome fusion. A. Different cytosolic proteins, such as Rab7, NSF (*N*-ethylmaleimide sensitive factor) and SNAPs (soluble NSF attachments proteins), tether endosomes with lysosomes or endosomes with endosomes. **B.** Two different *trans*-SNARE complexes induce either homotypic late endosome fusion (VAMP8-dependent) or heterotypic late endosome-lysosome fusion (VAMP7-dependent). **C.** Vesicle fusion is dependent on the release of lumenal Ca^{2+} (only shown for heterotypic fusion). Reformation of dense-core lysosomes from the endolysosome hybrid organelle requires the loss and retrieval of proteins. Adapted from Luzio et al., 2007.

Heterotypic late endosome-lysosome fusion starts with organelle tethering involving the formation of links between the two structures (***Figure 13A***). For this process, the HOPS complex is thought to be an important player, possibly in conjunction with Rab7 (Luzio et al., 2010). Subsequently, fusion depends on a core protein machinery that includes cytosolic factors and the formation of a SNAREpin composed of an R-SNARE and three Q-SNAREs (one each of Qa-, Qb- and Qc- SNAREs) (Luzio et al., 2007; Weber et al., 1998). For heterotypic late endosome-lysosome fusion, the Q-SNAREs are syntaxin-7, Vti1b and syntaxin-8

(Qa-, Qb- and Qc- SNAREs, respectively), whereas the R-SNARE is VAMP7. Interestingly, the Q-SNAREs required for homotypic late endosome fusion are the same, however the R-SNARE is VAMP8 instead of VAMP7 (***Figure 13B***) (Luzio et al., 2009; Pryor et al., 2004).

VAMP7 is a protein of particular interest since it is known to be present in numerous combinatorial SNARE complexes (***Table 2***), many of which involve lysosomes. Its presence on the lysosome membrane might help the definition of the lysosome and regulate its fusion with late endosomes. Furthermore, VAMP7 is involved in lysosome fusion with the plasma membrane, where it forms a *trans*-SNARE complex with syntaxin-4 and SNAP23 (Luzio et al., 2009; Rao et al., 2004).

Table 2 – VAMP7 can associate with several Q-SNAREs and form different combinatorial *trans*-SNARE complexes. Adapted from Luzio et al., 2007.

Qa-SNARE	Qb-SNARE	Qc-SNARE	Qb/c-SNARE	Function
Syntaxin-7	Vti1B	Syntaxin-8		Late endosome-lysosome fusion
Syntaxin-7	Vti1	Syntaxin-8		Macropinosome fusion
Syntaxin-4			SNAP23	Lysosome-plasma membrane fusion
Syntaxin-3			SNAP23	Vesicle-apical plasma membrane fusion
Syntaxin-1			SNAP25	Vesicle-neurite plasma membrane fusion

The final stages of late endosome-lysosome fusion are also dependent on calmodulin and Ca^{2+} (***Figure 13C***), which is released from the lumen of the organelles and allows phospholipid bilayer fusion (Pryor et al., 2000). After complete heterotypic fusion, the formation of a transient hybrid organelle called endolysosome takes place, which can be referred to as a "cell stomach" where degradation occurs. Here, hydrolase precursors are proteolytically cleaved into active forms, thus contributing to the degradative environment of the endolysosome. Finally, endolysosomes undergo content condensation and membrane-retrieval processes to remove endosomal membrane proteins and recycle SNAREs. In this way there is reformation of classical lysosomes (***Figure 10***), which are Lamp-1-positive but M6PR-negative spherical dense storage organelles (Luzio et al., 2010).

An important feature of endosomal maturation is the progressive acidification of the endosome luminal pH, which is regulated by vATPases. This protein associates with the membrane of endosomes and lysosomes, mediating the acidification of early endosomes (pH around 6.5-6.0), late endosomes (pH around 6.0-5.0) and lysosomes (where pH can drop to values around 4.5). The low pH provides not only an optimal environment for hydrolytic reactions, but is also essential for membrane trafficking and for the sorting and routing of cargo molecules (Maxfield and Yamashiro, 1987).

Phagosome maturation

Phagosome maturation is analogous to the mechanisms of endosome maturation and endolysosome formation, and is also divided into early, late and lysosome-interacting stages. Early phagosomes share many similarities with early endosomes. For example they are Rab5-positive and this small GTPase is also required for the transition to the late phagosome stage. Likewise, Rab5-to-Rab7 conversion regulates phagosome maturation and is important for the acquisition of lysosomal enzymes through the fusion with lysosomes. This is accompanied by the centripetal movement of phagosomes, which is essentially regulated by the same players that control movement of endosomes in the cell (Fairn and Grinstein, 2012). About 20 other Rab GTPases have been detected on phagosomes, such as Rab2, Rab10, Rab22a, Rab20 or Rab39 (Cardoso et al., 2010; Roberts et al., 2006; Seto et al., 2011; Trost et al., 2009), however little is known about how they coordinate phagosome maturation.

Phagosomes also interact with lysosomes to form a hybrid organelle called phagolysosome, which degrades phagocytosed particles. It has been reported that some events of phagosome-lysosome fusion occur by thin tubular extensions and there is also the requirement of Ca^{2+} (Stockinger et al., 2006), which is similar to the mechanisms of late endosome-lysosome fusion. VAMP7 is also recruited to the phagolysosome and, together with syntaxin-7, might be important for phagosome-lysosome fusion (Braun et al., 2004; Collins et al., 2002).

C. The ER as a hub for inter-organelle communication

In addition to the role of small vesicles in the trafficking of cargo between different intracellular compartments, an additional important player is the ER. The ER is the largest membrane-bound organelle in the eukaryotic cell. It has a complex architecture, spreading throughout the cytoplasm as one continuous membrane-enclosed network that surrounds a single lumen. The ER is divided into three major domains/morphologies, which include the outer nuclear membrane, the peripheral ER cisternae that extend all the way to the plasma membrane, and an interconnected tubular network (also called tubular ER). Since the ER lumen is continuous, it means that the different domains are established through the segregation and assembly of some membrane proteins into different parts of the ER (English and Voeltz, 2013; Friedman and Voeltz, 2011).

The ER serves as the entry site into the secretory pathway, allowing folding and maturation of the vast majority of secreted and membrane-bound proteins. Additionally, it is involved in cellular lipid biosynthesis. The ER is also extremely important in regulating Ca^{2+} homeostasis, and actively maintains gradients for various small molecules across its membrane. Even though this organelle always maintains its membrane continuity, it is also highly dynamic, constantly changing its structure. For this purpose, binding to and movement along MTs is of crucial importance. In this way, the ER contacts with almost every other organelle in the cell (including mitochondria, endosomes, lysosomes, Golgi, peroxisomes and the plasma membrane), thus acting as a main hub for inter-organelle communication (Borgese et al., 2006; English and Voeltz, 2013; Friedman and Voeltz, 2011; Stefan et al., 2013). The coordination of different cellular functions with other organelles can be achieved via the establishment of membrane contact sites (MCSs), which are regions where the membranes of two organelles are closely apposed, typically 10-30 nm apart (Toulmay and Prinz, 2011).

The shape of the ER is constantly changing. Moreover, the different ER domains have different shapes, which is mainly due to varied membrane curvature of these domains. Whereas the membranes of the nuclear envelope and of the peripheral ER cisternae are relatively flat and have low curvature, the tubular ER has high membrane curvature in cross-section along the length of the tube

(English and Voeltz, 2013; Zurek et al., 2011). This is mainly due to the presence of proteins that generate and maintain membrane curvature, such as the reticulon family of integral membrane proteins. Reticulons are ER proteins that contain two long transmembrane domains, which form wedge-shaped insertions into the membrane. In this way, these domains expand the area of the outer leaflet compared with the inner leaflet of the bilayer and thus generate high membrane curvature in the ER tubules (Stachowiak et al., 2013; Zurek et al., 2011).

In the following sections, it will only be addressed how the ER contacts and communicates with the plasma membrane, with endosomes and with the Golgi.

ER communication with the plasma membrane

Many of the proteins and lipids synthesized in the ER have to be transported to the plasma membrane. In a similar way, remodeling of the plasma membrane, together with changes in its molecular composition, induce biosynthesis changes in the ER. However, there is no evidence that secretory vesicles derived from the ER fuse with the plasma membrane, neither that endocytic vesicles from the plasma membrane fuse with the ER. Therefore, transfer of information between the two structures is likely to occur independently of vesicle trafficking (Stefan et al., 2013). It is now thought that large regions of the plasma membrane have an underlying network of cortical ER (cER), which can be closely apposed to the plasma membrane (***Figure 14***) and form MCSs that are observed in different cell types (Toulmay and Prinz, 2011). Nevertheless, how ER-plasma membrane MCSs are established at a molecular level, is still poorly understood.

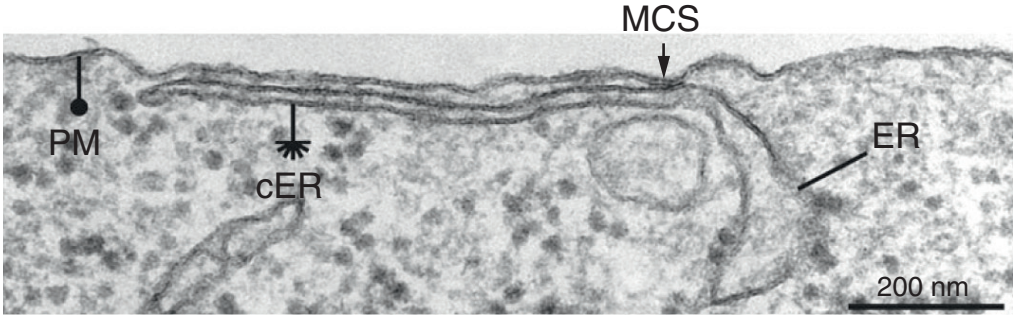

Figure 14 – Electron microscopy image of a membrane contact site (MCS) formed between the ER and the plasma membrane, in HeLa cells. The cortical ER (cER) is depleted of ribosomes, as compared to internal ER membranes, and is in close proximity to the plasma membrane (PM). An example of a tight MCS enriched in electron-dense material is shown (arrow) (Orci et al., 2009).

ER-plasma membrane contacts are important for different functions. They have been identified as sites of phosphatidylinositol metabolism, namely by regulating PtdIns(4)P levels, which is controlled by VAMP-associated proteins (VAPs, such as VAP-A or VAP-B) (Stefan et al., 2013). These sites are also implicated in the control of Ca^{2+} levels and non-vesicular sterol transfer (English and Voeltz, 2013).

ER communication with the endocytic system

The ER has also been shown to interact with endosomes, late endosomes and lysosomes, via the formation of MCSs. Immuno-electron microscopy data showed that the ER-localized phosphatase PTP1B interacts with the EFG receptor on the surface of endosomes, and localizes to ER-endosome MCSs (Eden et al., 2010). This suggests that ER proteins might modify endocytosed cargoes. Additionally, it has been suggested that early endosome movements might be coordinated with ER dynamics, and these two compartments might be temporally and physically tightly linked (Friedman and Voeltz, 2011; Friedman et al., 2010). Additionally, the ER directly interacts with late endosomes and lysosomes, most likely forming MCSs. It has been proposed that these interactions monitor and regulate cholesterol levels in endocytic organelles, which affects trafficking of endocytic vesicles in a VAP-A-dependent manner (Rocha et al., 2009).

ER communication with the Golgi (COPI and COPII trafficking)

Electron microscopy studies showed that the ER also establishes membrane contacts with the Golgi, which might regulate the transfer of proteins and non-vesicular lipid transport (Glick and Nakano, 2009; Mogelsvang et al., 2004). However, the proteins regulating the tethering between the ER and Golgi membranes at contact sites remain unknown (English and Voeltz, 2013). Additionally, there is bidirectional vesicular trafficking between the ER and the Golgi, which constitutes a vital gateway to the endomembrane system. ER-to-Golgi membrane trafficking (anterograde transport) and Golgi-to-ER (retrograde transport) membrane trafficking are mechanistically similar. In both cases, a carrier vesicle is formed on the donor organelle and then in transported and fuses with the target organelle (Brandizzi and Barlowe, 2013; Szul and Sztul, 2011). Nevertheless, different protein machineries regulate the trafficking fidelity and

directionality: coat protein complex II (COPII) regulates anterograde transport from the ER; and COPI regulates the retrograde transport from the Golgi (***Figure 15***).

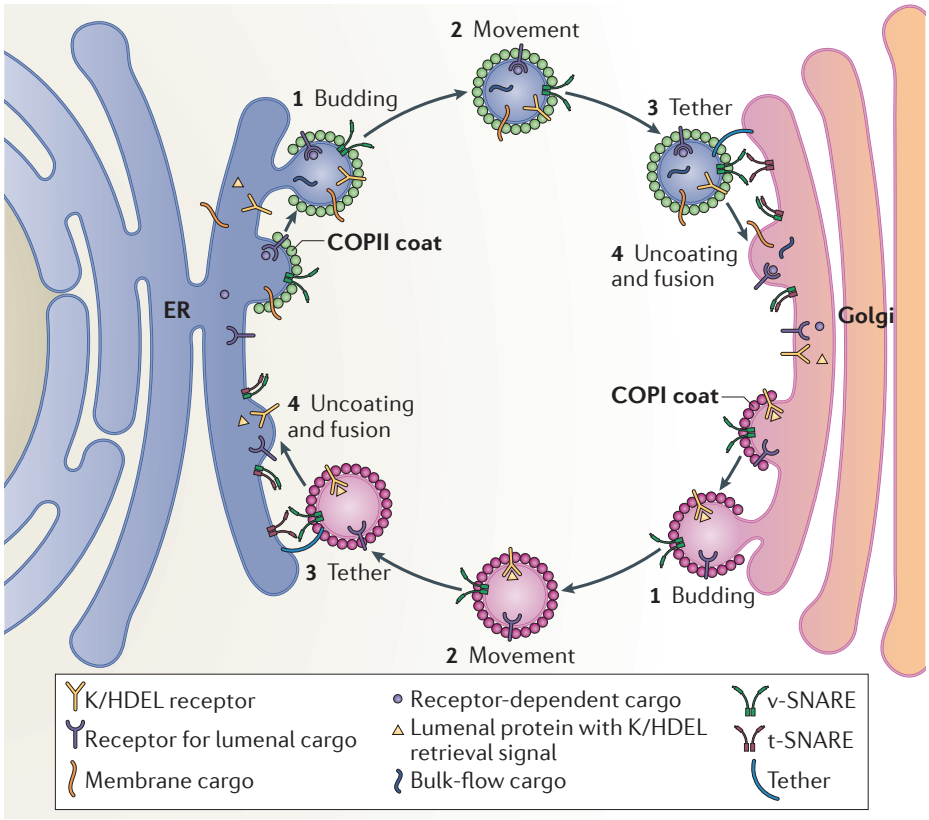

Figure 15 – Bidirectional membrane trafficking between the ER and the Golgi is mediated by COPI and COPII-coated vesicles. Transport of cargo between the ER and the Golgi requires budding (1), movement (2), tethering (3), and uncoating and fusion (4) of COPI and COPII-coated vesicles with their respective compartments. COPII-vesicles mediate cargo trafficking from the ER to the Golgi, whereas COPI-vesicles are involved in cargo trafficking from the Golgi to the ER. COPI facilitates the retrieval of luminal proteins containing K/HDEL signals that are recognized by the K/HDEL receptor. Vesicle fusion is regulated by v-SNAREs and t-SNAREs (Brandizzi and Barlowe, 2013).

To exit the ER, cargos are packaged into COPII-coated vesicles at specialized regions on the surface of the ER membrane, called ER exit sites (ERES) or transitional ER. ERES are morphologically recognizable by the absence of ribosomes and the presence of many 200-500 nm long membrane protrusions. Eukaryotic cells have a variable number or ERES that are scattered along the ER with some concentration in an area adjacent to the Golgi (Fan et al., 2003; Szul and Sztul, 2011). ERES are enriched in COPII and appear as discrete punctae during fluorescence imaging of COPII coat proteins. Additionally, these sites are likely to generate numerous COPII-coated vesicles that then transport cargo to the

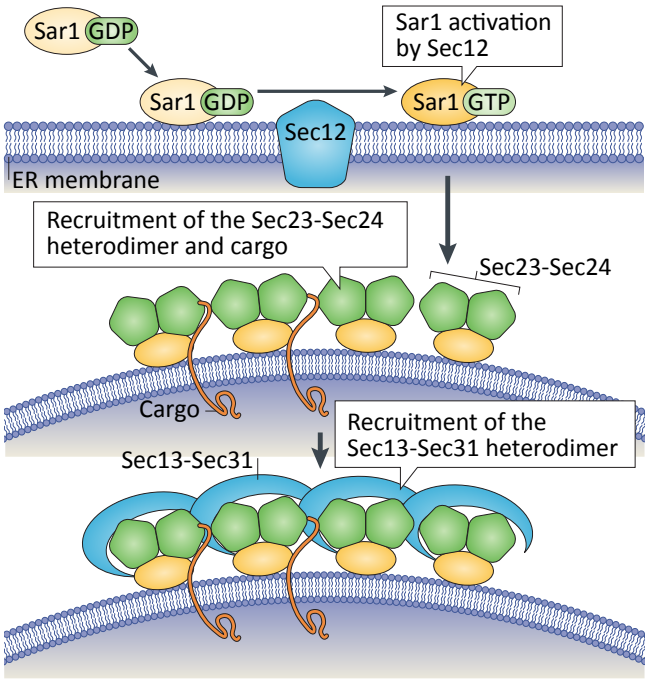

Figure 16 – Molecular details of the COPII coat complex assembly. Adapted from Brandizzi et al. 2013.

next compartment in the secretory pathway, the ER-Golgi intermediate compartment (ERGIC) (Jensen and Schekman, 2011; Szul and Sztul, 2011). COPII-coated vesicles formation follows a defined sequence of molecular events. In specific regions of the ER membrane there is tethering and activation of the small GTPase Sar1, which is catalyzed by the Sec12 GEF. Since Sec12 is an ER-localized membrane protein, it restricts Sar1 activity to the ER. Active Sar1 then recruits Sec23 and Sec24, initiating membrane curvature. Subsequently, these proteins act as a platform for the recruitment of Sec13 and Sec31 to the COPII coat, which is essential to generate membrane curvature and a spherical structure (***Figure 16***). The process of vesicle fission is then completed by the inactivation and release of Sar1, leading to the formation of an intact vesicle that buds out of the ER (Jensen and Schekman, 2011; Lord et al., 2013). In this way, Sar1 activity regulates the first step of COPII-coat assembly (when bound to GTP) and the last step of vesicle budding and release from the ER (when bound to GDP).

It is thought that COPII-coated vesicles that bud from the ER are then generally released to the cytosol and associate with the MTs plus end (***Figure 17***). Upon fission of vesicles from the ER, Sec13 and Sec31 are released from the coated vesicles, whereas the Sec23-Sec24 dimer is partially retained. Since the ERES are oriented towards the juxtaposed ERGIC, vesicles then reach this target compartment, in a MT-dependent manner, and are tethered possible though the interaction between Sec23 and TRAPPI (transport protein particle I) tethering complex. Subsequent vesicle fusion with the target membrane is regulated by SNAREs, such as Sec22 and syntaxin-5 (Brandizzi and Barlowe, 2013; Lord et al., 2013). Even though it has been widely accepted that COPII-coated vesicles are released from ERES to the cytosol and then travel to the target compartment,

recent data in yeast show that regions of the Golgi can approach and contact the ERES. This, together with the collapse of COPII coats, enables cargo capture into the Golgi, thus ensuring efficient and targeted cargo transport from the ERES to the Golgi (Kurokawa et al., 2014).

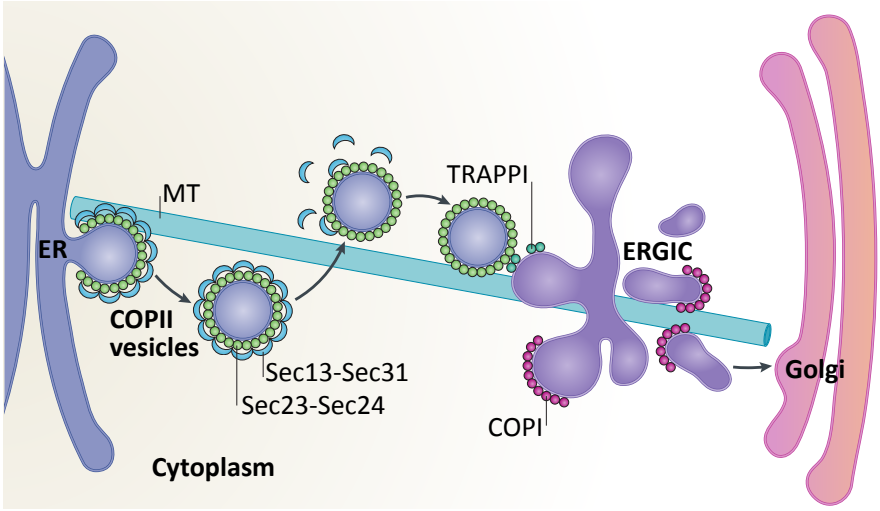

Figure 17 – The ER-Golgi interface in eukaryotic cells. COPII-coated vesicles that bud from the ERES are released into the cytoplasm and travel along MTs to the ERGIC. In parallel, there is depolymerization of the Sec13-Sec31 cage. Vesicles eventually tether with the ERGIC, in a Sec23 and TRAPPI-dependent manner. COPI mediates cargo transport from the ERGIC to toward the Golgi, as well as recycling back to the ER membrane (not shown in this scheme). Adapted from Brandizzi and Barlowe, 2013.

The ERGIC can also form COPI-coated vesicles that are generated from anterograde carriers as they move towards the Golgi. Though, the most biological relevant role of COPI-coated vesicles is to regulate retrograde transport from the Golgi to back the ER (Szul and Sztul, 2011). The COPI complex consists of a heptameric (α, β, β', γ, δ, ε, ζ) complex, also called coatomer. Two main subcomplexes then form the coatomer: the γ-COP-δ-COP-ζ-COP-β-COP tetrameric complex, which constitutes the inner layer core; and the α-COP-β'-COP-ε-COP trimeric complex, which forms the outer layer of the COPI coat. COPI is recruited to membranes by activated Arf1 GTPases. Once activated by ARFGEFs, Arf1 recruits preassembled COPI coats to the Golgi membrane, which then facilitates transport out of the Golgi and ERGIC (Brandizzi and Barlowe, 2013; Jackson, 2014; Szul and Sztul, 2011). Interestingly, several studies also show that inhibition of the retrograde transport route leads to the collapse of anterograde trafficking (Lippincott-Schwartz et al., 1989; Niu et al., 2005; Richter

et al., 2007; Sciaky et al., 1997). Thus, it is likely that the integrity of the anterograde pathway depends on the homeostasis of the retrograde pathway, which guarantees not only the retrieval of resident proteins that escape the ER but also facilitates the recycling of lipids back to the ER.

Chapter 4

Invasive Bacteria – Master Hijackers of Cellular Processes

Pathogenic bacteria can cause diseases that are devastating for humans and other animals. During their long lasting coexistence and coevolution with their hosts, many of these bacteria have developed diverse strategies to survive in the host, either replicating outside the cells of the infected organism or within the host-cell cytoplasm. In this way, these so called intracellular bacterial pathogens avoid the harsh extracellular environment and many immune defense mechanisms, such as circulating antibodies or complement-induced destruction. Furthermore, professional phagocytic cells, such as macrophages, engulf pathogenic bacteria (such as *Mycobacterium tuberculosis* and *Legionella pneumophila*). The pathogens have evolved ways to impair phagosome maturation and fusion with lysosomes, thus avoiding their degradation. Other bacteria use an arsenal of virulence factors (or effectors) that subvert the host cell cytoskeleton and endocytic machineries. In this way, these so called invasive bacteria (such as *Salmonella enterica, Shigella flexneri* or *Listeria monocytogenes*) trigger their own uptake into non-phagocytic cells, such as epithelial cells, and are internalized into an endocytic membrane-bound vacuole (***Figure 18***). These bacteria also modify their internalization vacuole, either to survive within it (intravacuolar lifestyle) or to promote its rupture and escape to the cytosol (cytosolic lifestyle) (Cossart and Helenius, 2014; Fredlund and Enninga, 2014; Ham et al., 2011; Kumar and Valdivia, 2009). In both cases, this requires a fine tuned manipulation of the host cell vesicular trafficking by the bacteria, which will be addressed in detail in this chapter.

Over the last decades, the combination of microbiology and cell biology into a new discipline, cellular microbiology (Cossart et al., 1996), has offered important insights into bacterial pathogenesis, transmission and dissemination. Moreover, the study of how bacteria hijack their host cells has also been crucial for the understanding of fundamental aspects of cell biology.

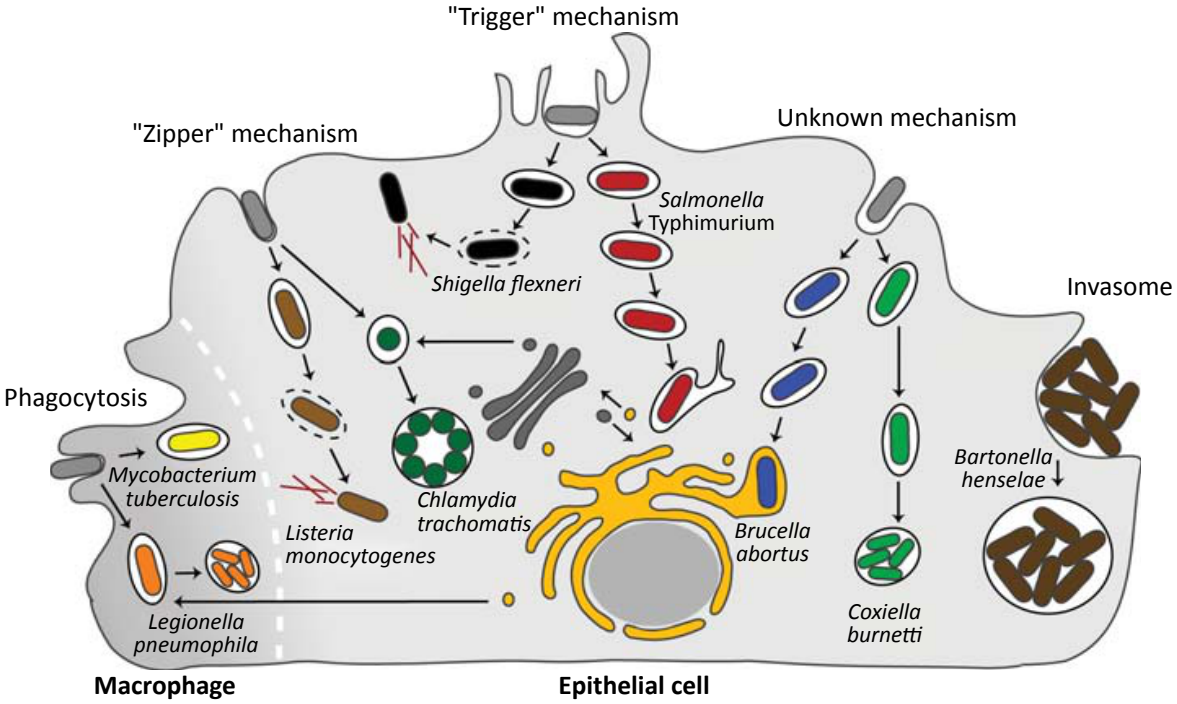

Figure 18 – Cellular invasion routes of intracellular bacterial pathogens and their intracellular fate. Some intracellular bacteria are phagocytosed by macrophages and then reside inside a modified phagosome. Whereas some bacteria can invade epithelial cells through an endocytosis-like "zipper" mechanism, other trigger massive membrane ruffling of the host cell surface, which is also accompanied by macropinocytosis ("trigger" mechanism). In the case of *Bartonella henselae*, specialized invasion structures called invasomes can be formed. Once inside the host cell, different bacteria have different fates: whereas some reside and replicate within a membrane-bound vacuole, others lyse this compartment and then replicate in the cytosol. Adapted from Cossart and Helenius, 2014.

A. Exploiting host cell mechanisms for bacterial entry

During bacterial-induced internalization into host cells, the bacterium plays the major and active role during the interplay between the two organisms. The other important player during this process is the host cell plasma membrane and underlying cytoskeleton, whose plasticity is exploited by the pathogen. Some invasive bacteria, such as *Listeria monocytogenes*, express surface proteins that bind to eukaryotic surface receptors, causing receptor clustering. In this way, signaling events are triggered that culminate in bacterial entry into epithelial cells, through a "zippering" process that involves relatively small cytoskeletal rearrangements and plasma membrane extensions for bacterial engulfment into an endocytic vacuole (***Figure 19A***).

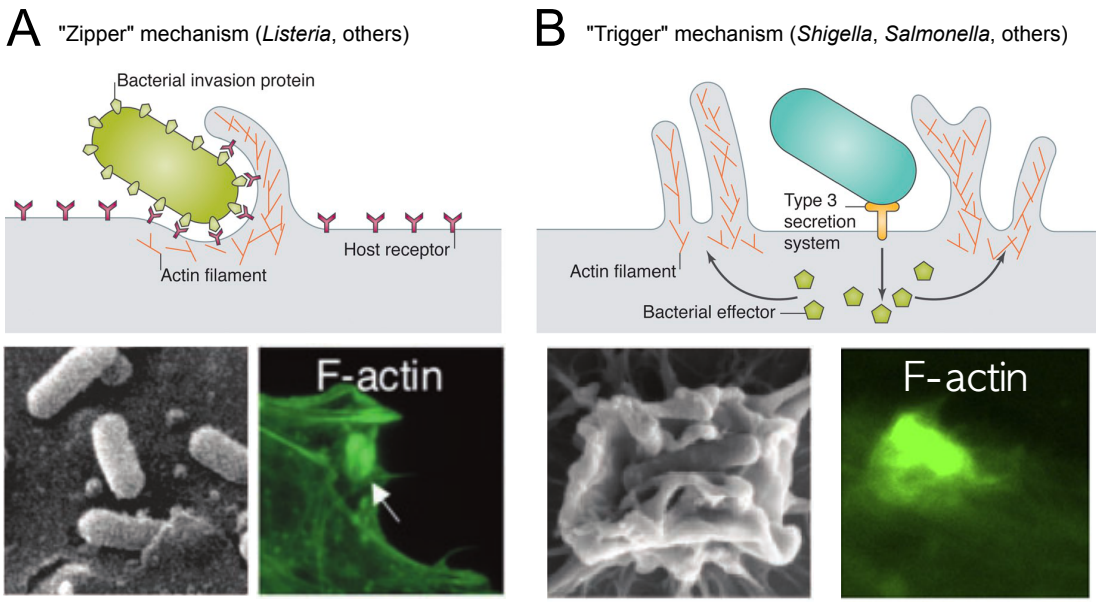

Figure 19 – Invasive bacteria hijack the actin cytoskeleton to promote invasion into epithelial cells. A. *Listeria* binds to the cell surface, via interactions between surface bacterial proteins and host cell receptors, and enter through a "zipper" mechanism, which involves minor actin rearrangements. **B.** Bacteria such as *Shigella* and *Salmonella* inject effector proteins into the host cell cytosol, via a type 3 secretion system (T3SS), leading to massive actin rearrangements and bacterial internalization via a "triggering" mechanism. On the lower panels, the perturbations on the host cell surface are shown, via scanning electron microscopy [left A and B (Cossart and Sansonetti, 2004)] or fluorescence microscopy [right A (Bierne et al., 2005) and B (Ehsani et al., 2012)]. Adapted from Haglund and Welch, 2011.

Other invasive bacteria, such as *Shigella flexneri* and *Salmonella enterica*, use dedicated needle-like secretion systems, called type III secretion systems (T3SSs). The T3SSs are essential virulence determinants of diverse Gram-negative bacteria and are used to inject virulence proteins into eukaryotic host target cells. T3SSs are complex syringe-like macromolecular machines (***Figure 20***) assembled in a hierarchical manner. They consist of the structural components of the export machinery itself (called injectisome), secreted proteins (including pore-forming translocators and effectors), chaperones and cytoplasmic regulators. The injectisome is made up of a basal body that spans both bacterial membranes, and an extracellular needle complex that protrudes from the bacterial surface. Both the basal body and the needle complex are hollow, containing a channel that acts as a tube for protein secretion. The needle complex terminates in a tip structure made of several copies of the tip protein. Upon *S. flexneri* or *S. enterica* contact with a host cell membrane, the T3SS exports two different categories of proteins: the translocators that form a pore in the target membrane, and the effectors that are translocated through the pore into the host cell (Deane et al.,

2010; Enninga and Rosenshine, 2009; Parsot, 2009). In this way there is the injection of a cocktail of bacterial effector molecules into the host cell cytosol. Here, the injected bacterial proteins can interact with and manipulate diverse host molecules. One of the first cellular consequences of T3SS effector injection is the manipulation of the host cell machinery that regulates the actin cytoskeleton dynamics, "triggering" massive cytoskeleton changes that cause the formation of macropinocytosis-like membrane ruffles and result in bacterial entry (***Figure 19B***) (Cossart and Helenius, 2014; Cossart and Sansonetti, 2004; Haglund and Welch, 2011; Rottner et al., 2005).

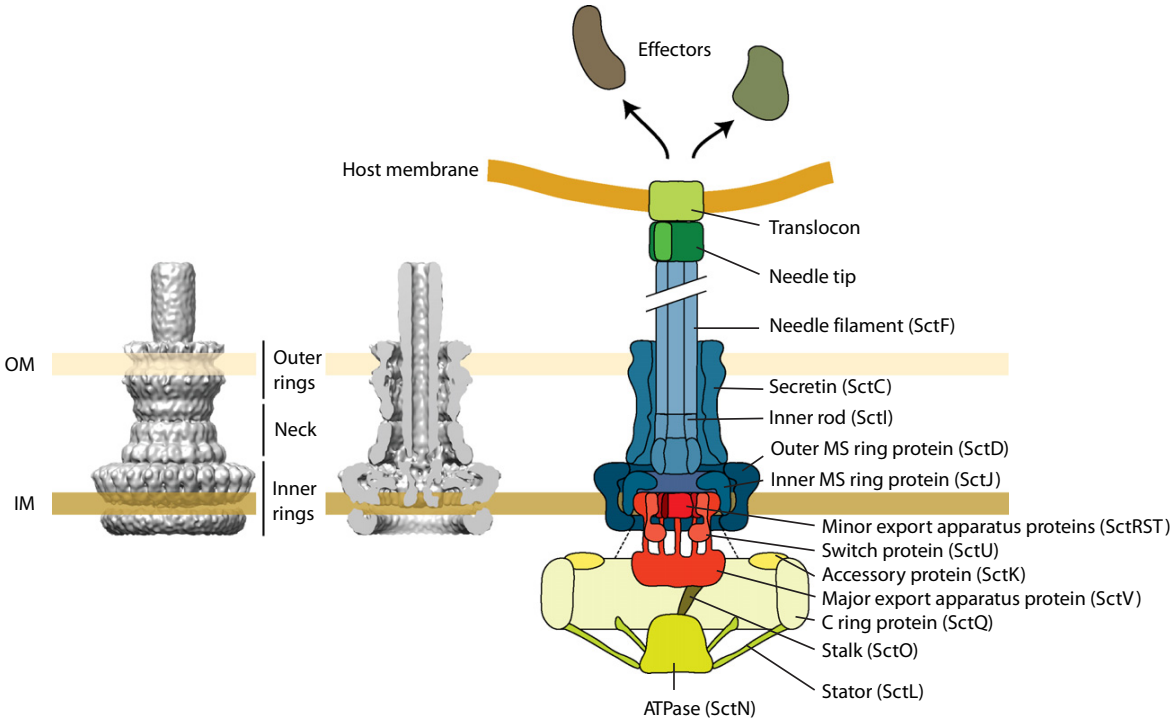

Figure 20 – Overview of the components of the type III secretion system. Left and middle panels depict, respectively, side and cut surface views representations of 3D reconstructions of needle complexes from *S. flexneri* and *S. enterica*, based on cryo-electron microscopic data. The right panel shows a schematic representation of the T3SS with all its components. Cytoplasmic components are shown in yellow, export apparatus components in red, base and needle components in blue, and needle tip and translocator proteins in green. The unified Sct names (secretion and cellular translocation) are shown. OM, bacterial outer membrane; IM, bacterial inner membrane; MS, membrane and supramembrane. Adapted from Diepold and Wagner, 2014.

Even though actin polymerization is of central importance in both processes, invasive bacteria also exploit the other components of the host cell cytoskeleton. Over the last decades this has helped the scientific community to understand the dynamics of the eukaryotic cytoskeleton regulation.

Listeria monocytogenes *entry by receptor signaling*

Listeria monocytogenes is a food-borne Gram-positive bacterial pathogen that preferentially infects immunocompromised hosts, eliciting a severe and often lethal disease, called listeriosis. In human hosts, clinical manifestations can range from gastroenteritis to severe systemic disease, such as meningitis, encephalitis, sepsis, and fetal infections that can result in abortion (Swaminathan and Gerner-Smidt, 2007). Classically, *L. monocytogenes* has been described to enter into epithelial cells through a "zipper" mechanism (Cossart and Sansonetti, 2004). This bacterium is able to bind to host cell surface receptors, through dedicated bacterial surface proteins called internalins. So far, the only two *L. monocytogenes* internalins that have been directly implicated in bacterial invasion are internalins A and B (InlA and InlB, respectively) (Pizarro-Cerdá et al., 2012). InlA interacts with E-cadherin, an adhesion molecule involved in the formation of adherens junctions in some epithelial barriers, and this promotes bacterial invasion in specific cellular subpopulations. InlB interacts with the hepatocyte growth factor receptor Met, promoting *L. monocytogenes* internalization into a broad range of cell types from epithelial origin. In this way, E-cadherin and Met are phosphorylated and ubiquitinated (via the ubiquitin ligases Hakai or Cbl, respectively), which leads to subsequent recruitment of the molecular machinery for clathrin-mediated endocytosis (Dab2, clathrin, dynamin, HIP1R, myosin-VI). In both cases, this coordinates local recruitment and activation of kinases and small GTPases that lead to Arp2/3 complex-dependent actin rearrangements and bacterial uptake (***Figure 21***). Given that myosin-VI has the ability to move towards the minus end of actin filaments, it is thought that it might pull the bacteria to the interior of the host cell. Ultimately, the actin remodeling is down-regulated by the recruitment of proteins such as cofilin or OCRL (reviewed in (Cossart and Helenius, 2014; Cossart and Roy, 2010; Pizarro-Cerdá et al., 2012)).

Interestingly, is was also shown that some members of the septin family (septin-2 and -9) are recruited to the entry site of *L. monocytogenes*, contributing to the anchorage of Met to the actin cytoskeleton and to bacterial entry in epithelial cells (Mostowy et al., 2009; 2011). Together, this highlights that *L. monocytogenes* entry into epithelial cells is a complex process that requires several host molecular machineries.

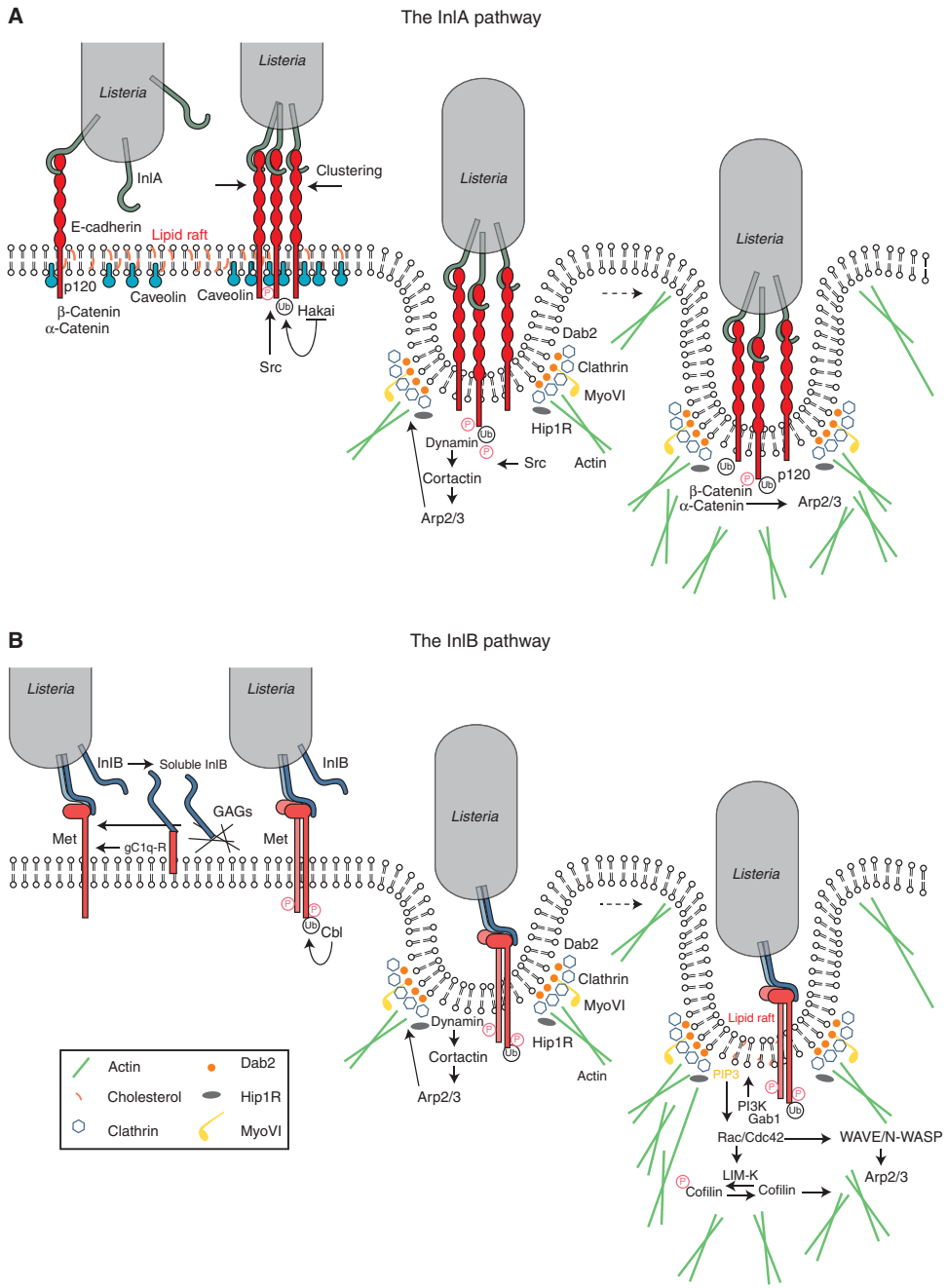

Figure 21 – InlA- and InlB-dependent *L. monocytogenes* invasion pathways. Binding of InlA to E-cadherin (A) or InlB to Met (B) lead to post-translational modifications of the receptors, recruitment of clathrin-mediated endocytosis machinery and initial actin reorganization. Subsequent receptor signaling results in further actin polymerization and bacterial internalization (Pizarro-Cerdá et al., 2012).

Shigella flexneri *entry by effector secretion*

Shigella spp. are Gram-negative, rod-shaped, facultative anaerobic, non-motile pathogenic bacteria that cause bacillary dysentery (shigellosis) in humans. Worldwide, shigellosis constitutes a significant public health burden, mostly in developing countries, where it is thought that about 160 million cases occur

annually, resulting in over 1 million deaths especially among children under the age of 5 years (Kotloff et al., 1999). This disease is transmitted by the fecal-oral route, usually by the ingestion of contaminated water or food, and is characterized by severe inflammatory destruction of the colonic epithelium. Currently, there is no vaccine available to prevent shigellosis, and the development of antibiotic resistance to multiple drugs is a growing problem (Phalipon and Sansonetti, 2007). The pathogenicity of these bacteria is mainly studied using the species *Shigella flexneri.*

S. flexneri pathogenicity is mainly related to a large virulence plasmid that encodes the mxi-spa pathogenicity island: this genetic element encodes proteins composing a T3SS and the effector proteins that are subsequently injected into the host cell (Parsot, 2009). Together, the T3SS and the translocated bacterial effectors are the main elements of bacterial invasion, survival and evasion of the host immune system. The *S. flexneri* T3SS is assembled during bacterial growth at 37ºC, however it is not active as the translocators and some effector are kept in the bacterial cytoplasm. However, within seconds upon bacterial contact with host cell membranes, the T3SS is activated and the translocators IpaB and IpaC are secreted through the needle complex to form a translocation pore (translocon) in the host plasma membrane, through which a cocktail of about 25-30 bacterial effectors can be injected into the host cytoplasm (Enninga et al., 2005; Parsot, 2009).

Only recently the cellular mechanisms eliciting the initial contact between *S. flexneri* and the host cell have been described. It was shown that the bacteria establish contacts and are captured by filopodial-like structures that emanate from the host cell, in a T3SS-dependent manner. These structures then retract, bringing the bacteria into contact with the host cell membrane, where invasion occurs (Romero et al., 2011). Then, *S. flexneri* adhesion to the host cell surface is facilitated by the interaction between the bacterial IpaB and CD44 receptor, which is present on the epithelial cell membrane in lipid raft-enriched areas, thus stimulating site-specific invasion (Skoudy et al., 2000). After contact with the host cell there is the formation of a translocon complex, which delivers a subset of effectors through the needle complex, both to the host cell membrane and into the host cytoplasm. These effectors include IpaA, IpaB, IpaC, IpgB1, IpgB2, IpgD and

VirA, and are involved in promoting bacterial entry into epithelial cells (***Figure 22***) by a "trigger" mechanism (Cossart and Sansonetti, 2004).

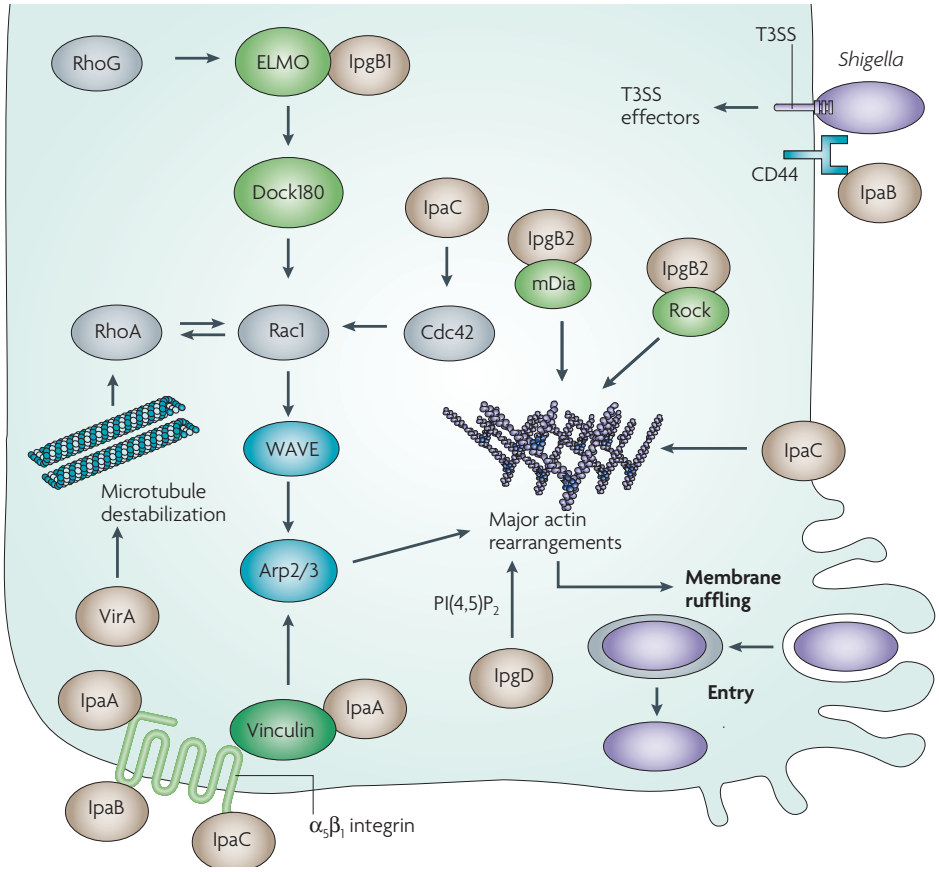

Figure 22 – Simplified model of the "trigger" mechanism in response to the stimulation of host cellular signaling by *Shigella flexneri* effectors. Bacterial contact with an epithelial cell membrane induces injection of a cocktail of effectors through the T3SS into the host cytoplasm. Several of the injected effectors directly or indirectly modulate Rho GTPases activity. This results in major actin rearrangements that lead to membrane ruffle formation in the bacterial entry site and efficient bacterial uptake. Adapted from Ogawa et al., 2008.

IpaA directly binds to human vinculin, a key component of focal adhesions, promoting its association with F-actin. In this way, IpaA induces vinculin-dependent capping of F-actin barbed ends, regulating actin polymerization/depolymerization dynamics at the sites of bacterial entry (Ramarao et al., 2007). Additionally, it has been proposed that IpaA targets β_1-integrin and stimulates the GTPase activity of RhoA, thus inducing the loss of actin stress fibers through a ROCK/myosin-II pathway (Demali et al., 2006). In this way, IpaA-mediated destruction of stress fibers might facilitate recycling of the free actin pool and contribute to membrane ruffle production. IpaC is an effector that is part of the

T3SS translocon, thereby integrating into the host cell plasma membrane at the bacterial entry site. Here, IpaC recruits and activates the Src tyrosine kinase, which in turn phosphorylates cortactin, an F-actin binding protein, thus leading to Arp2/3 complex activation and actin polymerization (Mounier et al., 2009). Moreover, activated cortactin binds to the adaptor protein CrK (a Src-related tyrosine kinase), further amplifying actin polymerization at the *S. flexneri* entry site (Bougnères et al., 2004).

At least two of the *S. flexneri* effectors (the IpgB1 and IpgB2 homologues) act as GEFs for small GTPases. IpgB1 binds the ELMO (engulfment and cell motility) protein and activates Rac1 through the ELMO/Dock180 pathway (***Figure 22***). In this way, it promotes Arp2/3 complex-dependent membrane ruffle formation (Handa et al., 2007) and allows rapid bacterial entry (Ehsani et al., 2012). Additionally, IpgB1 mimics the function of RhoG in producing membrane ruffles during *S. flexneri* entry (Ohya et al., 2005). IpgB2 has the ability to mimic RhoA activity, binding to mDia1 and to ROCK, thus promoting actin nucleation and stress fiber formation (Alto et al., 2006; Orchard and Alto, 2012). IpgD is a PtdIns(4,5)P_2 phosphatase that specifically depletes PtdIns(4,5)P_2 into PtdIns(5)P, which might help to loosen the connection between cortical actin and the plasma membrane, therefore facilitating membrane extensions (Cossart and Helenius, 2014). Finally, VirA, a cysteine protease, is injected into the host cytoplasm near the site of bacterial entry, inducing local MT degradation, and possible contributing to ruffle formation through the crosstalk between RhoA and Rac1 (Ogawa et al., 2008; Yoshida et al., 2002).

Together, the molecular mechanisms by which *S. flexneri* invades epithelial cells require an elaborated, choreographed activity of different effectors, which stimulate several host cell signaling pathways, resulting in actin polymerization and remodeling of the cell surface shape.

Salmonella *entry by effector secretion*

Bacteria of the genus *Salmonella* can cause salmonellosis, which is among the most common enteric diseases in humans. Salmonellae are Gram-negative, facultative intracellular and rod-shaped bacterial pathogens, ranging in size from 0.7 to 1.5 μm in diameter and 2 to 5 μm in length, and are generally motile with peritrichous flagella. Molecular methods have shown that the genus *Salmonella* is

composed of only two different species (*S. enterica* and *S. bongori*) that are further distinguished into seven distinct subgenera or subspecies (subspecies I, II, IIIa, IIIb, IV, V and VI). Out of these, and on the basis of their flagellar and lipopolysaccharide (LPS) antigens, more than 2500 *Salmonella* serovars have been identified (***Table 3***) (Agbaje et al., 2011; Brenner et al., 2000). Salmonellae can adapt to a wide range of conditions. They are broadly distributed and are capable of infecting a wide range of animals, including men, leading to several manifestations of disease.

Table 3 – *Salmonella* species and subspecies, the number of serovars and their usual habitats, according to the Kauffmann-White scheme. Adapted from Brenner et al., 2000.

***Salmonella* species and subspecies**	**Number of serovars**	**Usual habitat**
S. enterica	**2557**	
S. enterica subsp. *enterica* (I)	1531	Warm-blooded animals
S. enterica subsp. *salamae* (II)	505	Cold-blooded animals and the environment
S. enterica subsp. *arizonae* (IIIa)	99	Cold-blooded animals and the environment
S. enterica subsp. *diarizonae* (IIIb)	336	Cold-blooded animals and the environment
S. enterica subsp. *houtenae* (IV)	73	Cold-blooded animals and the environment
S. enterica subsp. *indica* (VI)	13	Cold-blooded animals and the environment
***S. bongori* (V)**	**22**	Cold-blooded animals and the environment
Total (genus *Salmonella*)	**2579**	

In humans, salmonellosis is caused by *Salmonella enterica* subsp. *enterica* that include both typhoidal and non-typhoidal *Salmonella* (NTS) serovars (***Table 4***). This disease can be characterized by enteric fever, self-limiting gastroenteritis, septicemia, focal infections and, in the case of some typhoidal strains, an asymptomatic carrier state. NTS-caused gastroenteritis is generally self-resolving in healthy adults, but it can also cause bacteremia and systemic infection in immunosuppressed hosts and in very young and older individuals. Salmonellosis is still endemic in most countries, where it is one of the most common causes of food-borne diseases, possibly affecting over 90 million people globally each year, and causes high economical losses (Majowicz et al., 2010). The pathogenicity of

this disease has been mostly studied by using *Salmonella enterica* serovars Typhimurium (hereafter referred as *Salmonella*) as a model to understand interactions with host cells.

Table 4 – Hosts and diseases caused by some examples of *Salmonella enterica* subsp. *enterica* serovars. Adapted from Haraga et al., 2008.

Salmonella enterica serovar	Host specificity	Disease and symptoms
Typhoidal		
Typhi; Paratyphi	Human-restricted	Enteric (typhoid) fever — abdominal pain, transient diarrhea or constipation, fever, salmon-colored maculopapular rash on the trunk
Non-typhoidal		
Typhimurium; Enteriditis	Broad-range	Gastroenteritis — abdominal pain, inflammatory diarrhea and vomiting

Salmonellosis is generally acquired by fecal-oral route, through the ingestion of contaminated water or food. Salmonellae are acid-tolerant, which promotes their survival in the low pH environment of the stomach. Therefore, the bacteria can travel to the small intestine, where they elicit profound inflammatory changes in the intestinal epithelium, including neutrophil and fluid infiltration into the intestinal lumen, which results in inflammatory diarrhea. *Salmonella* can be engulfed by phagocytes in the intestinal lumen, or it can traverse the epithelial barrier through microfold (M) cells that are present at Peyer's patches. Alternatively, *Salmonella* has developed sophisticated mechanisms to invade the non-phagocytic intestinal enterocytes, promoting their own endocytosis, which facilitates the avoidance of neutrophil-mediated killing (Haraga et al., 2008; LaRock et al., 2015).

Similarly to *S. flexneri*, *Salmonella* pathogenicity is dependent on T3SSs and dedicated effectors. However, *Salmonella* possesses two distinct T3SSs, encoded by the pathogenicity islands 1 (SPI-1) and 2 (SPI-2), respectively, which are present on the bacterial chromosome. The SPI-1-encoded T3SS (T3SS-1) allows the secretion of early effectors crucial for bacterial entry into epithelial host cells, whereas the SPI-2-encoded T3SS (T3SS-2) is activated after bacterial internalization and it is required for intracellular survival and the establishment of a replicative niche inside the host cell. However, it is now believed that some effectors from both T3SSs act at the same time and might have overlapping functions (Agbor and McCormick, 2011; Brawn et al., 2007; Srikanth et al., 2011).

Together, the two *Salmonella* T3SSs inject more than 30 effector proteins into the host cell, in a time-regulated manner and with the intention of manipulate several eukaryotic cell functions (Agbor and McCormick, 2011; Figueira and Holden, 2012; McGhie et al., 2009).

Several factors, such as osmolarity, pH, growth density and aeration levels, have been proposed to induce the expression of T3SS-1 components and effectors, whose transcription is regulated by the master regulator HilA. After assembly of the secretion system, direct and intimate contact between *Salmonella* and the host cell membrane is necessary for the activation of the T3SS-1, which is accompanied by the formation of the translocon pore in the host plasma membrane, formed by the effectors SipB and SipC (Bajaj et al., 1996; Eichelberg and Galán, 1999; Lara-Tejero et al., 2011). After the successful activation of the T3SS-1, at least 11 effectors are known to be injected into the host epithelial cell (Agbor and McCormick, 2011; van der Heijden and Finlay, 2012), “triggering” a bacterial entry process that is characterized by the extremely rapid appearance of host cell membrane ruffles. This resembles the *S. flexneri* invasion process described before. Massive and localized actin and plasma membrane rearrangements are mostly mediated by a subset of five *Salmonella* T3SS-1 effectors (SipA, SipC, SopB, SopE and SopE2) (***Figure 23***) (LaRock et al., 2015).

SipA and SipC bind directly to actin at the site of insertion of the T3SS-1 translocon, thus promoting bacterial entry. SipA inhibits actin depolymerization, through the inhibition of the filament-severing activities of cofilin and gelsolin (McGhie et al., 2004). Additionally, SipA increases F-actin bundling by enhancing the localized activity of T-plastin (Zhou et al., 1999a; 1999b). After translocon insertion, SipC can cause actin bundle and nucleation, thus promoting *Salmonella* invasion (Hayward and Koronakis, 1999; Myeni and Zhou, 2010). Moreover, it was shown that SipC interacts directly with Exo70, a component of the exocyst complex that mediates docking and fusion of exocytic vesicles with the plasma membrane, which might act as a source of membrane for the expanding ruffle (Nichols and Casanova, 2010).

The effector protein SopB is a phosphoinositide phosphatase that affects several cellular pathways during infection. It can generate PtdIns(3)P by recruiting Rab5 and hVPS34 to membranes (Mallo et al., 2008), and increased levels of this phosphatidylinositol seem to recruit VAMP8 to the entry site, which is important for

Salmonella entry (Dai et al., 2007). During bacterial entry into epithelial cells, SopB recruits annexin A2, which functions as a platform for actin rearrangements (Jolly et al., 2013). Additionally, SopB targets the SH3-containing GEF (SGEF) and promotes RhoG activation, thus participating in actin remodeling at the host cell plasma membrane (Patel and Galán, 2006). Whereas SopB activates a GEF, SopE and SopE2 (two effectors that are about 70% identical) mimic host GEFs, binding to Rho GTPases and activating them. SopE acts on Cdc42 and Rac1, whereas SopE2 seems to be specific for Cdc42 (Hardt et al., 1998; Stender et al., 2000; van der Heijden and Finlay, 2012). Activation of Rac1 by SopE triggers the recruitment of N-WASP and WAVE regulatory complex (WRC) to the plasma membrane. Here, ARNO (a Arf1 GEF) recruitment (possibly via SopB-induced PtdIns(3)P generation) and activation also takes place, via the simultaneous binding of GTP-bound Arf6 (***Figure 23***). Activated ARNO then activates Arf1, which in turn activates WRC. Thus, bacterial SopE and host ARNO cooperate to recruit and activate WRC, resulting in Arp2/3 complex-mediated membrane ruffling and *Salmonella* entry into epithelial cells (Humphreys et al., 2012; 2013). Recent work suggests that SopE can also activate RalA, a GTPase that is required for exocyst assembly, and then induce host cell membrane ruffling (Nichols and Casanova, 2010). After bacterial entry, the architecture of the cytoskeleton is restored, which is mediated by SptP, an effector with GAP activity that inactivates both Rac1 and Cdc42 (Fu and Galán, 1999).

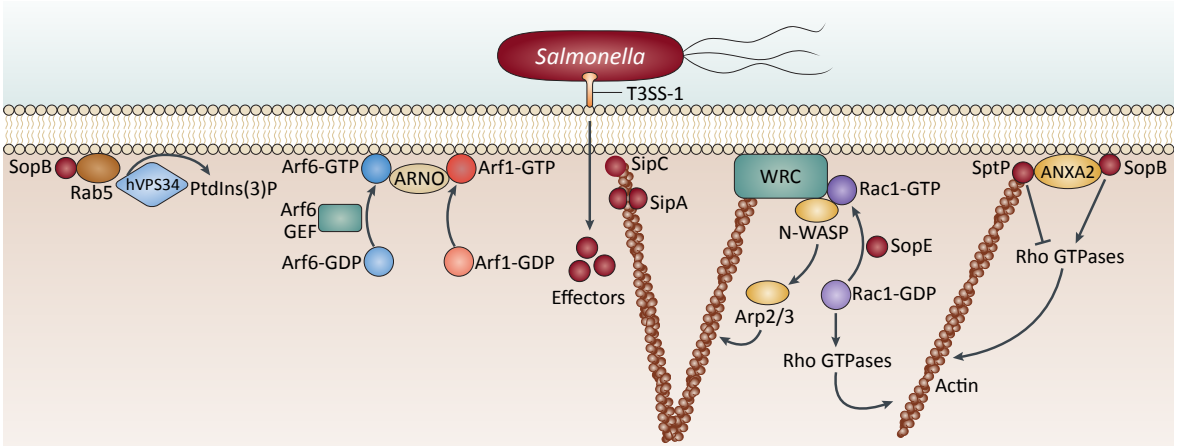

Figure 23 – Simplified model of the "trigger" mechanism in response to the stimulation of host cellular signaling by *Salmonella* effectors. Following *Salmonella* contact with epithelial host cells, injection of effectors through the T3SS-1 mediate cytoskeletal rearrangements and bacterial internalization. ANXA2, Annexin A2. Adapted from LaRock et al., 2015.

Recent data also suggest the existence of a novel membrane ruffling-independent mechanism for *Salmonella* entry, which operates independently of Arp2/3 complex. It was shown that this entry mechanism relies on myosin-II contractility at invasion sites, through the activation of RhoA/Rho kinase signaling pathway, in a SopB-dependent manner (Hänisch et al., 2010; 2011). Additionally, it was recently shown that *Salmonella* can invade epithelial cells in a T3SS-independent manner, which might be important under certain conditions. At least two non-fimbrial outer membrane proteins (Omps), Rck and PagN, can mediate bacterial "zipper"-like invasion of non-phagocytic cells. Rck-mediated entry is dependent on Arp2/3 complex, Rac1 and Cdc42, which induce actin rearrangements that result in membrane ruffling and bacterial internalization (Mijouin et al., 2012; Rosselin et al., 2010). PagN binds to cell surface heparin sulfate proteoglycans, mediating *Salmonella* adhesion and invasion (Lambert and Smith, 2009). It is likely that these alternate invasion mechanisms, when used in combination with T3SS-1-mediated entry, might help provide cell and host specificity.

B. Bacteria exploit the host intracellular environment to survive

After internalization, invasive bacterial pathogens are surrounded by a host cell membrane and are enclosed within a membrane-bound vacuole, which is thought to derive mostly from the plasma membrane. Since the host cell has efficient ways to destroy invading bacteria, the latter have evolved diverse strategies to survive and proliferate within the host. Many intracellular bacterial pathogens modulate their vacuoles by hijacking the host cell endomembrane system: they can either rupture the vacuole to reach the host cell cytoplasm (cytosolic lifestyle), or build a replicative niche inside the vacuole (intravacuolar lifestyle) (***Figure 18***). Each lifestyle has important consequences for both the infected cell and the invading pathogen, since the different niches have distinct physiological environments. By rupturing their vacuole, cytosolic bacterial pathogens, such as *L. monocytogenes*, *S. flexneri*, and *Francisella tularensis*, have direct access to the cytoplasm, which is a rich source of nutrients.

Nevertheless, they face other challenges, notably the cytoplasmic innate immune system that can induce inflammatory responses and autophagy-mediated bacterial degradation (Fredlund and Enninga, 2014; Ray et al., 2009). In contrast, intravacuolar bacteria, such as *Salmonella*, *L. pneumophila*, *M. tuberculosis* and *Chlamydia trachomatis*, must actively avoid vacuolar maturation into a degradative compartment, as well as subvert host cellular trafficking to obtain nutrients. However, the formation of a compartmentalized and unique pathogen-containing organelle allows them to avoid most of the host cell defense mechanisms (Cossart and Helenius, 2014; Creasey and Isberg, 2014; Kumar and Valdivia, 2009).

Even though each bacterial pathogen usually adopts a specific intracellular lifestyle, recent studies have described that some intravacuolar bacteria, namely *Salmonella* and *M. tuberculosis*, can also access the host cytoplasm (Fredlund and Enninga, 2014; Malik-Kale et al., 2011; Simeone et al., 2012).

Listeria *and* Shigella *rupture the vacuole and grow in the host cytoplasm*

Escape from the bacteria-containing vacuole to the host cytoplasm is a crucial step in the life cycle of cytosolic invasive bacteria (***Figure 24***). Most of these pathogens are found free in the cytoplasm within 30 minutes after entry into the host cell, which means that vacuolar rupture occurs very rapidly. For many years it has been thought that this process was exclusively driven by bacterial effectors, but it is now clear that vacuolar rupture depends on the intricate interplay between host and bacterial factors (Fredlund and Enninga, 2014; Ray et al., 2009; 2010).

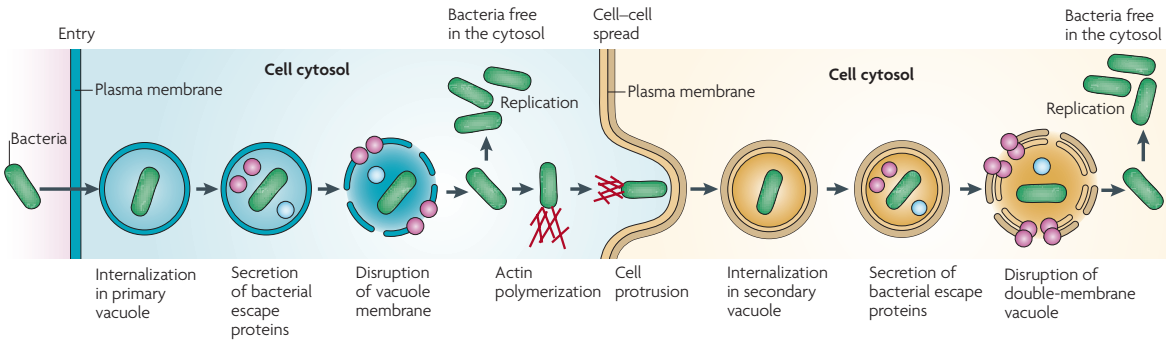

Figure 24 – The intracellular lifestyle of cytosolic bacteria, such as *L. monocytogenes* and *S. flexneri* (Ray et al., 2009).

In the case of *L. monocytogenes*, vacuolar rupture occurs 15 minutes upon internalization, and its mechanism has been studied in some detail. It has been proposed to be mediated mostly by the bacterial effectors listeriolysin O (LLO) and type C phosphatases. LLO is a secreted effector that oligomerizes and inserts into cholesterol-enriched domains of the vacuolar membrane, forming pores that destabilize and rupture the vacuole. In this way, *L. monocytogenes* avoids fusion with lysosomes. LLO production is tightly regulated, and this enzyme is optimally active only when the vacuole is slightly acidified (pH 5.5) (Beauregard et al., 1997; Hamon et al., 2012). LLO activity is also regulated by host factors, such as the γ-interferon-inducible lysosomal thiol reductase (GILT) (Singh et al., 2008). Moreover, *L. monocytogenes* secretes phosphatidylinositol-phospholipase C (PI-PLC) and phosphatidylcholine-phospholipase C (PC-PLC), which are required for vacuolar escape into the cytosol, and disruption of the double-membrane vacuole during cell-to-cell spread, respectively (Marquis and Hager, 2000; Smith et al., 1995).

After internalization, *S. flexneri* also escapes rapidly from the vacuole into the host cytoplasm. Several recent studies that allow tracking of vacuolar rupture in real time, by fluorescence microcopy, revealed that this process occurs in less than 10 minutes after bacterial entry (Ehsani et al., 2012; Paz et al., 2010; Ray et al., 2010). Over the last years, novel insights have been made into the rupture of the *S. flexneri* containing vacuole, which is changing the previous paradigm of a bacterial-induced mechanism. It was initially proposed that T3SS effectors could play a role in vacuolar rupture, within macrophages. In particular, it was proposed that the T3SS translocon proteins, IpaB and IpaC, could form a pore complex in cholesterol-rich membrane domains of the vacuole, causing its disruption and subsequent bacterial escape to the cytosol (Hayward et al., 2005; High et al., 1992). However, the role of these bacterial effectors during vacuolar escape in epithelial cells was never confirmed, since they are also required for invasion (High et al., 1992; Ogawa et al., 2008). After vacuolar rupture and bacterial escape to the cytoplasm, there is the formation of a pool of smaller vesicles derived from vacuolar membrane remnants, whose associated proteins are polyubiquitinated. Then, the autophagy marker microtubule-associated protein light chain 3 (LC3) and the adaptor p62 are recruited, as well as inflammasome components and caspase-1, and the membrane remnants are targeted to autophagic degradation

(Dupont et al., 2009; Ehsani et al., 2012). This suggests that the location of vacuolar rupture constitutes a site for the establishment of a signaling platform within the host cell. Recently, a high-content small interfering RNA (siRNA) study showed that several host proteins induce *S. flexneri* vacuolar membrane rupture (Mellouk et al., 2014), specifically Rab11, a component of the host ERC. It was shown that the conversion of PtdIns(4,5)P_2 to PtdIns(5)P, by the bacterial effector IpgD, results in the recruitment of Rab11-positive vesicles to the invasion site and around the bacteria-containing vacuole, before its rupture. In this way, *S. flexneri* promotes vacuolar rupture through the modulation of host vesicles.

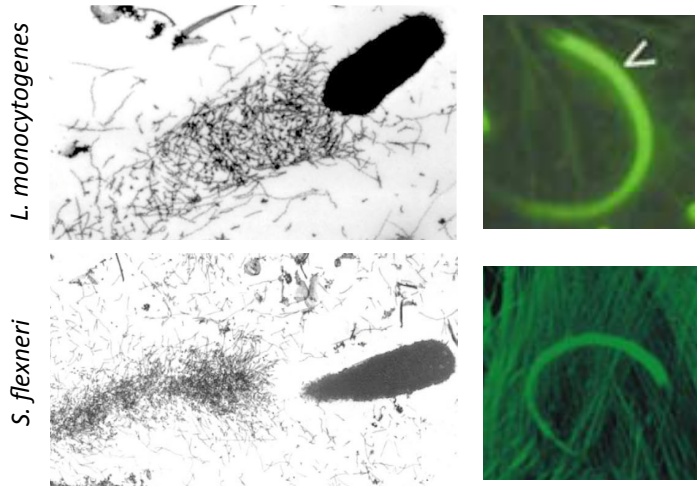

Figure 25 – Intracellular actin comet tails induced by *L. monocytogenes* (top) and *S. flexneri* (bottom). The left panels show electron microscopy data (Gouin et al., 2005), and the right panels show fluorescently labeled actin comet tails (Egile et al., 1999; Gouin et al., 2004).

Once in the host cytoplasm, *L. monocytogenes* and *S. flexneri* subvert the host cytoskeleton machinery by expressing effectors that induce actin polymerization at the surface of one bacterial pole. In this way, bacteria induce the formation of a so-called actin comet tail that propels bacteria within the host cytoplasm, moving them intra- and intercellularly. Intracellular bacterial motility can reach speeds of 10-87 μm/minute, for *L. monocytogenes*, or 3-26 μm/minute, for *S. flexneri* (Ray et al., 2009; Stevens et al., 2006). Structurally, actin comet tails formed by these two bacterial pathogens are composed of short, highly branched crosslinked actin filaments that can leave a long trail behind one of the bacterial poles (***Figure 25***). In the case of *L. monocytogenes*, the effector ActA is expressed at one of the bacterial poles, and it directly interacts with and activates the Arp2/3 complex (***Figure 26***). Thus, ActA mimics the activity of N-WASP,

functioning as a NPF (Gouin et al., 2005; Stevens et al., 2006). It has been proposed, from *in vitro* reconstitution experiments, that *L. monocytogenes* propulsion in the host cytoplasm might require an initial Arp2/3 complex-dependent nucleation step, followed by an Arp2/3 complex-independent tail-elongation phase that necessitates fascin and results in the formation of F-actin bundles (Brieher et al., 2004). As for *S. flexneri*, it induces the formation of actin comet tails by expressing the outer membrane protein IcsA (also called VirG) at one pole. IcsA directly interacts with and recruits a host cell NPF (N-WASP), which in turn activates the Arp2/3 complex to form an actin comet tail (***Figure 26***) (Stevens et al., 2006).

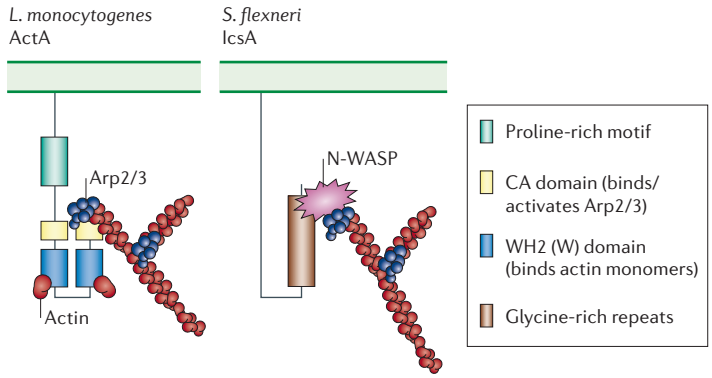

Figure 26 – Mechanisms of intracellular bacterial actin-based motility, induced by *L. monocytogenes* and *S. flexneri*. *Listeria* ActA directly interacts with Arp2/3 complex, through the central and acidic (CA) regions. In this way there is Arp2/3 activation. *Shigella* IcsA recruits N-WASP to the bacterial surface, through a glycine-rich domain, which in turn activates the Arp2/3 complex. Adapted from Stevens et al., 2006.

Bacterial escape from the endocytic vacuole to the cytoplasm allows them to escape degradation within the endolysosomal pathway. Nevertheless, the host cytoplasm also contains a range of innate immune defense mechanisms, such as antimicrobial peptides and the Nod-like receptors (NLRs). An additional component of the host defense against cytosolic pathogens is autophagy, a degradative pathway by which cytosolic contents, organelles and pathogens are delivered to lysosomes as part of cellular homeostasis (He and Klionsky, 2009). Though, cytosolic bacteria have developed strategies to interact and modify the autophagic pathway, in order to promote their survival. Once in the host cytoplasm, *L. monocytogenes* avoid autophagic degradation by expressing the phospholipases PI-PLC and PL-PLC, by a mechanism that remains to be

addressed (Birmingham et al., 2007; Py et al., 2007). In the case of *S. flexneri*, the IcsA effector, which is required for actin-based motility, also induces autophagy in the host cytoplasm, by binding the autophagic protein Atg5 (Ogawa et al., 2005). Moreover, septins are recruited to the IcsA-mediated actin comet tail, forming cage-like structures that prevent intracellular bacterial motility, entrapping and targeting *S. flexneri* to autophagic degradation (Mostowy and Cossart, 2011; Mostowy et al., 2010). To evade autophagy, *S. flexneri* secretes the T3SS effector IcsB, which competitively binds to IcsA and prevent Atg5-dependent recognition and septin cage entrapment (Mostowy et al., 2010; Ogawa et al., 2005).

Legionella *builds a replicative vacuole inside host cells*

Legionella pneumophila, the causative agent of the potentially fatal pneumonia Legionnaires' disease, is an accidental human pathogen that replicates intracellularly within environmental protozoa and alveolar macrophages (Hilbi et al., 2011; Isberg et al., 2009). After being phagocytosed, *L. pneumophila* secretes around 300 effectors into the host cell, via the Dot/Icm type IV secretion system (T4SS), some of which drive maturation of the *Legionella*-containing vacuole (LCV). Different cellular microbiology studies and proteomic analysis of purified LCVs revealed that this unique compartment intercepts the secretory vesicle trafficking pathway, interacts with the ER and communicates with the endosomal pathway without fusing with lysosomes (Hilbi and Haas, 2012; Hoffmann et al., 2014; Hubber and Roy, 2010; Isberg et al., 2009; Urwyler et al., 2009). Maintenance of the LVC is Dot/Icm-dependent, because non-virulent Δ*dot/icm* mutants escape to the cytosol of infected cells soon after invasion (Molmeret et al., 2007). By recruiting vesicles derived from the ER, the LCV matures into a specialized ER-like compartment that supports bacterial growth (***Figure 27***). *L. pneumophila* has the ability to subvert the functions of the GTPase Rab1 (a ER-to-Golgi traffic regulator) and of the v-SNARE Sec22b, in order to facilitate the transport and fusion of ER-derived vesicle with the LCV (Kagan et al., 2004). Additional evidence indicating that vesicles that exit the ER fuse with the LCV includes the presence of ER-derived proteins on the vacuole, such as glucose-6-phosphatase and protein disulphide isomerase, as detected by electron microscopy (Robinson and Roy, 2006).

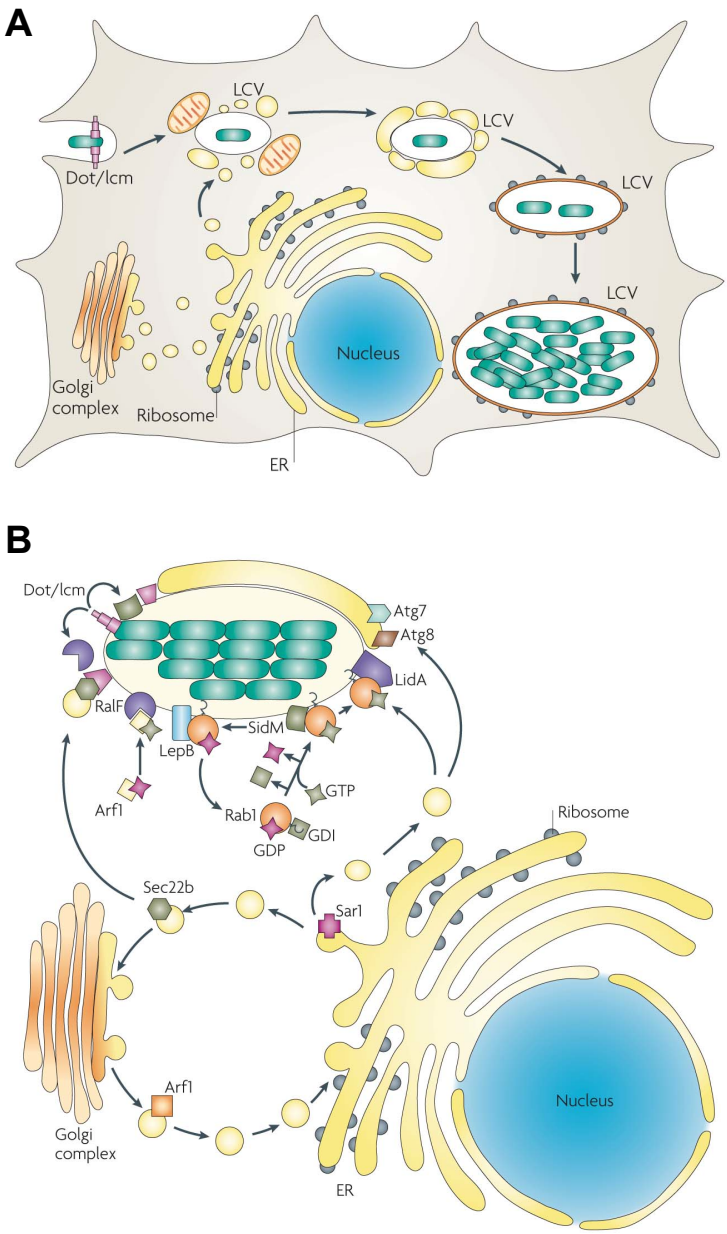

Figure 27 – The *L. pneumophila* intracellular lifestyle. A. After uptake into amoebae or macrophages, the LCV escapes transport to the endolysosomal pathway and it interacts with mitochondria and ER-derived vesicles. Eventually, the LCV matures into an ER-like compartment, covered with ribosomes, where the bacteria replicate. **B.** Several Dot/Icm T4SS effectors associate with the LCV and recruit host proteins involved in vesicle trafficking, such as Sec22b, Rab1 and Arf1. The host proteins Atg7 and Atg8 also associate with the LCV, possibly as a result of autophagic membrane recruitment to the vacuole. Adapted from Isberg et al., 2009.

The LCV is also decorated with host small GTPases involved the regulation of secretory or endosomal trafficking (Arf1, Rab4, Rab5, Rab7, Rab8 and Rab11), whose activity can be regulated by bacterial effectors (Hoffmann et al., 2014; Kagan and Roy, 2002; Urwyler et al., 2009). Additionally, *L. pneumophila* utilizes PtdIns(4)P and PtdIns(3)P on the LCV membrane to anchor bacterial effectors to the vacuole (Hilbi and Haas, 2012; Ragaz et al., 2008), and interferes with the

retrograde and lysosomal pathways. The Dot/Icm T4SS effector RidL, which localizes to the LCV membrane, binds the subunit Vps29 of the retromer complex, inhibiting retrograde endosome-Golgi trafficking and promoting intracellular bacterial replication (Finsel et al., 2013), and the effector SidK, which inhibits vATPase, prevents LCV acidification (Xu et al., 2010).

Since *L. pneumophila* uses a T4SS to inject effectors across host membranes, it is likely that it could also cause LCV membrane damage and compromise its integrity. Even though it has been described that this bacterium escapes into the host cytoplasm late in infection, this still needs further investigation (Kumar and Valdivia, 2009; Molmeret et al., 2004). Interestingly, it was recently shown that the bacterial effector SdhA is required to maintain the integrity of the LCV membrane in macrophages, which allows intracellular bacterial replication (Creasey and Isberg, 2012).

Salmonella *life inside a vacuole – nesting to grow*

After internalization into the host cell, *Salmonella* reside within the *Salmonella*-containing vacuole (SCV). This is a unique and modified membrane-bound compartment that, through the action of both T3SS-1 (SPI-1 effectors) and T3SS-2 (SPI-2 effectors), enables intravacuolar bacterial survival and replication. The SCV is subjected to different stages of maturation (early, maturing, and late), each associated with the presence of different host cell factors on the vacuole (Malik-Kale et al., 2011).

It has been shown that, immediately after formation, the early SCV [< 30 minutes post-invasion (p.i.)] shares some similarities with early endosomes and undergoes rapid membrane remodeling (***Figure 28***). This is mostly driven by the activities of the T3SS-1 effector SopB (a homologue of the *S. flexneri* effector IpgD), which is translocated during bacterial entry and then persists in the host cell for several hours (Drecktrah et al., 2005; Kubori and Galán, 2003). SopB is located on the cytosolic side of the SCV, where it recruits the small GTPase Rab5 to the SCV membrane. This in turn recruits the Rab5-interacting protein Vps34, a PI(3)K that phosphorylates PtdIns into PtdIns(3)P on the SCV membrane, which is necessary for the recruitment of EEA-1 and VAMP8 (Dai et al., 2007; Mallo et al., 2008; Scott et al., 2002). It has been suggested that the presence of PtdIns(3)P on the SCV stimulates fusion with other vesicles containing PtdIns(3)P, which might

bring nutrients required for bacterial growth (Hernandez et al., 2004). SopD is another T3SS-1 effector that may act cooperatively with SopB during the initial steps of SCV biogenesis (Bakowski et al., 2007).

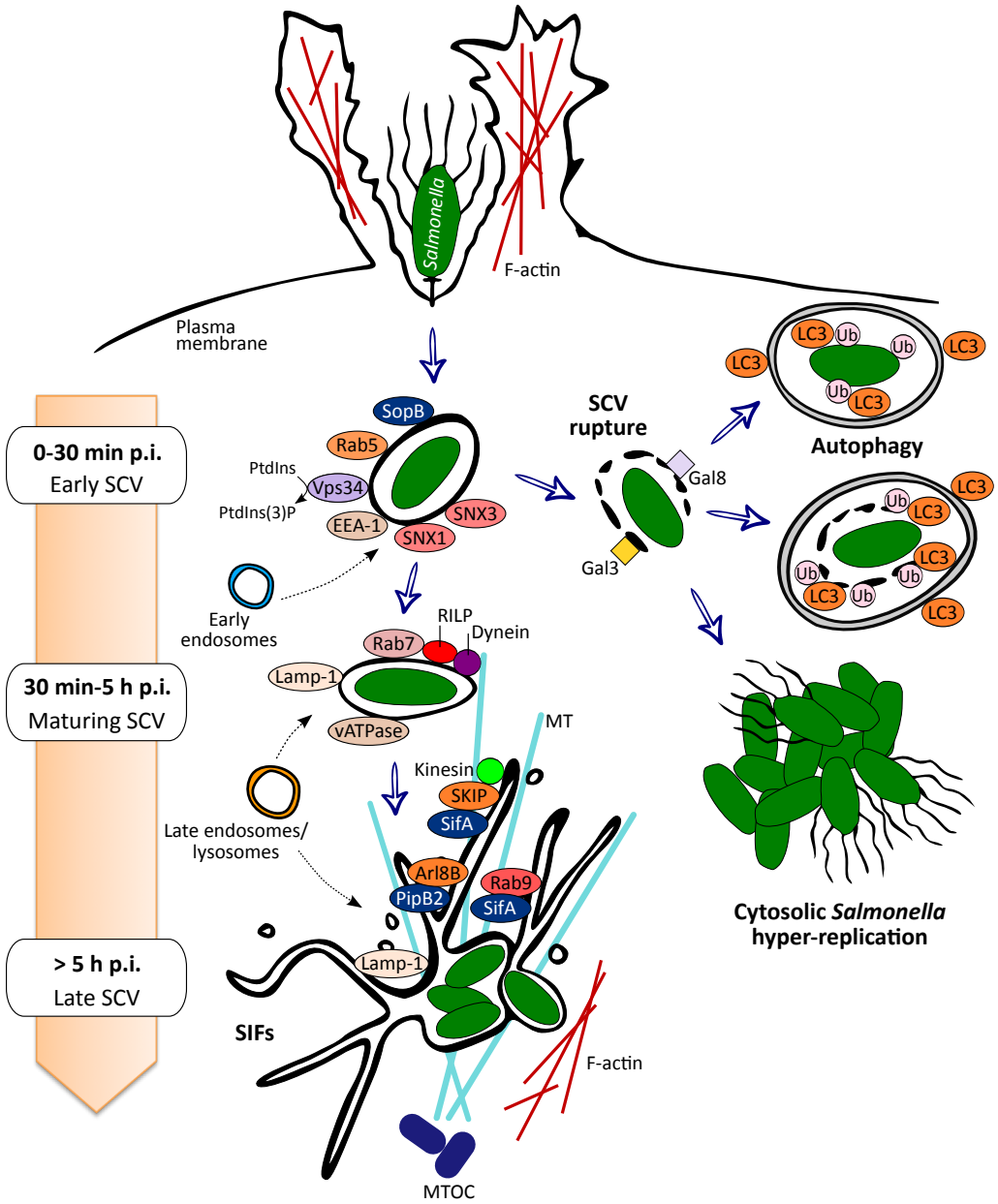

Figure 28 – Biogenesis and maturation of the *Salmonella*-containing vacuole (SCV), and the bimodal lifestyle of intracellular *Salmonella*, in epithelial cells. Invasive *Salmonella* use T3SS-1 to inject effectors into the host cell and promote actin-mediated ruffling and bacterial internalization into a modified vacuole, the SCV. The SCV then undergoes successive maturation steps, with extensive remodeling of its membrane. T3SS-2 effectors are required for SCV maturation and for its positioning in a perinuclear location, close to the MTOC. In the figure, the bacterial effectors SopB, SifA and PipB2, are depicted in dark blue. Some SCVs do not undergo maturation, and instead are ruptured, either releasing bacteria into the host cytosol or being targeted by the autophagy system. In the late SCV there is *Salmonella* replication and the formation of dynamic membrane tubules. For reasons of simplicity, only the Lamp-1-enriched *Salmonella*-induced filaments (SIFs) are represented. Cytosolic bacteria that have escaped autophagy start to hyper-replicate, and become activated for T3SS-1 and flagella. See text for details.

Moreover, within 15 minutes p.i., there is the recruitment of SNX1 to the SCV, in a SopB-dependent manner, which promotes exclusion of CI-M6PR from the SCV (Bujny et al., 2008). Since the CI-M6PR is used to deliver soluble lysosomal enzymes to lysosomes and it is generally excluded from the SCV at later time-points, this was first seen as evidence for the lack of lysosomal fusion with the SCV (Garcia-del Portillo and Finlay, 1995). Nevertheless, this has been controversial (Oh et al., 1996) and recent data clearly indicate that the SCV dynamically interacts with the host cell endolysosomal system (Drecktrah et al., 2007). Therefore, an alternative explanation for the exclusion of the CI-M6PR from the SCV is that it is still recruited to the early SCV but is then efficiently removed in a SNX1-dependent manner (Bujny et al., 2008). This implies that *Salmonella* might not avoid interactions between the SCV and lysosomes but, alternatively, can control host trafficking pathways to remove unwanted factors. SopB also mediates recruitment of SNX3 to the early SCV, which is important for vacuole maturation (Braun et al., 2010). Therefore, it is likely that SopB-mediated PtdIns modulation on the SCV membrane is crucial for SCV formation and maturation.

After the formation of the SCV, the T3SS-2 is induced and there is secretion of SPI-2 effectors across the SCV membrane. Upregulation and delivery of SPI-2 T3SS effectors across the SCV membrane into the host cytoplasm is a precisely controlled process. It involves the ordered assembly of the secretion apparatus on the cell surface, followed by the secretion of effectors that form de needle complex and the translocon pore (formed by SseB, SseC and SseD) (Chakravortty et al., 2005). Activation of genes encoding the secretion apparatus is mediated by two-component regulatory systems, in response to the slightly acidic pH (pH of around 5) and poor nutritional status of the SCV lumen. After assembly of the translocon pore on the SCV membrane, the pH of the host cytosol is sensed by an unknown component of the T3SS-2. Subsequently, a SPI-2-encoded regulatory complex in the bacteria dissociates, derepressing the translocation of proteins, and about 30 different bacterial effectors are injected across the SCV membrane into the host cytoplasm (Figueira and Holden, 2012; van der Heijden and Finlay, 2012), which leads to vacuole maturation. The intermediate or maturing SCV (between 30 minutes and 5 hours p.i.) then undergoes extensive membrane remodeling. Rab5 is depleted from the SCV, and this acquires late endosome/lysosomal markers, such as Rab7, Lamp-1 and vATPase (***Figure 28***). However, the maturing SCV is

generally not enriched in lysosomal hydrolases (Rathman et al., 1997; Schroeder et al., 2011; Steele-Mortimer et al., 1999; Steele-Mortimer, 2008). At the same time, the SCV moves to the perinuclear region of the host cell, in close proximity to the Golgi and to the MTOC. This is mediated by RILP that links active Rab7 to the MT-based motor dynein, forming a complex that mediates centripetal movement of the SCV (Guignot and Servin, 2008; Harrison et al., 2004; Marsman et al., 2004). Additionally, movement of the SCV to the MTOC, and maintenance at that position, involve at least three T3SS-2 effectors (SseF, SseG, and SifA) and two T3SS-1 effectors (SipA and SopB) (Abrahams and Hensel, 2006; Brawn et al., 2007; Ibarra and Steele-Mortimer, 2009). For example, at later stages, SifA plays a role in maintaining the perinuclear position, by binding Rab7 and therefore blocking interaction between RILP and Rab7, which impairs dynein recruitment (Bakowski et al., 2008). Interestingly, the activity of the actin based motor myosin-II is also implicated in SCV positioning, in a process that involves SopB and activation of ROCK (Wasylnka et al., 2008). Maintaining the SCV in close proximity to the Golgi may facilitate interception of transport vesicles to obtain nutrients and/or membrane. This is thought to be important for promoting bacterial replication, which is initiated 3-4 hours p.i. (Bakowski et al., 2008; Ramsden et al., 2007).

The last stages of SCV maturation (> 5 hours p.i.) are characterized by concomitant intravacuolar bacterial replication and formation of complex networks of membrane tubules that extend from the SCV and spread throughout the entire cell (Drecktrah et al., 2008; Liss and Hensel, 2015; Schroeder et al., 2011). This is induced by a set of *Salmonella* effectors, mostly secreted by the T3SS-2. One of these effectors is SifA, which is essential for the formation of *Salmonella*-induced filaments (SIFs) (***Figure 28***). SIFs are dynamic, Lamp-1-enriched membrane tubules that extend from the SCV along a scaffold of MTs, and they appear to derive solely from late endocytic compartments, as seen by fluorescence live imaging. The composition of SIFs is similar to that of the SCV membrane, containing Lamp proteins, Rab7, vATPase, cholesterol and low levels of cathepsin D (Brumell et al., 2001; Drecktrah et al., 2008). SIF formation also involves at least three host cell proteins: the plus end directed MT motor kinesin-1; the Arf GTPase Arl8B; and the kinesin-binding protein SKIP (SifA and kinesin-interacting protein). In fact, kinesin recruitment to the SCV and its subsequent activation are critical

steps in late SCV maturation (Boucrot et al., 2005). SifA links the SCV to the MT network through its interaction with SKIP, thereby regulating the levels of kinesin on the SCV. Nevertheless, kinesin-1 recruitment is driven by the T3SS-2 effector PipB2 (Henry et al., 2006) and the host Arl8B (Kaniuk et al., 2011). In this way, *Salmonella* translocates an effector that recruits kinesin and a different one that downmodulates the amount of this motor protein at the SCV surface. By doing this, bacteria control the dynamics of membrane exchange of the SCV, regulating the extension of SIFs towards the cell periphery in a precise manner. Interestingly, in the absence of the SKIP-SifA complex, there is excessive accumulation of kinesin on the SCV, which eventually leads to SCV membrane disruption, as result of an imbalanced membrane flow or of disproportional motor forces on the SCV (Boucrot et al., 2005; Ramsden et al., 2007). Additionally, SifA has important roles in the bacterial growth within the late SCV. When bound to SKIP, SifA sequesters the host Rab9 to the SCV, blocking Rab9-dependent retrograde trafficking of immature lysosomal enzymes to the TGN. As a result, detoxified lysosomes lacking hydrolytic enzymes become available for fusion with the SCV, which promotes *Salmonella* survival (McGourty et al., 2012). Recently, it was also shown that *Salmonella* recruits a PLEKHM1, Rab7 and HOPS complex to the SCV, in a SifA-dependent manner, which further promotes the fusion of detoxified lysosomes with the late the SCV (McEwan et al., 2014).

Despite the numerous studies on the molecular players responsible for SIF formation, its biogenesis has been mostly studied using light microscopy. This has inherent limitations, because with such approaches many of the ultrastructural details cannot be identified. Therefore, recent efforts have been made to resolve the ultrastructure of these filaments, by combining fluorescence microscopy with electron microscopy, a technique named correlative light and electron microscopy (CLEM). In particular, the correlation of confocal microscopy with transmission electron microscopy (TEM) showed that SIF formation initiates as single-membrane tubular compartments (leading SIFs), which then convert into double-membrane tubules (trailing SIFs) during maturation, in a SseF- and SseG-dependent manner (Krieger et al., 2014). Moreover, TEM showed the presence of host ribosomes, small membrane vesicles, MTs and F-actin inside double-membrane SIFs. Based on these novel observations, the authors proposed novel insights into the SIF biogenesis. Lateral extension of SIF membranes around the

guiding MT filaments might entrap portions of the cytosol, MTs and/or F-actin. Even though this appears to be a reversible process in the initial phase of SIF formation, during time there is membrane closure, which results in completely closed double-membrane tubules. The inner lumen of the double-membrane SIFs is derived from the host cytoplasm, whereas the outer lumen derives from the luminal content of vesicles that fuse with the SCV and the SIFs, and these two lumina seem to be connected to the lumen of the SCV. This interconnection might then allow the continuous interchange of luminal content inside the SIFs, to be delivered to *Salmonella* within the SCV.

In addition to SIFs, other tubular networks emanate from the late SCV, such as *Salmonella*-induced SCAMP3 (secretory carrier membrane protein 3) tubules (SISTs) (Mota et al., 2009) and Lamp-1-negative tubules (LNTs) (Schroeder et al., 2010). The biological role of all these *Salmonella*-induced tubules is still not fully understood (Schroeder et al., 2011), and it is unclear whether any of them are formed *in vivo*. Nevertheless, over the last years the scientific community has started to understand the role of these structures. Isolation of *Salmonella*-induced tubules and identification of their proteome composition revealed the presence of proteins derived from the TGN, recycling endosomes, ER and additional host organelles (Vorwerk et al., 2015). This suggests that membranes from different origins associate with the late SCV and with *Salmonella*-induced tubules, which points to the possibility that *Salmonella* might use these tubules to intercept host cell vesicles for nutritional or membrane requirements, or to dilute the lysosomal content within the SCV (Liss and Hensel, 2015).

After the proper localization of the SCV in the perinuclear region, close to the MTOC, T3SS-2 effectors also drive the formation of an F-actin meshwork in the vicinity of the SCV (***Figure 28***). This vacuole-associated actin polymerization is associated with SCV membrane integrity and is important for bacterial replication (Bakowski et al., 2008; Méresse et al., 2001). Altogether, analysis of the interactions between the SCV, at different stages of its maturation, and the host cell machinery have shown that *Salmonella* hijacks different components of the host cell to promote intracellular growth.

Salmonella *dual lifestyle – it can also escape the vacuole*

For many years, the SCV has been considered as the primary intracellular niche for *Salmonella* replication. However, a small proportion of infecting bacteria escape from the SCV to the host cytoplasm, as vacuolar membrane damage during the early or maturing stages has also been observed (***Figure 28***). Damage to the SCV membrane promotes the accumulation of galectin-3 and galectin-8, which recruit nuclear dot protein 52 (NDP52) to initiate autophagy (Thurston et al., 2012). In epithelial cells, both cytosolic *Salmonella* and damaged SCVs can be ubiquitinated, and are therefore recognized by the adaptor proteins NDP52 and p62, which leads to the recruitment of the autophagy protein LC3. In fact, it was observed that these autophagy markers are present in approximately 20% of the SCVs, 1 hour p.i. (Birmingham and Brumell, 2006; Birmingham et al., 2006; Jo et al., 2013). Ultimately, the autophagy pathway can clear these cytosolic *Salmonella* and damaged SCVs.

Nevertheless, recent data show that some bacteria that have escaped from the SCV can also evade autophagic degradation. In approximately 9% of infected epithelial cells, cytoplasmic *Salmonella* can replicate very rapidly, at much faster rates than those observed within the SCV (20 minutes per generation), which is termed hyper-replication (***Figure 28***). In fact, several hours after bacteria internalization, hyper-replicating *Salmonella* can fill almost the entire host cytosol. Quantitative microscopic techniques demonstrated that these cells can harbor more than 100 bacteria (Knodler et al., 2010), and that more than half of the total bacterial population are cytosolic, by 7-8 hours p.i. (Knodler et al., 2014). Interestingly, although cytosolic hyper-replicating *Salmonella* only occur in a minority of infected cells, they account for a significant proportion of the net bacterial replication (Malik-Kale et al., 2012). *Salmonella* hyper-replication is T3SS-2-independent, which suggests that the decision to leave the SCV is upstream of vacuole maturation. Additionally, cytosolic bacteria are activated for T3SS-1 and flagellated, and it was observed that epithelial cells harboring hyper-replicating *Salmonella* undergo inflammatory cell death and are extruded from monolayers, releasing a large number of invasive and motile bacteria. This suggests that hyper-replicating *Salmonella* might be primed for additional rounds of invasion once these bacteria are released into the extracellular milieu (Knodler et al., 2010).

Therefore, it is clear that *Salmonella* has a bimodal lifestyle inside epithelial cells, as it is adapted to survive both within the SCV and in the host cytosol. Moreover, intracellular *Salmonella* growth can be different, depending on its localization within the host cell.

Chapter 5

Understanding Cell Biology Through Organelle Proteomics

Cellular functions depend largely on the protein composition of the different organelles, which dynamically changes with time due to multiple interactions with other compartments. Nevertheless, most protein components of the cell are still poorly characterized. Therefore, approaches to identify all these proteins are instrumental to understand organelle functions in detail. The development of mass spectrometry (MS)-based proteomic technologies facilitated studies in the area of global organelle proteomics (Taylor et al., 2003a), which have become powerful methods for studying intracellular compartments, their components and dynamics. Additionally, combining large-scale proteomics studies with traditional cell biology techniques is providing valid strategies to the functional characterization of organelles and the molecules they interact with in a signaling pathway for example (Brunet et al., 2003). Organelle-associated proteins can be localized in the lumen of an organelle, at its membrane, or more or less loosely attached to the membrane periphery. Interestingly, many of the known proteins are believed to be associated with membranes. These proteins are particularly challenging to analyze with many proteomic techniques, however several recent technological advancements have led to a substantial increase in membrane protein representation in large datasets (Savas et al., 2011; Wu and Yates, 2003).

A. Subcellular fractionation by density gradient centrifugation

Over the last decades, the study of organelle proteomics has became increasingly important, as demonstrated by the growing number of annual publications (***Figure 29***). Many of the organelle proteomics studies begin with the isolation of an enriched fraction that contains the organelle of interest (Gatto et al., 2010; Yates et al., 2005), through the use of subcellular fractionation methods.

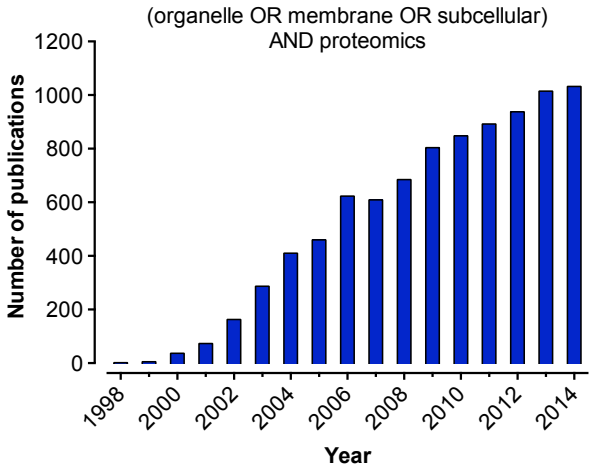

Figure 29 – Number of publications per year in the field of organelle proteomics. The PubMed query is shown on top of the figure.

Subcellular fractionation allows the separation of organelles according to their physical and biological properties. The most usual strategy consists of mechanically disrupting or homogenizing the cell, in a detergent-free isotonic buffer solution, in order to release all the organelles and other cellular constituents as a free suspension of intact individual components. Then, several techniques exploiting the physical and biological parameters of the different compartments can be used to isolate organelles and membranes. Among those, equilibrium ultracentrifugation in a density gradient is considered to be the most effective. In this way, it is possible to separate all the different organelles on the basis of their distinct densities: after reaching equilibrium in the gradient, a specific organelle will be positioned in an area (called “fraction”) where its density matches the density of the surrounding medium. In this way, several organelles can be purified to obtain nearly pure fractions (Graham and Rickwood, 1997). Even though high enrichments can be achieved, many endosomal compartments have similar physical properties. Thus, a particular fraction of interest might contain some degree of contamination from a different organelle. Despite this limitation, subcellular fractionation proved to be crucial for the identification and characterization of several organelles, as exemplified by the groundbreaking work performed by George Palade, Christian de Duve and Albert Claude, during the 1950s and 1960s (Bergeron et al., 2010).

Other techniques used to separate subcellular fractions, alone together with centrifugation, include immuno-isolation, affinity electrophoresis, free-flow electrophoresis or direct alteration of the physical properties of an organelle.

B. Mass spectrometry-based proteomics

The principles of MS-based proteomics

MS is a way to accurately identify the type and amount of a molecule, by measuring its mass-to-charge ratio (m/z). Given that mass analysis uses electromagnetic fields in a vacuum, molecules first have to be subjected to electrospray ionization. In this technique, molecules such as peptides are dissolved in liquid that passes through a needle at high electrical potential. The applied voltage causes the liquid to disperse into small, highly charged droplets, which evaporate and transfer the molecules into the gas phase in an ionized form. After electrospray ionization, electrically charged molecules are transferred into the vacuum of a mass spectrometer and their m/z ratio is determined by their trajectories in an electric field. Popular mass analyzers include, for example, quadrupole-time of flight (TOF) instruments, where the m/z is determined by the time ions need to travel through an electric field to arrive at a detector. Alternatively, ions can be captured in a linear ion trap, where they can be accumulated and manipulated for further analysis. This can be used in combination with an Orbitrap, a type of ion trap mass analyzer where ions oscillate along and around a central spindle-shaped electrode, and that enables extremely accurate m/z measurements and a high mass spectrometric resolution. The high resolution allows the mass spectrometer to distinguish hundreds of thousands of different peptides from each other, which is crucial for their accurate identification and quantification (Walther and Mann, 2010). Nevertheless, it can be difficult to measure the mass of entire proteins (“top-down proteomics”), because the m/z differences of distinct proteins with similar compositions are small. Therefore, for most experiments it is measured the m/z ratio of peptides derived from the entire proteins, after enzymatic cleavage (“bottom-up proteomics”). As the peptides are electrosprayed, the mass spectrometry yields a MS-spectrum of m/z ratios. Then the acquisition software selects a preset number of peptides in the mass spectra and isolates each one of them, to fragment them in the mass spectrometer and to measure the mass spectra of the fragments, which allows peptide sequence identification. This is called tandem mass spectrometry (MS/MS). The data are then scanned through an amino acid sequence database that calculates and

predicts a sequence for each peptide, which enables protein identification. The most popular commercially available peptide search engines are Mascot and Sequest (Cox and Mann, 2011; Walther and Mann, 2010).

In experiments where it is necessary to determine the protein composition of an organelle or a protein complex, it is crucial to accurately detect specific proteins in complex mixtures. In addition, increasing layers of complexity are generated when proteins are digested to peptides. Thus, several approaches can be used to reduce complexity. Initial techniques involved the separation of soluble proteins by two-dimensional gel electrophoresis (2DGE), followed by protein excision from the gel, digestion with a protease, and analysis by MS techniques, such as matrix-assisted laser desorption/ionization-time of flight (MALDI-TOF). However, 2DGE has significant limitations for the separation of transmembrane proteins, and the extraction of hundreds of spots from the gel is extremely time-consuming (Molloy et al., 1998; Yates et al., 2005). Therefore, the most widely method is to separate the proteins by one-dimensional SDS-PAGE (sodium dodecyl sulfate-polyacrylamide gel electrophoresis), which effectively solubilizes membrane proteins, due to the detergent SDS. Proteins can then be subjected to in-gel digestion by a protease, and the remaining peptides are extracted from the gel. Alternatively, it is possible to digest proteins in-solution, avoiding the tedious steps of gel separation and extraction (Walther and Mann, 2010). In these two last examples (SDS-PAGE proteins separation followed by in-gel digestion, or protein digestion in-solution) it is then essential to resolve and detect peptides with high accuracy. To this end, peptides can be separated according to their hydrophobicity, by very low flow high-performance liquid chromatography (HPLC) that is linked directly to a tandem mass spectrometer through electronspary ionization (this technique is called LC-MS/MS, for liquid chromatography-tandem mass spectrometry). This allows extremely high efficiency, yielding peptide spectra that are sufficiently well resolved for a comprehensive detection of hundreds of proteins present in a complex sample (Walther and Mann, 2010; Yates et al., 2005).

Novel LC-MS/MS-based proteomics methodologies generate gigabytes of high resolution data per day and per mass spectrometer, which need to be analyzed by computational tools. For this, a computational proteomics workflow has been developed, based on the use of the MaxQuant algorithms for the analysis of large

MS datasets. MaxQuant is equipped with its own search engine, called Andromeda, and enables peak detection in the raw data with a high peptide identification rate, as well as peptide quantification (Cox and Mann, 2008; Cox et al., 2011).

Quantitative proteomics

Usually it is more important to determine how protein levels change between different conditions, than it is to know just whether a protein is present or not. In this regard, quantification is of central importance in MS-based proteomics, and it can determine the absolute amount of each of the proteins in a mixture or their relative change between two or more conditions. There are two main approaches to turn MS quantitative: stable isotope-labeling or label-free methods (Cox and Mann, 2011; Ong and Mann, 2005).

One of the labeling approaches that has recently gained popularity is called iTRAQ (isobaric tag for relative and absolute quantitation), where digested peptides are chemically modified with isobaric tags. iTRAQ uses up to eight isobaric tags (even though usually only four tags are used in simultaneous) that react with primary amine groups of peptides. During MS analysis, the tags are further fragmented into low mass reporter ions with a tag-specific mass, and then the relative peak intensities of the different reporter ions are used to derive the relative abundance of the corresponding peptides and proteins (Ong and Mann, 2005; Sadowski et al., 2006; Walther and Mann, 2010). Alternatively, peptides can be metabolically labeled, as in the SILAC (stable isotope labeling by amino acids in cell culture) approach. SILAC procedure consists of growing two cell populations in media. One of the cell populations is fed with normal (called “light”) amino acids, whereas the other population is fed with stable (nonradioactive) “heavy” ^{13}C- and ^{14}N-labeled forms of lysine and/or arginine. When cells grow in this “heavy” medium, cells will integrate the “heavy” amino acids into all proteins in the course of several cell doublings. In this way, after protein digestion and MS analysis, the “heavy” labeled proteome is distinguishable from the “light” control proteome by a characteristic mass shift, and the relative intensity of the peaks reflects the relative abundance of the proteins in the mixture (Ong and Mann, 2005; Walther and Mann, 2010).

A label-free quantitative MS methodology is becoming increasingly used. Here, the basic principle is to align and compare the signals of the same eluting peptides from separate LC-MS/MS runs, which allows calculating differences in peak intensities of the same peptides detected in each run. This approach is usually less accurate than the isotope labeling techniques. Nevertheless, in combination with sophisticated algorithms, label-free quantification can be a robust alternative, mostly because it can be applied to any cell type without the need of introducing isotopes (Cox and Mann, 2011; Luber et al., 2010; Walther and Mann, 2010).

Insights from organelle proteomics

The analysis of organelles using proteomics methods is an active field of research, and significant progress is being made in order to define the proteomes of different organelles. For this, subcellular fractionation approaches can be combined with MS-based proteomics to detect and measure proteins in purified organelles (Yates et al., 2005). The mitochondrial proteome was determined after organelle purification by sucrose gradient fractionation, followed by SDS-PAGE protein separation and LC-MS/MS, which identified hundreds of factors associated with this organelle (Pflieger et al., 2002; Taylor et al., 2002; 2003b). Similarly, proteins associated with the Golgi (Wu et al., 2000), clathrin-coated vesicles (Blondeau et al., 2004; Wasiak et al., 2002), the ER lumen (Knoblach et al., 2003), the ERGIC (Breuza et al., 2004) or peroxisomes (Marelli et al., 2004) were determined after subcellular fractionation and MS.

As described in the previous chapters of this thesis, there are complex mechanisms of intracellular communication and contact sites between organelles. This complexity makes it hard to evaluate the biological significance of proteins that are usually associated with one organelle but are detected in the proteome of a different organelle. Additionally, different organelles can have similar physical properties, which means that during biochemical subcellular fractionation they can co-fractionate together, and thus some proteins can be associated with multiple organelle fractions. This shows that not all proteins in a fraction are bona fide constituents of the organelle of interest, but might be instead a result of subcellular fractionation artifacts or contaminants. Nevertheless, it is not possible to exclude that these proteins could also be of biological significant. One of the simplest

solutions to the difficulty in obtaining pure organelles fractions is to perform “subtractive proteomics”, in which the inventory of proteins that are found in a control state or fraction are subtracted from an experimental state or organelle-enriched fraction (Yates et al., 2005). The remaining proteins only detected in the target fraction are thus considered to be enriched in components of the organelle of interest. It is also possible to combine this with quantitative proteomics, where the relative abundance of proteins present in a target and similar control fractions is compared. A quantitative subtractive proteomics has the main advantage of discriminating between true protein members of the organelle and background hits. It is however important that the two fractions under comparison share as much as possible of technical variability to avoid systematic biases that would invalidate the entire approach (Gatto et al., 2010).

C. The proteome of bacteria-containing vacuoles: the Holy Grail

More than twenty years ago, scientists started making important contributions to the understanding of the protein composition of phagosomes (Desjardins et al., 1994). Using phagocytes as cellular model, phagosomes containing inert, low-density latex beads (latex bead-containing phagosomes, or LBPs) were first isolated by subcellular fractionation. Given that LBPs have a lower density than most other organelles, they float after ultracentrifugation and thus can be isolated with a very high degree of purity. Over the last two decades, several subsequent studies have been performed, which, with the development of more sensitive mass spectrometers, identified hundreds of proteins associated with LBPs (Campbell-Valois et al., 2012; Garin et al., 2001; Rogers and Foster, 2007; Stuart et al., 2007; Trost et al., 2009). These studies, together with many others, helped to understand phagosome biogenesis and maturation, as well as to identify novel sources of membrane during the process (Li et al., 2010; Rogers and Foster, 2008).

Phagocytosed latex beads are an excellent tool to understand normal phagosome maturation, but some of the most interesting aspects of phagosome maturation involve the ability of intracellular bacterial pathogens to manipulate the

normal maturation process, as described in chapter 4B. However, in the field of host-pathogen interactions, isolation and protein identification of bacteria-containing phagosomes is considered a “Holy Grail” in phagosome proteomics, and only a few studies have been successfully performed. One example is the determination of LCV protein composition. Since *L. pneumophila*, through its T4SS, injects and selectively anchors the effector SidC into the LCV membrane, it is possible to isolate this compartment by using immuno-magnetic separation followed by density gradient centrifugation (Hoffmann et al., 2013; Urwyler et al., 2009). The proteomics analysis of isolated LCVs revealed more than 670 (in amoeba) or 1150 (in macrophages) host proteins (Hoffmann et al., 2014). Many of these factors are Rab GTPases, which corroborates that LCVs communicates with different cellular signaling and vesicle trafficking pathways. It was also possible to isolate enriched fractions containing *Mycobacterium bovis* bacillus Calmette-Guérin (BCG)-containing phagosomes, through subcellular fractionation methodologies, and determine their proteome composition (Lee et al., 2010). This revealed the presence of 447 host proteins on the BCG-containing phagosomes. Finally, recent work established a novel protocol for the isolation of *Salmonella*-modified membranes (Vorwerk et al., 2015), which include all host cell membranes modified by activities of intracellular *Salmonella* (such as the late SCV, SIFs, SISTs and other unknown membrane structures). Using fractionation followed by affinity immuno-precipitation and subtractive LC-MS/MS analysis, the authors identified 247 host proteins uniquely associated with *Salmonella*-modified membranes. The analysis revealed that these membranes are enriched in proteins derived from the TGN, recycling endosomes, ER and other host organelles.

“Ceux qui préfèrent leurs principes à leur bonheur. Ils refusent d'être heureux en dehors des conditions qu'auparavant ils ont fixées à leur bonheur. S'ils le sont, par surprise, les voilà désemparés - malheureux d'être privés de leur malheur.”

– Albert Camus; in Carnets III: Mars 1951-Décembre 1959

PART II

GOALS OF THE PROJECT

Many of the molecular events during *S. flexneri* or *Salmonella* infection of host epithelial cells have been studied during the last decades. As described in the introduction of this thesis, these two pathogens are able to manipulate the host cell, entering in an endocytic vacuole that is then subjected to different outcomes: either its membrane integrity is lost with consequently bacterial escape to the host cytosol; or its membrane integrity is maintained, supporting intravacuolar bacterial replication. Inside epithelial cells, whereas the *Shigella*-containing vacuole is invariably ruptured, it is clear that *Salmonella* has a bimodal lifestyle, as it is adapted to survive both within the SCV and in the host cytosol. Moreover, intracellular *Salmonella* growth can be different, depending on its localization within the host cell. Nevertheless, the molecular mechanisms of vacuolar membrane rupture and bacterial escape to the host cytosol are not completely understood and require further studies. Thus, the aims of this doctoral project were to better understand the molecular mechanisms involved in the maturation and/or membrane rupture of vacuoles containing invasive bacterial pathogens. At the molecular level, these processes are characterized by a high degree of spatial and temporal organization. Therefore, the main goals of this project were to identify the repertoire of proteins that constitute the bacteria-containing vacuoles and to pinpoint their intracellular localization, in both space and time. For this, we followed two main technical approaches: biochemical isolation of bacteria-containing vacuoles to determine their protein composition, and real time fluorescence microscopy of infected cells to follow the dynamic intracellular localization of host proteins.

As membrane rupture is a critical step during the maturation of bacteria-containing vacuoles, it needs to be spatiotemporally monitored with precision. For this, we used an approach based on the specific recruitment of cytosolic galectins to the site of vacuolar membrane rupture. The use of fluorescently tagged galectin-3 has been successfully used to follow the precise moment of *S. flexneri* escape into the host cytosol, in real time (Paz et al., 2010; Ray et al., 2010).

PART III

RESULTS

The main results of this doctoral project are presented in this thesis in the format of two published manuscripts. In the first manuscript, we studied the dynamic recruitment of several host small GTPases to the site of *S. flexneri* entry into epithelial cell, and correlated this with subsequent vacuolar rupture, by time-lapse fluorescence microscopy. With this, it was possible to show that bacterial entry and vacuolar rupture follow precise kinetics, in relation to the recruitment of some host factors.

In the second manuscript, which was the main project of my project, we isolated and determined the protein composition of the *Salmonella*-containing vacuole, at different stages of its maturation. This identified hundreds of host proteins specifically and dynamically recruited to the SCV. Additionally, we followed the interactions of some host factors and intracellular compartments with the SCV, by fluorescence microscopy and large volume three-dimensional electron microscopy by FIB/SEM (focused ion beam/scanning electron tomography), and studied their functional role in the maturation of the SCV. This work showed that the SCV dynamically interacts with different host cell organelles, which is important both for vacuolar maturation and vacuolar membrane rupture. Moreover, SCV communication with different organelles affects intracellular *Salmonella* localization and growth.

Manuscript 1 – "Hierarchies of host factor dynamics at the entry site of *Shigella flexneri* during host cell invasion"

Soudeh Ehsani[1], José Carlos Santos[1,2], Cristina D. Rodrigues[1], Ricardo Henriques[3], Laurent Audry[1], Christophe Zimmer[3], Philippe Sansonetti[4,5], Guy Tran Van Nhieu[6,7], Jost Enninga[1]

1. Unit of Dynamics of Host-Pathogen Interactions, Institut Pasteur, Paris, France
2. Graduate Program in Areas of Basic and Applied Biology (GABBA), Universidade do Porto, Portugal
3. Group "Imagerie et Modélisation", Institut Pasteur, Paris, France; CNRS URA 2582
4. Unit "Pathogénie Microbienne Moléculaire", Institut Pasteur, Paris, France
5. INSERM unit 789, Paris, France
6. Interdisciplinary research group "Intercellular communication of microbial infection", College de France, Paris, France
7. INSERM unit 1050, Paris, France

Contribution to this manuscript

I contributed extensively for this work. Together with Soudeh Ehsani, we performed most of the experiments presented in the manuscript, except the ones presented in Figure 4 and Figure S2 (performed by Cristina Rodrigues and Ricardo Henriques), and Figure 6 (performed solely by Soudeh Ehsani). Data presented in Figures 3 and 5 was performed solely by myself. Together with Soudeh Ehsani and Jost Enninga, we assembled all figures, except Figures 4 and Figure S2. I also contributed to text editing and manuscript revision.

State of publication

Published in *Infection & Immunity*, in July 2012.

IAI
Journals.ASM.org

Hierarchies of Host Factor Dynamics at the Entry Site of *Shigella flexneri* during Host Cell Invasion

Soudeh Ehsani,[a] José Carlos Santos,[a,b] Cristina D. Rodrigues,[a] Ricardo Henriques,[c] Laurent Audry,[a] Christophe Zimmer,[c] Philippe Sansonetti,[d,e] Guy Tran Van Nhieu,[f,g] and Jost Enninga[a]

Group Dynamics of Host-Pathogen Interactions, Institut Pasteur, Paris, France[a]; Doctoral Program in Areas of Basic and Applied Biology (GABBA), Universidade do Porto, Porto, Portugal[b]; Group Imagerie et Modélisation, Institut Pasteur, Paris, France[c]; Unit Pathogénie Microbienne Moléculaire, Institut Pasteur, Paris, France[d]; INSERM Unit 789, Paris, France[e]; Interdisciplinary Research Group Intercellular Communication of Microbial Infection, College de France, Paris, France[f]; and INSERM Unit 1050, Paris, France[g]

***Shigella flexneri*, the causative agent of bacillary dysentery, induces massive cytoskeletal rearrangement, resulting in its entry into nonphagocytic epithelial cells. The bacterium-engulfing membrane ruffles are formed by polymerizing actin, a process activated through injected bacterial effectors that target host small GTPases and tyrosine kinases. Once inside the host cell, *S. flexneri* escapes from the endocytic vacuole within minutes to move intra- and intercellularly. We quantified the fluorescence signals from fluorescently tagged host factors that are recruited to the site of pathogen entry and vacuolar escape. Quantitative time lapse fluorescence imaging revealed simultaneous recruitment of polymerizing actin, small GTPases of the Rho family, and tyrosine kinases. In contrast, we found that actin surrounding the vacuole containing bacteria dispersed first from the disassembling membranes, whereas other host factors remained colocalized with the membrane remnants. Furthermore, we found that the disassembly of the membrane remnants took place rapidly, within minutes after bacterial release into the cytoplasm. Super-resolution visualization of galectin 3 through photoactivated localization microscopy characterized these remnants as small, specular, patchy structures between 30 and 300 nm in diameter. Using our experimental setup to track the time course of infection, we identified the *S. flexneri* effector IpgB1 as an accelerator of the infection pace, specifically targeting the entry step, but not vacuolar progression or escape. Together, our studies show that bacterial entry into host cells follows precise kinetics and that this time course can be targeted by the pathogen.**

Invasive pathogens such as *Shigella flexneri*, *Salmonella enterica*, or *Listeria monocytogenes* are capable of subverting host factors to induce their uptake into typically nonphagocytic epithelial and/or endothelial cells (32). This is achieved via bacterial constituents or adhesive molecules present on the pathogen surface, the secretion of soluble bacterial factors, or the translocation of effectors into the host cell through specialized molecular injection devices. Independent of the mode of interaction, the internalization process is rapid for all studied pathogens, requiring only a few minutes and featuring a complex and coordinated interplay between host and bacterial factors.

After ingestion of spoiled food or water, as few as 10 to 100 bacteria are sufficient to cause an infection resulting in mucosal ulceration and bloody diarrhea, qualifying *Shigella* as a potent enteroinvasive pathogen (20). Upon contact of *S. flexneri* with an epithelial cell, the injection of effectors through the type III secretion system (T3SS) leads to the formation of a signaling platform consisting of the bacterial translocon complex constituents IpaB and IpaC and the targeting of host factors through injected effectors (25, 37). Together, these induce a complex rearrangement of the cortical cytoskeletal components, resulting in the formation of lamelipodia that engulf the pathogen and lead to its uptake. These events are coordinated by bacterial effectors, e.g., IpgB1 and IpgB2, IpgD, or IpaC, and host factors, mainly the small GTPases of the Rho family, Rac, Cdc42, and kinases, such as Abl and Src (4, 7, 38). Apart from GTPases and kinases, other signaling molecules have been implicated in the entry process of *S. flexneri*, namely, inositol signaling, which is targeted by IpgD (7).

Examplarily, the bacterial effector IpgB1 mimics RhoG at the host plasma membrane and interferes with the ELMO/Dock180 pathway (12, 27). Furthermore, the homologous effector IpgB2, together with IpgB1, orchestrates bacterial entry through their GEF activities, which have been reported for both of them *in vitro* (11, 18). The activation of the GTPases induces members of the WASP family verprolin-homologous protein family (WAVE) that in turn activate the actin-nucleating Arp2-Arp3 complex. Additionally, it has been suggested that the C terminus of IpaC is involved in the activation of the kinase Src (24). In turn, Src and another tyrosine kinase, Abl, play a role in the bacterial entry process via the phosphorylation of CrkII at the plasma membrane, which leads to the recruitment of phosphorylated cortactin to the *S. flexneri* entry site (3, 5).

Upon internalization, *S. flexneri* is surrounded by an endocytic vacuole that is subsequently ruptured, thereby releasing the pathogen into the host cellular cytoplasm (6, 35). We have recently shown that the rupture happens within minutes after uptake and can be spotted using fluorescently labeled galectin 3 as a marker for the disassembled membranes (30, 34). It is believed that the membrane remnants are then processed into smaller ves-

Received 29 December 2011 **Returned for modification** 22 January 2012
Accepted 12 April 2012
Published ahead of print 23 April 2012
Editor: J. B. Bliska
Address correspondence to Jost Enninga, jostenn@pasteur.fr.
Supplemental material for this article may be found at http://iai.asm.org/.

doi:10.1128/IAI.06391-11

icles, and it has been shown that they are targeted to the autophagy machinery by the tethering of autophagy markers to the site of ruptured membranes, which in turn leads to the induction of signaling pathways (8). Further, it has been found that autophagy-associated signaling is also triggered from *S. flexneri* surrounded by septin structures termed septin cages (22, 23).

The dynamic recruitment of host factors to the forming vacuole and to the membrane remnants upon vacuolar disruption is still poorly understood. So far, only a few studies have tracked bacterial entry into living host cells in real time compared to investigations that used endpoint assays (2, 24, 29, 34). Therefore, we aimed at obtaining a more precise picture of the temporal events surrounding the entry of *S. flexneri*. HeLa cells were transfected with a set of host factors, and the time course of their tethering to the site of bacterial entry and the disassembly of the endocytic vacuole was monitored. This allowed us to delineate the functional hierarchies of host factor recruitment during the entry process, which involves different families of signaling molecules, namely, kinases or GTPases. We observed the simultaneous recruitment of the small GTPases Rac, RhoA, and Cdc42 and of the kinases Src and Abl to the site of bacterial entry, which contrasted with a specific sequence of events for their dispersal during the process of vacuolar rupture. Further, we show that the vacuolar membranes disassemble rapidly upon release of the pathogen into the cytoplasm. Finally, we revealed that the bacterial effector IpgB1 is responsible for the rapid entry of bacteria into the host and propose that it acts as a pacemaker of infection.

MATERIALS AND METHODS

Cell culture and infection assays. All cell culture reagents were purchased from Invitrogen unless otherwise stated. Human epithelial HeLa cells were cultured in Dulbecco's modified Eagle's medium (DMEM) supplemented with 10% (vol/vol) fetal bovine serum (FBS), 50 μg/ml penicillin, 50 μg/ml streptomycin, and 2 mM L-glutamine at 37°C, 5% CO_2. All live-cell fluorescence microscopy was performed in EM buffer (120 mM NaCl, 7 mM KCl, 1.8 mM $CaCl_2$, 0.8 mM $MgCl_2$, 5 mM glucose, 25 mM HEPES, pH 7.3).

Overnight bacterial cultures were inoculated at a 1/100 dilution in tryptic casein soy broth (TCSB) with the appropriate antibiotic if required and grown to an optical density at 600 nm (OD_{600}) of ~0.3. Before infection, the bacteria were washed with PBS and coated with poly-L-lysine (Sigma Corp.) at a final concentration of 10 μg/ml to facilitate bacterial adhesion to cells. After 10 min of incubation at room temperature, the bacteria were washed 2 times with PBS, resuspended in the medium of the cells that were prepared for infection, and used immediately.

Bacterial strains. The following *S. flexneri* strains were used: *S. flexneri* M90T (wild type), *S. flexneri* M90T expressing dsRed, BS176 (no virulence plasmid), an *ipgB1* strain (nonpolar mutant of the effector IpgB1), and the complemented *ipgB1*/pHA61 strain (these strains were described previously [11, 36, 19]). All bacterial strains were grown in TCSB at 37°C. The growth medium was supplemented with kanamycin (100 μg/ml) or ampicillin (50 μg/ml), depending on the resistance of the strain used.

Plasmids and transfection. For the expression of actin-mOrange, the mOrange coding sequence was inserted into the actin-EGFP-C3 plasmid by excising the enhanced green fluorescent protein (EGFP) sequence at the NheI/XhoI sites and inserting the mOrange sequence (the primers used were as follows: 5′, AGAGCTGCTAGCATGGTGAGCAAGGGCGAGGA, and 3′, AGAGTCCTCGAGATCTGAGTCCGGACTTCTACAGCTCGTCCATGC). The construct was verified by sequencing. For the expression of galectin 3-tandem Eos fluorescent protein (tdEos), the tdEos coding sequence was inserted in the peGFP-N1 plasmid (BD Biosciences Clontech) by excising the EGFP at the BamHI/NotI sites and inserting the tdEos sequence (the primers used were as follows: 5′, AGCTGGATCCATCCACCGGTCGCCACCATG, and 3′, AGTCGCGGCCGCTCTAGAGTCGCGGCCGCTTA) and by inserting the galectin 3 coding sequence at the KpnI/BamHI sites (the primers used were as follows: 5′, ATGCGGTACCCGCCACCATGGCAGACAATTTTTCGCTC, and 3′, GCATGGATCCGTATCATGGTATATGAAGCACT). The construct was verified by sequencing. The other plasmids have been described previously, as follows: pEGFP-galectin 3 (30), pEGFP-actin (24), pOrange-galectin 3 (34), pOrange-RhoA (34), pEYFP-RhoA (17), pEYFP-Rac1 (17), pOrange-Rac1 (34), pEGFP-Abl (5), and pEGFP-Src (24).

For transfection of samples that were processed for indirect immunofluorescence, HeLa cells were plated on 12-well plates containing glass coverslips at a density of 2×10^4 cells per coverslip (diameter, 12 mm; thickness, 0.13 to 0.17 mm) 24 h before transfection. For transfection of samples that were processed for live-cell imaging, HeLa cells were seeded into glass bottom dishes 35 mm in diameter at a density of 2×10^5 cells per dish (Mattek) or 96-well glass bottom plates (Nunc) at a density of 3×10^4 cells per plate 24 h before transfection.

Microscopy and image analysis. Bacterial invasion was measured in real time on a Leica DM or Nikon inverted microscope equipped with a heated stage, using a 40× N-Plan Objective for simultaneous phase-contrast imaging (Leica or Nikon), and fluorescence imaging was performed with excitation at 465 to 500 nm (fluorescein isothiocyanate [FITC]) and 532 to 554 nm (rhodamine), and emission was detected with 516- to 556-nm (FITC) and 573- to 613-nm (rhodamine) filters. Images were captured using a Cascade 512B camera or a CoolSnap2 camera (Roeper Scientific). Images were acquired in the two fluorescent channels and in *trans* every 30 s or 90 s. Time lapse series were analyzed with the freeware program ImageJ (http://rsb.info.nih.gov/ij/) and further processed using Excel (Microsoft).

Superresolution imaging. Glass coverslips (diameter, 18 mm; thickness, 1) were cleaned using acetone (high-grade pure) treatment for 1 h, followed by overnight treatment with a potassium hydroxide solution at 0.1 M and extensive cleaning with autoclaved ultrapure water.

HeLa cells were maintained in DMEM F-12 medium (without phenol red) supplemented with 4% FBS and 1% penicillin/streptomycin. Forty-eight hours before bacterial infection, HeLa cells were seeded on the treated coverslips and transfected with 1.5 μg of the plasmid galectin 3-tdEos. For the infection assay, *S. flexneri* M90T bacterial cultures were prepared as previously described. Galectin 3-tdEos-transfected cells were incubated for 45 min with *S. flexneri* M90T at a multiplicity of infection of 100. Afterward, samples were fixed with 2% paraformaldehyde for 30 min at 37°C, washed, and incubated with 0.5 μl of fluorescent beads (2 mM 0.1-μm TetraSpeck microspheres, fluorescent blue/green/orange/dark red; Invitrogen) for 30 min. For imaging, coverslips were mounted in PBS.

Photoactivated localization microscopy (PALM) imaging was performed on a home-made setup, previously described in detail (1, 15), based on a Nikon Ti-E eclipse microscope system. For tdEos activation and imaging, the system uses a solid-state laser with an emission wavelength at 488 nm (Spectra Physics, Japan) and diode lasers with emission wavelengths at 405 nm and 561 nm (Spectra Physics, Japan). Observations were performed with a 100× oil immersion objective (numerical aperture [NA], 1.49) and detected by an electron-multiplying charge-coupled device (EM-CCD) camera (Ixon DV887ECS-BV; Andor, Belfast, Northern Ireland). Imaging was performed with a final magnification of ×150, corresponding to a pixel size of 107 nm. Sequences of 50,000 to 100,000 wide-field fluorescence images compatible with PALM were acquired with a 50-ms exposure time. During acquisition of PALM image sequences, the 561-nm laser power was kept constant for readout of the tdEos activated state, and the 405-nm laser was pulsed at decreasing frequencies adjusted manually to maintain a stable number of active fluorophores per frame. The imaging parameters were set using the μManager freeware (http://www.micro-manager.org/), and laser control was achieved with custom software (15).

After acquisition, each sequence of raw diffraction-limited images was processed with ImageJ and QuickPALM (15). The QuickPALM software

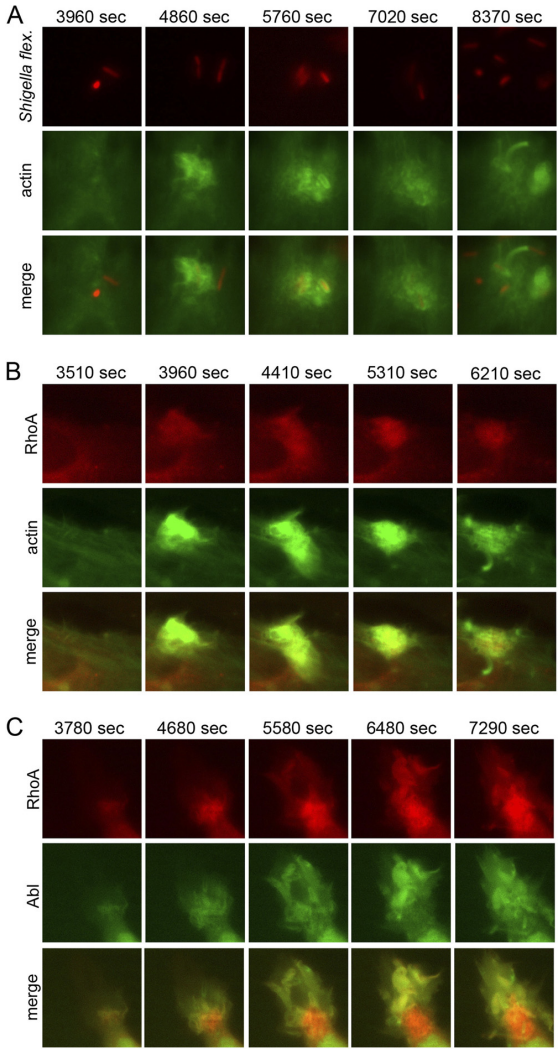

FIG 1 Sequential recruitment and dispersal of host molecules involved in the entry of *S. flexneri* into epithelial cells. (A) HeLa cells transfected with actin-EGFP were challenged with *S. flexneri* expressing dsRed and monitored by time lapse fluorescence microscopy. The recruitment of actin to the entry site highlights the successive internalization steps, bacterial contact, focus formation, collapse of the entry focus, and intracytoplasmic bacteria moving along actin tails. (B) Simultaneous tracking of host cellular actin and the small GTPase RhoA at the entry site shows that they are both recruited to the bacterial entry site at the same time. (C) Simultaneous tracking of the host cellular kinase Abl and the GTPase RhoA at the entry site shows that they are both recruited at the same time. Abl is tethered to the apical edges of the forming foci, whereas RhoA spreads diffusely through the focus and is enriched around the vacuole containing bacteria. Representative data from 5 to 10 independent experiments are shown.

computed the positions of individual molecules and reconstructed super-resolution images with an initial arbitrary pixel size of 10 nm by superimposing Gaussian spots with a full-width-Hald-maximum (FWHM) of 30 nm centered on these positions. The imaged fluorescent beads were used as fiducial markers for drift correction. To estimate the average resolution,

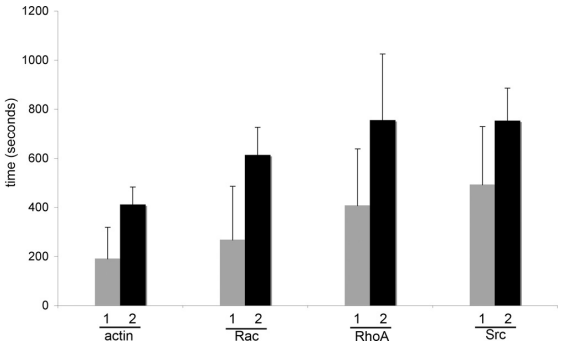

FIG 2 Quantification of the sequence of recruitment of bulk actin, small GTPases, and kinases to the entry site of *S. flexneri*. The images were quantified by thresholding from the image sequences displayed in Fig. 1 (see Materials and Methods for details). Actin, small GTPases, and kinases are rapidly recruited to the pathogen entry site (between 200 and 400 s after contact), and these factors reach their peak at the entry foci between 425 and 725 s after bacterial contact. The standard deviations (SD) (error bars) indicate high variance of the events temporally, making it impossible to delineate clear hierarchies of recruitment. 1, delay of host factor recruitment to the pathogen entry site upon bacterial contact; 2, time window between host factor recruitment and the time point with the peak of the individual foci before their disassembly. Data from 5 to 10 independent experiments are shown.

23 small clusters of galectin 3-tdEos were aligned by their center of mass, and the FWHM of the superimposed clusters was calculated, yielding an estimated resolution of 28 nm.

RESULTS

Numerous studies have described the recruitment of the host actin cytoskeleton, regulatory factors like small GTPases of the Rho family, and tyrosine kinases to the entry site of enteroinvasive bacteria, such as *Shigella* or *Salmonella* (9, 31). The studies discovered a growing family of host proteins involved in the entry process. We aimed at studying the spatiotemporal hierarchies between some representative host protein family members at the bacterial entry site throughout the successive steps of internalization during cell challenge with *S. flexneri* wild type and the *ipgB1* mutant strain.

Host proteins involved in cytoskeletal rearrangements are recruited simultaneously to the *S. flexneri* entry site. Figure 1A (for more detail, see Movie S1 in the supplemental material) displays a series of time lapse images of actin-GFP-transfected HeLa cells challenged with dsRed-expressing *S. flexneri*. These images confirm the well-documented massive actin rearrangements upon host cellular contact with the bacterium. We used such image series to establish a quantification procedure with the open-source software ImageJ to determine the time points when the accumulation of a host factor became detectable at the site of bacterial entry and when it reached its maximum at the entry site before the disassembly of the individual entry focus. These quantifications were performed in order to decipher the order of host factor recruitment at the bacterial entry site. As a control, we compared the bacterial entry kinetics in transfected cells with those of nontransfected cells and found no significant differences. We then went on to challenge HeLa cells with *S. flexneri* cotransfected with fluorescently tagged actin and members of the small GTPase family. Figure 1B (for more detail, see Movie S2 in the supplemental mate-

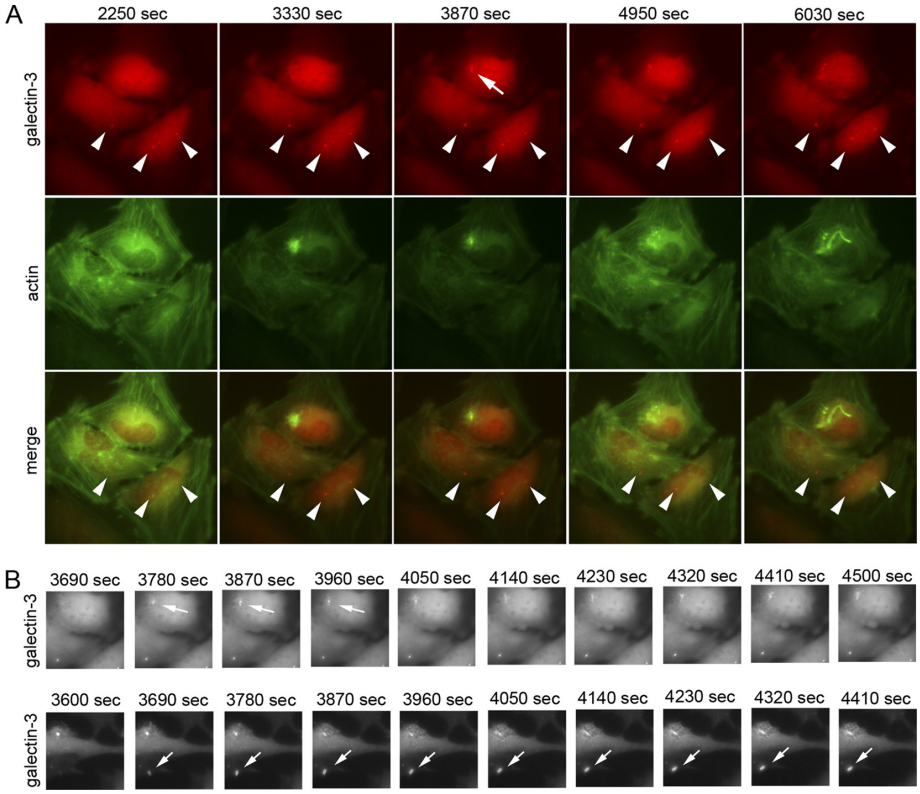

FIG 3 Rapid assembly and disassembly of galectin 3 around the ruptured membranes after vacuolar escape of *S. flexneri*. (A) Galectin 3 flags the membrane remnants upon vacuolar rupture of the pathogen. The remnants (indicated by the arrow) are typically present only for a few minutes upon membrane rupture and cannot be distinguished from background signal (arrowheads) at later time points. (B) In some instances, galectin 3 remains associated with the membrane remnants (arrows) for hours after escape from the vacuole. Representative data from at least 10 independent experiments are shown.

rial) shows that actin and RhoA are simultaneously recruited at the entry site upon challenge. Similar results were obtained with other small GTPases, such as Rac1 or Cdc42 (data not shown). Tyrosine kinase recruitment was exemplarily studied using Abl (Fig. 1C; for more detail, see Movie S3 in the supplemental material) and Src (24) (see Fig. S1 in the supplemental material) fused to EGFP. Cotransfection of Abl and RhoA showed that both were recruited to the bacterial entry site at the same time points; however, their localizations differed upon recruitment. Abl was located at the distal tips of the forming membrane ruffles, whereas the GTPases, such as RhoA, were spread throughout the entry focus or around the entering bacterium, as was previously shown for Src (24, 25). This was expected, since distinct functions during the entry process have previously been attributed to the different recruited host factors (25, 28).

Next, we quantified the fluorescence intensities at the *S. flexneri* entry sites, setting stringent thresholds in the ImageJ software. The time point of the start of host factor recruitment was determined as the time point when fluorescence values were at least 50% above the background levels before bacterial contact. Then, we determined the time span between this time point and the time point of bacterial contact that could be identified in the TRANS channel (1 in Fig. 2). Second, we measured the mean fluorescence intensity in the area of bacterial entry and determined the time point when it reached its maximum. We then subtracted the time point of bacterial contact from the time point when a maximum mean fluorescence intensity was present within the entry focus. This was used to determine the time it took to reach maximal host factor recruitment, coordinating the cytoskeletal rearrangements at the entry site (2 in Fig. 2). Figure 2 depicts the summary of these quantifications for the recruitment of actin, Rac1, RhoA, and Src. Strikingly, we found that all these factors are recruited simultaneously at the bacterial entry site upon bacterial contact, and the large standard deviations show pronounced variability at the single-cell level (Fig. 2, columns numbered 1). Further, recruitment of the analyzed host factors appeared rapidly upon contact, within 200 to 400 s. Similar results were obtained when analyzing the time it took to reach maximal recruitment of host factors to the entry foci. Here, we found again that the maxima were reached within similar time intervals for all measured host factors and that the standard deviations were pronounced for all analyzed scenarios, highlighting large variability in the kinetics of the entry process. We also realized that there is some variability in the diminishing of the recruited host factor signals at the entry site, e.g., the massive early actin recruitment disappeared before the RhoA sig-

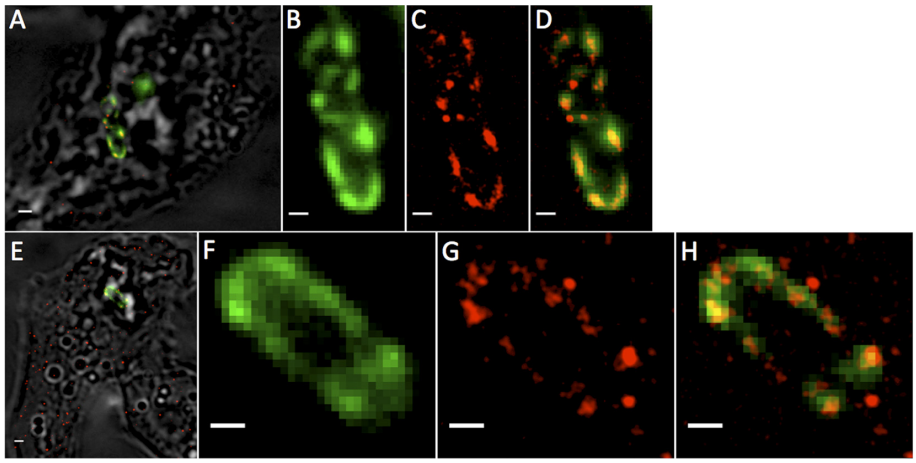

FIG 4 High-resolution analysis of disassembling vacuoles by superresolution microscopy. (A to H) HeLa cells transfected with galectin 3-tdEos fluorescent protein (tdEosFP) were infected with *S. flexneri* M90T. PALM shows galectin 3-tdEos being organized in heterogeneous patchy clusters in the bacterial enveloping vacuoles. The images correspond to two different acquisitions representative of a total of 7 cells from 2 independent experiments. (A and E) Merges of the bright-field (gray), wide-field epifluorescence (green), and superresolution PALM (red) images. (B to D and F to H) Zoomed images of the bacterial region. (B and F) Wide-field epifluorescence. (C and G) PALM imaging. (D and H) Merges of wide-field epifluorescence and PALM imaging. Scale bars: A and E, 1,000 nm; B to D and F to H, 500 nm.

nal in Fig. 1B. However, we have not been able to establish a reliable algorithm to quantify this phenomenon.

Disassembly of the ruptured vacuolar membrane remnants is highly dynamic. We went on to investigate the subsequent step of *S. flexneri* invasion, bacterial escape from the endocytic vacuole. In particular, we were interested in tracking the fate of the disassembling membranes that constituted the endocytic vacuole containing bacteria using the recently described marker galectin 3 (30). It has been shown that fluorescently tagged galectin 3 is recruited to the bacterial entry site within seconds after vacuolar rupture and that it targets the disassembling membranes surrounding the bacterium (30, 34). By cotransfecting HeLa cells with actin-EGFP and galectin 3-mOrange, we confirmed this rapid recruitment of galectin 3 to the entering bacteria, which highlights the ruptured membranes as "bacterial ghost-like" structures (Fig. 3A and B, top; see Movie S1 in the supplemental material for more details). Strikingly, our time lapse experiments demonstrated that the galectin 3 vacuolar-membrane-wrapping signal was very short-lived, disappearing within 5 to 15 min after bacterial escape from the vacuole (Fig. 3A, arrow). At later time points, the galectin 3 signal was similar to background signals in cells that were not invaded by *S. flexneri* (compare the specific signal, indicated by an arrow, and the nonspecific background signals, indicated by arrowheads, in Fig. 3A). In a few cases, galectin 3 highlighted the bacterial ghost-like structures for more than 30 min without disassembling into smaller membrane vesicles. However, it turned out to be difficult to quantify the extent of this phenomenon, due to the heterogeneity of the measured signal (Fig. 3B, arrows in the bottom row). Together, these findings show the rapid processing of the disassembling membranes at the bacterial entry site that are subsequently targeted to autophagy (8).

To analyze the membrane disassembly in more detail, we performed PALM, which achieves a 10-fold increase in resolution over the classical optical limit in microscopy (roughly 30 nm versus 300 nm) (1, 16). PALM imaging of the photoactivatable tdEos fused to galectin 3 was used to obtain superresolution insight into the cellular localization of the protein upon the rupture of the vacuole containing bacteria.

HeLa cells were transfected with galectin 3-tdEos and infected with *S. flexneri* M90T. We selected seven different individual fixed cells featuring visible galectin 3 staining accumulating around the ruptured membranes of the invading bacteria and superresolved them through PALM imaging. Two representative samples are shown in Fig. 4A to D (first example) and E to H (second example). PALM allowed us to discern small patchy accumulations of galectin 3 in the vicinity of the bacteria (Fig. 4C and G). Importantly, no structures with a lumen (resembling vesicles) could be observed. Further analyses of the cluster sizes of these small accumulations of galectin 3 permitted us to observe a distribution of sizes ranging from 30 nm (the estimated resolution of PALM images) to 300 nm in diameter (see Fig. S2 in the supplemental material). These structures are beyond the resolution limit of standard wide-field epifluorescence microscopy and thus cannot be accurately discerned by standard imaging methods (Fig. 4B and F). Larger clusters of galectin 3 with diameters between 100 and 200 nm are found predominantly in the vicinity of the disassembling bacterial vacuole, but not in the rest of the host cellular cytoplasm (see Fig. S2 in the supplemental material), indicating the vacuolar degradation surrounding the bacteria.

We then investigated the localization of the simultaneously recruited host factors (Fig. 1 and 2) at the site of the vacuole containing bacteria around the time of vacuolar escape. In contrast to their recruitment to the entry site, we found that the disassembly process showed a higher level of organization with regard to the temporal sequence of events. We found that the accumulated actin surrounding the bacteria within vacuoles diminished before the recruitment of galectin 3 (Fig. 5A and C; for more detail, see Movie S5 in the supplemental material). Interestingly, the galectin

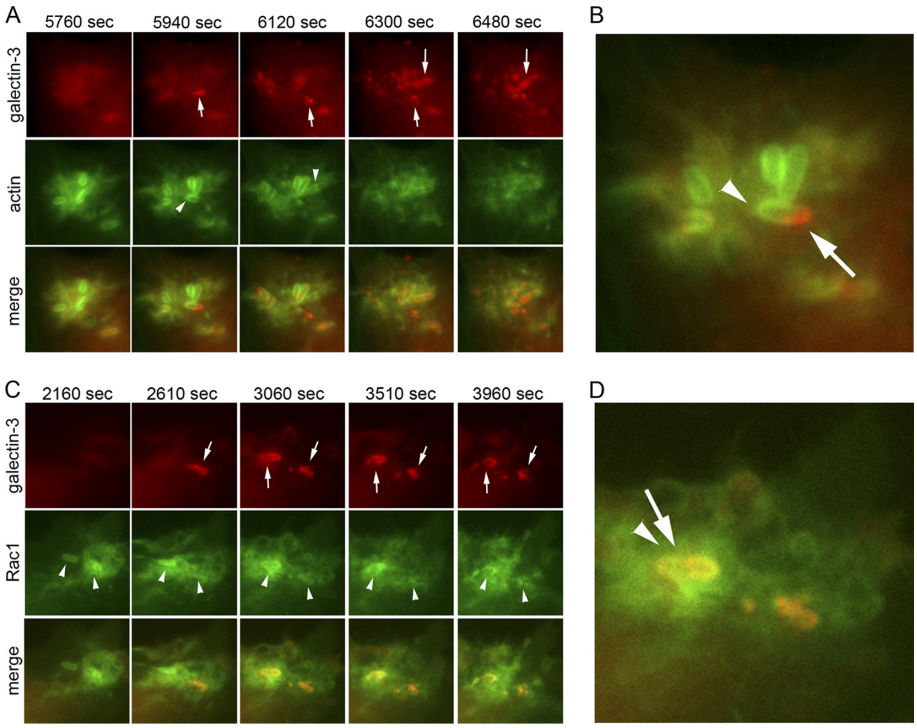

FIG 5 Hierarchies of host factor dispersal from the disassembling vacuoles. (A) HeLa cells were cotransfected with galectin 3-mOrange (arrow, red) and actin-EGFP (arrowhead, green) before being challenged with *S. flexneri*. Time lapse microscopy shows that actin disperses from the vacuole containing bacteria before its disassembly. Staining of the two factors is mutually exclusive. (B) Enlargement of an image from panel A. The arrowhead shows the actin signal (green) surrounding one moiety of a bacterium, and the arrow shows the other moiety with galectin 3 accumulation (red). (C) HeLa cells were cotransfected with galectin 3-mOrange (arrow, red) and Rac1-EGFP (arrowhead, green) before being challenged with *S. flexneri*. Rac1 surrounds the entering bacteria and remains associated with the galectin 3-positive membrane remnants after vacuolar rupture. (D) Enlargement of an image from panel C. The arrowhead and arrow point to the overlapping signal (orange) of Rac and galectin 3. Representative data from 7 independent experiments are shown.

3 (arrowheads) and actin (arrows) signals around the disassembling vacuoles were mutually exclusive. Furthermore, actin could not be readily identified around smaller vesicular structures potentially derived from disassembling vacuoles at later time points after the escape of *S. flexneri* to the cytoplasm. In contrast, the small GTPase Rac1 was also recruited to the vacuole containing bacteria; however, it remained located around the membrane remnants upon vacuolar rupture, colocalizing with galectin 3 (Fig. 5B and D; for more detail, see Movie S6 in the supplemental material). The tyrosine kinase Src (24) (see Fig. S1 in the supplemental material) is also recruited to the *Shigella*-containing vacuole, but this event was not seen with the kinase Abl and the small GTPase RhoA, which were both recruited rather diffusely or at the distal ends of the forming entry foci (Fig. 1). Together, these findings show that, despite simultaneous recruitment of the investigated host factors to the entering bacteria, the sequence of events during vacuolar disassembly appear to be temporally well organized.

IpgB1 accelerates the pace of invasion by *S. flexneri*. It has been reported that the *S. flexneri* T3SS effector IpgB1 mimics small GTPases to promote their entry into epithelial host cells (11, 12, 27). Using low multiplicities of infection (MOIs) (between 1 and 5) and following bacterial internalization at successive time points by gentamicin protection assay, we found that the *ipgB1* strain showed reduced entry. However, increasing the load of challenging bacteria or increasing the time periods of infection impeded the readout of this endpoint assay (data not shown). Therefore, we chose to track the dynamics of the time course of internalization and the recruitment of host factors to the bacterial entry site using the *ipgB1* mutant with the aim of measuring the effects on the entry kinetics. Performing time lapse microscopy on HeLa cells transfected with the host factors shown in Fig. 1 and 2, we found that the *ipgB1* mutant was able to enter host cells; however, the time periods of host factor recruitment to the bacterial contact site and entry were massively reduced (Fig. 6A and C; see Fig. S3 and Movie S7 in the supplemental material) compared to the wild-type bacteria (Fig. 6B and C; see Fig. S3 in the supplemental material). The wild-type phenotype was restored when the *ipgB1* complemented strain was used (see Fig. S3 in the supplemental material).

We also tested whether IpgB1 affected the subsequent step of vacuolar maturation and escape of the bacteria into the cytoplasm. To do this, we performed time lapse microscopy on HeLa cells coexpressing fluorescent actin and galectin 3, challenged with either the wild-type, *ipgB1*, or complemented strain (Fig. 7). Again, we found that the entry of the *ipgB1* strain was delayed (Fig. 7A;

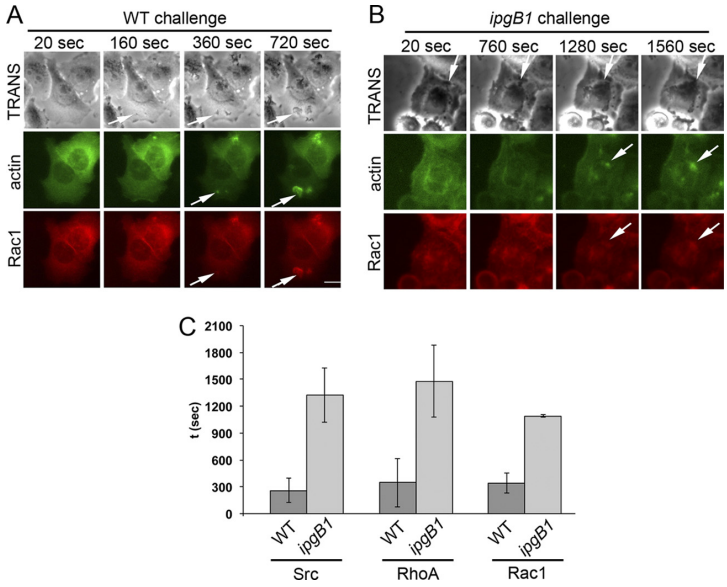

FIG 6 The *S. flexneri ipgB1* strain enters HeLa cells, but at a reduced rate. (A) Time lapse microscopy of cells cotransfected with actin and Rac1 and challenged with the *S. flexneri* wild-type strain. Arrows show bacterial entry sites. (B) Cells transfected similarly to those in panel A and challenged with an *S. flexneri ipgB1* mutant. Arrows show bacterial entry sites. (C) Quantification of the entry dynamics of the *S. flexneri* wild-type (WT) and *ipgB1* strains was performed using the time-lapse image series. Data from 5 independent experiments are shown. The error bars indicate SD.

see Movie S8 in the supplemental material). Interestingly, we identified some actin accumulation around the bacteria in contact with the host plasma membrane (Fig. 7A, middle; for more detail see Fig. S4 in the supplemental material), hinting at the involvement of multiple pathways for actin cytoskeletal rearrangement. Quantifying the time course of vacuolar escape, we were not able to measure significant differences between the *ipgB1*, the wild-type, and the complemented strains (Fig. 7B). In conclusion, the data presented in Fig. 6 and 7 suggest that IpgB1 represents a bacterial T3SS effector that accelerates the pace of *S. flexneri* entry into host cells as a means to boost bacterial infectivity but that it does not impact the subsequent steps.

DISCUSSION

Using time lapse microscopy, we demonstrated the simultaneous recruitment of host small GTPases and kinases to the site of *S. flexneri* entry into epithelial cells. Even though it is evident that bacterial invasion has to be highly organized, the functional hierarchies between the involved host factors have not been identified with precision (2, 7). So far, hierarchies of small GTPases have been described only in the case of *Salmonella* infection (28, 29).

Simultaneous host factor recruitment (Fig. 1 and 2) may call into question the importance of strict hierarchies during cellular invasion or may highlight the fact that the entry process is following not only one pathway, but multiple pathways, as previously proposed for *S. enterica* (13, 14). However, it also highlights the limitations of the performance of our microscopes with regard to both spatial and temporal resolution. Another fact that has to be considered is the activation of the signaling molecules involved; for example, GTPases can switch between GDP- and GTP-bound states, and kinases can be activated via phosphorylation. Such activities have already been taken into account by some studies on host-pathogen interactions, for example, in the case of *Yersinia*, using functionalized fluorescence resonance energy transfer (FRET) probes for the GTP state of small GTPases (39). Nevertheless, these studies require a high level of experimental sophistication, impeding its broad use throughout the scientific community. Considering the manifold and seemingly contradictory functions of the injected bacterial effectors on the host, such as actin polymerization via IpaC and its depolymerization via IpaA, we suggest that future studies will be required to reveal the precise recruitment of host factors and their dispersal (24). This will be facilitated once the precise enzymatic functions of the injected effectors have been revealed.

It is possible to track the step of vacuolar escape of *S. flexneri* with more precision. Recently, we have shown that this event takes place rapidly upon internalization (26, 34). Vacuolar escape has also been found for other cytoplasmic bacteria, for example, *Listeria* and *Rickettsia* (35). Strikingly, in this study, we show the rapid disassembly of the membrane remnants (Fig. 3) that have been reported to be coated with autophagy markers upon vacuolar rupture (8). This shows that the signaling events leading to the "digestion" of the membrane remnants have to be very rapid, efficient, and transient. PALM microscopy revealed the heterogeneous, patchy nature of the membrane remnants (Fig. 4). First, we found that the disassembled membranes were not hollow, highlighting their multilayered or micellar organization. Second, their resolvable size distribution spanned 30 to 300 nm (see Fig. S1 in the supplemental material). Based on these observations, we suggest that the membrane remnants are eventually disassembled or recycled, not only by a single mechanism, but by multiple mech-

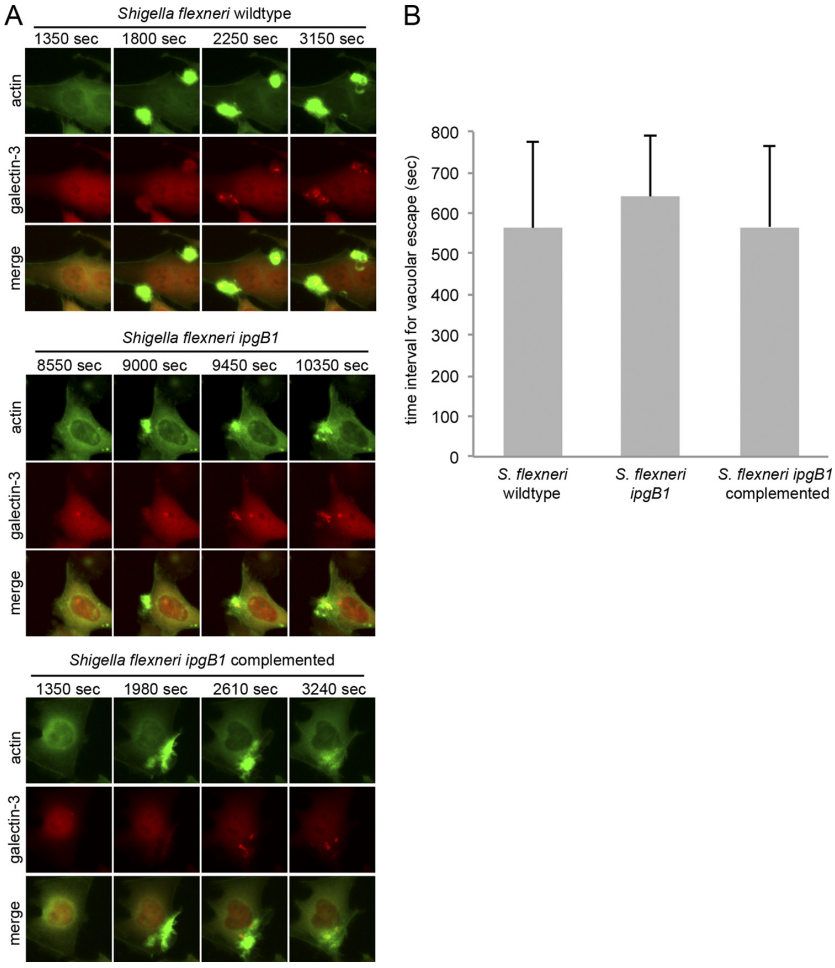

FIG 7 Effects of *Shigella* IpgB1 on entry and vacuolar disassembly. (A) Time lapse microscopy of HeLa cells cotransfected with actin-EGFP and galectin 3-mOrange challenged with the wild-type strain, with the *ipgB1*strain, or with the *ipgB1* strain complemented with IpgB1. The *ipgB1* mutant escaped efficiently from the endocytic vacuole. (B) Quantification of the time intervals between entry focus formation and escape of *S. flexneri* wild-type, *S. flexneri ipgB1*, and complemented strains from vacuoles. The wild-type bacteria escaped from the vacuoles at the same rate as the *ipgB1* mutant. Representative data from 4 independent experiments are shown. The error bars indicate SD.

anisms. Further, it is likely that the heterogeneous vesicular remnants result in the induction of multiple signaling pathways.

Taking advantage of our single-cell-based assays, we also found that some bacteria remained vacuole bound in vesicles coated with actin. It would be interesting to investigate the fate of these vacuole-bound bacteria, for example, if they are also targeted to the autophagy pathway. So far, it has been reported that cytoplasmic bacterial pathogens can be trapped within septin cages that send specific signals to trigger autophagy (22, 23). In addition to these signaling events, we suggest that future studies investigate whether septins can also be recruited to *S. flexneri* trapped within actin-coated vacuoles and whether the signals emanating from the trapped vacuolar bacteria are different from the signals emanating from cytoplasmic bacteria trapped in septin cages.

Where *S. flexneri* succeeded in escaping from the endocytic vacuoles, we noted that the dispersal of the host factors surrounding the cytoplasmic escaping bacteria appeared to be more organized than the recruitment during the initial steps of entry (Fig. 5). Since the membrane remnants appear to be targeted to the autophagy machinery, it will be important to investigate whether the sequential recruitment and dispersal of host factors around these remnants impacts the signaling cascades emanating from them.

Challenging host cells with a number of bacterial mutants, for example, with the translocon component IpaB or IpaC, results in very little or no invasion of the host cells (10). In contrast, mutant strains for other effectors show attenuated and subtle invasion phenotypes. One of these is the GEF IpgB1 that interferes with the ELMO/Dock180 pathway at the host plasma membrane upstream of the small GTPases (12, 27). An *S. flexneri* mutant strain for IpgB1 and IpgB2 was as invasive as the wild-type strain, indicating

that these homologous effectors have contradictory functions (11). In this work, we show that IpgB1 increases the pace of bacterial invasion, and we propose that the attenuated invasion phenotype of the *ipgB1* strain is caused by an alteration of the overall invasion time course (Fig. 6). This identified a bacterial T3SS effector as a pacemaker for infection targeting one precise step of the entry process. Strikingly, subsequent steps, such as the delay between entry and vacuolar escape, were not affected in the *ipgB1* mutant strain (Fig. 7). Often, loss-of-function studies of pathogen invasion, either using mutants or performing gene silencing via small interfering RNAs, result in phenotypes with a somewhat reduced but far from complete loss of infectivity (21). This can be a result of cellular plasticity or redundancy of host factor function. For example, this has been shown for *S. enterica*, which enters host cells via a pathway including the Arp2-Arp3 complex or via a myosin II-dependent pathway (13, 14). Nevertheless, pathway plasticity/redundancy is only one explanation of attenuated phenotypes. Consequently, we suggest that future studies should focus on the implication of merely kinetic effects of invasion, and we propose that time lapse investigations are perfectly suited for such studies. We are convinced that such kinetic studies will shift our idea of the functions of numerous bacterial effectors and involved host factors during the dynamic interplay between pathogens and their hosts.

Our results indicate the rapidity of events around the entering pathogens and also highlight the fact that perturbation of the system results in altered time courses of the invasion process. Microscopy-based high-throughput screens have become widely popular to investigate host-pathogen interactions in single cells (33). For the most part, they are performed as endpoint assays yielding only a single time point of the investigated events. Screens performed by different research groups investigating the same phenomenon have yielded different, even opposing, results (33). One possible explanation lies in the limitations of the assays used for the studies. Having described galectin 3 as a marker for vacuolar rupture, our work underlines the fact that it is particularly suited for time lapse investigation (30). On the other hand, the rapid disassembly of the membrane remnants upon rupture hampers efficient signal detection at later time points of infection (Fig. 3). Therefore, care must be taken in choosing the appropriate time points when using galectin 3 in endpoint assays in fixed samples.

ACKNOWLEDGMENTS

We thank C. Parsot, R. Tsien, J. Swanson, and A. M. Pendergast for providing us with plasmids and/or bacterial strains. We are particularly thankful to M. Lelek for support in the PALM experiments. We acknowledge the members of the PFID at the Institut Pasteur for excellent microscopy support.

S.E. was supported by a grant from the Fondation Schlumberger pour l'Education et la Recherche. J.C.S. and C.D.R. were the recipients of fellowships from the Portuguese Fundação para a Ciência e Tecnologia, FCT (SFRH/BD/51006/2010 and SFRH/BPD/41004/2007, respectively). C.D.R. is presently a Marie Curie fellow.

REFERENCES

1. **Betzig E, et al.** 2006. Imaging intracellular fluorescent proteins at nanometer resolution. Science **313**:1642–1645.
2. **Bobard A, Mellouk N, Enninga J.** 2011. Spotting the right location—imaging approaches to resolve the intracellular localization of invasive pathogens. Biochim. Biophys. Acta **1810**:297–307.
3. **Bougneres L. Girardin SE, et al.** 2004. Cortactin and Crk cooperate to trigger actin polymerization during Shigella invasion of epithelial cells. J. Cell Biol. **166**:225–235.
4. **Bourdet-Sicard R, et al.** 1999. Binding of the Shigella protein IpaA to vinculin induces F-actin depolymerization. EMBO J. **18**:5853–5862.
5. **Burton EA, Plattner R, Pendergast AM.** 2003. Abl tyrosine kinases are required for infection by Shigella flexneri. EMBO J. **22**:5471–5479.
6. **Clerc P, Sansonetti PJ.** 1987. Entry of Shigella flexneri into HeLa cells: evidence for directed phagocytosis involving actin polymerization and myosin accumulation. Infect. Immun. **55**:2681–2688.
7. **Dunn JD, Valdivia RH.** 2010. Uncivil engineers: Chlamydia, Salmonella and Shigella alter cytoskeleton architecture to invade epithelial cells. Future Microbiol. **5**:1219–1232.
8. **Dupont N, et al.** 2009. Shigella phagocytic vacuolar membrane remnants participate in the cellular response to pathogen invasion and are regulated by autophagy. Cell Host Microbe **6**:137–149.
9. **Ehsani S, Rodrigues CD, Enninga J.** 2009. Turning on the spotlight—using light to monitor and characterize bacterial effector secretion and translocation. Curr. Opin. Microbiol. **12**:24–30.
10. **Enninga J, Mounier J, Sansonetti P, Tran Van Nhieu G.** 2005. Secretion of type III effectors into host cells in real time. Nat. Methods **2**:959–965.
11. **Hachani A, et al.** 2008. IpgB1 and IpgB2, two homologous effectors secreted via the Mxi-Spa type III secretion apparatus, cooperate to mediate polarized cell invasion and inflammatory potential of Shigella flexenri. Microbes Infect. **10**:260–268.
12. **Handa Y, et al.** 2007. Shigella IpgB1 promotes bacterial entry through the ELMO-Dock180 machinery. Nat. Cell Biol. **9**:121–128.
13. **Hanisch J, et al.** 2010. Molecular dissection of Salmonella-induced membrane ruffling versus invasion. Cell Microbiol. **12**:84–98.
14. **Hanisch J, et al.** 2011. Activation of a RhoA/myosin II-dependent but Arp2/3 complex-independent pathway facilitates Salmonella invasion. Cell Host Microbe **9**:273–285.
15. **Henriques R, et al.** 2010. QuickPALM: 3D real-time photoactivation nanoscopy image processing in ImageJ. Nat. Methods **7**:339–340.
16. **Hess ST, Girirajan TP, Mason MD.** 2006. Ultra-high resolution imaging by fluorescence photoactivation localization microscopy. Biophys. J. **91**:4258–4272.
17. **Hoppe AD, Swanson JA.** 2004. Cdc42, Rac1, and Rac2 display distinct patterns of activation during phagocytosis. Mol. Biol. Cell **15**:3509–3519.
18. **Huang Z, et al.** 2009. Structural insights into host GTPase isoform selection by a family of bacterial GEF mimics. Nat. Struct. Mol. Biol. **16**:853–860.
19. **Konradt C, et al.** 2011. The Shigella flexneri type three secretion system effector IpgD inhibits T cell migration by manipulating host phosphoinositide metabolism. Cell Host Microbe **9**:263–272.
20. **Kotloff KL, et al.** 1999. Global burden of Shigella infections: implications for vaccine development and implementation of control strategies. Bull. World Health Organ. **77**:651–666.
21. **Misselwitz B, et al.** 2011. RNAi screen of Salmonella invasion shows role of COPI in membrane targeting of cholesterol and Cdc42. Mol. Syst. Biol. **7**:474.
22. **Mostowy S, et al.** 2010. Entrapment of intracytosolic bacteria by septin cage-like structures. Cell Host Microbe **8**:433–444.
23. **Mostowy S, et al.** 2011. p62 and NDP52 proteins target intracytosolic Shigella and Listeria to different autophagy pathways. J. Biol. Chem. **286**:26987–26995.
24. **Mounier J, et al.** 2009. The IpaC carboxyterminal effector domain mediates Src-dependent actin polymerization during Shigella invasion of epithelial cells. PLoS Pathog. **5**:e1000271. doi:10.1371/journal.ppat.1000271.
25. **Nhieu GT, Enninga J, Sansonetti P, Grompone G.** 2005. Tyrosine kinase signaling and type III effectors orchestrating Shigella invasion. Curr. Opin. Microbiol. **8**:16–20.
26. **Nothelfer K, Dias Rodrigues C, Bobard A, Phalipon A, Enninga J.** 2011. Monitoring Shigella flexneri vacuolar escape by flow cytometry. Virulence **2**:54–57.
27. **Ohya K, Handa Y, Ogawa M, Suzuki M, Sasakawa C.** 2005. IpgB1 is a novel Shigella effector protein involved in bacterial invasion of host cells. Its activity to promote membrane ruffling via Rac1 and Cdc42 activation. J. Biol. Chem. **280**:24022–24034.
28. **Patel JC, Galan JE.** 2006. Differential activation and function of Rho GTPases during Salmonella-host cell interactions. J. Cell Biol. **175**:453–463.
29. **Patel JC, Galan JE.** 2008. Investigating the function of Rho family GTPases during Salmonella/host cell interactions. Methods Enzymol. **439**:145–158.

30. **Paz I, et al.** 2010. Galectin-3, a marker for vacuole lysis by invasive pathogens. Cell Microbiol. **12**:530–544.
31. **Perrett CA, Jepson MA.** 2007. Applications of cell imaging in Salmonella research. Methods Mol. Biol. **394**:235–273.
32. **Pizarro-Cerda J, Cossart P.** 2006. Bacterial adhesion and entry into host cells. Cell **124**:715–727.
33. **Prudencio M, Lehmann MJ.** 2009. Illuminating the host—how RNAi screens shed light on host-pathogen interactions. Biotechnol. J. **4**:826–837.
34. **Ray K, et al.** 2010. Tracking the dynamic interplay between bacterial and host factors during pathogen-induced vacuole rupture in real time. Cell Microbiol. **12**:545–556.
35. **Ray K, Marteyn B, Sansonetti PJ, Tang CM.** 2009. Life on the inside: the intracellular lifestyle of cytosolic bacteria. Nat. Rev. Microbiol. **7**:333–340.
36. **Sansonetti PJ, Ryter A, Clerc P, Maurelli AT, Mounier J.** 1986. Multiplication of Shigella flexneri within HeLa cells: lysis of the phagocytic vacuole and plasmid-mediated contact hemolysis. Infect. Immun. **51**: 461–469.
37. **Schroeder GN, Hilbi H.** 2008. Molecular pathogenesis of Shigella spp.: controlling host cell signaling, invasion, and death by type III secretion. Clin. Microbiol. Rev. **21**:134–156.
38. **Terry CM, et al.** 2008. The C-terminus of IpaC is required for effector activities related to Shigella invasion of host cells. Microb. Pathog. **45**:282–289.
39. **Wong KW, Mohammadi S, Isberg RR.** 2006. Disruption of RhoGDI and RhoA regulation by a Rac1 specificity switch mutant. J. Biol. Chem. **281**: 40379–40388.

Supplemental information from Manuscript 1

Supplemental figure 1 Ehsani et al

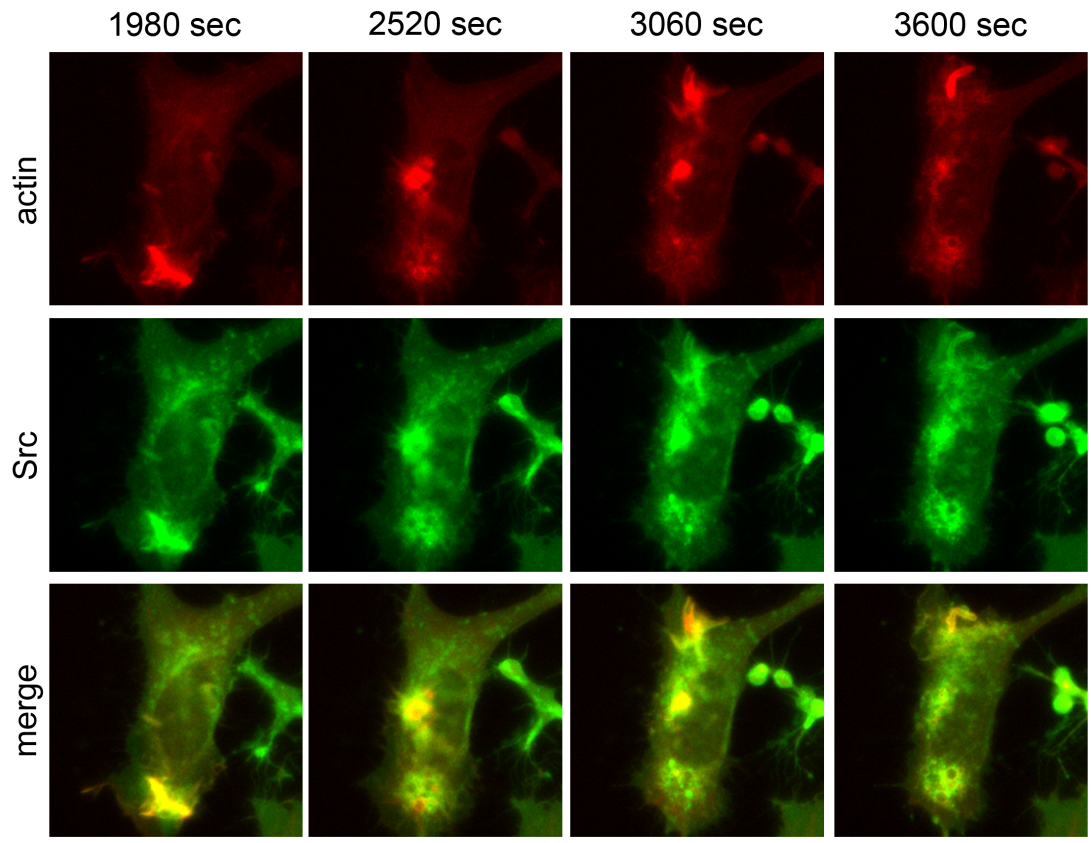

Sequential recruitment and dispersal of host Src in the entry of *S. flexneri* into epithelial cells.

HeLa cells co-transfected with actin-mOrange (red) and Src-GFP (green) were challenged with *S. flexneri* M90T afaI and monitored by time-lapse fluorescent microscopy. Both host factors are recruited to the bacterial entry site at the same time, and are then also tethered to the bacterial-containing vacuole.

Representative data is shown from 3 independent experiments.

Supplemental figure 2 Ehsani et al

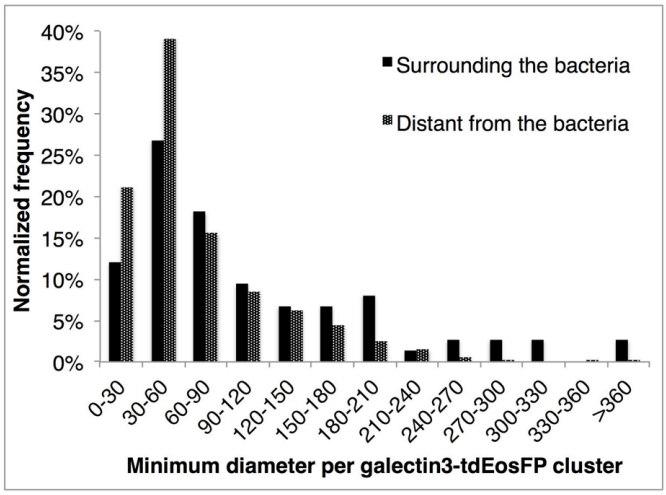

Histogram of the minimum diameters of galectin-3-tdEosFP clusters both surrounding and distant from the infecting *Shigella flexneri* M90T bacteria inside HeLa cells.

Analysis done over 4 cells visualized by PALM super-resolution microscopy in similar conditions. Minimum diameter calculated as the minimum distance between any two points along the individual clusters boundary.

Supplemental figure 3 Ehsani et al

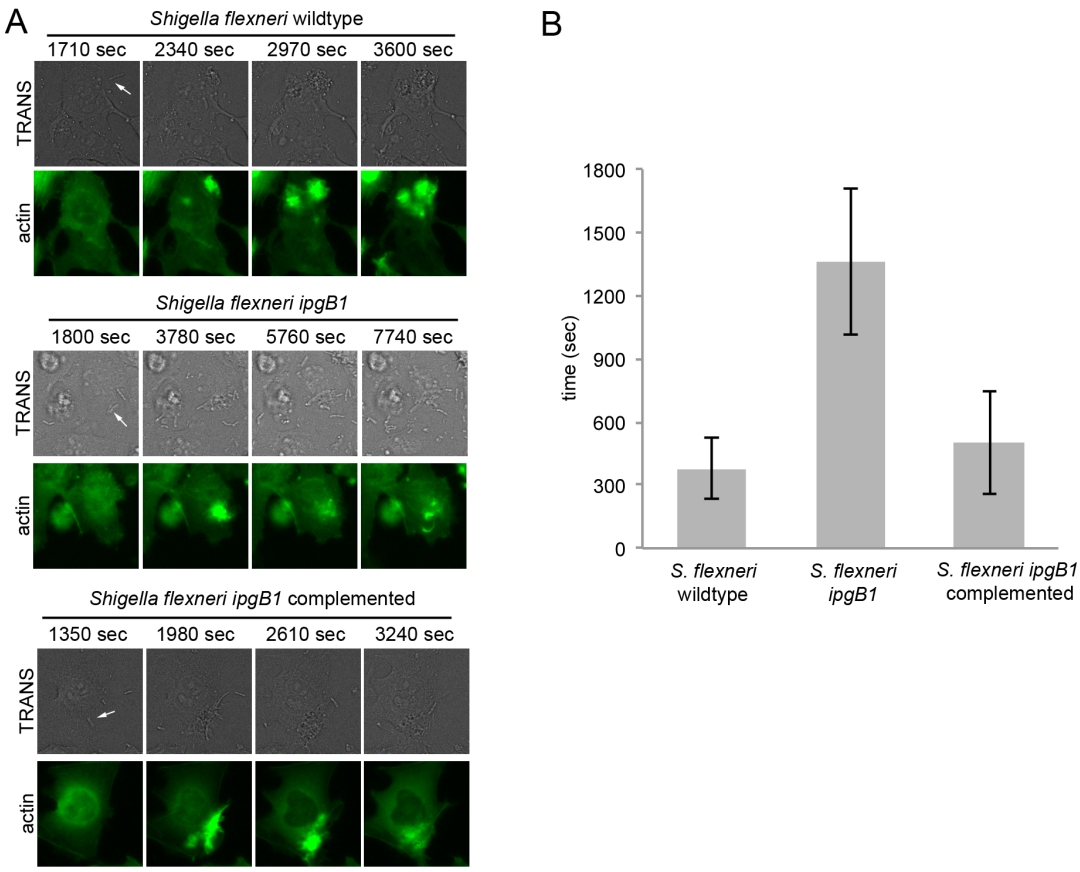

The effect of *S. flexneri* IpgB1 on bacterial entry into HeLa cells.

A) Time-lapse microscopy of cells transfected with actin-eGFP and challenged either with *S. flexneri* wildtype, *ipgB1* or the complemented strain. Arrows point to the event of bacterial contact with the host cell, at the indicated time point.

B) Quantification of the time interval between bacterial contact with the host cell and focus onset for *S. flexneri* wildtype, *S. flexneri ipgB1* and the corresponding complemented strain.

Data is shown from 3 independent experiments, error bars are SD.

Supplemental figure 4 Ehsani et al

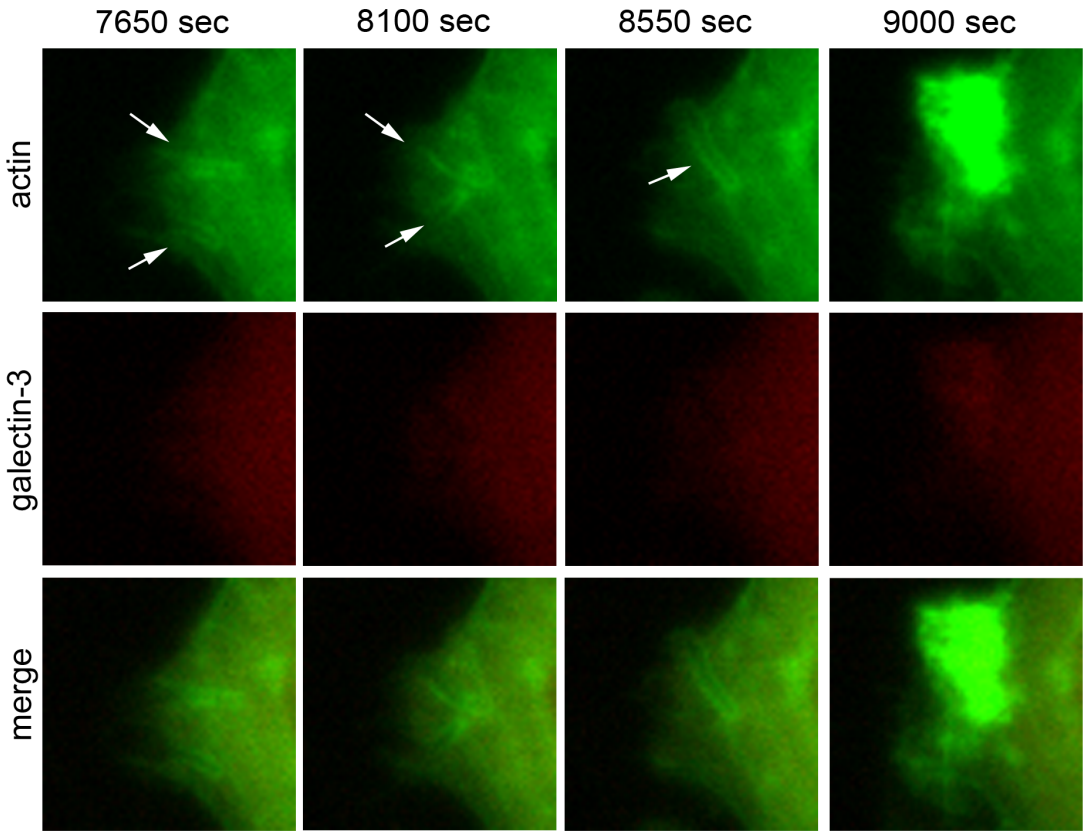

Entry of *S. flexneri ipgB1* into HeLa cells.

Upon contact of the bacteria with the host cell the entry is delayed when comparing to the wildtype strain (see **figure 6** and **supplemental figure 3**). During this time period there is the accumulation of actin around the bacteria in contact with the host plasma membrane (arrows).

Data is shown from 5 independent experiments.

Supplemental Movie Legends

Movie S1. Time-lapse movie corresponding to Fig. 1A: Infection of actin-GFP-transfected cells with *Shigella flexneri* expressing the dsRed protein.

Movie S2. Time-lapse movie corresponding to Fig. 1B: HeLa cells cotransfected with actin-eGFP and RhoA-mOrange challenged with *Shigella flexneri*.

Movie S3. Time-lapse movie corresponding to Fig. 1C: HeLa cells cotransfected with RhoA-mOrange and Abl-eGFP challenged with *Shigella flexneri*.

Movie S4. Time-lapse movie corresponding to Fig. 3: HeLa cells cotransfected with actin-eGFP and galectin-3–mOrange challenged with *Shigella flexneri*.

Movie S5. Time-lapse movie corresponding to Fig. 5A: HeLa cells cotransfected with galectin-3–mOrange and actin-eGFP challenged with *Shigella flexneri*.

Movie S6. Time-lapse movie corresponding to Fig. 5B: HeLa cells cotransfected with Rac1-citrin and galectin-3–mOrange challenged with *Shigella flexneri*.

Movie S7. Time-lapse movie corresponding to Fig. 6A: HeLa cells cotransfected with Rac1-mOrange and actin-eGFP challenged with the *ipgB1* mutant.

Movie S8. Time-lapse movie corresponding to Fig. 7A: HeLa cells cotransfected with actin-eGFP and galectin-3–mOrange challenged with the *ipgB1* mutant.

Movies S1-**S8** are shown on the Electronic Annex, on the attached CD.

Manuscript 2 – "The COPII complex and lysosomal VAMP7 determine intracellular *Salmonella* localization and growth"

José Carlos Santos[1,2], Magalie Duchateau[3], Jennifer Fredlund[1], Allon Weiner[1], Adeline Mallet[4], Christine Schmitt[4], Mariette Matondo[3], Véronique Hourdel[3], Julia Chamot-Rooke[3,5] and Jost Enninga[1]

1. Unit of Dynamics of Host-Pathogen Interactions, Institut Pasteur, Paris, France
2. Graduate Program in Areas of Basic and Applied Biology (GABBA), Universidade of Porto, Portugal
3. Structural Mass Spectrometry and Proteomics Unit, Institut Pasteur, Paris, France
4. Plate-forme Microscopie Ultrastructurale, Institut Pasteur, Paris, France
5. CNRS UMR3528, Paris, France

Contribution to this manuscript

For this manuscript, I contributed to all parts of the work. For nearly one and a half years I developed and optimized the protocol for the biochemical purification of SCVs, in parallel with the assay for assessing SCV integrity. In collaboration with Magalie Duchateau, from the Structural Mass Spectrometry and Proteomics Unit of the Institut Pasteur, we optimized the best conditions to analyze the SCV enriched fraction by LC-MS/MS. The quantitative analysis of the SCV proteome was performed by Mariette Matondo and Véronique Hourdel. Nonetheless, I also extensively discussed the methodologies for data analysis with them, Julia Chamot-Rooke and Jost Enninga. I performed the evaluation of hyper-replicating *Salmonella* together with Jennifer Fredlund. For the CLEM, I imaged the samples by fluorescence spinning disk confocal microscopy, Christine Schmitt prepared the Epon blocks and Adeline Mallet performed the FIB/SEM acquisition. All these steps were performed with crucial help from Allon Weiner, who also helped me and taught me how to do the data correlation, analysis and segmentation with the Amira software. I prepared all the figures presented in the manuscript and I wrote the entire manuscript, with the proofreading of Jennifer Fredlund and Jost Enninga.

State of publication

Accepted for publication in *Cellular Microbiology*, in June 2015.

Cellular Microbiology (2015) doi:10.1111/cmi.12475

The COPII complex and lysosomal VAMP7 determine intracellular *Salmonella* localization and growth

José Carlos Santos,[1,2] Magalie Duchateau,[3] Jennifer Fredlund,[1] Allon Weiner,[1] Adeline Mallet,[4] Christine Schmitt,[4] Mariette Matondo,[3] Véronique Hourdel,[3] Julia Chamot-Rooke[3,5] and Jost Enninga[1]*

[1]*Unit of Dynamics of Host-Pathogen Interactions, Institut Pasteur, Paris, France.*
[2]*Graduate Program in Areas of Basic and Applied Biology (GABBA), University of Porto, Porto, Portugal.*
[3]*Structural Mass Spectrometry and Proteomics Unit, Institut Pasteur, Paris, France.*
[4]*Plate-forme Microscopie Ultrastructurale, Institut Pasteur, Paris, France.*
[5]*CNRS UMR3528, Paris, France.*

Summary

Salmonella **invades epithelial cells and survives within a membrane-bound compartment, the *Salmonella*-containing vacuole (SCV). We isolated and determined the host protein composition of the SCV at 30 min and 3 h of infection to identify and characterize novel regulators of intracellular bacterial localization and growth. Quantitation of the SCV protein content revealed 392 host proteins specifically enriched at SCVs, out of which 173 associated exclusively with early SCVs, 124 with maturing SCV and 95 proteins during both time-points. Vacuole interactions with endoplasmic reticulum-derived coat protein complex II vesicles modulate early steps of SCV maturation, promoting SCV rupture and bacterial hyper-replication within the host cytosol. On the other hand, SCV interactions with VAMP7-positive lysosome-like vesicles promote *Salmonella*-induced filament formation and bacterial growth within the late SCV. Our results reveal that the dynamic communication between the SCV and distinct host organelles affects both intracellular *Salmonella* localization and growth at successive steps of host cell invasion.**

Received 15 April, 2015; revised 22 May, 2015; accepted 12 June, 2015. *For correspondence. E-mail jostenn@pasteur.fr; Tel. (+33) 1 44 38 94 13; Fax (+33) 1 40 61 35 83.

Introduction

Salmonella enterica serovar Typhimurium (*Salmonella*) is a Gram-negative enteric pathogen that can cause acute gastroenteritis in humans after ingestion of contaminated food or water. Salmonellosis is one of the most common sources of food-borne disease in humans and is a major public health and economic burden worldwide (Majowicz *et al.*, 2010; Agbor and McCormick, 2011). A key aspect of *Salmonella* virulence is its ability to invade and survive within non-phagocytic intestinal epithelial cells, processes driven by two type III secretion systems (T3SS1 and T3SS2) that together inject more than 30 effector proteins into the host cell (Haraga *et al.*, 2008; Figueira and Holden, 2012).

Host cell invasion is mostly mediated by T3SS1-injected effectors, triggering fast and massive rearrangements of the actin cytoskeleton (Zhou *et al.*, 2001; Scott *et al.*, 2005; Patel and Galán, 2006) followed by the formation of plasma membrane (PM) ruffles and *Salmonella* engulfment into the *Salmonella*-containing vacuole (SCV). The SCV is a unique, modified membrane-bound compartment that enables bacterial survival and replication. The early SCV [< 30 min post-invasion (p.i.)] has been shown to share some similarities with early endosomes, namely an association with phosphatidylinositol 3-phosphate, Rab5, Vps34, early endosomal antigen-1 (EEA-1) and sorting nexins -1 and -3 (Hernandez *et al.*, 2004; Bujny *et al.*, 2008; Mallo *et al.*, 2008; Steele-Mortimer, 2008; Braun *et al.*, 2010). The maturing SCV [between 30 min and 5 h p.i.] undergoes extensive membrane remodelling and acquires late endosome/lysosomal markers, such as Rab7, lysosomal-associated membrane-associated protein-1 (Lamp-1) and vacuolar ATPase (vATPase) (reviewed in Steele-Mortimer, 2008; Schroeder *et al.*, 2011). This is accompanied by movement of the SCV along microtubules (MTs) to a juxtanuclear position adjacent to the MT-organizing centre (Harrison *et al.*, 2004). Maintaining the SCV in the perinuclear region is thought to be important for promoting bacterial replication, which is initiated 3–4 h p.i. (Ramsden *et al.*, 2007a,b; Bakowski *et al.*, 2008). The last stages of SCV maturation (> 5 h p.i.), mostly mediated by T3SS2 effectors, are characterized by concomitant intravacuolar bacterial replication and formation of Lamp-1-enriched membrane tubules, named *Salmonella*-induced filaments (SIFs), that extend from the SCV along MTs (Drecktrah *et al.*, 2008). SIFs are highly dynamic structures and can spread throughout the entire

cell to form a complex network. They are also enriched in vATPase, Rab7 and cholesterol (Brumell *et al*., 2001). In addition to SIFs, other tubular networks emanate from the late SCV, such as *Salmonella*-induced SCAMP3 tubules (Mota *et al*., 2009) and Lamp-1-negative tubules (Schroeder *et al*., 2010). However, the biological role of all these *Salmonella*-induced tubules remains largely unknown (Schroeder *et al*., 2011). Membrane damage during the early or maturing stage has also been described for some SCVs, which gives bacteria access to the host cell cytosol. This can allow for bacterial detection and degradation by autophagy mechanisms (Jo *et al*., 2013). Nevertheless, recent data show that in approximately 9% of infected epithelial cells, these cytoplasmic bacteria can replicate at much faster rates than those within an SCV (doubling time of ~ 20 min); this is termed hyper-replication (Knodler *et al*., 2010; Malik-Kale *et al*., 2012). Thus, intracellular *Salmonella* growth can be different depending on its localization within the host cell.

Proteomics has been used to reveal the protein composition of phagosomes (Desjardins *et al*., 1994; Gagnon *et al*., 2002; Stuart *et al*., 2007; Rogers and Foster, 2008). Other proteomics studies have reported the protein composition of bacteria-containing vacuoles, such as *Legionella pneumophila* (Shevchuk *et al*., 2009; Urwyler *et al*., 2009; Hoffmann *et al*., 2014) or *Mycobacterium bovis* BCG (Lee *et al*., 2010), and have given important insights into the mechanisms of intracellular bacterial survival. In this study, we applied a quantitative proteomics approach to identify novel host factors associated with the SCV at different stages of its maturation. We reproducibly isolated SCVs and determined their protein composition. Using functional and correlative ultrastructural approaches, we then characterized and showed that two specific SCV–protein interactions affect intracellular *Salmonella* growth. We demonstrate that early interactions between the SCV, the endoplasmic reticulum (ER) and the coat protein complex II (COPII) complex promote cytoplasmic *Salmonella* localization and hyper-replication. At late stages, bacterial growth is regulated by interactions between intact SCVs and VAMP7-positive lysosome-like vesicles, which also determine SIF formation.

Results

Purification of SCVs from infected epithelial host cells

We developed a fractionation methodology to obtain a subcellular fraction highly enriched in intact SCVs that could be used to determine the SCV proteome. Vacuoles were isolated at two time-points of *Salmonella* infection representing two stages of SCV maturation: 30 min, corresponding to the early SCV; and 3 h, corresponding to the maturing SCV. Later stages of SCV maturation were not isolated, as bacterial replication and *Salmonella*-induced tubule formation interfere with our purification procedures. In order to obtain intact SCVs with sufficient purity, we performed careful cell homogenization and centrifugal separation in density gradients. SCV integrity was quantified in the post-nuclear supernatant (PNS) after cell homogenization, by a novel ELISA-based assay (Fig. 1; see *Experimental procedures* for details). In this assay, non-vacuolarized *Salmonella* adhere to an immobilized antibody and are then quantified by a secondary, biotinylated antibody, whereas vacuolarized bacteria do not adhere and are thus not counted (Fig. 1A, left panel). Total bacteria in each sample were also determined using this method by first subjecting samples to osmotic shock in order to rupture the SCVs and free all vacuolarized bacteria. In order to evaluate the robustness of our assay and to quantify the number of non-vacuolarized *Salmonella* in the PNS, a standard curve with known amounts of bacteria was generated and statistically validated (Fig. S1A and B). In the non-infected control PNS, to which a known amount of bacteria was added, the percentage of non-vacuolarized and total, osmotically shocked, *Salmonella* was the same (Fig. 1A, right panel). At the two time-points of infection, non-vacuolarized *Salmonella* accounted for only 16% of the total number of bacteria in the PNS, indicating that the vast majority of SCVs are intact after cell homogenization.

Fig. 1. Isolation of highly enriched and intact SCVs from infected host cells.
A. *Salmonella*-infected HeLa cells were mechanically homogenized in an isotonic buffer and the SCV integrity in the PNS was tested by ELISA. Non-infected PNS supplemented with a known amount of added bacteria was used as control. A small aliquot of sample was subjected to a sandwich ELISA, either at isotonic conditions (non-treated) or after osmotic shock. Data are represented as the mean ± SEM from three independent and representative experiments.
B. The different PNSs (non-infected control, 30 min and 3 h infection) were fractionated by ultracentrifugation in a density gradient and the number of *Salmonella* in each fraction (F1 to F12) was determined by counting CFUs (black bars). Simultaneously, the density of each fraction (expressed in g cm^{-3}) was measured in a refractometer and plotted together in the same graph (white dots). Data represent the mean ± SEM from five independent experiments.
C. Aliquots of fractions F6 to F8 were subjected to the ELISA method described in (A). Data show the mean ± SEM from three independent and representative experiments.
D. All fractions F1 to F12 and the PNS were tested using markers for the following compartments: early endosomes (EEA-1 and Rab5), late endosomes and lysosomes (Lamp-1), Golgi (GM130), peroxisomes (catalase), mitochondria (TOM22) and ER (calreticulin). The organelle distribution in the density gradients was the same in the non-infected control (left panel), 30 min (right panel) and 3 h (Fig. S2). *Salmonella* distribution, detected with a specific anti-*Salmonella* LPS antibody, was the same in the 30 min (right panel) and 3 h (Fig. S2) fractionations. All *P*-values were determined using the Student's *t*-test.

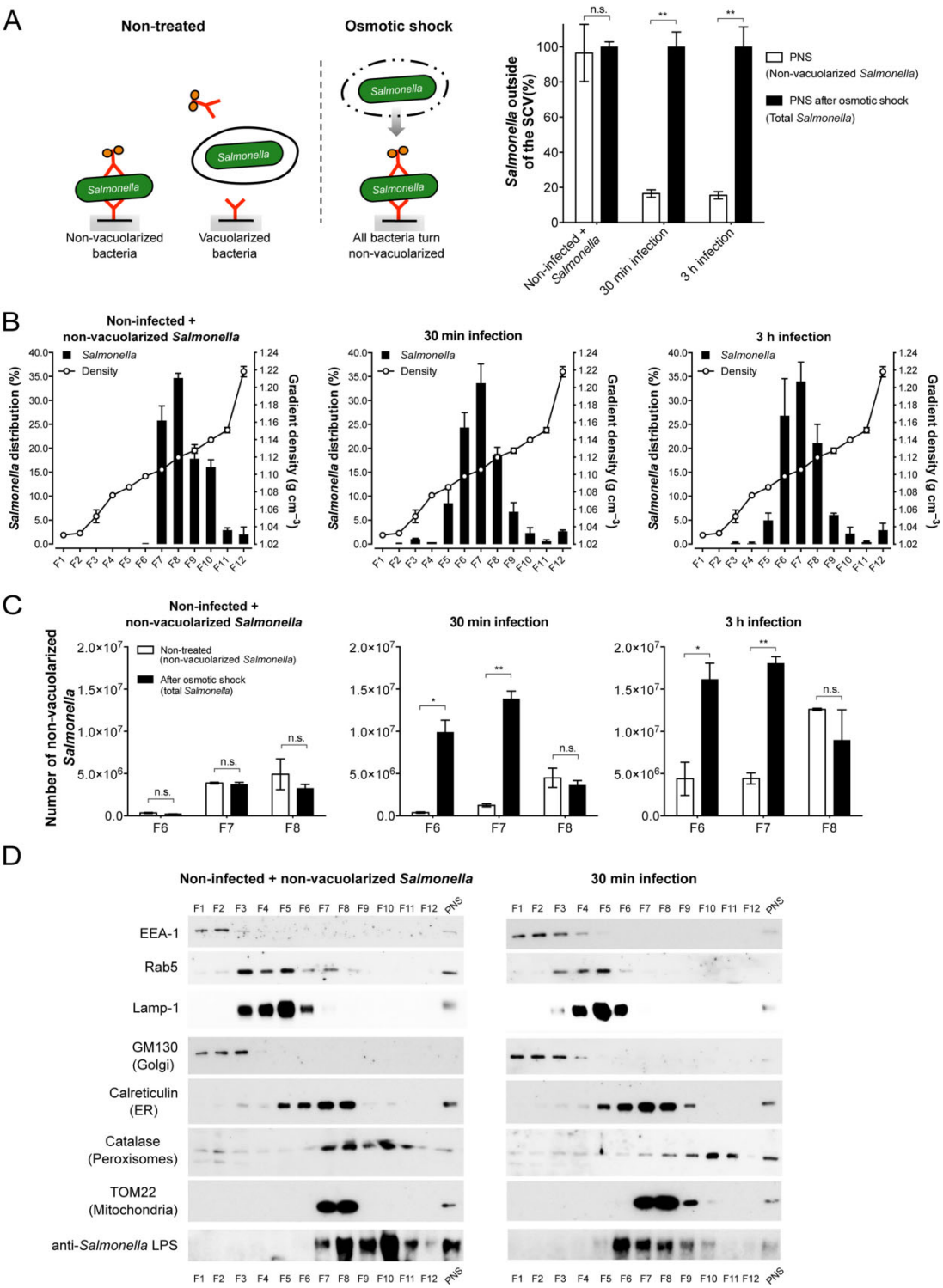

We performed five independent infection experiments, followed by ultracentrifugation, with highly reproducible linear density gradients (Fig. S1C). This separated SCVs from remaining subcellular organelles. To determine the SCV position within the gradient, we measured the number of colony forming units (CFUs) of total *Salmonella* in each fraction. As a control, we added *Salmonella* to a non-infected PNS before fractionation and found that the majority of non-vacuolarized bacteria (Fig. 1B, left panel) accumulated in fractions F7 and F8 (1.11 and 1.12 g cm^{-3} respectively). In contrast, the fractionation of the infected PNS, both at 30 min and 3 h (Fig. 1B, middle and right panels), led to a 500-fold enrichment of total bacteria in fraction F6 (1.10 g cm^{-3}). We next evaluated SCV integrity in fractions F6 to F8 by ELISA. The number of non-vacuolarized bacteria in fractions F6 and F7 was significantly lower than the total *Salmonella* as determined by osmotic shock (Fig. 1C, middle and right panels). This indicates that the bacteria in these two fractions were mostly within intact SCVs. In contrast, fraction F8 contained solely non-vacuolarized *Salmonella*, as no increase was seen after osmotic shock. Thus, in fractions F6 and F7, we successfully isolated intact SCVs and separated them from non-vacuolarized bacteria.

We assessed the separation efficiency of different subcellular organelles by Western blot (Fig. 1D). As expected, the Golgi apparatus and early endosomes showed a low density (between 1.03 and 1.09 g cm^{-3}), whereas peroxisomes had a high density (between 1.12 and 1.15 g cm^{-3}) and did not overlap with fractions F6 and F7. Late endosomes/lysosomes accumulated mostly in F5 (1.09 g cm^{-3}) but also showed partial overlap with the SCV-enriched fraction F6. The ER displayed a broad distribution within the gradient, spanning from F5 to F8 (1.09 to 1.12 g cm^{-3}) and overlapped with the SCV fractions. This distribution can be explained by the complex structure of the ER and its heterogeneous physical properties. Importantly, the tested conditions led to the accumulation of mitochondria only in fractions F7 and F8 (1.11–1.12 g cm^{-3}), not overlapping with the SCV fraction, F6. For all tested antibodies, equal results were obtained for the 30 min (Fig. 1D, right panel) and 3 h fractionation (Fig. S2). We successfully isolated intact and highly enriched SCVs in fraction F6, which we then used to determine the protein composition of the SCV.

The dynamic quantitative host protein composition of the SCV

To determine the repertoire of host proteins enriched at the SCV at the two time-points, we used a label-free quantitative mass spectrometry (MS)-based proteomics approach. We compared the relative protein abundance in the SCV fraction (30 min or 3 h) with a non-infected control fraction, prepared in parallel. MS data obtained from five independent experiments were analysed by MaxQuant, both for protein identification and quantification (Cox and Mann, 2008; Luber *et al*., 2010). As protein abundance from contaminating organelles should not differ between the tested conditions (Rao *et al*., 2009), factors that are enriched in the SCV can be identified through their positive fold-change ratio compared with the control.

Analysis of the entire MS data set identified 2522 host proteins, 392 of which (~ 15%) showed a statistically significant fold-change increase at one or both of the two time-points of infection (Fig. 2A and Fig. S3A and B and Tables S1 and S2). In detail, 173 proteins were enriched solely at the 30 min SCV (red), 124 uniquely at the 3 h SCV (green) and 95 at both time-points (orange) (Fig. 2A). These three specific subsets of host factors (only 30 min SCV; only 3 h SCV; 30 min + 3 h SCV; complete list is in Table S3) reflect how SCV protein composition is altered during its maturation. An overview of some selected proteins dynamically associated with the SCV can be found in Table S4.

The identified proteins were grouped according to their putative subcellular localization or biological function by gene ontology analysis. We detected a significant enrichment of ER-, Golgi- and vesicle-derived proteins, all of which decreased with time. Also, lysosome-derived proteins were exclusively increased in the 30 min SCV (Fig. 2B). We observed significant enrichment of proteins involved in ER to Golgi vesicle-mediated transport at the 30 min SCV or at both time-points (Fig. S3C). Together, these data highlight that SCV protein composition dynamically varies with time and that specific biological processes are implicated at each step of SCV maturation.

Several host proteins identified by our quantitative approach were previously described to be associated with the SCV (Rathman *et al*., 1997; Steele-Mortimer *et al*., 1999; Harrison *et al*., 2004; Boucrot *et al*., 2005; Smith *et al*., 2007; Thurston *et al*., 2012) or involved in *Salmonella* infection (Criss and Casanova, 2003; Hänisch *et al*., 2010; Jolly *et al*., 2014), confirming the potential of our work (Fig. 2C and Table S4). Importantly, we also identified several novel host proteins associated with the SCV (Tables S3 and S4). Among them, we were particularly interested in ER-derived proteins, all the factors from the coat protein complex II (COPII) machinery and lysosome-derived proteins (Fig. 2C).

Early SCV interactions with ER-derived COPII complex promote vacuolar rupture and cytoplasmic Salmonella *growth through hyper-replication*

A key finding in our quantitative proteomic analysis was that approximately 20% of the proteins enriched in early SCVs were derived from the ER (Fig. 2B and Table S3 for

A

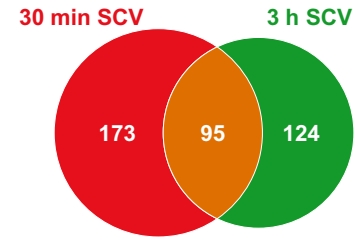

Number of host proteins enriched in the SCV

B

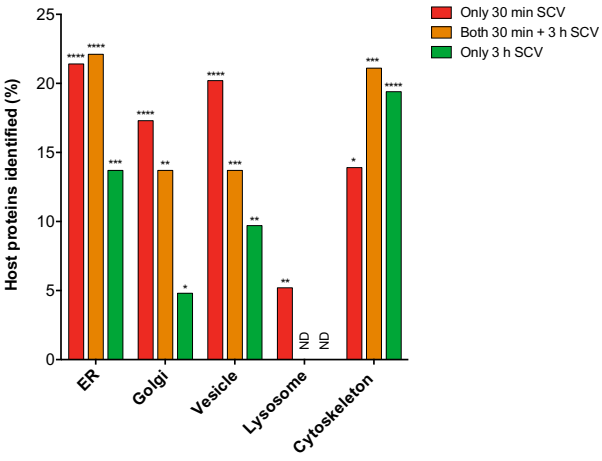

C

Known SCV associated proteins	Early SCV	Maturing SCV
Dynactin	n.d.	+
Dynein	+	+
Galectin-3	+	–
Kinesin light chain 1	n.d.	+
Kinesin light chain 2	n.d.	+
Kinesin-1 heavy chain	+	+
Lysosomal acid phosphatase	+	–
Rab-4a	+	n.d.
Rab-7a	+	n.d.
vATPase	+	n.d.

Proteins known to be involved in *Salmonella* infection	Early SCV	Maturing SCV
Arp2/3 complex	+	n.d.
Actin	+	n.d.
Annexin A2	+	n.d.
Filamin	+	+
Tropomyosin-4	+	n.d.
Tubulin	n.d.	+

ER-derived proteins	Early SCV	Maturing SCV
Calnexin	+	+
Reticulon-4	+	n.d.
VAP-A	+	–
VAP-B	+	–

COPII-complex proteins	Early SCV	Maturing SCV
Sec13	+	n.d.
Sec23	+	+
Sec24	+	n.d.
Sec31	+	n.d.

Lysosome-derived proteins	Early SCV	Maturing SCV
Cathepsin B	+	–
Cathepsin Z	+	–
CI Man-6-P receptor	+	n.d.
Dipeptidyl peptidase 2	+	–

+ (enriched relative to control)
– (depleted relative to control)
n.d. (no diference relative to control)

Fig. 2. The SCV protein composition dynamically changes during vacuole maturation. Protein data from fraction F6 of each condition (control, 30 min and 3 h) was analysed with label-free quantitation algorithms (MaxQuant software). Relative host protein abundances were compared between the control and any two infection time-points. Proteins enriched at a specific time-point were considered as SCV constituents. A positive fold-change was considered when the abundance ratio 30 min/control or 3 h/control was > 1.3 ($\log_2$ fold-change > 0.387) with a *P*-value < 0.05.
A. Thirty minute SCV-enriched proteins were compared with 3 h SCV-enriched proteins and a Venn diagram was built.
B. The host proteins enriched in the SCV were grouped according to their subcellular localization. For each term, the analysis was performed for the proteins enriched uniquely either at the 30 min SCV (only 30 min SCV, red bars) or at the 3 h SCV (only 3 h SCV, green bars) or for the proteins enriched at both time-points (both 30 min + 3 h SCV, orange bars). The graphs show the percentage of host proteins enriched at the SCV, relative to the total number of proteins identified in each condition. Statistics were performed by determining the *P*-values (EASE score, as mentioned in the *Experimental procedures*) and show the robustness of gene-term enrichment for each condition. ND, non-enriched factors in comparison with the control.
C. Selected proteins enriched in the early (30 min) or maturing (3 h) SCV are shown with a '+' symbol.

Fig. 3. The SCV contacts with the host cell ER.
A. Log_2 fold-change in ER-derived protein abundance in the SCV-enriched fraction compared with the non-infected control from five independent MS/MS experiments. Relative protein abundances were considered different when the log_2 fold-change > 0.387 (red line) or < −0.387 (green line), with a *P*-value < 0.05. Statistics are relative to the non-infected control for each protein.
B–D. HeLa cells were infected with *Salmonella* (B) or *Salmonella*-dsRed (D), fixed at different time-points and immunostained for calnexin or reticulon-4 respectively. F-actin was stained with phalloidin and DNA with DAPI (cyan). Representative confocal microscopy images are shown. In (B), arrows indicate the site of bacterial entry, for which calnexin accumulation at the different time-points was quantified (C) from three independent experiments. Scale bars represent 10 μm.
E and F. Fluorescence confocal microscopy was followed by large-volume FIB/SEM of the same *Salmonella*-infected cell. (E) Confocal image of an infected cell is shown in the upper left corner, together with the region that was imaged by FIB/SEM (white box). Corresponding zoomed 3D views are shown for the native and segmented fluorescent signals (middle and lower left panel, respectively), together with the volume of FIB/SEM acquisition. A 3D view of the FIB/SEM acquisition is depicted in the upper middle panel. Using Amira software, the bacteria (blue), the SCVs lumen (yellow) and the ER (red) were segmented (upper right panel). The FIB/SEM segmentation was correlated with reticulon-4 fluorescent signal, showing overlap between the ER segmentation and the fluorescence (lower right panel). (F) A xy-view FIB/SEM section shows a site of contact between the SCV and the ER membrane (upper panel, white box). A corresponding partial 3D segmentation showing the bacteria (blue), the SCV lumen (yellow) and the ER (red) is presented in the lower panel.

details). Figure 3A depicts some of these host factors, such as calnexin, which was previously described to be associated with phagosomes (Gagnon *et al*., 2002) and with the *Legionella*-containing vacuole (LCV) (Lu and Clarke, 2005; Ragaz *et al*., 2008). Hence, we investigated its subcellular localization during *Salmonella* infection by immunofluorescence microscopy. Fast and transient calnexin accumulation at the invasion site was observed, which peaked at 10 min p.i. (Fig. 3B, upper panel; quantification in Fig. 3C), and by 30 min p.i., we observed calnexin accumulation around some of the SCVs (Fig. 3B, magnifications). Reticulon-4 immunostaining was used to observe tubular ER during bacterial infection. Unlike calnexin, reticulon-4 did not consistently accumulate at the *Salmonella* entry site (data not shown); however, we observed that the early SCV seemed to be wrapped by ER filaments (Fig. 3D, insets for details). Additionally, Western blot analysis of the isolated subcellular fractions confirmed enrichment of reticulon-4 in the 30 min fraction F6 (Fig. S4A).

The precise nature of the SCV–ER interactions could not be determined by light microscopy due to its resolution limit. Therefore, we applied an emerging technique, termed correlative-focused ion beam/scanning electron tomography (C-FIB/SEM). Fluorescence microscopy and large-volume ultrastructural tomography are combined in a single three-dimensional (3D) data set, allowing for precise identification of molecules of interest within the ultrastructural volume. This technique was previously used in our laboratory to characterize the host cell environment around the *Shigella*-containing vacuole (Mellouk *et al*., 2014). In short, cells were infected with *Salmonella* for 30 min and fixed. The ER was labelled with a reticulon-4 antibody followed by indirect immunofluorescence, DNA (bacteria and host cell nuclei) was stained and cells were imaged by confocal microscopy followed by FIB/SEM tomography at the exact same location (Fig. 3E, see *Experimental procedures* for details). The two data sets were then correlated and combined into a single data set presented here. DAPI and reticulon-4 fluorescent signals were segmented by thresholding (left middle and lower panels) and the corresponding FIB/SEM data (upper middle and right panels) show the segmentation of bacteria (blue) and of the SCV lumen (yellow). After superimposing the ER fluorescent signal with the FIB/SEM data, we could segment the ER ultrastructure (red). Strikingly, in all data sets ($n = 4$) the SCVs were surrounded by ER (Fig. 3E, lower right panel). Moreover, in all data sets we could observe membrane interactions between the ER and SCVs (Fig. 3F and Fig. S4B show different data sets; in Video Clip S1, ER contacts with multiple SCVs are also observed) that resembled membrane contact sites (MCS) (Orci *et al*., 2009; Eden *et al*., 2010; Stefan *et al*., 2013). Therefore, we conclude that there is membrane contact between the early SCV and the ER.

Interestingly, we found that the early SCV proteome was enriched in all constituents of the COPII complex, namely Sec13, Sec23, Sec24 and Sec31 [proteins form a complex leading to vesicle budding from the ER membrane and the transport of cargo to the Golgi or the cell surface (Haucke, 2003; Sato, 2004; Lord *et al*., 2013)]. Using immunofluorescence microscopy, we observed the accumulation of COPII complex around a small percentage of intracellular *Salmonella* (8–15%), as seen by Sec13-positive bacteria (Fig. 4B and C and Fig. S4C). This confirmed our proteomic data and also suggested a potential link between the ER and some of the early SCVs, possibly via COPII-coated vesicles.

To examine if COPII affects the intracellular *Salmonella* lifestyle, we measured bacterial growth within epithelial cells using gentamicin assays (Elsinghorst, 1994), after inhibiting COPII function via Sec13 siRNA treatment. *Salmonella* entry into HeLa cells, measured 1 h p.i., was not affected after Sec13 knockdown (data not shown). Strikingly, Sec13-depletion impaired intracellular bacterial growth from 3 h p.i. onwards, as compared with the control (Fig. 4D). These data show that the COPII complex is crucial for bacterial growth within the host cell. Then, we tested if there was a functional link between the

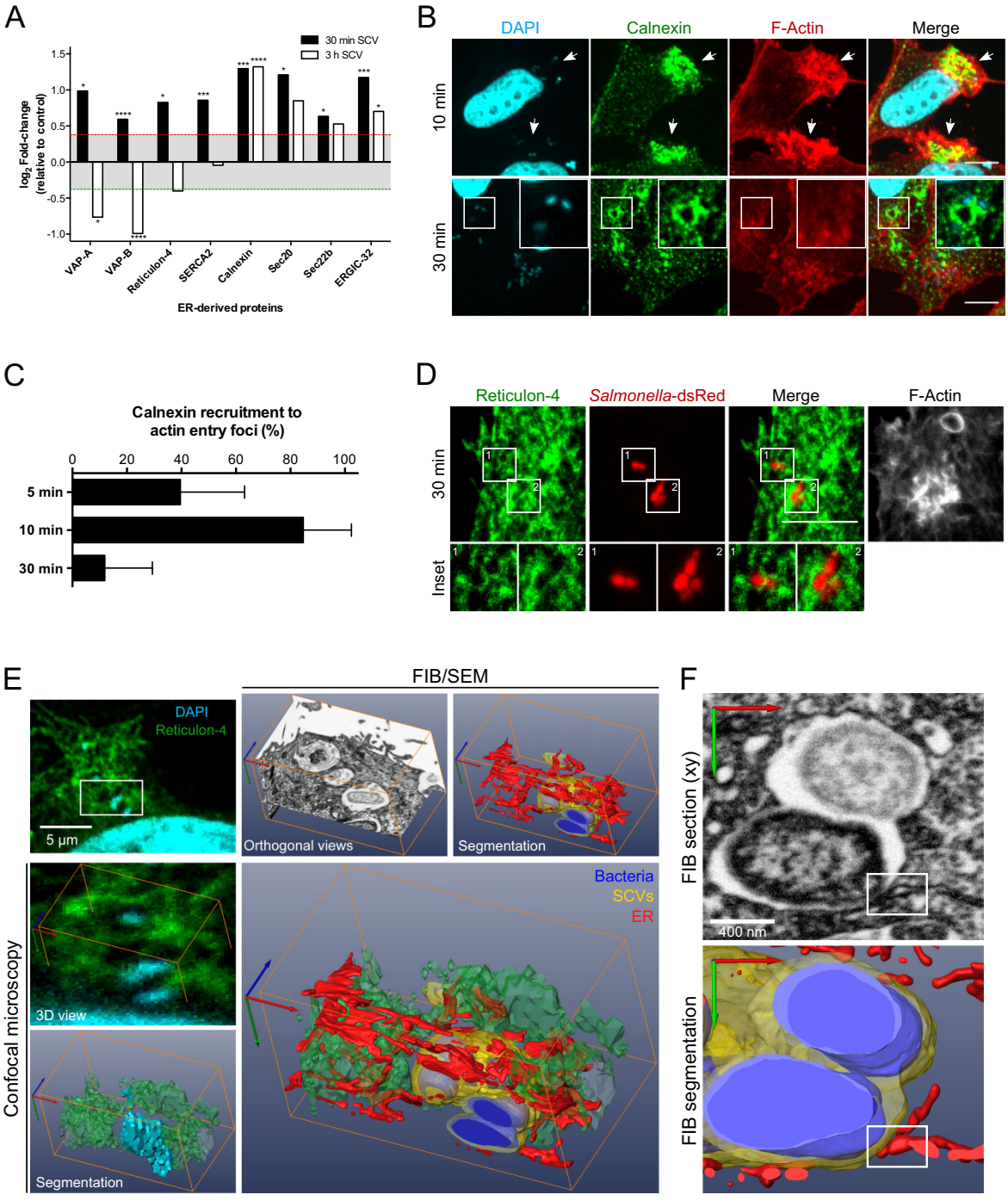

COPII complex and bacterial hyper-replication within the cytosol, which requires SCV rupture (Knodler *et al.*, 2010; 2014; Malik-Kale *et al.*, 2012). By 6 and 9 h p.i., we found COPII localizing to bacterial-shaped structures in 100% of the cells with hyper-replicating *Salmonella* (Fig. S4D and E), although only surrounding some of the bacteria. These structures were specific to bacterial hyper-replication, as they were absent in infected cells not containing

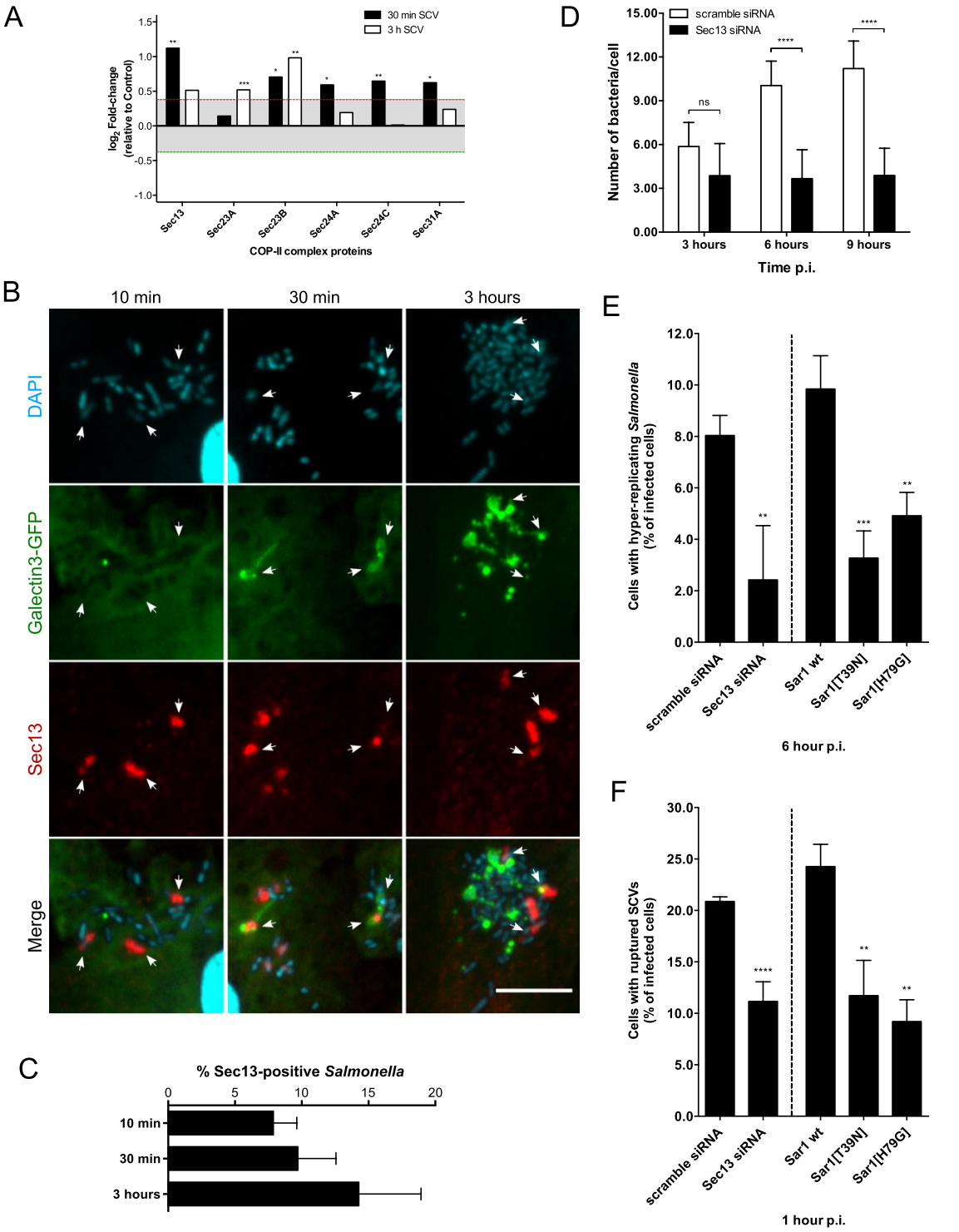

Fig. 4. COPII vesicle assembly and accumulation on the early SCV promotes vacuolar rupture and *Salmonella* hyper-replication.
A. Log_2 fold-change in COPII complex-derived protein abundance in the SCV-enriched fraction compared with the non-infected control from five independent MS/MS experiments. Relative protein abundances were considered different when the log_2 fold-change > 0.387 (red line) or < −0.387 (green line) with a *P*-value < 0.05. Statistics are relative to the non-infected control for each protein.
B and C. HeLa cells expressing galectin-3-GFP were infected with *Salmonella*, fixed at different time-points and immunostained for Sec13. In (B), DNA was stained with DAPI (cyan). Representative confocal microscopy images show association of Sec13 around intracellular bacteria. Arrows point to Sec13-positive (10 min) or Sec13- and galectin-3-positive bacteria (30 min and 3 h). The graph in (C) shows the percentage of Sec13-poisitive *Salmonella* by counting at least 100 intracellular bacteria from three independent experiments performed in triplicate.
D. Cells were treated with scramble or Sec13 siRNA and infected with *Salmonella*. Gentamicin was added to kill all extracellular bacteria, then host cells were lysed at the indicated time-points of infection and the number of viable intracellular bacteria was counted by CFUs. The graph shows the mean ± SEM number of bacteria normalized to the number of cells counted for each siRNA after trypsinization of a non-infected well. Sec13-knockdown level was assessed by Western blot as described in the *Experimental procedures*.
E and F. Cells in 96-well plates were treated with scramble or Sec13 siRNA, for 72 h, or transfected with plasmids expressing either Sar1 wt- or the mutants Sar1[T39N]-CFP or Sar1[H79G]-CFP for 24 h. After 1 or 6 h of infection with *Salmonella*-dsRed, cells were fixed and imaged by fluorescence microscopy. Vacuolar rupture was quantified by assessing the presence of intracellular bacteria positive for galectin-3-GFP. Bacterial hyper-replication was determined as described in the *Experimental procedures*. In the Sar1-transfected cells, only those expressing CFP were used in the quantification. All *P*-values were determined using the two-way analysis of variance test for multiple comparisons from three independent experiments performed in triplicate (D) or quadruplicate (E–G). Scale bars represent 10 μm.

hyper-replicating bacteria. This suggested that the COPII complex is directly implicated in promoting *Salmonella* hyper-replication. To test this, cells were transfected with Sec13 siRNA and the percentage of infected cells containing hyper-replicative bacteria was determined 6 h p.i. by fluorescence microscopy. Sec13 depletion significantly decreased the number of cells with hyper-replicating *Salmonella* (Fig. 4E) as compared with the control. To assess if COPII vesicles were specifically associated with SCVs that undergo rupture, we used fluorescent galectin-3 as a marker for vacuolar lysis (Paz *et al*., 2010; Ehsani *et al*., 2012). SCV rupture was observed as soon as 30 min p.i., occurring in SCVs that were also positive for the COPII complex (Fig. 4B). Moreover, we could not detect any galectin-3 positive bacteria by 10 min p.i., suggesting that vacuolar damage happens after the initial accumulation of COPII vesicles at the early SCV.

We then asked if COPII function was involved in SCV rupture. By 1 h p.i., Sec13 knockdown significantly reduced the percentage of infected cells with ruptured SCVs (Fig. 4F), which were identified by the presence of galectin-3-positive bacteria. These results suggest that COPII complex assembly is important for SCV rupture and *Salmonella* hyper-replication. To confirm this, we overexpressed two different Sar1 mutants, Sar1[T39N] or Sar1[H79G], which are, respectively, constitutively inactive or active (Ward *et al*., 2001; Schindler and Schekman, 2009). In this way, it is possible to perturb either the first step of COPII complex assembly or the final step of COPII vesicle release. Interestingly, inhibition of either of these steps resulted in impairment of *Salmonella* hyper-replication (Fig. 4E), and the upstream event of SCV rupture (Fig. 4F), in a similar manner as Sec13 knockdown.

Altogether, these data indicate that COPII vesicles accumulate at the early SCV and the latter physically interacts with the ER. Moreover, COPII assembly promotes SCV rupture followed by bacterial hyper-replication in the host cytosol.

Salmonella *growth within the late SCV is regulated by interactions with lysosome-like vesicles*

Our quantitative proteomics data confirmed that the SCV also interacts with lysosomes (Fig. 2B and C) (Oh *et al*., 1996; Drecktrah *et al*., 2007). Associated proteins included cathepsins, the cation-independent mannose-6-phosphate receptor (CI-M6PR), dipeptidyl peptidase 2, palmitoyl protein thioesterase 1 (PPT-1) and Rab-7a. Especially, they were enriched in the early SCV and then depleted in the maturing SCV (Figs 2C and 5A). We also observed the same trend for VAMP7 (see also Fig. S4A), a lysosomal v-SNARE protein essential for heterotypic, late endosome-lysosome fusion (Luzio *et al*., 2007). This protein was interesting to us as it has been associated with intracellular growth of other bacteria, such as *Chlamydiae trachomatis* and *Coxiella burnetii* in epithelial cells (Delevoye *et al*., 2008; Campoy *et al*., 2013). Moreover, in the early SCV, we observed the enrichment of syntaxin-4, a t-SNARE that binds VAMP7 leading to lysosomal fusion with the PM (Luzio *et al*., 2010). By using fluorescently labelled VAMP7, we found that VAMP7-positive vesicles were recruited to the early SCV, as most of the bacteria were positive by 30 min p.i. (Fig. 5B, arrows and 5C). Additionally, the number of VAMP7-positive bacteria significantly decreased during SCV maturation, corroborating our quantitative proteomics data. Co-immunostaining for the lysosomal marker Lamp-1 showed colocalization with VAMP7 on cytosolic vesicles and around bacteria (Fig. 5B and D). By time-lapse microscopy, we observed that VAMP7-positive vesicles accumulating around the early SCV are acidic, as they were positive for LysoTracker (Fig. S5; Video Clips S2–S4). Interestingly, as the SCV matures, we observed that VAMP7 either transiently dispersed from the SCV (Fig. S5A and B; Video Clips S2 and S3) or not (Fig. S5C; Video Clip S4). However, in all cases we observed a diminishing of LysoTracker signal around the SCV (Fig. S5; Video Clips S2–S4). Together with the proteomics data, this suggests that vesicles with

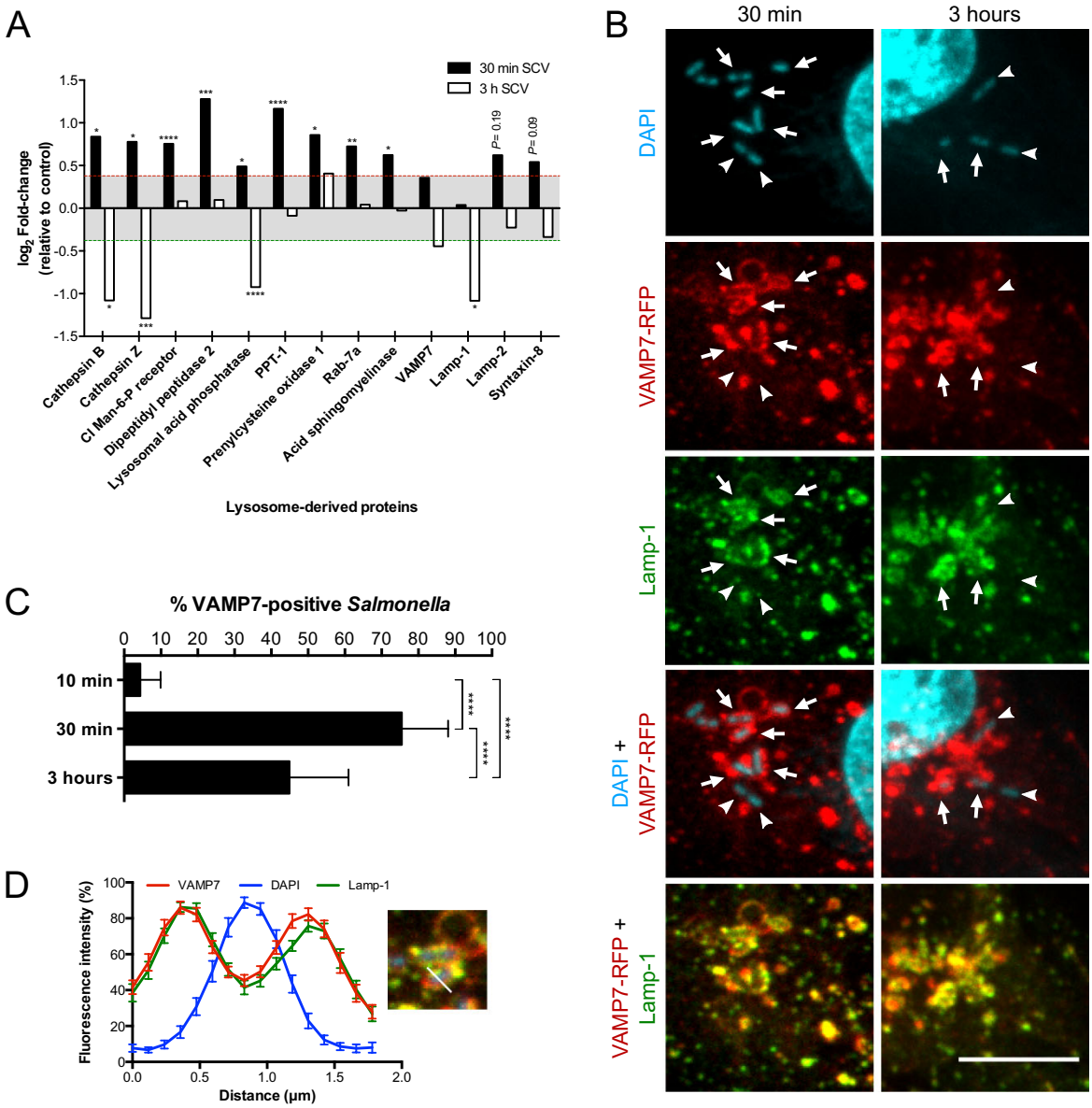

Fig. 5. The early SCV is enriched in lysosomal proteins.
A. The graph shows the $\log_2$ fold-change in lysosomal protein abundance in the SCV-enriched fraction compared with the non-infected control from five independent experiments. Relative protein abundances were considered different when the $\log_2$ fold-change > 0.387 (red line) or < –0.387 (green line) with a *P*-value < 0.05. Statistics are relative to the non-infected control for each protein.
B–D. Cells were transfected with VAMP7-RFP, infected with *Salmonella* and fixed at different time-points. In (B), infected cells were immunostained for Lamp-1 and bacteria were labelled with DAPI. Arrows and arrowheads point to VAMP7-positive or -negative *Salmonella* respectively. Representative confocal microscopy images are shown. The graph in (C) shows the percentage of VAMP7-poisitive *Salmonella* by counting at least 100 intracellular bacteria from three independent experiments performed in triplicate. Line-scan analysis (D) of VAMP7-RFP and Lamp-1-positive SCVs at 30 min p.i. The graph shows the mean ± SEM relative fluorescence intensity from 25 SCVs. *P*-values were determined using the two-way analysis of variance test for multiple comparisons from three independent experiments performed in triplicate. Scale bars represent 10 µm.

lysosomal characteristics directly interact with the SCV at early stages of its maturation, followed by depletion of lysosomal content. Lysosome-like vesicle fusion with the SCV were directly visualized by C-FIB/SEM. Cells were transfected with VAMP7-RFP, infected with *Salmonella* for 30 min and fixed. Figure 6A (Video Clip S5) shows that VAMP7- and Lamp-1-positive structures in the bacterial vicinity (upper panels) correlate to vesicles that surround and interact with the SCVs, as seen by overlaying the fluorescence signals with the ultrastructural data (middle and lower panels). Importantly, detailed analysis of different areas within the C-FIB/SEM data (Fig. 6B) depicts an SCV fused with a VAMP7/Lamp-1-positive vesicle (left panels, yellow arrows). Moreover, we also observed membrane invagination of a VAMP7/Lamp-1-positive vesicle into a SCV (right panels, red arrows), most likely representing the early steps of vesicle fusion. Thus, C-FIB/SEM data clearly show that the early SCV interacts and fuses with lysosome-like vesicles in its vicinity.

We then investigated the involvement of VAMP7 on *Salmonella* growth during longer time-courses of epithelial cell infection. Depletion of this protein did not affect bacterial entry into host cells (data not shown) and did not alter intracellular *Salmonella* growth until 6 h p.i. (Fig. 7A). In contrast, VAMP7 knockdown stalled bacterial growth at later time-points (> 6 h p.i.). This effect was not due to impaired bacterial escape from the SCV and replication in the cytosol, as VAMP7 knockdown did not affect *Salmonella* hyper-replication (Fig. S6A). As described earlier (Figs 2B and 5A), we obtained decreased lysosomal protein content in the maturing SCV (around 3 h). Interestingly, time-lapse microscopy indicated a resurging, massive, VAMP7 accumulation around the late SCV (> 5 h p.i.), often forming tubular structures resembling SIFs (Fig. S5B and C; Video Clips S3 and S4), but these did not label with LysoTracker. We evaluated and confirmed this hypothesis, as VAMP7 colocalizes with Lamp-1 in the SIFs (Fig. 7B, time-lapse microscopy is shown in Fig. S6B and Video Clip S6). Moreover, VAMP7 is important for SIF formation, as we observed a significant decrease in the number of infected cells with SIFs after VAMP7 depletion (Fig. 7C).

Together, we show that the early SCV fuses with VAMP7-positive lysosome-like vesicles, but these do not seem to be important for the initial steps of intracellular *Salmonella* growth. Moreover, the lysosomal content is quickly depleted from the SCV during its maturation process. At later time-points, VAMP7-positive vesicles with reduced acidic activity are recruited to the late SCV, where they contribute to SIF formation and establishment/maintenance of the replicative bacterial niche.

Discussion

In this work, a quantitative proteomics approach was used to identify novel host proteins associated with the SCV. We show how the dynamic interaction between this unique organelle and different host cell compartments regulates bacterial growth during SCV maturation in different ways (Fig. 7D). Within the first hours of infection, the COPII complex regulates SCV integrity, inducing *Salmonella* access to the host cell cytosol and hyper-replication. At later stages, interactions between the SCV and lysosome-like vesicles promote SIF formation and intravacuolar bacterial growth.

We used fractionation methodologies based on density gradients to successfully isolate early (modified mostly by the bacterial T3SS1) or maturing SCVs (modified by the bacterial T3SS1 and T3SS2). Vacuoles in late stages of maturation were not isolated, as bacterial replication and the complex structure of membrane tubules formed by the SCV would interfere with the biochemical purification. The isolated SCVs were highly enriched and largely free from other organelles, most importantly from mitochondria-derived contaminants. We assessed SCV integrity through a non-biased ELISA assay, rather than the electron microscopy (EM) used in other studies (Gagnon *et al*., 2002; Shevchuk *et al*., 2009), due to the challenges of handling, preparation and image interpretation of isolated cellular fractions for EM. To circumvent the limitations of biochemical SCV isolation and incomplete organelle separation (Rogers and Foster, 2007; Walther and Mann, 2010), we performed a label-free quantitative subtractive proteomics analysis from five independent infection experiments. The inventory of the target SCV fraction was compared with a related non-infected control fraction. The remaining proteins enriched in the SCV fraction can be considered specific SCV components. Our stringent quantification has some limitations, potentially missing some true hits if they are also present to some extent as contaminants in the control fraction. A likely example is Lamp-1, which is known to localize to maturing and late SCVs (Steele-Mortimer, 2008), but was excluded by our quantification procedure. Still we identified about 400 host proteins enriched in the SCV fraction at different stages of maturation, including many factors not previously known to associate with this compartment. Interestingly, we found that the SCV proteome is enriched in factors derived from the host ER, COPII vesicles and lysosomes. Therefore, we investigated how the interactions between these subcellular compartments and the SCV affect intracellular bacterial growth.

Although it remains debated, several proteomics studies provided evidence that the ER associates with the phagosome and is an important source of membrane for phagocytosis (Gagnon *et al*., 2002; Guermonprez *et al*.,

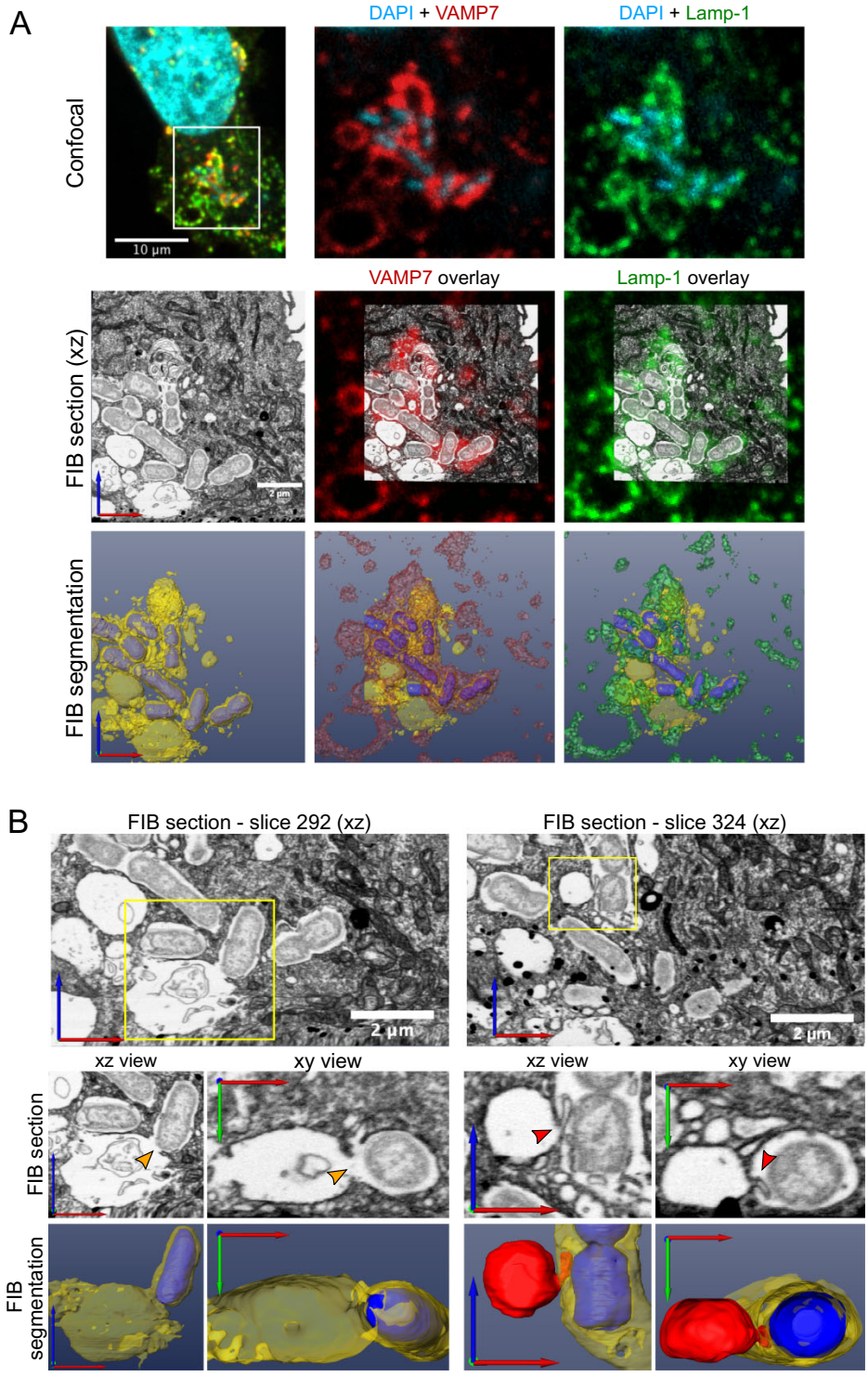

Fig. 6. The early SCVs fuse with lysosome-like vesicles in their vicinity. Fluorescence confocal microscopy was followed by large-volume FIB/SEM of the same *Salmonella*-infected cell.
A. Confocal image of an infected cell is shown in the upper left panel, together with the region that was imaged by FIB/SEM (white box). Corresponding zoomed images for DAPI and VAMP7 or DAPI and Lamp-1 are shown in the upper middle and right panels respectively. A xz-view FIB/SEM section is shown in the middle left panel, together with the overlay with VAMP7 or Lamp-1 fluorescent signals (middle and right panels respectively). The FIB/SEM segmentation is shown in the lower left corner (bacteria in blue; SCVs and vesicles in yellow) together with the superimposition with the VAMP7 or Lamp-1 segmented fluorescent signals (lower middle and right panels respectively).
B. Zoomed images of different FIB/SEM sections are shown, together with the respective segmentations, both in the xz and xy views. In the left panels, yellow arrows point to the site of SCV fusion with a lysosome (bacteria were segmented in blue; SCV and fused lysosome in yellow). In the right panels, red arrows point to the site of lysosomal membrane invagination into the SCV (bacteria were segmented in blue; SCV in yellow and lysosome in red). Amira software was used to present the data. The figure shows one representative C-FIB/SEM data set ($n = 3$).

2003; Houde *et al*., 2003). Our data support this hypothesis, as the early SCV was enriched in ER proteins. Moreover, we observed the recruitment of ER protein calnexin to the bacterial entry site, which could suggest that the ER provides membrane for PM ruffles (Gagnon *et al*., 2002) and *Salmonella* uptake. We additionally speculate that calnexin accumulation at the entry site could be important for *Salmonella* uptake, as this protein was previously shown to control phagocytosis of particles (Müller-Taubenberger *et al*., 2001) and *L. pneumophila* (Fajardo *et al*., 2004), possibly by modulating actin. Other quantitative proteomics studies support the hypothesis of ER-phagosome association by showing that the ER accounts for approximately 20% of the early phagosome proteome (Campbell-Valois *et al*., 2012), in agreement with our analysis in which the same percentage of ER protein enrichment was found at the early SCV. Finally, our C-FIB/SEM approach resolves the controversy about ER interactions with the SCV as we could visualize them directly. We hypothesize that the ER and the SCV are connected via MCS, which might regulate several functions at the interface, such as lipid transfer or modification, Ca^{2+} signalling, phosphatidylinositol metabolism (English and Voeltz, 2013; Stefan *et al*., 2013) or membrane fission (Rowland *et al*., 2014). Moreover, ER-SCV MCS could be promoted through interactions between Rab7 and the ER protein VAP-A. We found these two proteins enriched in our early SCV proteome and they were previously described to act as a scaffold for the formation of ER-late endosome MCS (Rocha *et al*., 2009). Even though we did not observe fusion between the SCV and the ER, it cannot be excluded and should be further investigated. We also found similarities between the proteomes of the SCV and the LCV (Hoffmann *et al*., 2014). ER-derived proteins such as the inositol 1,4,5-trisphosophate, atlastin-3, Rab-2a, Sec20, Sec22b, reticulon-4, VAP-A and VAP-B are enriched in the vacuoles containing *Salmonella* or *Legionella*, pointing to possible similar mechanisms of interaction with the ER.

A striking piece of evidence pointing to the existence of SCV-ER communication is that all the components of the COPII complex were enriched in the early SCV proteome. Importantly, COPII assembly regulates *Salmonella* replication within epithelial cells via Sar1 GTPase activity. We propose that COPII accumulation on the SCV destabilizes vacuolar integrity, through a mechanism that needs to be determined, promoting *Salmonella* release into the cytosol and hyper-replication. Intracellular *L. pneumophila* growth is also promoted by Sar1-mediated COPII activity. However, in this case, COPII activity enables exiting vesicles from the ER to fuse with the LCV to promote the formation of a replicative organelle (Kagan and Roy, 2002; Robinson and Roy, 2006). Thus, it seems that both *Salmonella* and *L. pneumophila* co-opt COPII vesicle activity for different vacuolar maturation outcomes (rupture vs. creation of a replicative organelle) that result in a similar advantage for the bacterium: intracellular growth. It has been recently shown for different bacterial pathogens that host proteins are involved in vacuolar rupture (Akimana *et al*., 2010; Davis *et al*., 2012; Mellouk *et al*., 2014). In the case of *Shigella flexneri*, which enters host cells similarly to *Salmonella*, vacuolar lysis and bacterial escape into the cytosol is mediated by several host GTPases, such as Cdc42, Rab-3b, Rab-4a, Rab-5a and Rab-11a (Mellouk *et al*., 2014). However, the COPII component Sec13 does not seem to be involved in the rupture of the *Shigella* vacuole. It would be interesting to address the common host proteins targeted by *Shigella* and *Salmonella* for destabilization of vacuolar membrane integrity. It is thought that ER tubules could be preferred sites for the formation of COPII vesicles at the ER exit sites (ERES) (Friedman and Voeltz, 2011). Moreover, markers for ERES are often found in close juxtaposition with other organelles (Hughes and Stephens, 2008; Kurokawa *et al*., 2014), which might allow fast, efficient and targeted routes of secretory transport (Budnik and Stephens, 2009). Taken together with our FIB/SEM data, we propose that the close proximity between the ER and the SCV facilitates COPII vesicle activity between ERES and the SCV. Recruitment of ER-derived vesicles to the SCV could be facilitated by Sec22b and syntaxin-4, which were enriched on the early SCV proteome. These proteins were previously described to act together, mediating the recruitment of ER components to phagosomes in dendritic cells (Cebrian *et al*., 2011).

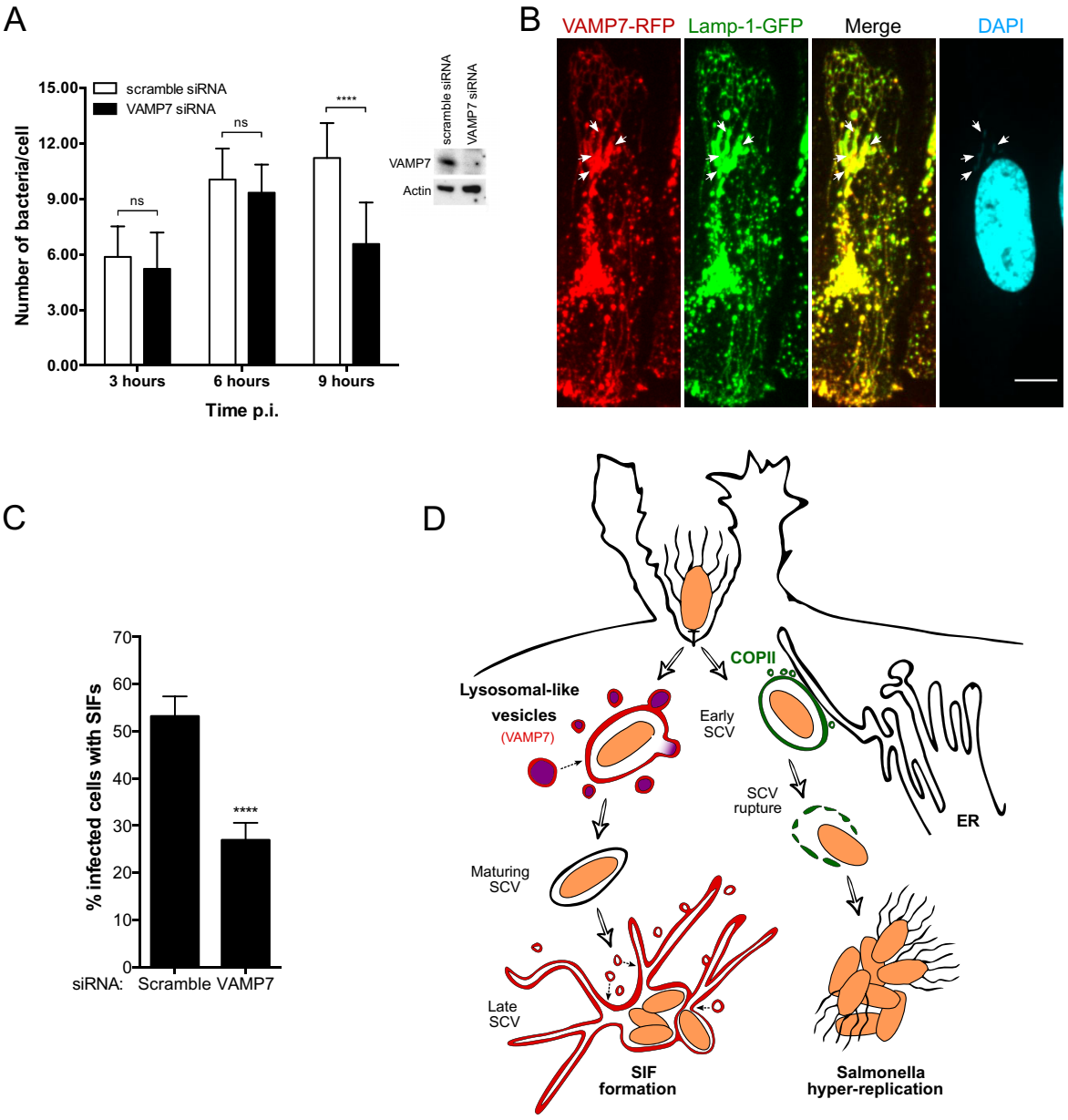

Lysosomal interaction with the SCV has remained a matter of debate. Initial studies pointed to the SCV avoiding fusion with late endosomes and lysosomes, as hydrolases and the M6PR were reported to be absent from the late SCV (Buchmeier and Heffron, 1991; Garcia-del Portillo and Finlay, 1995; Rathman *et al.*, 1997; Hashim *et al.*, 2000). This is, however, controversial (Oh *et al.*, 1996) and has been recently questioned, as extensive dynamic interactions between the lysosomal system and the SCV were observed during vacuole maturation (Drecktrah *et al.*, 2007). Intriguingly, our proteomics data show that the early SCV is enriched in lysosomal proteins, pointing to a model where the early SCV remains accessible to incoming lysosomal content that does not take place at later time-points of vacuole maturation. Such direct interactions were visualized by C-FIB/SEM, in which we observed fusion events of VAMP7/Lamp-1-positive vesicles with the early SCV. Thus, fusion between

Fig. 7. VAMP7 recruitment to the late SCV is important for bacterial replication within the vacuole and SIF formation.
A. HeLa cells were treated with scramble or VAMP7 siRNA and infected with *Salmonella*. Gentamicin was added to kill all extracellular bacteria. Then, cells were lysed at the indicated time-points of infection and the number of viable intracellular bacteria was counted by CFUs. The graph shows the mean ± SEM number of bacteria normalized to the number of cells counted for each siRNA after trypsinization of a non-infected well. *P*-values were determined using the two-way analysis of variance test for multiple comparisons from three independent experiments performed in triplicate. VAMP7-knockdown level was evaluated by Western blot as described in the *Experimental procedures*.
B. Cells were double transfected with VAMP7-RFP and Lamp-1-GFP and infected with *Salmonella* for 16 h. Cells were imaged by confocal microscopy without fixation, in order to preserve SIFs structure.
C. Cells were treated with scramble or VAMP7 siRNA and, 24 h later, transfected with Lamp-1-mCherry. After infection with *Salmonella*-GFP for 16 h, the number of infected cells containing SIFs was counted by confocal microscopy. Results presented in the graph show the mean ± SEM percentage of infected cells with SIFs from three independent experiments performed in triplicate. Thirty infected cells per condition were counted. *P*-values were determined using the Student's *t*-test.
D. Model for VAMP7 and COPII contribution to SCV maturation and *Salmonella* growth in epithelial cells. The early SCV is enriched and fuses with acidic lysosome-like vesicles (red with purple fill). The lysosomal content, including VAMP7, is then temporarily depleted from the maturing SCV. At later stages, VAMP7-positive vesicles with decreased acidity (red) associate again with the late SCV, promoting SIF formation and *Salmonella* replication within the vacuole. There is also contact between the early SCV and the host cell ER. COPII complex (green) assembly and accumulation around the early SCV promote vacuolar rupture, bacterial escape into the host cytosol and hyper-replication. Scale bars represent 10 μm.

lysosome-like vesicles and the early SCV could be part of a normal mechanism of vacuole maturation. When the vacuole reaches the stage of the maturing SCV, it contains fewer lysosomal proteins, such as VAMP7. One possible explanation is that *Salmonella* could control recycling pathways in the host cell to remove unwanted proteins from the SCV in order to avoid degradation, as previously suggested (Bujny *et al.*, 2008). Moreover, interaction with the ER might modulate SCV maturation, as the acquisition of ER-derived membranes to phagosomes was shown to alter normal phagosomal maturation in dendritic cells (Cebrian *et al.*, 2011). Interestingly, we show here that interactions between SCVs and VAMP7-positive vesicles do not play a role in the establishment of the early and maturing SCV.

Surprisingly, at later time-points (> 5 h p.i.), we verified that VAMP7-positive but LysoTracker-negative vesicles are recruited to the late SCV and also to SIFs. Our data also show that VAMP7 is important for SIF formation and *Salmonella* replication exclusively within the late SCV. Due to the role of VAMP7 on vesicle fusion, we hypothesize that this cellular mechanism could provide membrane for SIF elongation and bacterial replication. Despite the late SCV being again enriched in lysosomal proteins such as VAMP7 and Lamp-1, it is LysoTracker negative. This confirms the hypothesis that the early SCV interacts with lysosomes, and that *Salmonella* actively reduces the lysosomal content/activity of its replicative niche during vacuole maturation (McGourty *et al.*, 2012). Moreover, as SIFs display reduced acidity, they might be involved in diluting the lysosomal proteins that are delivered to the SCV (Schroeder *et al.*, 2011). In the future, it will be interesting to identify bacterial effectors that control the successive cycles of interactions between the SCV and the lysosomal system. It could also be informative to compare our data with SCV remodelling in macrophages, as SCV-lysosome fusions have been reported in those cells (Oh *et al.*, 1996), or with intestinal epithelia, where the mechanisms of SCV maturation are largely unknown.

In summary, quantitative proteomic analysis of the SCV combined with cell biology techniques revealed that this unique and specialized organelle interacts with several host cell compartments. We demonstrate that *Salmonella* growth within epithelial cells is regulated by the interactions between the SCV and either the ER or the lysosomal system, in distinct ways. ER-derived COPII-vesicle activity promotes SCV rupture and *Salmonella* hyper-replication within the cytosol, while successive interactions between the SCV and VAMP7-positive vesicles regulate bacterial growth within the SCV, by promoting formation of SIFs.

Experimental procedures

Bacterial strains

The following *Salmonella* strains were used: SL1344 (wild type), SL1344 pM965 (*Salmonella*-GFP) and SL1344 expressing dsRed (*Salmonella*-dsRed). Bacteria were grown in lysogeny broth (LB) medium supplemented with 0.3 M NaCl at 37°C in an orbital shaker. LB was supplemented with streptomycin (50 μg ml^{-1}) and, when appropriate, with ampicillin (50 μg ml^{-1}).

Plasmids, siRNAs and cell transfection

HeLa cells were plated either on 12-well plated containing glass coverslips (1×10^5 cells per well) or into 96-well glass bottom plates (Greiner) (7×10^3 cells per well) 24 h before plasmid transfection. Cells were then transfected with one or two expression plasmids using the X-tremeGENE 9 DNA Transfection Reagent (Roche) for 24 or 48 h, according to the manufacturer's instructions. The pRFP-VAMP7 plasmid was kindly provided by Thierry Galli (Institut Jacques Monod, Université Paris 7). The plasmids encoding the CFP-tagged Sar1, Sar1[T39N] and Sar1[H79G] were a kind gift from Franck Perez (Institut Curie). All siRNAs SMARTpool were obtained from Dharmacon: VAMP7 (6845), Sec13 (6396), non-specific non-targeting pool. Cells were reversed transfected for 72 h with Lipofectamine RNAiMAX (Life Technologies) reagent according to the manufacturer's instructions. Protein knockdown efficiency was assessed by Western blot, by lysing cells with RIPA buffer at 4°C. Equal protein

amounts were separated in a SDS-PAGE gel, transferred to a nitrocellulose membrane and immunoblotted with Sec13 or VAMP7 specific antibodies. An actin antibody was used as loading control.

Cell culture and infection assays

All cell culture reagents were purchased from Invitrogen unless otherwise stated. Human epithelial HeLa cells (clone CCL-2 from the American Type Culture Collection (ATCC)) were cultured in Dulbecco's modified eagle's medium supplemented with 10% (v/v) fetal bovine serum (FBS) at 37°C, 5% CO_2. All live-cell fluorescence microscopy and infection assays were performed in EM buffer (120 mM NaCl, 7 mM KCl, 1.8 mM $CaCl_2$, 0.8 mM $MgCl_2$, 5 mM glucose, 25 mM HEPES, pH 7.3). For invasion experiments, overnight bacterial cultures were subcultured 1/20 and grown until late exponential/early stationary phase. Before infection, bacteria were gently washed with PBS and resuspended in EM buffer. Except for live-cell microscopy, bacteria were added to the cells at a multiplicity of infection (MOI) of 100, incubated for 5 min at room temperature and then at 37°C for 10 min, so that a synchronized infection could be followed. Non-internalized bacteria were washed three times with warm EM buffer and incubated up to 30 min at 37°C. Extracellular bacteria were killed by adding EM containing 50 μg ml^{-1} gentamicin for 1 h. The concentration of gentamicin was then decreased to 10 μg ml^{-1} for the remainder of the experiment and 10% FBS was added to the medium. At the desired time-points, the cells were either processed for fractionation, enumeration of intracellular bacteria or fixed for immunofluorescence analysis. To count the number of intracellular bacteria, infected cells were gently washed with PBS and lysed with ice-cold distilled water containing 0.2% Triton X-100 for 5 min. Bacteria were then serially diluted and plated onto LB agar.

Cell fractionation and isolation of the SCV

For the isolation of the SCV, approximately 6×10^7 HeLa cells were used in T225 flasks. Cells were infected as described before and, at the selected time-points (30 min or 3 h), they were extensively washed with ice-cold homogenization buffer (HB: 250 mM sucrose, 0.5 mM ethylene glycol tetraacetic acid (EGTA), 20 mM HEPES-KOH pH 7.4, supplemented with complete protease inhibitors and 5 μg ml^{-1} cytochalasin-D), detached and then homogenized in HB with a Dounce homogenizer. All steps were performed at 4°C. Between 30 and 40 strokes were performed, until more than 80% free nuclei were visible. Nuclei and intact cells were removed by performing three sequential centrifugations, at 100 g (1000 rpm) for 5 min each, in order to obtain the PNS. In parallel, a non-infected control was prepared. In order to separate all the subcellular organelles, the PNS was loaded on top of a 10–25% (1.06–1.15 g cm^{-3}) linear OptiPrep (Sigma) gradient with a 50% (1.22 g cm^{-3}) cushion, in a 14×89 mm ultracentrifuge tube (Beckman), and then centrifuged at 210000 g (35000 rpm) for 4 h at 4°C, in a SW-41 swinging bucket rotor, with low acceleration and slow brake. Approximately 5×10^7 bacteria were added to the non-infected control PNS. After ultracentrifugation, 1.0 ml fractions were collected from the top to the bottom of the gradient and each fraction was analysed by measuring its refractive index, the number of bacteria by CFUs and the organelle separation efficiency by Western blot. Equal amount of proteins in each fraction were analysed by Western blot. The following primary antibodies were used: mouse anti-EEA-1 (1:2500, BD Biosciences), mouse anti-Rab5 (1:2000, BD Biosciences), rabbit anti-Lamp-1 (1:2000, Abcam), mouse anti-GM130 (1:1000, BD Biosciences), rabbit anti-Catalase (1:2500, Abcam), mouse anti-Calreticulin (1:2000, Abcam), mouse anti-TOM22 (1:2000, Sigma), rabbit anti-VAMP7 (1:2000, Pierce), rabbit anti-*Salmonella* Lipopolysaccharide (LPS) (1:20000, Abcam) and mouse anti-reticulon-4 (1:2000, Thermo-Scientific). The secondary antibodies were diluted 1:10000 (anti-mouse-HRP and anti-rabbit-HRP, Amersham).

ELISA for quantification of intact SCVs

The bottom of the wells of an ELISA plate (Nunc) was coated with a polyclonal rabbit anti-*Salmonella* antibody (Abcam) in PBS and incubated overnight at 4°C. Blocking was carried out by incubating the wells with a 2% BSA solution at room temperature for 90 min. Samples from the PNS or from F6 to F8 were added to the wells and incubated for 1 h at room temperature. As a control, an aliquot from the same sample was subjected to osmotic shock by incubation with distilled water. Standard curves were generated by adding known amounts of bacteria in 1:2 dilution series. Bacteria were then detected by incubation with the same antibody, biotinylated in 2% BSA. Signal was quantified at 450 nm after sequential incubation with streptavidin peroxidase (Sigma) and *o*-Phenylenediamine dihydrochloride (Sigma).

Sample preparation for MS, data processing and analysis

Each experiment was carried out in five biological replicates. After density centrifugation, 150 μl of fraction F6, which was highly enriched is intact SCVs, was subjected to methanol/chloroform protein precipitation (Wessel and Flügge, 1984). Proteins were then separated in by one-dimensional SDS-PAGE in order to eliminate OptiPrep contaminations, each lane was cut into 10 slices and in-gel tryptic digestion was performed as described previously (Wilm *et al.*, 1996). Peptides were finally extracted in 50 mM NH_4HCO_3/acetonitrile/formic acid (42.5/42.5/5), dried down and reconstituted in H_2O/acetonitrile/formic acid (98/2/0.1) before LC-MS/MS analysis. Tryptic digests were analysed by nanoLC-MS/MS using an Ultimate 3000 RSLC system (Dionex, Thermo-Scientific, Waltham, MA, USA) coupled to the nanoelectrospray ion source of a Q-Exactive mass spectrometer (Thermo-Scientific, Bremen, Germany). One microgram of each digest was loaded on a C-18 μ-precolumn (C-18 PepMap100, 5 μm, 100 Å, Dionex, Thermo-Scientific, Waltham, MA, USA) at a flow rate of 30 μl min^{-1} of solvent A and the separation was performed using an in-house packed 15 cm nano-HPLC column (75 μm inner diameter) with C-18 resin (3 μm particles, 100 Å pore size, Reprosil C-18, Dr. Maisch GmbH). Peptides were separated at a flow rate of 300 nl min^{-1} using a gradient of 2% to 55% solvent B for 30 min, followed by a 10 min washing step at 100% solvent B and a reconditioning step at 2% B for 20 min. Solvent A was H_2O/acetonitrile/formic acid (98/2/0.1) and solvent B was H_2O/acetonitrile/formic acid (20/80/0.08). NanoLC-MS/MS experiments were conducted in data-dependent acquisition mode. A resolution of 70 000 (at *m/z* 400) was used for MS scans. The 10 most intense ions were selected for HCD frag-

mentation and fragments were analysed in the orbitrap. A dynamic exclusion window of 30 s was used. Raw files were processed with MaxQuant software (version 1.3.0.5) (Cox and Mann, 2008; Luber *et al*., 2010). Protein identification was carried out using Andromeda (Cox *et al*., 2011) against a concatenated database including *Salmonella* strain SL1344 proteins (tax 216597 – 4657 proteins) and human proteins (tax 9606 – 20233 proteins). Trypsin was chosen as specific enzyme with a maximum number of two miscleavages. Possible modifications included carbamidomethylation (Cys, fixed), oxidation (Met, variable) and N-terminal acetylation (variable). Mass tolerance for MS was set to 20 ppm for the first search then 6 ppm for the main search and 10 ppm was used for MS/MS. The 'match between run' option was selected with a maximal retention time window of 2 min. Five amino acids were required as minimum peptide length. A false discovery rate of 1% was used for the identification. *Salmonella*, reverse and contaminant proteins were excluded and only proteins identified with a minimum of two peptides were considered. Statistical relative protein quantification was performed with the peptide intensities extracted from the 'peptides.txt' MaxQuant output file using MSstats R package (Choi *et al*., 2014). MSstats enables protein significance analysis between different conditions (here control, 30 min and 3 h p.i.) and statistical protein quantification from label-free LC-MS experiments. The gene ontology analysis was performed with DAVID/EASE tools (Huang *et al*., 2009a,b) (http://david.abcc.ncifcrf.gov/).

Microscopy and image analysis

Time-lapse microscopy of living cells was performed at 37°C in a PerkinElmer UltraView spinning disk confocal microscope with a 40 ×/1.3 NA oil objective. Every 10, 20 or 30 min, a stack of 15 z-planes (500 nm step size) was acquired sequentially. In 4% paraformaldehyde (PFA)-fixed samples, the following antibodies were used after cell permeabilization with 0.5% saponin for 10 min: mouse anti-Sec13 (1:100, Abnova), mouse anti-reticulon-4 (1:300, Thermo Scientific), rabbit anti-calnexin (1:100, Stressgen), rabbit anti-Lamp-1 (1:500, Abcam), Alexa Fluor 488-conjugated anti-mouse or anti-rabbit (1:200, Life Technologies) and Cy5-conjugated anti-rabbit (1:200, Life Technologies). Z-stacks of 300 nm step size were acquired with a 60 ×/1.2 NA water objective. The following excitation lasers were used: 405, 488, 561 or 640 nm. Fluorescence emission was detected with 445 (W60), 525 (W50), 615 (W70) or 705 (W90) nm filters respectively. All images were further analysed with ImageJ and FiJi softwares. All confocal microscopy derived images shown correspond to maximum 3D projections.

Correlative-focused ion beam/scanning electron large-volume tomography

HeLa cells grown on MatTek dishes with a finder grid were fixed with 0.1% glutaraldheyde (GA) and 4% PFA for 15 min. After confocal microscopy imaging using a 60 ×/1.3 NA water objective, positions of interest were marked at 10 × magnifications. Then cells were fixed overnight with 2.5% GA in 0.1 M HEPES pH 7.2 and post fixed in 1% osmium/1.5% potassium ferrocyanide in 0.1M HEPES for 1 h. Samples were treated for 30 min with 1% tannic acid and 1 h with 1% osmium tetroxide, rinsed in water and dehydrated in an ethanol series of 25%, 50%, 75%, 90% and 100% (5 min each). Cells were embedded in hard Epon resin. After resin polymerization, Epon blocks were mounted on a SEM stub and coated with a 25 nm layer of gold/palladium. Samples were placed in an Auriga FIB/SEM system (Zeiss) and the site of interest previously visualized by light microscopy was relocated using the imprint of the gridded dish in the Epon. Site was prepared and data acquired using ATLAS 3D software (Zeiss) using the backscatter detector at 2 kV with pixel sizes of 5 nm (Fig. 2E and F) or 10 nm (Fig. 5 and Fig. S4B). Slice thickness was 10 nm in all acquisitions. Stack alignment was performed with ImageJ and 3D visualization, data correlation, manual segmentation and video clips with Amira (FEI).

Quantification of cells containing hyper-replicating bacteria

Identification of cells containing hyper-replicating bacteria was performed using fluorescence microscopy. HeLa cells were infected with dsRed-expressing *Salmonella* and fixed at 6 h p.i., stained with DRAQ5 to enable computer segmentation and imaged on a Perkin Elmer, Opera spinning disk microscope. Images were analysed using Columbus software (Perkin Elmer) to quantify the red intensity (representing bacteria) per cell and defining intensity thresholds for uninfected, infected and hyper-replicating cells. The percentage of hyper-replication was defined as the number of cells containing hyper-replicating bacteria divided by the total number of infected cells.

Statistical analysis

Statistical analyses were performed in GraphPad Prism software v6, or MSstats R package for MS data. Significance was referred as *, **, *** and **** for P-values < 0.05, < 0.01, < 0.001 and < 0.0001 respectively.

Acknowledgements

We would like to thank all the members of the Dynamics of host-pathogen interaction (DIHP) unit, Paul Lazarow and Randy Schekman for productive discussions. We thank T. Gally and F. Perez for fluorescent constructs. This work was supported by a PhD fellowship from the Portuguese Fundação para a Ciência e a Tecnologia (SFRH/BD/51006/2010) to JCS; a Pasteur Foundation Fellowship to JF; and fellowships from the Pasteur-Weizmann Council, EMBO and the Fondation pour la Recherche Médicale to AW. JE is member of the LabEx consortium IBEID and is supported by the Institut Pasteur CARNOT-MIE and the PTR (grant number PTR-460) programmes. JE also acknowledges support of an European Research Council (ERC) starting grant for this work (Rupteffects, Nr. 261166).

The platform microscopie ultrastructurale was supported by France Bioimaging.

Author contributions

JCS, JC-R and JE designed the study. JCS performed all experiments with the help of JF and AW, except mass

spectrometry performed by MD. AM and CS performed electron microscopy sample preparation and data acquisition. Data were analysed by JCS, MD, JF, AW, MM and VH. JCS and JE wrote the manuscript.

Conflict of interest

The authors declare that they have no conflict of interest.

References

Agbor, T.A., and McCormick, B.A. (2011) *Salmonella* effectors: important players modulating host cell function during infection. *Cell Microbiol* **13:** 1858–1869.

Akimana, C., Al-Khodor, S., and Abu Kwaik, Y. (2010) Host factors required for modulation of phagosome biogenesis and proliferation of *Francisella tularensis* within the cytosol. *PLoS ONE* **5:** e11025.

Bakowski, M.A., Braun, V., and Brumell, J.H. (2008) *Salmonella*-containing vacuoles: directing traffic and nesting to grow. *Traffic* **9:** 2022–2031.

Boucrot, E., Henry, T., Borg, J.-P., Gorvel, J.-P., and Méresse, S. (2005) The intracellular fate of *Salmonella* depends on the recruitment of kinesin. *Science* **308:** 1174–1178.

Braun, V., Wong, A., Landekic, M., Hong, W.J., Grinstein, S., and Brumell, J.H. (2010) Sorting nexin 3 (SNX3) is a component of a tubular endosomal network induced by *Salmonella* and involved in maturation of the *Salmonella*-containing vacuole. *Cell Microbiol* **12:** 1352–1367.

Brumell, J.H., Tang, P., Mills, S.D., and Finlay, B.B. (2001) Characterization of *Salmonella*-induced filaments (Sifs) reveals a delayed interaction between *Salmonella*-containing vacuoles and late endocytic compartments. *Traffic* **2:** 643–653.

Buchmeier, N.A., and Heffron, F. (1991) Inhibition of macrophage phagosome-lysosome fusion by *Salmonella typhimurium*. *Infect Immun* **59:** 2232–2238.

Budnik, A., and Stephens, D.J. (2009) ER exit sites – localization and control of COPII vesicle formation. *FEBS Lett* **583:** 3796–3803.

Bujny, M.V., Ewels, P.A., Humphrey, S., Attar, N., Jepson, M.A., and Cullen, P.J. (2008) Sorting nexin-1 defines an early phase of *Salmonella*-containing vacuole-remodeling during *Salmonella* infection. *J Cell Sci* **121:** 2027–2036.

Campbell-Valois, F.-X., Trost, M., Chemali, M., Dill, B.D., Laplante, A., Duclos, S., *et al*. (2012) Quantitative proteomics reveals that only a subset of the endoplasmic reticulum contributes to the phagosome. *Mol Cell Proteomics* **11:** M111.016378.

Campoy, E.M., Mansilla, M.E., and Colombo, M.I. (2013) Endocytic SNAREs are involved in optimal *Coxiella burnetii* vacuole development. *Cell Microbiol* **15:** 922–941.

Cebrian, I., Visentin, G., Blanchard, N., Jouve, M., Bobard, A., Moita, C., *et al*. (2011) Sec22b regulates phagosomal maturation and antigen crosspresentation by dendritic cells. *Cell* **147:** 1355–1368.

Choi, M., Chang, C.-Y., Clough, T., Broudy, D., Killeen, T., MacLean, B., and Vitek, O. (2014) MSstats: an R package for statistical analysis of quantitative mass spectrometry-based proteomic experiments. *Bioinformatics* **30:** 2524–2526.

Cox, J., and Mann, M. (2008) MaxQuant enables high peptide identification rates, individualized p.p.b.-range mass accuracies and proteome-wide protein quantification. *Nat Biotechnol* **26:** 1367–1372.

Cox, J., Neuhauser, N., Michalski, A., Scheltema, R.A., Olsen, J.V., and Mann, M. (2011) Andromeda: a peptide search engine integrated into the MaxQuant environment. *J Proteome Res* **10:** 1794–1805.

Criss, A.K., and Casanova, J.E. (2003) Coordinate regulation of *Salmonella enterica* serovar Typhimurium invasion of epithelial cells by the Arp2/3 complex and Rho GTPases. *Infect Immun* **71:** 2885–2891.

Davis, M.J., Gregorka, B., Gestwicki, J.E., and Swanson, J.A. (2012) Inducible renitence limits *Listeria monocytogenes* escape from vacuoles in macrophages. *J Immunol* **189:** 4488–4495.

Delevoye, C., Nilges, M., Dehoux, P., Paumet, F., Perrinet, S., Dautry-Varsat, A., and Subtil, A. (2008) SNARE protein mimicry by an intracellular bacterium. *PLoS Pathog* **4:** e1000022.

Desjardins, M., Huber, L.A., Parton, R.G., and Griffiths, G. (1994) Biogenesis of phagolysosomes proceeds through a sequential series of interactions with the endocytic apparatus. *J Cell Biol* **124:** 677–688.

Drecktrah, D., Knodler, L.A., Howe, D., and Steele-Mortimer, O. (2007) *Salmonella* trafficking is defined by continuous dynamic interactions with the endolysosomal system. *Traffic* **8:** 212–225.

Drecktrah, D., Levine-Wilkinson, S., Dam, T., Winfree, S., Knodler, L.A., Schroer, T.A., and Steele-Mortimer, O. (2008) Dynamic behavior of *Salmonella*-induced membrane tubules in epithelial cells. *Traffic* **9:** 2117–2129.

Eden, E.R., White, I.J., Tsapara, A., and Futter, C.E. (2010) Membrane contacts between endosomes and ER provide sites for PTP1B-epidermal growth factor receptor interaction. *Nat Cell Biol* **12:** 267–272.

Ehsani, S., Santos, J.C., Rodrigues, C.D., Henriques, R., Audry, L., Zimmer, C., *et al*. (2012) Hierarchies of host factor dynamics at the entry site of *Shigella flexneri* during host cell invasion. *Infect Immun* **80:** 2548–2557.

Elsinghorst, E.A. (1994) Measurement of invasion by gentamicin resistance. *Methods Enzymol* **236:** 405–420.

English, A.R., and Voeltz, G.K. (2013) Endoplasmic reticulum structure and interconnections with other organelles. *Cold Spring Harb Perspect Biol* **5:** a013227.

Fajardo, M., Schleicher, M., Noegel, A., Bozzaro, S., Killinger, S., Heuner, K., *et al*. (2004) Calnexin, calreticulin and cytoskeleton-associated proteins modulate uptake and growth of *Legionella pneumophila* in *Dictyostelium discoideum*. *Microbiology* **150:** 2825–2835.

Figueira, R., and Holden, D.W. (2012) Functions of the *Salmonella* pathogenicity island 2 (SPI-2) type III secretion system effectors. *Microbiology* **158:** 1147–1161.

Friedman, J.R., and Voeltz, G.K. (2011) The ER in 3D: a multifunctional dynamic membrane network. *Trends Cell Biol* **21:** 709–717.

Gagnon, E., Duclos, S., Rondeau, C., Chevet, E., Cameron, P.H., Steele-Mortimer, O., *et al.* (2002) Endoplasmic reticulum-mediated phagocytosis is a mechanism of entry into macrophages. *Cell* **110:** 119–131.

Garcia-del Portillo, F., and Finlay, B.B. (1995) Targeting of *Salmonella typhimurium* to vesicles containing lysosomal membrane glycoproteins bypasses compartments with mannose 6-phosphate receptors. *J Cell Biol* **129:** 81–97.

Guermonprez, P., Saveanu, L., Kleijmeer, M., Davoust, J., Van Endert, P., and Amigorena, S. (2003) ER-phagosome fusion defines an MHC class I cross-presentation compartment in dendritic cells. *Nature* **425:** 397–402.

Haraga, A., Ohlson, M.B., and Miller, S.I. (2008) *Salmonellae* interplay with host cells. *Nat Rev Microbiol* **6:** 53–66.

Harrison, R.E., Brumell, J.H., Khandani, A., Bucci, C., Scott, C.C., Jiang, X., *et al.* (2004) *Salmonella* impairs RILP recruitment to Rab7 during maturation of invasion vacuoles. *Mol Biol Cell* **15:** 3146–3154.

Hashim, S., Mukherjee, K., Raje, M., Basu, S.K., and Mukhopadhyay, A. (2000) Live *Salmonella* modulate expression of Rab proteins to persist in a specialized compartment and escape transport to lysosomes. *J Biol Chem* **275:** 16281–16288.

Haucke, V. (2003) Vesicle budding: a coat for the COPs. *Trends Cell Biol* **13:** 59–60.

Hänisch, J., Ehinger, J., Ladwein, M., Rohde, M., Derivery, E., Bosse, T., *et al.* (2010) Molecular dissection of *Salmonella*-induced membrane ruffling versus invasion. *Cell Microbiol* **12:** 84–98.

Hernandez, L.D., Hueffer, K., Wenk, M.R., and Galán, J.E. (2004) *Salmonella* modulates vesicular traffic by altering phosphoinositide metabolism. *Science* **304:** 1805–1807.

Hoffmann, C., Finsel, I., Otto, A., Pfaffinger, G., Rothmeier, E., Hecker, M., *et al.* (2014) Functional analysis of novel Rab GTPases identified in the proteome of purified *Legionella*-containing vacuoles from macrophages. *Cell Microbiol* **16:** 1034–1052.

Houde, M., Bertholet, S., Gagnon, E., Brunet, S., Goyette, G., Laplante, A., *et al.* (2003) Phagosomes are competent organelles for antigen cross-presentation. *Nature* **425:** 402–406.

Huang, D.W., Sherman, B.T., and Lempicki, R.A. (2009a) Systematic and integrative analysis of large gene lists using DAVID bioinformatics resources. *Nat Protoc* **4:** 44–57.

Huang, D.W., Sherman, B.T., and Lempicki, R.A. (2009b) Bioinformatics enrichment tools: paths toward the comprehensive functional analysis of large gene lists. *Nucleic Acids Res* **37:** 1–13.

Hughes, H., and Stephens, D.J. (2008) Assembly, organization, and function of the COPII coat. *Histochem Cell Biol* **129:** 129–151.

Jo, E.-K., Yuk, J.-M., Shin, D.-M., and Sasakawa, C. (2013) Roles of autophagy in elimination of intracellular bacterial pathogens. *Front Immunol* **4:** 97.

Jolly, C., Winfree, S., Hansen, B., and Steele-Mortimer, O. (2014) The Annexin A2/p11 complex is required for efficient invasion of *Salmonella* Typhimurium in epithelial cells. *Cell Microbiol* **16:** 64–77.

Kagan, J.C., and Roy, C.R. (2002) *Legionella* phagosomes intercept vesicular traffic from endoplasmic reticulum exit sites. *Nat Cell Biol* **4:** 945–954.

Knodler, L.A., Vallance, B.A., Celli, J., Winfree, S., Hansen, B., Montero, M., and Steele-Mortimer, O. (2010) Dissemination of invasive *Salmonella* via bacterial-induced extrusion of mucosal epithelia. *Proc Natl Acad Sci USA* **107:** 17733–17738.

Knodler, L.A., Nair, V., and Steele-Mortimer, O. (2014) Quantitative assessment of cytosolic *Salmonella* in epithelial cells. *PLoS ONE* **9:** e84681.

Kurokawa, K., Okamoto, M., and Nakano, A. (2014) Contact of cis-Golgi with ER exit sites executes cargo capture and delivery from the ER. *Nat Commun* **5:** 3653.

Lee, B.-Y., Jethwaney, D., Schilling, B., Clemens, D.L., Gibson, B.W., and Horwitz, M.A. (2010) The *Mycobacterium bovis* bacille Calmette-Guerin phagosome proteome. *Mol Cell Proteomics* **9:** 32–53.

Lord, C., Ferro-Novick, S., and Miller, E.A. (2013) The highly conserved COPII coat complex sorts cargo from the endoplasmic reticulum and targets it to the golgi. *Cold Spring Harb Perspect Biol* **5:** a013367.

Lu, H., and Clarke, M. (2005) Dynamic properties of *Legionella*-containing phagosomes in *Dictyostelium amoebae*. *Cell Microbiol* **7:** 995–1007.

Luber, C.A., Cox, J., Lauterbach, H., Fancke, B., Selbach, M., Tschopp, J., *et al.* (2010) Quantitative proteomics reveals subset-specific viral recognition in dendritic cells. *Immunity* **32:** 279–289.

Luzio, J.P., Pryor, P.R., and Bright, N.A. (2007) Lysosomes: fusion and function. *Nat Rev Mol Cell Biol* **8:** 622–632.

Luzio, J.P., Gray, S.R., and Bright, N.A. (2010) Endosome-lysosome fusion. *Biochem Soc Trans* **38:** 1413–1416.

McGourty, K., Thurston, T.L., Matthews, S.A., Pinaud, L., Mota, L.J., and Holden, D.W. (2012) *Salmonella* inhibits retrograde trafficking of mannose-6-phosphate receptors and lysosome function. *Science* **338:** 963–967.

Majowicz, S.E., Musto, J., Scallan, E., Angulo, F.J., Kirk, M., O'Brien, S.J., *et al.* (2010) The global burden of nontyphoidal *Salmonella* gastroenteritis. *Clin Infect Dis* **50:** 882–889.

Malik-Kale, P., Winfree, S., and Steele-Mortimer, O. (2012) The bimodal lifestyle of intracellular *Salmonella* in epithelial cells: replication in the cytosol obscures defects in vacuolar replication. *PLoS ONE* **7:** e38732.

Mallo, G.V., Espina, M., Smith, A.C., Terebiznik, M.R., Alemán, A., Finlay, B.B., *et al.* (2008) SopB promotes phosphatidylinositol 3-phosphate formation on *Salmonella* vacuoles by recruiting Rab5 and Vps34. *J Cell Biol* **182:** 741–752.

Mellouk, N., Weiner, A., Aulner, N., Schmitt, C., Elbaum, M., Shorte, S.L., *et al.* (2014) *Shigella* subverts the host recycling compartment to rupture its vacuole. *Cell Host Microbe* **16:** 517–530.

Mota, L.J., Ramsden, A.E., Liu, M., Castle, J.D., and Holden, D.W. (2009) SCAMP3 is a component of the *Salmonella*-induced tubular network and reveals an interaction between bacterial effectors and post-Golgi trafficking. *Cell Microbiol* **11:** 1236–1253.

Müller-Taubenberger, A., Lupas, A.N., Li, H., Ecke, M., Simmeth, E., and Gerisch, G. (2001) Calreticulin and

calnexin in the endoplasmic reticulum are important for phagocytosis. *EMBO J* **20:** 6772–6782.
Oh, Y.K., Alpuche-Aranda, C., Berthiaume, E., Jinks, T., Miller, S.I., and Swanson, J.A. (1996) Rapid and complete fusion of macrophage lysosomes with phagosomes containing *Salmonella typhimurium*. *Infect Immun* **64:** 3877–3883.
Orci, L., Ravazzola, M., Le Coadic, M., Shen, W.-W., Demaurex, N., and Cosson, P. (2009) From the Cover: STIM1-induced precortical and cortical subdomains of the endoplasmic reticulum. *Proc Natl Acad Sci USA* **106:** 19358–19362.
Patel, J.C., and Galán, J.E. (2006) Differential activation and function of Rho GTPases during *Salmonella*-host cell interactions. *J Cell Biol* **175:** 453–463.
Paz, I., Sachse, M., Dupont, N., Mounier, J., Cederfur, C., Enninga, J., *et al*. (2010) Galectin-3, a marker for vacuole lysis by invasive pathogens. *Cell Microbiol* **12:** 530–544.
Ragaz, C., Pietsch, H., Urwyler, S., Tiaden, A., Weber, S.S., and Hilbi, H. (2008) The *Legionella pneumophila* phosphatidylinositol-4 phosphate-binding type IV substrate SidC recruits endoplasmic reticulum vesicles to a replication-permissive vacuole. *Cell Microbiol* **10:** 2416–2433.
Ramsden, A.E., Holden, D.W., and Mota, L.J. (2007a) Membrane dynamics and spatial distribution of *Salmonella*-containing vacuoles. *Trends Microbiol* **15:** 516–524.
Ramsden, A.E., Mota, L.J., Münter, S., Shorte, S.L., and Holden, D.W. (2007b) The SPI-2 type III secretion system restricts motility of *Salmonella*-containing vacuoles. *Cell Microbiol* **9:** 2517–2529.
Rao, P.K., Singh, C.R., Jagannath, C., and Li, Q. (2009) A systems biology approach to study the phagosomal proteome modulated by mycobacterial infections. *Int J Clin Exp Med* **2:** 233–247.
Rathman, M., Barker, L.P., and Falkow, S. (1997) The unique trafficking pattern of *Salmonella typhimurium*-containing phagosomes in murine macrophages is independent of the mechanism of bacterial entry. *Infect Immun* **65:** 1475–1485.
Robinson, C.G., and Roy, C.R. (2006) Attachment and fusion of endoplasmic reticulum with vacuoles containing *Legionella pneumophila*. *Cell Microbiol* **8:** 793–805.
Rocha, N., Kuijl, C., van der Kant, R., Janssen, L., Houben, D., Janssen, H., *et al*. (2009) Cholesterol sensor ORP1L contacts the ER protein VAP to control Rab7-RILP-p150 Glued and late endosome positioning. *J Cell Biol* **185:** 1209–1225.
Rogers, L.D., and Foster, L.J. (2007) The dynamic phagosomal proteome and the contribution of the endoplasmic reticulum. *Proc Natl Acad Sci USA* **104:** 18520–18525.
Rogers, L.D., and Foster, L.J. (2008) Contributions of proteomics to understanding phagosome maturation. *Cell Microbiol* **10:** 1405–1412.
Rowland, A.A., Chitwood, P.J., Phillips, M.J., and Voeltz, G.K. (2014) ER contact sites define the position and timing of endosome fission. *Cell* **159:** 1027–1041.
Sato, K. (2004) COPII coat assembly and selective export from the endoplasmic reticulum. *J Biochem* **136:** 755–760.
Schindler, A.J., and Schekman, R. (2009) In vitro reconstitution of ER-stress induced ATF6 transport in COPII vesicles. *Proc Natl Acad Sci USA* **106:** 17775–17780.
Schroeder, N., Henry, T., de Chastellier, C., Zhao, W., Guilhon, A.-A., Gorvel, J.-P., and Méresse, S. (2010) The virulence protein SopD2 regulates membrane dynamics of *Salmonella*-containing vacuoles. *PLoS Pathog* **6:** e1001002.
Schroeder, N., Mota, L.J., and Méresse, S. (2011) *Salmonella*-induced tubular networks. *Trends Microbiol* **19:** 268–277.
Scott, C.C., Dobson, W., Botelho, R.J., Coady-Osberg, N., Chavrier, P., Knecht, D.A., *et al*. (2005) Phosphatidylinositol-4,5-bisphosphate hydrolysis directs actin remodeling during phagocytosis. *J Cell Biol* **169:** 139–149.
Shevchuk, O., Batzilla, C., Hägele, S., Kusch, H., Engelmann, S., Hecker, M., *et al*. (2009) Proteomic analysis of *Legionella*-containing phagosomes isolated from *Dictyostelium*. *Int J Med Microbiol* **299:** 489–508.
Smith, A.C., Heo, W.D., Braun, V., Jiang, X., Macrae, C., Casanova, J.E., *et al*. (2007) A network of Rab GTPases controls phagosome maturation and is modulated by *Salmonella enterica* serovar Typhimurium. *J Cell Biol* **176:** 263–268.
Steele-Mortimer, O. (2008) The *Salmonella*-containing vacuole: moving with the times. *Curr Opin Microbiol* **11:** 38–45.
Steele-Mortimer, O., Méresse, S., Gorvel, J.P., Toh, B.H., and Finlay, B.B. (1999) Biogenesis of *Salmonella typhimurium*-containing vacuoles in epithelial cells involves interactions with the early endocytic pathway. *Cell Microbiol* **1:** 33–49.
Stefan, C.J., Manford, A.G., and Emr, S.D. (2013) ER-PM connections: sites of information transfer and inter-organelle communication. *Curr Opin Cell Biol* **25:** 434–442.
Stuart, L.M., Boulais, J., Charriere, G.M., Hennessy, E.J., Brunet, S., Jutras, I., *et al*. (2007) A systems biology analysis of the *Drosophila* phagosome. *Nature* **445:** 95–101.
Thurston, T.L., Wandel, M.P., von Muhlinen, N., Foeglein, A., and Randow, F. (2012) Galectin 8 targets damaged vesicles for autophagy to defend cells against bacterial invasion. *Nature* **482:** 414–418.
Urwyler, S., Nyfeler, Y., Ragaz, C., Lee, H., Mueller, L.N., Aebersold, R., and Hilbi, H. (2009) Proteome analysis of *Legionella* vacuoles purified by magnetic immunoseparation reveals secretory and endosomal GTPases. *Traffic* **10:** 76–87.
Walther, T.C., and Mann, M. (2010) Mass spectrometry-based proteomics in cell biology. *J Cell Biol* **190:** 491–500.
Ward, T.H., Polishchuk, R.S., Caplan, S., Hirschberg, K., and Lippincott-Schwartz, J. (2001) Maintenance of Golgi structure and function depends on the integrity of ER export. *J Cell Biol* **155:** 557–570.
Wessel, D., and Flügge, U.I. (1984) A method for the quantitative recovery of protein in dilute solution in the presence of detergents and lipids. *Anal Biochem* **138:** 141–143.
Wilm, M., Shevchenko, A., Houthaeve, T., Breit, S., Schweigerer, L., Fotsis, T., and Mann, M. (1996) Femtomole sequencing of proteins from polyacrylamide gels by nano-electrospray mass spectrometry. *Nature* **379:** 466–469.

Zhou, D., Chen, L.M., Hernandez, L., Shears, S.B., and Galán, J.E. (2001) A *Salmonella* inositol polyphosphatase acts in conjunction with other bacterial effectors to promote host cell actin cytoskeleton rearrangements and bacterial internalization. *Mol Microbiol* **39:** 248–259.

Supporting information

Additional Supporting Information may be found in the online version of this article at the publisher's web-site:

Fig. S1. (Related to Fig. 1). Validation of the ELISA assay and density gradients quality.
A–B. The bottom of the wells of an ELISA plate was coated with an anti-*Salmonella* antibody and known amounts of bacteria were added in 1:2 dilution series. *Salmonella* were then detected by incubation with a biotinylated anti-*Salmonella* antibody and streptavidin peroxidase. Signal was quantified at 450 nm, correlated to number of bacteria per ml and plotted as linear-linear (A) or log-log (B).
C. After ultracentrifugation of the different PNSs, 12 fractions were collected (F1–F12) from the top to the bottom of the gradients. The refractive index was measured in each fraction, using a refractometer, and then the density (in g cm^{-3}) was calculated. The graph shows the mean ± SEM from 15 different gradients from five independent experiments.
Fig. S2. (Related to Fig. 1). Subcellular organelle distribution in the 3 h infection fractionation.
All fractions F1 to F12 and the PNS were tested using markers for the following compartments: early endosomes (EEA-1 and Rab5), late endosomes and lysosomes (Lamp-1), Golgi (GM130), peroxisomes (catalase), mitochondria (TOM22) and ER (calreticulin). *Salmonella* distribution was assessed with a specific anti-*Salmonella* LPS antibody.
Fig. S3. (Related to Fig. 2). Relative protein quantitative differences between the different protein subsets and gene ontology analysis.
A–B. Volcano plots of relative protein abundance differences between the control fraction and the 30 min SCV fraction (A) or the 3 h SCV fraction (B), as a function of statistical significance. Relative protein abundances were considered different when the $\log_2$ fold-change >0.387 or <–0.387, with a *P*-value <0.05. Proteins with no statistically significant abundance difference between conditions are represented in gray. Proteins enriched at the 30 min SCV are depicted in red (A), whereas proteins enriched at the 3 h SCV are shown in green (B). In both graphs, factors enriched in the control non-infected fraction are shown in blue. Values correspond to the average fold-changes of five independent experiments.
C. The host proteins enriched in the SCV were subjected to gene ontology analysis and grouped according to their biological process. For each term, the analysis was performed for the proteins enriched uniquely either at the 30 min SCV (only 30 min SCV, red bars) or at the 3 h SCV (only 3 h SCV, green bars) or for the proteins enriched at both time-points (both 30 min + 3 h SCV, orange bars). The graphs show the percentage of host proteins enriched at the SCV, relative to the total number of proteins identified in each condition. Statistics were performed by determining the *P*-values (EASE score) and show the robustness of gene-term enrichment for each condition. ND, non-enriched factors in comparison with the control.
Fig. S4. (Related to Figs 3 and 4). The SCV contacts with the host cell ER and the COPII complex accumulates around intracellular *Salmonella*.
A. Equal amounts of protein from subcellular fractions F3 to F7 were immunoblotted, using markers for reticulon-4 or VAMP7.
B. Cells infected with *Salmonella* for 30 min were fixed and imaged by fluorescence confocal microscopy followed by FIB/SEM. Several yz-views are shown, corresponding to different acquisition planes, and depict sites of membrane contact between the SCV and the ER (arrowheads). We show here a different data set from the one shown on Fig. 3E–F. (b, bacteria; s, SCV lumen).
C. Cells were infected with *Salmonella*-dsRed, fixed at different time-points and immunostained for Sec13 (green). DNA was stained with DAPI (cyan). Representative confocal microscopy images show the association of Sec13 around intracellular bacteria. Arrows point to Sec13-positive bacteria.
D. HeLa cells were infected with *Salmonella*-dsRed, fixed at different time-points and immunostained for Sec13. DNA was stained with DAPI (cyan). Images show representative infected cells with or without hyper-replicating *Salmonella* after confocal microscopy analysis. Arrows point to Sec13-positive structures resembling bacterial-shaped membrane remnants.
E. The percentage of infected cells containing Sec13-positive bacterial-shaped membrane remnants was determined by counting 50 cells with or without hyper-replicating bacteria, from triplicate wells. Scale bars correspond to 10 μm.
Fig. S5. (Related to Video Clips S2–S4). VAMP7-positive lysosome-like vesicles are recruited to the early SCV, which then gets depleted in acidic content.
HeLa cells were transfected with VAMP7-RFP for 48 h, treated with LysoTracker deep red at 50 nM for 30 min and infected with GFP-expressing *Salmonella* at a MOI of 30. Infected cells were then imaged by time-lapse confocal microscopy. After 30 min cells were washed and 50 μg ml^{-1} gentamicin was added for 1 h. The concentration of gentamicin was then decreased to 10 μg ml^{-1} for the remainder of the experiment and 10% FBS was added to the medium. Arrows point to intracellular bacteria. Scale bar corresponds to 10 μm. Representative data from five independent experiments are shown.
Fig. S6. (Related to Fig. 7 and Video Clip S6). VAMP7 does not affect *Salmonella* hyper-replication but is recruited to SIFs.
A. HeLa cells were treated with scramble or VAMP7 siRNA for 72 h and infected with dsRed-expressing *Salmonella* for 6 h. Cells were then fixed, counterstained with DRAQ5 and imaged by fluorescence microscopy. Statistics were determined using the Student's *t*-test. ns, not significant. Data from three independent experiments are shown.
B. Cells were transfected with VAMP7-RFP and Lamp-1-GFP and infected with *Salmonella*. Gentamicin was added to kill extracellular bacteria and cells were then imaged by time-lapse confocal microscopy every 10 min. Arrows indicate SIF tubules. Representative data from three independent experiments are shown.
Table S1. Relative protein abundances at the 30 min SCV compared with the non-infected control for the complete list of host proteins identified by proteomics.
Table S2. Relative protein abundances at the 3 h SCV compared with the non-infected control for the complete list of host proteins identified by proteomics.

Table S3. Complete list of host proteins enriched in the SCV at 30 min, 3 h or at both time-points.
Table S4. Selected host proteins enriched in the SCV identified by proteomics.
Video Clip S1. (Related to Fig. 3E and F – 38 MB; 1 min and 11 s). Ultrastructural characterization of ER interactions with the early SCV. Successive FIB/SEM sections are shown in the xy-view and show sites of membrane contact between SCVs and the ER (arrowheads). The bacteria (blue), the SCV lumen (yellow) and the ER (red) were segmented using Amira software.
Video Clip S2. (Related to Fig. S5A – 771 KB; 20 s). HeLa cells were transfected with VAMP7-RFP (red) and lysosomes were stained with LysoTracker deep red (purple). Cells were then infected with *Salmonella*-GFP (green) and imaged by confocal microscopy. VAMP7- and LysoTracker-positive vesicles accumulate around the early SCV, in the first 2 h of infection. Then the SCV loses both markers and by 5 h p.i. gets again enriched in VAMP7 but not LysoTracker. Scale bar corresponds to 10 μm.
Video Clip S3. (Related to Fig. S5B – 1.3 MB; 30 s). HeLa cells were transfected with VAMP7-RFP (red) and lysosomes were stained with LysoTracker deep red (purple). Cells were then infected with *Salmonella*-GFP (green) and imaged by confocal microscopy. VAMP7- and LysoTracker-positive vesicles accumulate around the early SCV, in the first 2 h of infection. Then the SCV loses both markers and by 5 h p.i. gets again enriched in VAMP7 but not LysoTracker. By 6 h p.i., bacterial replication is observed, together with VAMP7-positive tubules emanating from the SCV. Scale bar corresponds to 10 μm.
Video Clip S4. (Related to Fig. S5C – 1.3 MB; 18 s). HeLa cells were transfected with VAMP7-RFP (red) and lysosomes were stained with LysoTracker deep red (purple). Cells were then infected with *Salmonella*-GFP (green) and imaged by confocal microscopy. VAMP7- and LysoTracker-positive vesicles accumulate around the early SCV, in the first 2.5 h of infection. Then the SCV loses LysoTracker and by 6 h p.i., bacterial replication is observed, together with VAMP7-positive tubules emanating from the SCV. Scale bar corresponds to 10 μm.
Video Clip S5. (Related to Fig. 6 – 49 MB; 1 min and 23 s). Ultrastructural characterization of the interactions between early SCVs and VAMP7/Lamp-1-positive vesicles. Fluorescence confocal microscopy of DAPI (blue), VAMP7 (red) and Lamp-1 (green) was followed by 3D FIB/SEM at the same cell. Segmentation of the bacteria (blue), vesicles and SCVs lumen (yellow) show that some VAMP7/Lamp-1-poisitive vesicles interact and fuse with the SCVs. Fluorescence staining of the bacteria was used as correlating fiducials.
Video Clip S6. (Related to Fig. S6B – 1.3 MB; 27 s). HeLa cells were transfected with VAMP7-RFP and Lamp-1-GFP and infected with *Salmonella*. Lamp-1- and VAMP7-positive SIFs emanate from the SCV 5 h p.i. Scale bar corresponds to 10 μm.

Supplemental information from Manuscript 2

Inventory of Supplemental information

Supplemental Figures

Fig. S1

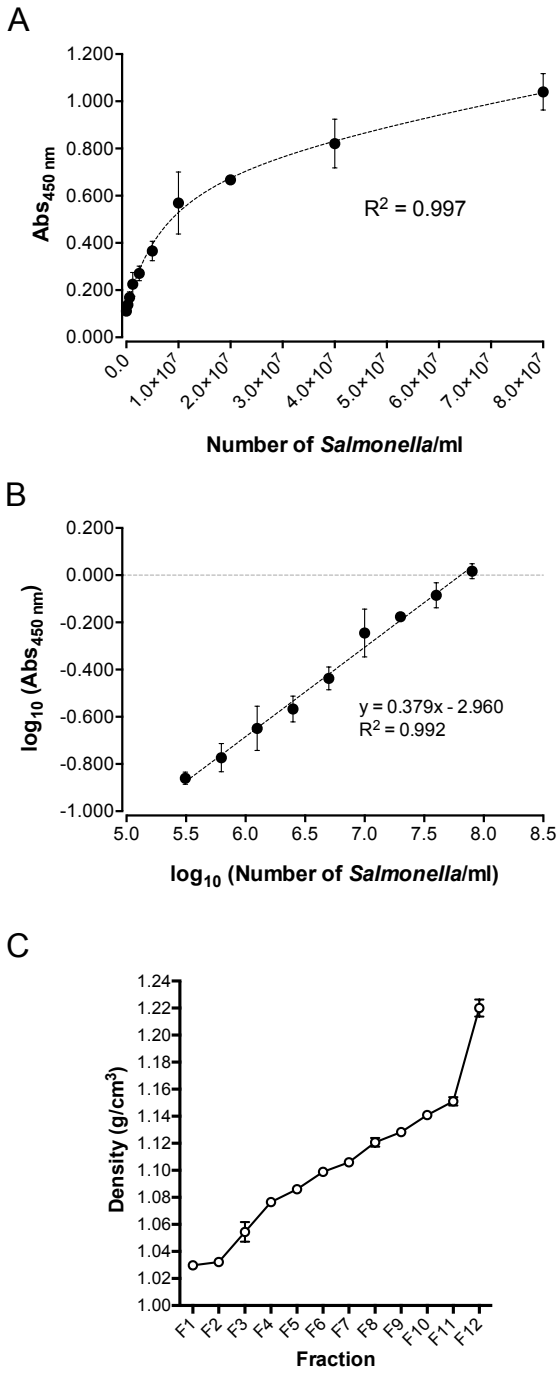

Fig. S1 (related to Fig. 1). **Validation of the ELISA assay and density gradients quality.**

A-B. The bottom of the wells of an ELISA plate was coated with an anti-*Salmonella* antibody and known amounts of bacteria were added in 1:2 dilution series. *Salmonella* were then detected by incubation with a biotinylated anti-*Salmonella* antibody and

streptavidin-peroxidase. Signal was quantified at 450 nm, correlated to number of bacteria/ml and plotted as linear-linear (A) or log-log (B).

C. After ultracentrifugation of the different PNSs, 12 fractions were collected (F1-F12) from the top to the bottom of the gradients. The refractive index was measured in each fraction, using a refractometer, and then the density (in g/cm^3) was calculated. The graph shows the mean ± SEM from 15 different gradients from 5 independent experiments.

Fig. S2

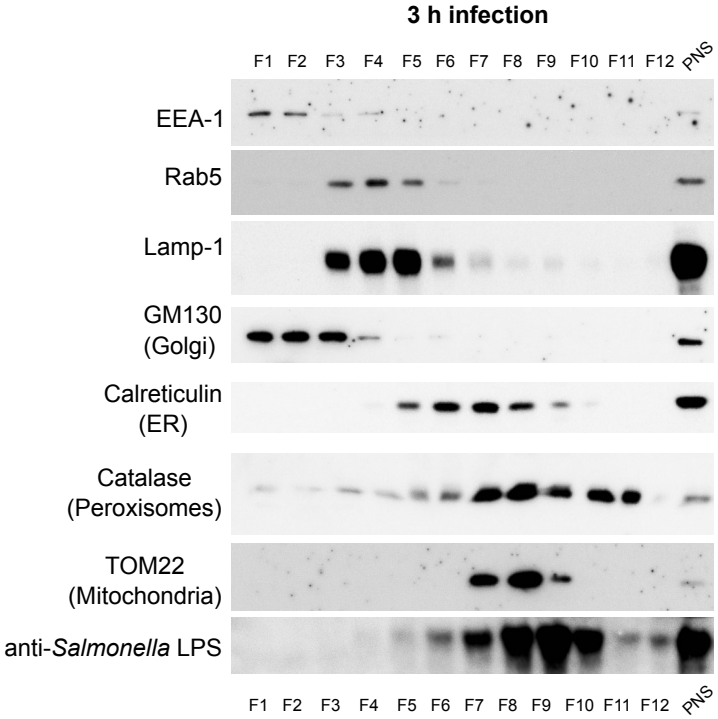

Fig. S2 (related to Fig. 1**). Subcellular organelle distribution in the 3 h infection fractionation.**

All fractions F1 to F12 and the PNS were tested using markers for the following compartments: early endosomes (EEA-1 and Rab5), late endosomes and lysosomes (Lamp-1), Golgi (GM130), peroxisomes (catalase), mitochondria (TOM22) and ER (calreticulin). *Salmonella* distribution was assessed with a specific anti-*Salmonella* LPS antibody.

Fig. S3

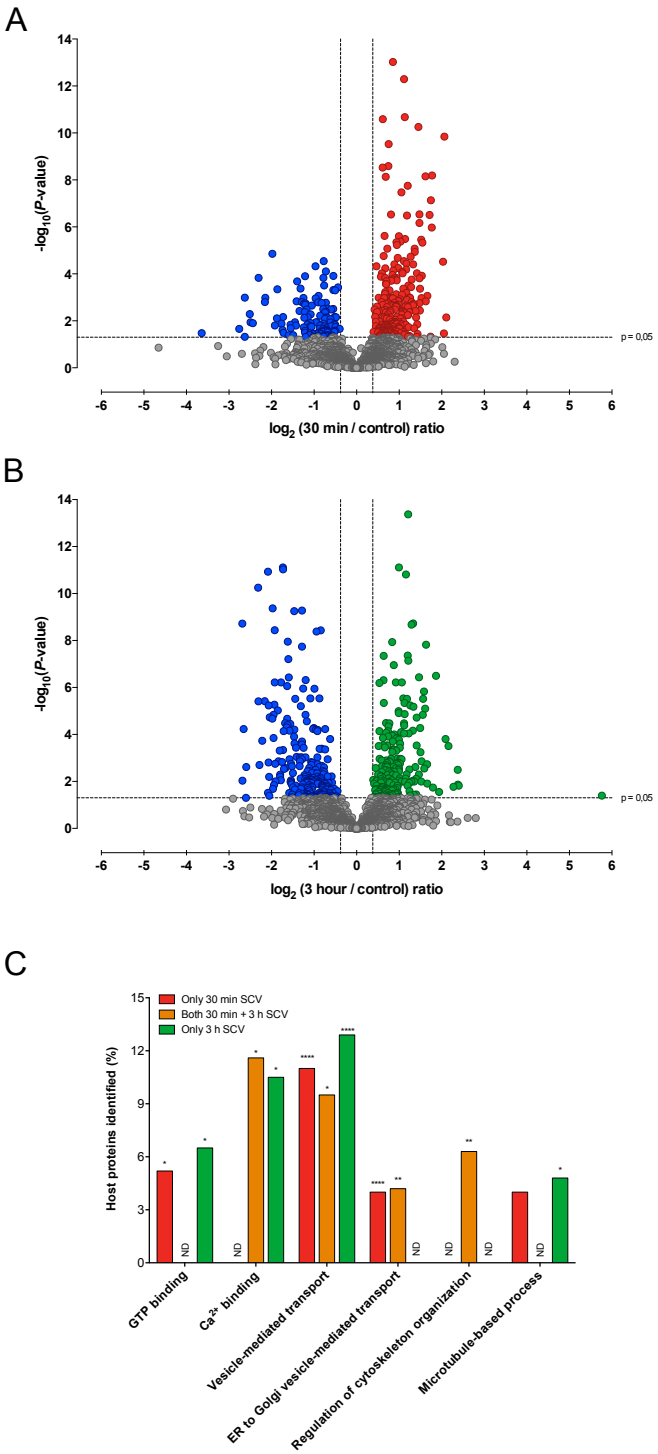

Fig. S3 (related to Fig. 2). **Relative protein quantitative differences between the different protein subsets and Gene Ontology analysis.**

A-B. Volcano plots of relative protein abundance differences between the control fraction and the 30 min SCV fraction (A) or the 3 h SCV fraction (B), as a function of statistical significance. Relative protein abundances were considered different when the $\log_2$ fold-change > 0.387 or < -0.387, with a *P*-value < 0.05. Proteins with no statistically significant

abundance difference between conditions are represented in gray. Proteins enriched at the 30 min SCV are depicted in red (A), whereas proteins enriched at the 3 h SCV are shown in green (B). In both graphs, factors enriched in the control non-infected fraction are shown in blue. Values correspond to the average fold-changes of 5 independent experiments.

C. The host proteins enriched in the SCV were subjected to gene ontology analysis and grouped according to their biological process. For each term, the analysis was performed for the proteins enriched uniquely either at the 30 min SCV (only 30 min SCV, red bars) or at the 3 h SCV (only 3 h SCV, green bars), or for the proteins enriched at both time-points (both 30 min + 3 h SCV, orange bars). The graphs show the % of host proteins enriched at the SCV, relative to the total number of proteins identified in each condition. Statistics were performed by determining the *P*-values (EASE score), and show the robustness of gene-term enrichment for each condition. ND – non enriched factors in comparison to the control.

Fig. S4

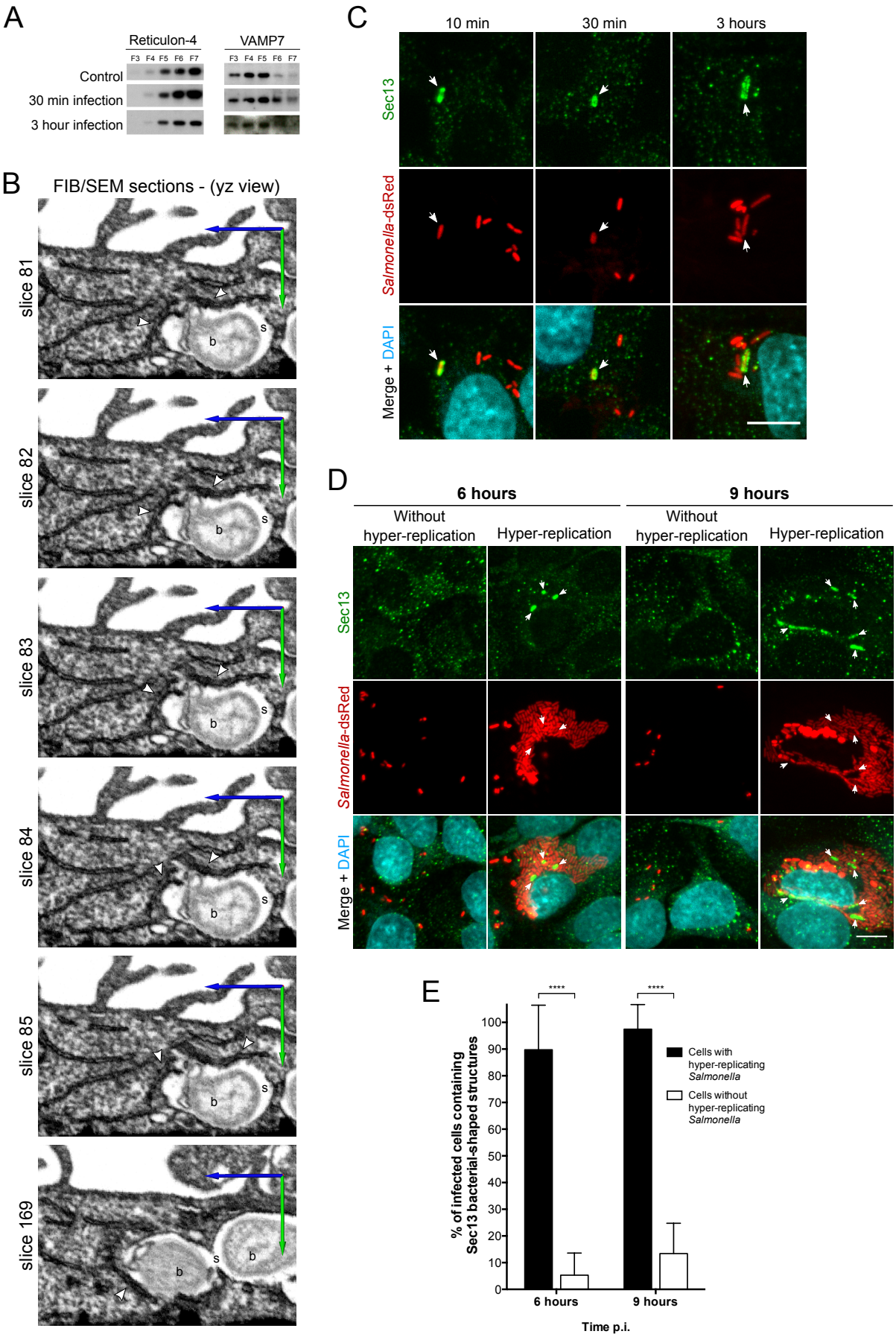
A
Reticulon-4
VAMP7
F3 F4 F5 F6 F7
Control
30 min infection
3 hour infection
B
FIB/SEM sections - (yz view)
slice 81
slice 82
slice 83
slice 84
slice 85
slice 169
b
s
C
10 min
30 min
3 hours
Sec13
Salmonella-dsRed
Merge + DAPI
D
6 hours
9 hours
Without hyper-replication
Hyper-replication
Sec13
Salmonella-dsRed
Merge + DAPI
E
% of infected cells containing Sec13 bacterial-shaped structures
0
10
20
30
40
50
60
70
80
90
100
****
****
6 hours
9 hours
Time p.i.
Cells with hyper-replicating Salmonella
Cells without hyper-replicating Salmonella

Fig. S4 (related to Fig. 3 and 4). **The SCV contacts with the host cell ER, and the COPII complex accumulates around intracellular *Salmonella*.**

A. Equal amounts of protein from subcellular fractions F3 to F7 were immunoblotted, using markers for reticulon-4 or VAMP7.

B. Cells infected with *Salmonella* for 30 min were fixed and imaged by fluorescence confocal microscopy followed by FIB/SEM. Several yz-views are shown, corresponding to different acquisition planes, and depict sites of membrane contact between the SCV and the ER (arrowheads). We show here a different dataset from the one shown on Figure 3E-F. (b - bacteria; s - SCV lumen).

C. Cells were infected with *Salmonella*-dsRed, fixed at different time-points and immunostained for Sec13 (green). DNA was stained with DAPI (cyan). Representative confocal microscopy images show the association of Sec13 around intracellular bacteria. Arrows point to Sec13-positive bacteria.

D. HeLa cells were infected with *Salmonella*-dsRed, fixed at different time-points and immunostained for Sec13. DNA was stained with DAPI (cyan). Images show representative infected cells with or without hyper-replicating *Salmonella* after confocal microscopy analysis. Arrows point to Sec13-positive structures resembling bacterial-shaped membrane remnants.

E. The percentage of infected cells containing Sec13-positive bacterial-shaped membrane remnants was determined by counting 50 cells with or without hyper-replicating bacteria, from triplicate wells.

Scale bars correspond to 10 µm.

Fig. S5

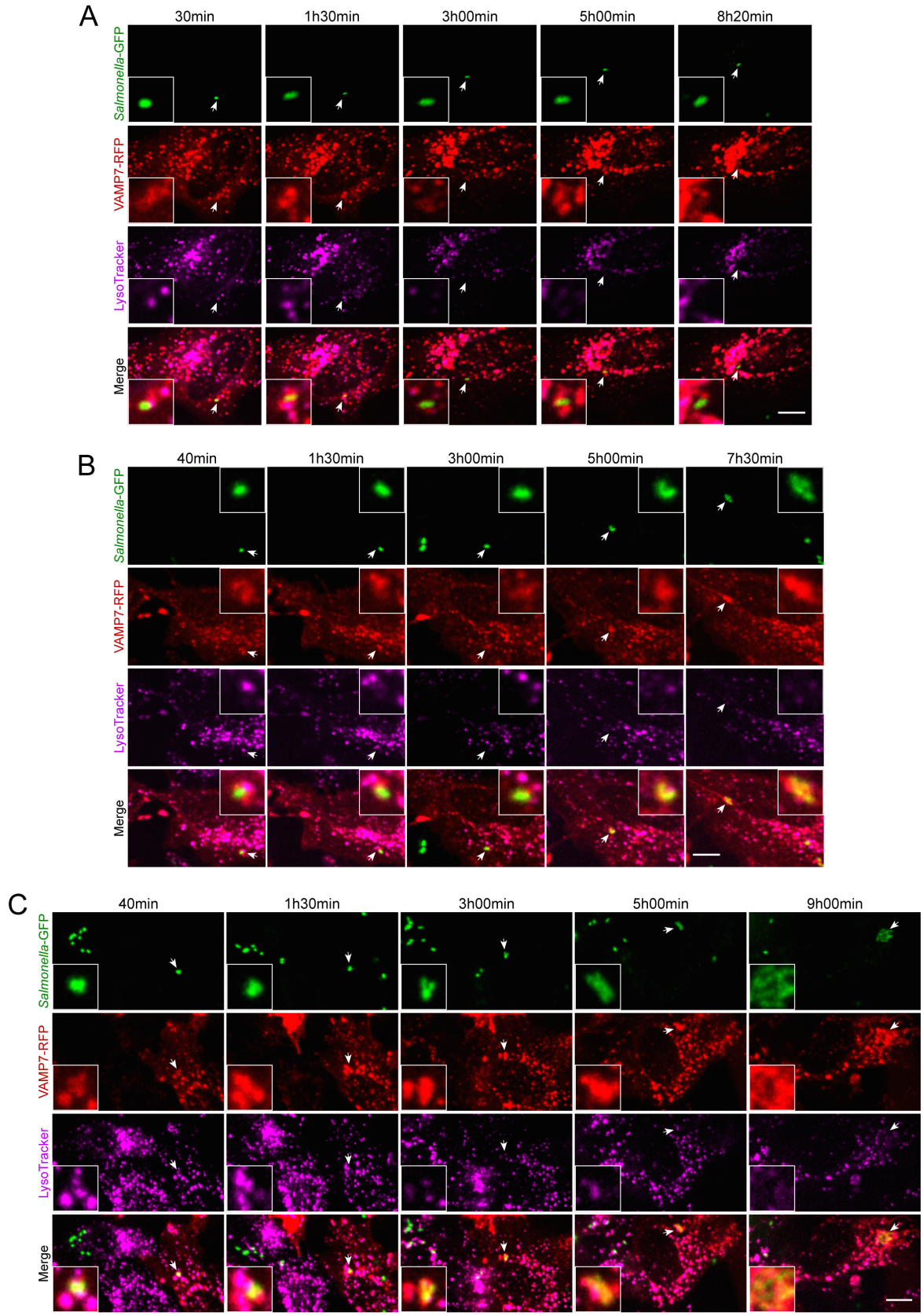

Fig. S5 (related to Supplemental Movies S2-S4). **VAMP7-positive lysosome-like vesicles are recruited to the early SCV, which then gets depleted in acidic content.**

HeLa cells were transfected with VAMP7-RFP for 48 h, treated with LysoTracker Deep Red at 50 nM for 30 min and infected with GFP-expressing *Salmonella* at a MOI of 30. Infected cells were then imaged by time-lapse confocal microscopy. After 30 min cells were washed and 50 µg/ml gentamicin was added for 1 h. The concentration of gentamicin was then decreased to 10 µg/ml for the remainder of the experiment and 10% FBS was added to the medium. Arrows point to intracellular bacteria. Scale bar corresponds to 10 µm. Representative data from 5 independent experiments are shown.

Fig. S6

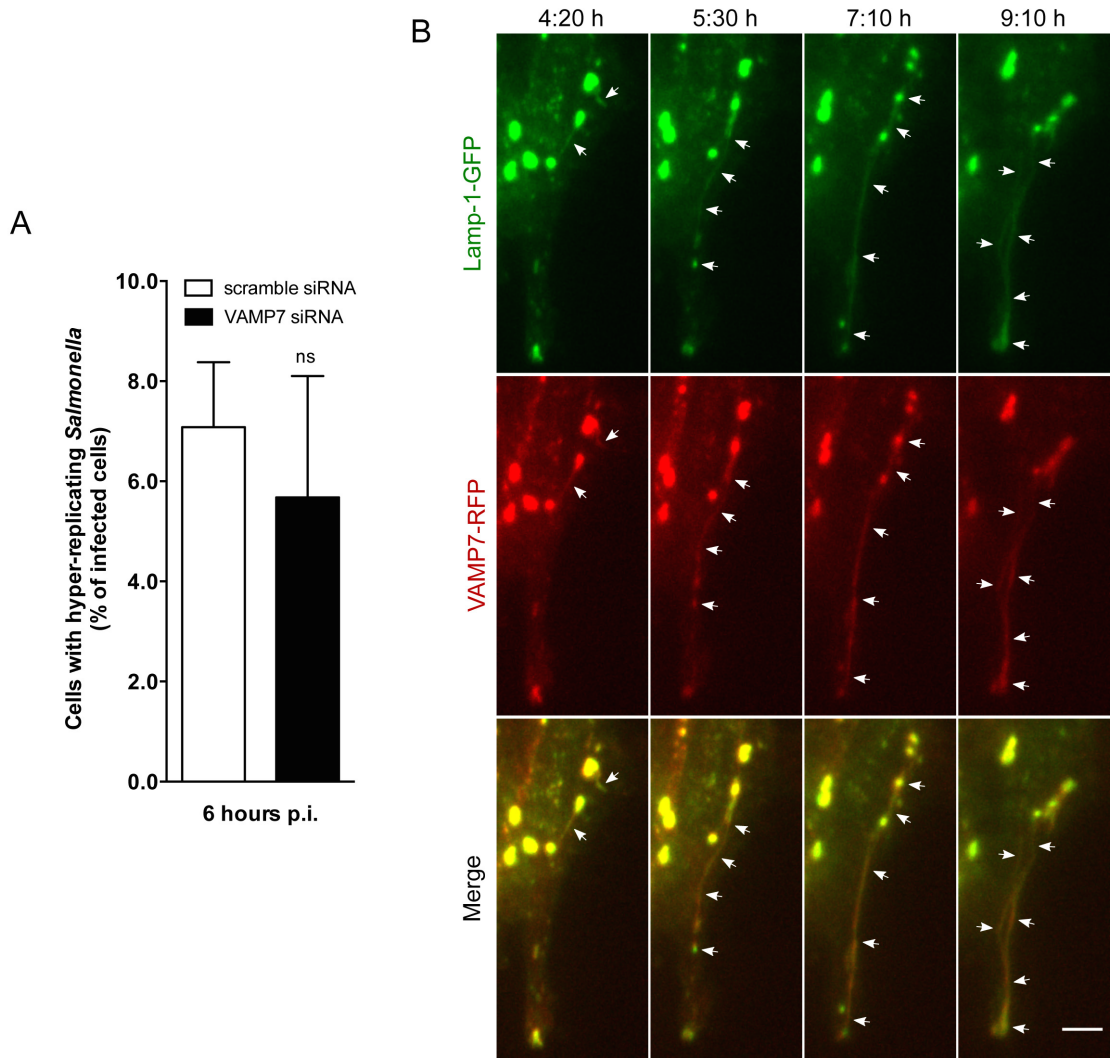

Fig. S6 (related to Fig. 7 and Movie S6). **VAMP7 does not affect *Salmonella* hyper-replication but is recruited to SIFs.**

A. HeLa cells were treated with scramble or VAMP7 siRNA for 72 h and infected with dsRed-expressing *Salmonella* for 6h. Cells were then fixed, counterstained with DRAQ5 and imaged by fluorescence microscopy. Statistics were determined using the Student's t test. ns = not significant. Data from 3 independent experiments are shown.

B. Cells were transfected with VAMP7-RFP and Lamp-1-GFP and infected with *Salmonella*. Gentamicin was added to kill extracellular bacteria and cells were then imaged by time-lapse confocal microscopy, every 10 minutes. Arrows indicate SIF tubules. Representative data from 3 independent experiments are shown.

Supplemental Movie Legends

Movie S1 (related to Fig. 3E-3F – 38 MB; 1 minute and 11 seconds).
Ultrastructural characterization of ER interactions with the early SCV. Successive FIB/SEM sections are shown in the xy-view and show sites of membrane contact between SCVs and the ER (arrowheads). The bacteria (blue), the SCV lumen (yellow) and the ER (red) were segmented using Amira software.

Movie S2 (related to Fig. S5A – 771 KB; 20 seconds).
HeLa cells were transfected with VAMP7-RFP (red) and lysosomes were stained with LysoTracker Deep Red (purple). Cells were then infected with *Salmonella*-GFP (green) and imaged by confocal microscopy. VAMP7- and LysoTracker-positive vesicles accumulate around the early SCV, in the first 2 h of infection. Then the SCV loses both markers and by 5 h p.i. gets again enriched in VAMP7 but not LysoTracker. Scale bar corresponds to 10 μm.

Movie S3 (related to Fig. S5B – 1.3 MB; 30 seconds).
HeLa cells were transfected with VAMP7-RFP (red) and lysosomes were stained with LysoTracker Deep Red (purple). Cells were then infected with *Salmonella*-GFP (green) and imaged by confocal microscopy. VAMP7- and LysoTracker-positive vesicles accumulate around the early SCV, in the first 2 h of infection. Then the SCV loses both markers and by 5 h p.i. gets again enriched in VAMP7 but not LysoTracker. By 6 h p.i. bacterial replication is observed, together with VAMP7-positive tubules emanating from the SCV. Scale bar corresponds to 10 μm.

Movie S4 (related to Fig. S5C – 1.3 MB; 18 seconds).
HeLa cells were transfected with VAMP7-RFP (red) and lysosomes were stained with LysoTracker Deep Red (purple). Cells were then infected with *Salmonella*-GFP (green) and imaged by confocal microscopy. VAMP7- and LysoTracker-positive vesicles accumulate around the early SCV, in the first 2.5 h of infection. Then the SCV loses Lysotracker and by 6 h p.i. bacterial replication is observed, together with VAMP7-positive tubules emanating from the SCV. Scale bar corresponds to 10 μm.

Movie S5 (related to Fig. 6 – 49 MB; 1 minute and 23 seconds).
Ultrastructural characterization of the interactions between early SCVs and VAMP7/Lamp-1-positive vesicles. Fluorescence confocal microscopy of DAPI (blue), VAMP7 (red) and Lamp-1 (green) was followed by 3D FIB/SEM at the same cell. Segmentation of the

bacteria (blue), vesicles and SCVs lumen (yellow) show that some VAMP7/Lamp-1-poisitive vesicles interact and fuse with the SCVs. Fluorescence staining of the bacteria was used as correlating fiducials.

Movie S6 (related to Fig. S6B – 1.3 MB; 27 seconds).
HeLa cells were transfected with VAMP7-RFP and Lamp-1-GFP and infected with *Salmonella*. Lamp-1- and VAMP7-positive SIFs emanate from the SCV 5 h p.i.. Scale bar corresponds to 10 µm.

Movies S1-**S6** are shown on the Electronic Annex, on the attached CD.

Supplemental Tables

Table S1. Relative protein abundances at the 30 min SCV comparing to the non-infected control, for the complete list of host proteins identified by proteomics.

Table S2. Relative protein abundances at the 3 h SCV comparing to the non-infected control, for the complete list of host proteins identified by proteomics.

Table S3. Complete list of host proteins enriched in the SCV, at 30 min, 3 h or at both time-points.

Table S4. Selected host proteins enriched in the SCV, identified by proteomics.

Tables S1-**S2** are shown on the Electronic Annex, on the attached CD.

Table S3 is shown on the Annexes at the end of this thesis.

Table S4 is shown on the following pages.

Table S4. Selected host proteins enriched in the SCV, identified by proteomics.[a]

Accession no.	Protein name	Subcellular localization	30 min SCV	3 h SCV	References
P61160	Actin-related protein 2 (Arp2)	Cytoskeleton	+	n.d,	(Criss and Casanova, 2003; Hänisch et al., 2010) [b]
P62736	Alpha-actin-2	Cytoplasm, cytoskeleton	+	n.d.	(Finlay et al., 1991) [b]
P07355	Annexin A2	PM, early endosomes, BCG-phagosome	+	n.d.	(Jolly et al., 2013; Lee et al., 2010) [b,c]
P08758	Annexin A5	Early endosomes, BCG-phagosome	n.d.	+	(Lee et al., 2010) [c]
P08133	Annexin A6	Cytoplasm, early endosomes	n.d.	+	
O95782	AP-2 complex subunit alpha-1	PM, coated pits	n.d.	+	
P63010	AP-2 complex subunit beta	PM, coated pits	n.d.	+	
Q9Y6D5	ARFGEF2	Golgi, endosomes, cytoskeleton	+	n.d.	
Q6DD88	Atlastin-3	ER	+	+	
P27824	Calnexin	ER, *Legionella*-Containing Vacuole (LCV), phagosomes	+	+	(Finsel et al., 2013; Gagnon et al., 2002) [c,d]
P35221	Catenin alpha-1 (Alpha E-catenin)	Cytoplasm, cytoskeleton, adherens junctions	n.d.	+	
O60716	Catenin delta-1 (p120 catenin)	Cytoplasm, nucleus, PM	n.d.	+	
P07858	Cathepsin B	Lysosomes, phagosomes	+	–	(Trost et al., 2009) [c]
Q9UBR2	Cathepsin Z	Lysosomes, phagosomes	+	–	(Trost et al., 2009) [c]
P11717	CI Man-6-P receptor	Lysosomes, phagosomes, LCV	+	n.d.	(Finsel et al., 2013; Trost et al., 2009) [d]
Q00610	Clathrin heavy chain 1	Coated pits	+	n.d.	
P06493	Cyclin-dependent kinase 1	Cytoskeleton, nucleus	+	n.d.	
P24941	Cyclin-dependent kinase 2	Cytoskeleton, endosomes	+	n.d.	
Q7L576	Cytoplasmic FMR1-interacting protein 1	Lamellipodia, cell ruffles	+	n.d.	
Q07065	Cytoskeleton-associated protein 4	ER, cytoskeleton	+	n.d.	
Q14008	Cytoskeleton-associated protein 5	Cytoskeleton	+	n.d.	
Q9UJW0	Dynactin subunit 4	Cytoskeleton, MTOC, SCV	n.d.	+	(Harrison et al., 2004) [b]
P50570	Dynamin-2	Cytoskeleton	n.d.	+	
Q14204	Dynein heavy chain, cytosolic	Cytoskeleton, SCV	+	+	(Guignot et al., 2004; Harrison et al., 2004) [b]
Q03001	Dystonin	Cytoskeleton, ER	+	n.d.	
P00533	EGF receptor	PM, ER, Golgi, endosomes	+	n.d.	
Q969X5	ERGIC-32	ER, Golgi	+	+	
Q9P0I2	ER membrane protein complex subunit 3	ER	+	n.d.	
Q96KP1	Exocyst complex component 2		n.d.	+	(Nichols and Casanova, 2010) [b]
O60645	Exocyst complex component 3		n.d.	+	(Nichols and Casanova, 2010) [b]
Q96A65	Exocyst complex component 4		n.d.	+	(Nichols and Casanova, 2010) [b]
O00471	Exocyst complex component 5		n.d.	+	(Nichols and Casanova, 2010) [b]
P21333	Filamin-A	Cytoskeleton	+	+	(Miao et al., 2003) [b]
O75369	Filamin-B	Cytoskeleton, phagosomes	+	+	(Miao et al., 2003; Trost et al., 2009) [b,c]
P09382	Galectin-1	Extracellular matrix	n.d.	+	
P17931	Galectin-3	Cytoplasm, SCV, phagosomes	+	–	(Garin et al., 2001; Thurston et al., 2012) [b,c]
P23258	Gamma-1-tubulin	Cytoskeleton, MTOC	n.d.	+	(Ramsden *et al.*, 2007) [b]
Q9BSJ2	Gamma-tubulin complex component 2	Cytoskeleton, MTOC	n.d.	+	(Ramsden *et al.*, 2007) [b]
P06744	Glucose-6-phosphate isomerase	Cytoplasm	+	+	
P04406	Glyceraldehyde-3-phosphate dehydrogenase (GAPDH)	Cytosol, phagosomes	+	n.d.	(Garin *et al.*, 2001) [c]
P13807	Glycogen synthase		n.d.	+	
Q14643	IP3 receptor isoform 1	ER	+	+	
Q14573	IP3 receptor isoform 3	ER	+	+	
Q07866	Kinesin light chain 1	Cytoskeleton, SCV	n.d.	+	(Boucrot *et al.*, 2005) [b]
Q9H0B6	Kinesin light chain 2	Cytoskeleton, SCV	n.d.	+	(Boucrot *et al.*, 2005) [b]
Q86UP2	Kinesin receptor	ER	+	n.d.	
P33176	Kinesin-1 heavy chain (KIF5B)	Cytoskeleton, SCV	+	+	(Boucrot *et al.*, 2005) [b]
Q99661	Kinesin-like protein KIF2C	Cytoskeleton	n.d.	+	
P11117	Lysosomal acid phosphatase	Lysosomes, SCV	+	–	(Garcia-del Portillo and Finlay, 1995; Rathman *et al.*, 1997) [b]

P46821	Microtubule-associated protein 1B	Cytoskeleton	+	n.d.	
P27816	Microtubule-associated protein 4	Cytoskeleton	+	+	
Q9NZM1	Myoferlin	PM, vesicles	+	n.d.	
P35579	Myosin-9	Cytoskeleton, phagosomes	+	+	(Diakonova *et al.*, 2002)[d]
Q13492	Phosphatidylinositol-binding clathrin assembly protein (PICALM)	Clathrin-coated pits, Golgi	+	+	
P42356	PI4-kinase alpha	Cytoplasm, membrane.	+	n.d.	
Q15149	Plectin	Cytoskeleton	+	+	
P20618	Proteasome gamma chain	Cytoplasm, nucleus	+	n.d.	
Q5VYK3	Proteasome-associated protein ECM29 homolog	ER, endosome, cytoskeleton, nucleus	+	+	
O75128	Protein cordon-bleu	PM, cytoskeleton, cell ruffles	+	n.d.	
Q9Y6W5	Protein WAVE-2	Cytoskeleton	n.d.	+	
Q969M3	Protein YIPF5	ER, Golgi, COPII-coated vesicles	+	–	
P61019	Rab-2a	ER, Golgi, phagosomes	+	n.d.	(Trost *et al.*, 2009)[c]
P20338	Rab-4a	Membrane, cytoplasm, SCV	+	n.d.	(Smith *et al.*, 2007)[b]
P20340	Rab-6	Golgi, endosomes	+	n.d.	(Stuart *et al.*, 2007)[c]
P51149	Rab-7a	Late endosomes, lysosomes, phagosomes, SCV	+	n.d.	(Stuart *et al.*, 2007; Smith *et al.*, 2007)[b,c]
Q9NQC3	Reticulon-4	ER	+	n.d.	
Q68EM7	Rho GTPase-activating protein 17	Membranes, cytoplasm	n.d.	+	
O75116	ROCK-II	PM, cytoskeleton	+	+	(Truong *et al.*, 2013)[b]
O75396	SEC22b	ERGIC, phagosomes	+	n.d.	(Lee *et al.*, 2010; Cebrian *et al.*, 2011)[c]
P55735	SEC13-related protein	COPII-coated vesicles	+	n.d.	
Q15436	SEC23-related protein A	COPII-coated vesicles	n.d.	+	
Q15437	SEC23-related protein B	COPII-coated vesicles	+	+	
O95486	SEC24-related protein A	COPII-coated vesicles	+	n.d.	
P53992	SEC24-related protein C	COPII-coated vesicles	+	n.d.	
O94979	SEC31-related protein A	COPII-coated vesicles	+	n.d.	
Q15019	Septin-2	Cytoplasm, cytoskeleton	+	n.d.	
Q9UHD8	Septin-9	Cytoplasm, cytoskeleton	+	+	
Q9P0V9	Septin-10	Cytoplasm, cytoskeleton	+	+	
P16615	SERCA2	ER	+	n.d.	
Q12846	Syntaxin-4	PM, phagosomes	+	+	(Cebrian *et al.*, 2011)[c]
Q86Y82	Syntaxin-12	Endosomes, Golgi	+	n.d.	
A5PLL7	Transmembrane protein 189	ER	+	n.d.	
Q9BTV4	Transmembrane protein 43	ER	+	–	
P43307	TRAP-alpha	ER	+	+	
P67936	Tropomyosin-4	Cytoskeleton	+	n.d.	(Finlay *et al.*, 1991)[b]
Q12792	Twinfilin-1	Cytoplasm, cytoskeleton	+	n.d.	
Q6IBS0	Twinfilin-2	Cytoplasm, cytoskeleton	+	n.d.	
P21283	V-ATPase subunit C 1	SCV	+	n.d.	(Steele-Mortimer *et al.*, 1999)[b]
P61421	V-ATPase subunit d 1	Membranes, SCV	+	–	(Steele-Mortimer et al., 1999)[b]
Q9P0L0	VAP-A	ER, phagosomes	+	–	(Garin et al., 2001)[c]
O95292	VAP-B	ER	+	–	
Q9Y3E0	Vesicle transport protein GOT1B	Golgi	+	n.d.	
Q12981	Vesicle transport protein SEC20	ER	+	n.d.	
P08670	Vimentin	Cytoplasm, phagosomes	+	+	(Garin et al., 2001)[c]
P18206	Vinculin	Cytoskeleton, PM, adherens junctions	+	n.d.	
Q12907	VIP36	ER, Golgi	+	n.d.	
Q9H0V9	VIP36-like protein	ER, Golgi	+	+	
Q9UID3	VPS51	Golgi, GARP complex	n.d.	+	
Q8N1B4	VPS52	Golgi, GARP complex	n.d.	+	

[a]See Table S3 for the complete set of host proteins enriched at the SCV.

[b]References relevant to *Salmonella*-host cell interactions.

[c]Proteins previously identified by proteome analysis of latex beads-containing phagosomes or bacteria-containing vacuoles.

[d]Proteins previously identified in bacteria-containing vacuoles or latex beads-containing phagosomes by non-proteome analysis.

+ (enriched relative to control)

– (depleted relative to control)

n.d. (no difference relative to control)

Supplementary References

Boucrot, E., Henry, T., Borg, J.-P., Gorvel, J.-P., and Méresse, S. (2005) The intracellular fate of Salmonella depends on the recruitment of kinesin. *Science* **308**: 1174–1178.

Cebrian, I., Visentin, G., Blanchard, N., Jouve, M., Bobard, A., Moita, C., *et al.* (2011) Sec22b regulates phagosomal maturation and antigen crosspresentation by dendritic cells. *Cell* **147**: 1355–1368.

Criss, A.K., and Casanova, J.E. (2003) Coordinate regulation of Salmonella enterica serovar Typhimurium invasion of epithelial cells by the Arp2/3 complex and Rho GTPases. *Infect Immun* **71**: 2885–2891.

Diakonova, M., Bokoch, G., and Swanson, J.A. (2002) Dynamics of cytoskeletal proteins during Fcgamma receptor-mediated phagocytosis in macrophages. *Mol Biol Cell* **13**: 402–411.

Finlay, B.B., Ruschkowski, S., and Dedhar, S. (1991) Cytoskeletal rearrangements accompanying salmonella entry into epithelial cells. *J Cell Sci* **99 (Pt 2)**: 283–296.

Finsel, I., Ragaz, C., Hoffmann, C., Harrison, C.F., Weber, S., van Rahden, V.A., *et al.* (2013) The Legionella Effector RidL Inhibits Retrograde Trafficking to Promote Intracellular Replication. *Cell Host Microbe* **14**: 38–50.

Gagnon, E., Duclos, S., Rondeau, C., Chevet, E., Cameron, P.H., Steele-Mortimer, O., *et al.* (2002) Endoplasmic reticulum-mediated phagocytosis is a mechanism of entry into macrophages. *Cell* **110**: 119–131.

Garcia-del Portillo, F., and Finlay, B.B. (1995) Targeting of Salmonella typhimurium to vesicles containing lysosomal membrane glycoproteins bypasses compartments with mannose 6-phosphate receptors. *J Cell Biol* **129**: 81–97.

Garin, J., Diez, R., Kieffer, S., Dermine, J.F., Duclos, S., Gagnon, E., *et al.* (2001) The phagosome proteome: insight into phagosome functions. *J Cell Biol* **152**: 165–180.

Guignot, J., Caron, E., Beuzón, C., Bucci, C., Kagan, J., Roy, C., and Holden, D.W. (2004) Microtubule motors control membrane dynamics of Salmonella-containing vacuoles. *J Cell Sci* **117**: 1033–1045.

Harrison, R.E., Brumell, J.H., Khandani, A., Bucci, C., Scott, C.C., Jiang, X., *et al.* (2004) Salmonella impairs RILP recruitment to Rab7 during maturation of invasion vacuoles. *Mol Biol Cell* **15**: 3146–3154.

Hänisch, J., Ehinger, J., Ladwein, M., Rohde, M., Derivery, E., Bosse, T., *et al.* (2010) Molecular dissection of Salmonella-induced membrane ruffling versus invasion. *Cell Microbiol* **12**: 84–98.

Jolly, C., Winfree, S., Hansen, B., and Steele-Mortimer, O. (2013) The Annexin A2/p11 complex is required for efficient invasion of Salmonella Typhimurium in epithelial cells. *Cell Microbiol*.

Lee, B.-Y., Jethwaney, D., Schilling, B., Clemens, D.L., Gibson, B.W., and Horwitz, M.A. (2010) The Mycobacterium bovis bacille Calmette-Guerin phagosome proteome. *Mol Cell Proteomics* **9**: 32–53.

Miao, E.A., Brittnacher, M., Haraga, A., Jeng, R.L., Welch, M.D., and Miller, S.I. (2003) Salmonella effectors translocated across the vacuolar membrane interact with the actin cytoskeleton. *Mol Microbiol* **48**: 401–415.

Nichols, C.D., and Casanova, J.E. (2010) Salmonella-directed recruitment of new membrane to invasion foci via the host exocyst complex. *Curr Biol* **20**: 1316–1320.

Ramsden, A.E., Mota, L.J., Münter, S., Shorte, S.L., and Holden, D.W. (2007) The SPI-2 type III secretion system restricts motility of Salmonella-containing vacuoles. *Cell Microbiol* **9**: 2517–2529.

Rathman, M., Barker, L.P., and Falkow, S. (1997) The unique trafficking pattern of Salmonella typhimurium-containing phagosomes in murine macrophages is independent of the mechanism of bacterial entry. *Infect Immun* **65**: 1475–1485.

Smith, A.C., Heo, W.D., Braun, V., Jiang, X., Macrae, C., Casanova, J.E., *et al.* (2007) A network of Rab GTPases controls phagosome maturation and is modulated by Salmonella enterica serovar Typhimurium. *J Cell Biol* **176**: 263–268.

Steele-Mortimer, O., Méresse, S., Gorvel, J.P., Toh, B.H., and Finlay, B.B. (1999) Biogenesis of Salmonella typhimurium-containing vacuoles in epithelial cells involves interactions with the early endocytic pathway. *Cell Microbiol* **1**: 33–49.

Stuart, L.M., Boulais, J., Charriere, G.M., Hennessy, E.J., Brunet, S., Jutras, I., *et al.* (2007) A systems biology analysis of the Drosophila phagosome. *Nature* **445**: 95–101.

Thurston, T.L.M., Wandel, M.P., Muhlinen, von, N., Foeglein, A., and Randow, F. (2012) Galectin 8 targets damaged vesicles for autophagy to defend cells against bacterial invasion. *Nature* **482**: 414–418.

Trost, M., English, L., Lemieux, S., Courcelles, M., Desjardins, M., and Thibault, P. (2009) The phagosomal proteome in interferon-gamma-activated macrophages. *Immunity* **30**: 143–154.

Truong, D., Brabant, D., Bashkurov, M., Wan, L.C.K., Braun, V., Heo, W.D., *et al.* (2013) Formin-Mediated Actin Polymerization Promotes Salmonella Invasion. *Cell Microbiol*.

Unpublished Results – The role of VAP-A and septin-9 during *Salmonella* infection of epithelial cells

VAP-A affects intracellular Salmonella *growth by promoting bacterial hyper-replication*

As observed on the **Manuscript 2** of the results section, a key finding in the quantitative proteomic analysis of the purified SCVs was that these were enriched in proteins derived from the ER. Moreover, our C-FIB/SEM data showed that the early SCV contacts with the host cell ER. In addition to the data presented in the published manuscript, we tried to follow the association of other ER proteins with the SCV by time-lapse fluorescence microscopy, through the use of fluorescently tagged Sec61β (a protein used as a general ER marker (Zurek et al., 2011)) or VAP-A (a factor enriched at the early SCV proteome). Nevertheless, this was technically complicated and the data interpretation was extremely challenging, as overexpression of ER-localized proteins resulted in abnormal protein localization. Therefore, and even though it seemed that these ER proteins were recruited to the *Salmonella* entry site (***Figure 30***; ***Movies SA1-SA2***), we could not conclude as weather the SCV associates with Sec61β and VAP-A.

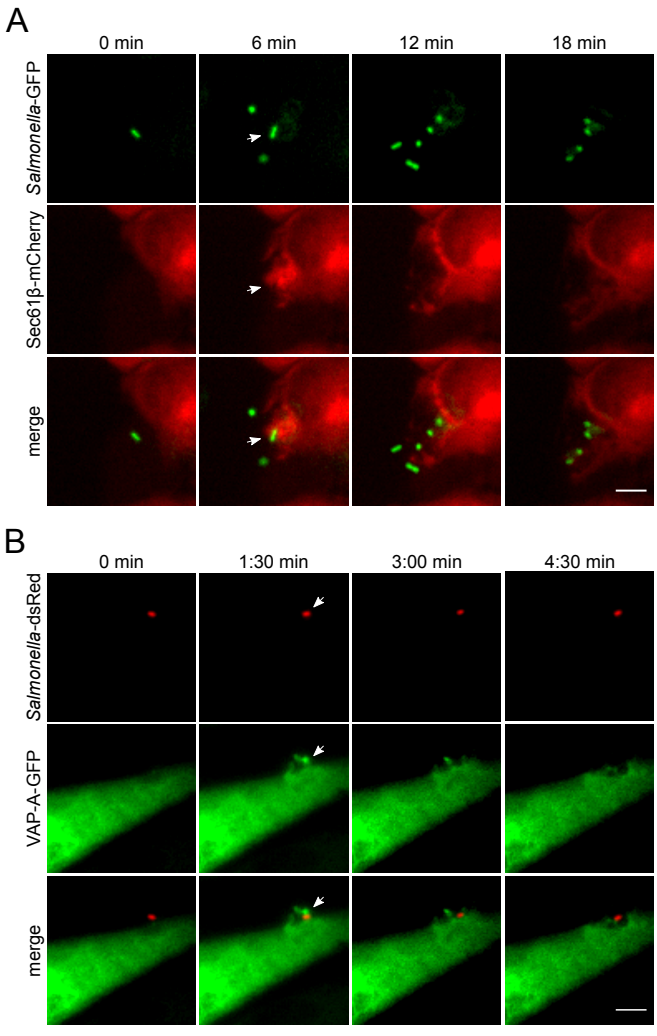

Figure 30 – ER dynamics during *Salmonella* infection of epithelial cells. HeLa cells were transfected with Sec61β-mCherry (**A**) or VAP-A-GFP (**B**), infected with GFP- or dsRed-expressing *Salmonella* and imaged by time-lapse epifluorescent microscopy. Arrows indicate the site of bacterial invasion. Representative data from 3 independent experiments are shown. See also ***Movies SA1-SA2***.

Interestingly, we found that the early SCV (30 minutes) was enriched in several proteins derived from the cER, such as SERCA2, reticulon-4, VAP-A and VAP-B (***Figure 3A*** of the **Manuscript 2**). The cER is a subcompartment that is involved in the establishment of MCSs between the ER and other organelles, and several of these contact sites contain the protein VAP-A, either as a structural component or as a targeting factor (Raiborg et al., 2015). Given that it seems that VAP-A is a crucial player in the formation of MCSs we tested if VAP-A knockdown affects the intracellular *Salmonella* lifestyle. We first measured bacterial entry and replication within epithelial cells using gentamicin assays, after VAP-A-depletion by siRNA treatment. *Salmonella* entry into HeLa cells, measured 1 hour p.i., was not affected after VAP-A knockdown (data not shown). Interestingly, VAP-A-depletion impaired intracellular bacterial growth from 3 hours p.i. onwards, as compared to the control (***Figure 31A***). These data show that VAP-A, and possibly the formation of MCSs, is important for bacterial growth within the host cell. Next, we assessed if VAP-A could be implicated in *Salmonella* hyper-replication within the host cytosol. Cells were transfected with VAP-A siRNA and the percentage of infected cells containing hyper-replicating bacteria was determined 6 hours p.i. by fluorescence microscopy. VAP-A-depletion significantly decreased the number of cells with hyper-replicating *Salmonella* (***Figure 31B***) as compared to the control, suggesting that VAP-A function is crucial for SCV membrane rupture and bacterial escape to the cytosol.

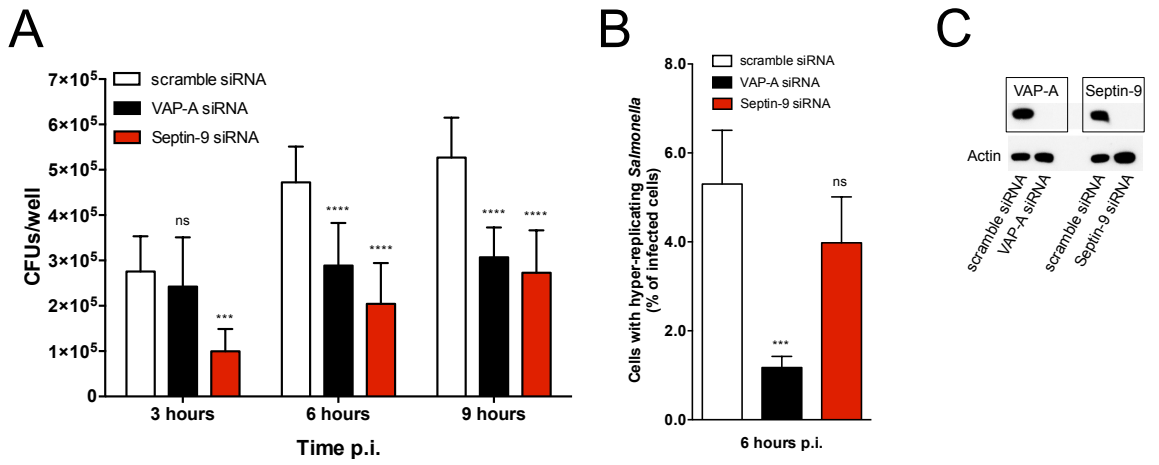

Figure 31 – The impact of VAP-A and septin-9 on different steps of *Salmonella* intracellular lifestyle. Cells were treated with scramble, VAP-A or septin-9 siRNA for 72 h and infected with *Salmonella*. (**A**) Gentamicin was added to kill all extracellular bacteria, then host cells were lysed at the indicated time-points of infection and the number of viable intracellular bacteria was counted by CFUs. The graph shows the mean ± SEM number of CFUs per well. (**B**) Cells in 96-well plates were fixed 6 h p.i. with *Salmonella*-dsRed, counterstained with DRAQ5 and imaged by fluorescence microscopy. (**C**) VAP-A and septin-9 knockdown levels were assessed by Western blot. All *P*-values were determined using the two-way ANOVA test for multiple comparisons from three independent experiments performed in triplicate.

Septin-9 promotes Salmonella *entry into epithelial host cells*

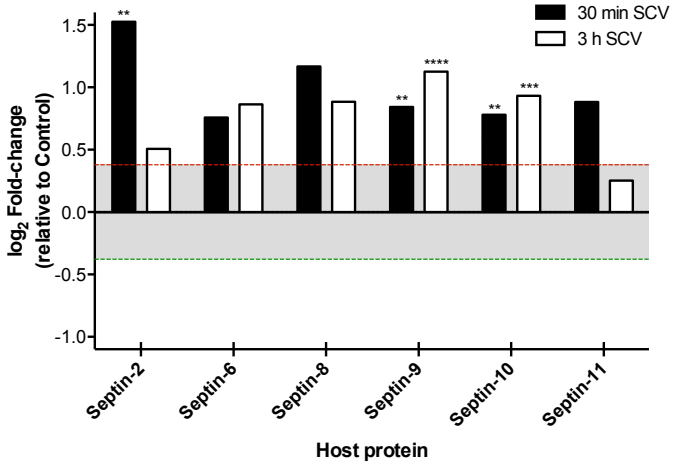

Figure 33 – The SCV is enriched in septins. The graph shows the log_2 fold-change in septins abundance, compared to the non-infected control, from 5 independent experiments. Relative protein abundances were considered different when the log_2 fold-change > 0.387 (red line) or < -0.387 (green line), with a *P*-value < 0.05. Statistics are relative to the non-infected control, for each protein.

Recently, septins have been implicated in ER linking with the plasma membrane during store-operated calcium entry (Sharma et al., 2013), as well as being associated with *S. flexneri* and *L. monocytogenes* invasion of epithelial cells (Mostowy et al., 2009). In this context, we were intrigued by the enrichment of different septins in the SCV as compared to the non-infected control (***Figure 32***), which suggested that septins might also be involved in *Salmonella* infection. Time-lapse fluorescent microscopy showed massive recruitment of septin-9 to the bacterial entry site (***Figure 33***; ***Movie SA3***), and septin-9 knockdown significantly impaired bacterial entry into the host cell (***Figure 31A***), but did not affect bacterial growth within the cell, since the bacterial load increased at a similar rate to the control. Moreover, these proteins did not have an impact on *Salmonella* hyper-replication within the host cell cytosol (***Figure 31B***). Together, these data show that septin-9 is recruited to the *Salmonella* invasion site and plays an important role during bacterial entry into epithelial cells.

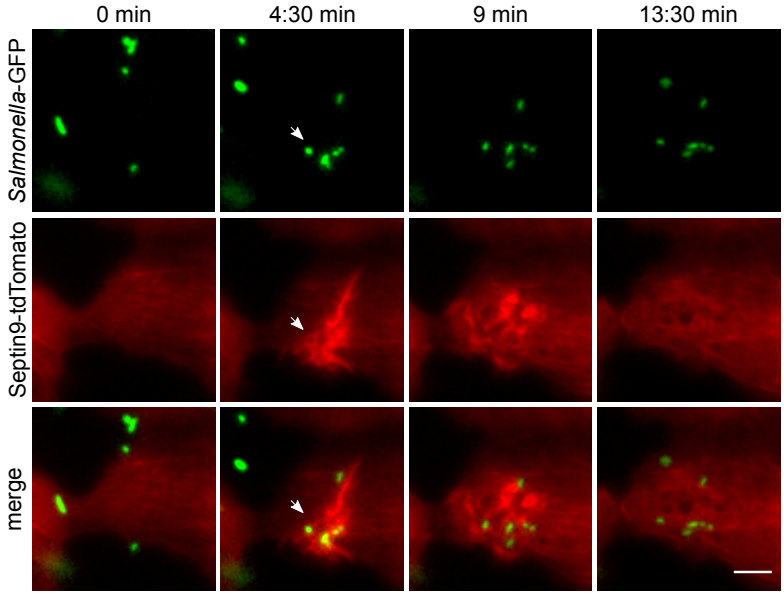

Figure 32 – Septin-9 is recruited to the site of *Salmonella* entry. HeLa cells were transfected with Septin-9-tdTomato, infected with GFP-expressing *Salmonella* and imaged by time-lapse epifluorescence microscopy. Arrows point to the site of bacterial entry. Scale bar corresponds to 10 µm. Representative data from 3 independent experiments are shown. See also ***Movie SA3***.

“A saudade não está na distância das coisas, mas numa súbita fractura de nós, num quebrar de alma em que todas as coisas se afundam.”

- Vergílio Ferreira; in Conta-Corrente 3

PART IV

DISCUSSION

During this doctoral project, I studied different steps of *S. flexneri* and *Salmonella* infection of epithelial host cells. After entering into the host cell, *S. flexneri* briefly resides within a membrane-bound vacuole that is ruptured within minutes, with subsequent bacterial escape into the host cytosol. *Salmonella* intracellular lifestyle, in epithelial cells, can be considered as more complex, as this bacterium can either survive within its endocytic vacuole (the so-called SCV) or escape into the host cytosol. This highlights that the formation and maturation of the bacteria-containing vacuole are steps of vital importance during bacterial invasion. In this regard, vacuolar maturation can either result in membrane damage, with bacterial escape into the cytosol, or maintenance of membrane integrity and establishment of a bacterial replicative niche. Despite that numerous studies over the last decades helped to understand the intracellular lifestyle of invasive bacteria, much is still unknown. Mostly because the molecular events of bacteria-containing vacuole maturation are extremely fast and dynamic. Additionally, it is important to understand these mechanisms at a spatiotemporal level. Thus, novel assays based on high-resolution time-lapse fluorescence microscopy have been developed, with a special focus on quantitative and systematic analysis, in order to achieve unprecedented spatiotemporal resolution. By combining these assays with ultrastructural studies on the same cell and biochemical characterization of the bacteria-containing vacuoles, it is possible to better understand how intracellular bacterial pathogens hijack the host cell environment to survive.

We started by using time-lapse fluorescence microscopy to characterize for the first time the hierarchical kinetics of host factor recruitment to the *S. flexneri* entry site and to the forming bacteria-containing vacuole. We could demonstrate that several host factors are dynamically recruited to the bacterial entry site. In more detail, there is the simultaneous recruitment of actin and of the small GTPases Rac1, RhoA and Cdc42, and of the kinases Src and Abl to the site of bacterial entry. This means that host proteins that act as a platform for cytoskeletal rearrangements are recruited altogether to the site of *S. flexneri* entry site. Interestingly, the bacterial effector IpgB1 increases the pace of bacterial invasion, by accelerating the recruitment of small GTPases and kinases. Whereas previous data suggested that a bacterial Δ*ipgB1* mutant strain could have impaired entry

into epithelial cells (Ohya et al., 2005), we showed in this work that this effector actually has a kinetic effect. Performing time-lapse microscopy was of crucial importance, as we could follow individual infected cells and quantify the recruitment of host proteins and bacterial entry. Thus, we could revise what was known before and demonstrate that the Δ*ipgB1* mutant also invades epithelial cells, but at a reduced pace. Consequently, it seems that *S. flexneri* injects T3SS effectors that can "trigger" and "accelerate" bacterial internalization into epithelial cells, which might act as a temporal mechanism to avoid the extracellular immune defense mechanisms.

We then investigated the localization of the same host factors at the site of the bacteria-containing vacuole and at the time of vacuolar rupture. The host laboratory where I performed my PhD project developed an approach to track vacuole membrane rupture in real time: fluorescently tagged galectin-3 targets disassembling membranes (Ray et al., 2010), forming "bacterial ghost-like structures". In contrast to the simultaneous recruitment of host small GTPases and kinases to the entry site, we found that vacuolar rupture follows a higher level of temporal organization. Often, we observed accumulation of actin around the bacteria inside vacuoles, forming actin cages that disperse before membrane rupture and galectin-3 recruitment. Interestingly, among the tested small GTPases and kinases, only Rac1 and Src were recruited to the *Shigella*-containing vacuole. However, these two factors remained localized around the bacteria after vacuolar rupture, colocalizing with galectin-3. This might point to a selective role of specific small GTPases and kinases during vacuolar rupture, depending on their localization, given that it was demonstrated that only some small GTPases, such as Rab11a, Cdc42 or Rab3, are implicated in the rupture of the *Shigella*-containing vacuole (Mellouk et al., 2014). Additionally, we found that the IpgB1 effector does not seem to be implicated in vacuolar rupture, acting solely during bacterial entry into epithelial cells. In the future it will be important to investigate if other small GTPases and kinases are also recruited to the site of vacuolar rupture, which could give us important clues about the intracellular signaling pathways that could be activated upon *S. flexneri* escape to the cytosol. Furthermore we could show in this PhD project that, during bacterial escape to the cytosol, galectin-3 is rapidly recruited to the site of vacuolar membrane rupture and then dispersed, thus having a short-lived signal. This highlights the importance of using time-lapse

fluorescent microscopy for studying vacuolar rupture, as the underlying biological processes are extremely dynamic.

With this part of the project we could show that the events during *S. flexneri* entry into epithelial cells and subsequent vacuolar rupture follow a dynamic sequence. Different host proteins are localized to distinct parts of the cell, most likely eliciting biological functions in a hierarchical manner. In the future, it will be important to investigate the host signaling pathways that are triggered upon vacuolar rupture. For this, it is vital to consider that the mentioned small GTPases and kinases have different activation status and can switch between “on” and “off” states. There are several functionalized fluorescence resonance energy transfer (FRET) biosensors to track the activity of small GTPases in correlation with their subcellular localization, in living cells (Aoki and Matsuda, 2009; Machacek et al., 2009; Pertz, 2010; Pertz and Hahn, 2004; Wang et al., 2005; Yoshida et al., 2009). This could give us important clues on how, when and where host proteins are activated during the steps of bacterial entry and vacuolar membrane disassembly.

Over the last 60 years, the knowledge that we have on cell biology has significantly improved by knowing the molecular constituents of the cell’s different components. In particular, discovering the protein composition of different organelles, such as phagosomes, has elucidated how they work at a molecular level, and how they interact with other cellular compartments. In this regard, it is very important to understand the protein composition of bacteria-containing vacuoles, in order to better understand the molecular mechanisms of vacuolar maturation and membrane disassembly. Therefore, we aimed to isolate and determine the proteome of bacteria-containing vacuoles in order to identify novel host proteins associated with these compartments.

A common criticism of subcellular fractionation is the possible presence of contaminants in the fraction of interest. Biochemical enrichment of an organelle is never perfect, because complete separation from all other organelles is essentially never achieved (Li et al., 2010; Rogers and Foster, 2007). Moreover, it is known that after ultracentrifugation in a density gradient, bacteria-containing vacuoles have densities closer to some other organelles, which is also observed in the data presented in this thesis (**Manuscript 2**, ***Figure 1***). Even after several rounds of gradient centrifugation, contaminants from different organelles may still be present

in a fraction of interest. This limitation has already been recognized by Christian de Duve, in 1974 (Duve, 1975). Nevertheless, with proper experimental design and data analysis, the existence of some contaminating proteins from other organelles might not prevent the determination of the relative abundance of proteins present in the bacteria-containing vacuole fraction. Therefore we decided to monitor the changes in protein abundance in a time-course experiment, always in comparison to a non-infected control fraction that does not contain bacteria-containing vacuoles (but all the other contaminants). It is possible to assume that a contaminant or non-specific protein would not change over time, and that specific vacuolar proteins show time-dependent fluctuation in their abundance (Li et al., 2010). Thus, we circumvented the limitations of biochemical bacteria-containing vacuole isolation and incomplete organelle separation by performing a label-free quantitative subtractive proteomics analysis. The inventory of the target vacuolar fraction was compared with a related non-infected control fraction and the remaining proteins enriched in the bacteria-containing vacuole fraction can thus be considered specific vacuolar components.

During this project, several months were spent for the development and optimization of a robust protocol for the enrichment of intact bacteria-containing vacuoles. We decided to use a continuous linear OptiPrep (a solution of iodixanol (Graham, 2002)) gradient for the subcellular fractionation. The high density and low viscosity of OptiPrep, when compared to equivalent sucrose solutions, facilitates the fractionation, allowing faster and better organelle separation. Additionally, by using linear gradients it is possible to increase separation efficiency and decrease organelle contamination across different fractions. We also optimized the range of gradient linearity (10-25%: that is 1.06-1.15 g/cm^3) in such a way that the fraction enriched in bacteria-containing vacuoles has the lowest levels of contaminants by other organelles. Is this way, is was possible to remove mitochondrial contaminants from the fraction of interest, which was thought to be one of the major problems, given that bacteria-containing vacuoles and mitochondria exhibit similar densities (Li et al., 2010; Rogers and Foster, 2007). Through the use of such methodology we could reproducibly obtain fractions enriched in intact SCVs, which had never been achieved before. We also made an effort to obtain fractions enriched in intact *Shigella*-containing vacuoles, but this proved to be extremely difficult. Firstly, *S. flexneri* ruptures its vacuole in

less than 10 minutes after bacterial entry, which means that the technical procedure needs to be quickly performed. Secondly, we think that the *Shigella*-containing vacuole is very fragile, as we could not reproducibly isolate it in an intact form after subcellular fractionation (data not presented in this thesis). Hence, we focused only on the characterization of the protein composition of the SCV. To assess SCV integrity in the isolated SCV-enriched fraction, we used a non-biased ELISA (enzyme-linked immunosorbent assay) method, rather than electron microscopy used in other studies (Gagnon et al., 2002; Shevchuk et al., 2009). Given that the ELISA assay is quantitative, we could measure the percentage of *Salmonella* inside intact vacuoles, in the entire fraction. With electron microscopy-based techniques, it would be very difficult to perform similar quantifications. Moreover, electron microscopy might not be as precise, as preparation of isolated cellular fractions would require either dehydration followed by chemical fixation certain to damage SCV integrity, or cryo-fixation by high pressure freezing or plunging. Both cryo approaches are not suited for isolated fractions, as high pressure freezing requires dense samples and plunging involves blotting of excess water, likely to disrupt SCV integrity.

In order to further circumvent the limitation that biochemical purification of organelles does not yield pure fractions, we performed label-free quantitative subtractive proteomics. By comparing the inventory of the target SCV fraction with a related non-infected control fraction, we obtained a list of proteins uniquely enriched the SCV. These proteins can be considered as specific SCV components. This MS-based approach is of central importance in organelle proteomics, as the risk and effect of contamination is explicitly included in the experimental design. Nevertheless, the quantitative proteomics approach applied in this project has some limitations, potentially missing some true hits. If proteins reach a certain threshold in the control fraction, they will be discarded in our subtraction. In fact, the stringent quality controls (5 independent experiments and subtraction from negative controls) led to the exclusion of some proteins from the final “hit-list”, but we still decided to be highly restrictive in this study to avoid false-positives. However this led to the lack of some proteins that are known to be present at the SCV, such as the case of Lamp-1, which is known to be localized to the maturing and late SCVs (Steele-Mortimer, 2008). Even though label-free quantitative proteomics is now very robust, it is usually less accurate than isotope-

based methods, such as SILAC or iTRAQ (Cox and Mann, 2011; Walther and Mann, 2010). Moreover, major challenges in label-free quantitative methods include difficulties to match thousands of peptides across samples, variability in LC-MS/MS that results in retention time shifts, and possible errors introduced by slight differences in sample fractionation steps (Luber et al., 2010).

Importantly, our quantitative proteomics analysis identified 392 host proteins enriched in the SCV fraction at different stages of maturation (30 minutes early SCV and 3 hour maturing SCV), including many factors not previously known to be associated with this compartment. Even though we predicted that the number of *Salmonella* proteins in the SCV enriched fraction would be lower than the total number of host proteins that constitute the SCV and different non-specific contaminants, we could still detected 238 *Salmonella* proteins in the SCV enriched fraction. This is a relatively good yield compared to the number of identified host proteins. Nevertheless, this project only focused on the host proteins that were enriched at the SCV fraction. The data showed that the SCV is enriched is several host proteins previously described to be either associated with this compartment (such as dynein, galectin-3, kinesin, Rab4a, Rab7a and vATPase) or involved in *Salmonella* infection (such as Arp2/3 complex, annexin A2, tropomyosin-4, filamin, tubulin and ROCK-2), which confirmed the potential of the results. For instance, the maturing 3 h SCV was enriched in a number of MT-associated proteins, such as kinesin, kinesin receptor, dynein and tubulin, which are most likely involved in the transport of the SCV along MTs towards the MTOC. Additionally, we identified several novel host proteins associated with the SCV, whose presence in this compartment dynamically varies depending on the SCV maturation stage (***Figure 34***). Among this group of novel SCV-associated proteins, we were particularly interested in factors derived from the host ER, COPII vesicles and lysosomes. Strikingly, we found that all the members of the COPII complex were enriched in the early SCV. This finding was extremely reproducibly in all independent experiments, which highlights that our quantitative MS-based method to determine the SCV proteome is robust.

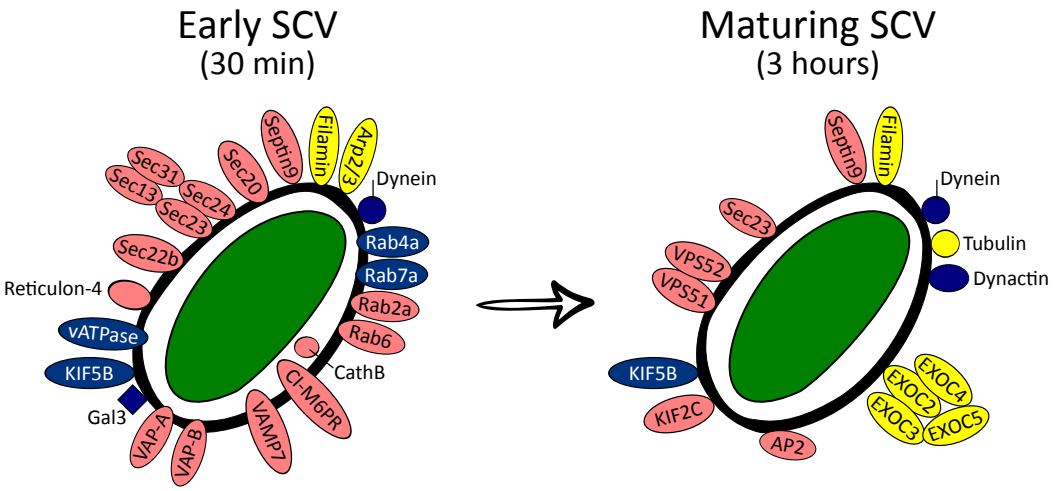

Figure 34 – Schematic representation of some host proteins associated with the SCV, at different stages of vacuolar maturation, as determined by quantitative proteomics. Factors in blue represent known SCV-associated proteins; factors in yellow represent proteins previously identified to be involved in *Salmonella* infection; factors in pink represent novel proteins associated with the SCV. The directionality of the proteins represented in this scheme, in relation to the SCV membrane, is hypothetical.

To validate the association of some host proteins with the SCV, we complemented the proteomics studies with fluorescence microscopy-based methods, both in fixed and living cells. Additionally, and given that we were extremely interested to understand the connectivity between the SCV and different host cell organelles, we used a novel C-FIB/SEM approach to characterize the ultrastructural details around the SCV. This provided important insights on the mechanisms of SCV maturation. By combining these different methodologies we showed that the SCV is enriched in proteins derived from the ER and that there is physical interaction between these two structures. Thus, our data helps clarifying one of the biggest controversies in the field of phagosome biogenesis: whether or not this compartment interacts with the ER (Gagnon et al., 2002; Guermonprez et al., 2003; Houde et al., 2003; Rogers and Foster, 2007; Touret et al., 2005). Additionally, we cannot exclude that the ER recruitment to the *Salmonella* entry site could also provide membrane that facilitates the formation of plasma membrane ruffles and bacterial uptake. Interestingly we detected the enrichment of Sec22b and Sec20 in the early SCV proteome. These two proteins are part of the same SNARE complex and might contribute to the fusion of ER-derived vesicles with the SCV as Sec22b was previously described to mediate the recruitment of ER components to phagosomes in dendritic cells (Cebrian et al.,

2011). ER-SCV interaction might also be facilitated by syntaxin-4, which interacts with Sec22b as part of the molecular machinery leading to the interaction between the ER and the phagosome (Cebrian et al., 2011). Based on our C-FIB/SEM data, we hypothesize that the SCV and the ER are connected via MCSs. These MCSs might be promoted through interactions between Rab7 and VAP-A, which were both enriched at the early SCV. Our proteomics data also showed that the early SCV is enriched in several cER proteins, such as SERCA2, reticulon-4, VAP-A and VAP-B, suggesting that the early steps of SCV formation recruit a significant amount of the cER. This could mean that during formation of the early SCV there is communication with specific ER subdomains. Moreover, several septins were enriched in the early SCV proteome. It was recently shown that septins tether with VAP proteins at plasma membrane-ER junctions, creating diffusion barriers that regulate Ca^{2+} trafficking at these sites (Chao et al., 2014; Sharma et al., 2013). Thus, we hypothesize that septin-9 recruitment to the *Salmonella* invasion site could define ER boundaries and therefore regulate bacterial entry or SCV maturation. Even though all our C-FIB/SEM datasets point to the existence of MCSs between the SCV and the ER, we cannot exclude that fusion might occur. Technically, it is complicated to observe such delicate biological events using C-FIB/SEM because of small artifacts introduced by chemical fixation and due to its lower resolution when compared to TEM tomography, for example. To circumvent this it would be important to perform cryo-fixation, in order to preserve the native cellular structures, coupled with TEM tomography. Moreover, our approach does not give information on dynamic biological events, so fusion, fission or contacts are hard to discern from each other. Therefore, the possibility of SCV-ER fusion should be addressed in the future through the use of more sophisticated techniques.

Furthermore, we found similarities between the proteomes of the SCV and the LCV (Hoffmann et al., 2014). ER-derived proteins such as inositol 1,4,5-trisphosphate, atlastin-3, Rab2a, Sec20, Sec22b, reticulon-4, VAP-A and VAP-B are enriched in the vacuoles containing *Salmonella* or *L. pneumophila*, suggesting similar mechanisms of interaction with the ER. We hypothesize that during maturation of a bacteria-containing vacuole, the default pathway might be interaction with the ER, since this organelle extends throughout the entire host cytosol. Though, we cannot rule out that other intracellular bacteria might have

mechanisms to actively avoid interactions between the ER and the bacteria-containing vacuole. This should be further investigated by using C-FIB/SEM methods, for example.

One of the most interesting findings of this project, which also points to the existence of SCV-ER communication, is that all the components of the COPII complex were enriched in the early SCV proteome. Additionally, we found that COPII vesicle assembly, via Sar1 GTPase activity, promotes SCV membrane rupture, *Salmonella* release into the host cytosol and bacterial hyper-replication. However, we still do not understand the precise mechanisms of SCV membrane disassembly, and this will need future investigation. We hypothesize that ER-SCV interactions could facilitate COPII vesicle activity between ERES and the SCV, due to close proximity. Thus, we envision one of two possible scenarios for COPII-mediated SCV membrane rupture. If one considers that the SCV and the ER are a single and connected structure, COPII vesicle budding out of the SCV might destabilize the vacuolar membrane, causing it to rupture. Alternatively, COPII vesicle budding out of the ER and subsequent insertion into the SCV membrane could promote to vacuolar rupture. Moreover, we present data that seem to indicate that VAP-A is important for SCV membrane rupture, because it promotes *Salmonella* hyper-replication. Given that VAP-A is an important constituent of MCSs between the ER and other organelles, we also hypothesize that the establishment of SCV-ER MCSs could facilitate vacuolar disassembly, through the induction of membrane fission (Rowland et al., 2014).

Together, the data presented in this thesis also helped elucidating the debate as whether or not the SCV interacts with lysosomes. We show that early SCVs are enriched in lysosomal proteins and fuse with VAMP7-positive lysosome-like vesicles. Then, in the maturing SCVs, there is depletion of the lysosomal content. This points to a model where the early SCV remains accessible to incoming lysosomal content that is then excluded from the SCV, to avoid intravacuolar bacterial degradation. Surprisingly, we found that at later time-points of vacuolar maturation there is again recruitment of VAMP7-poisitive vesicle to the late SCV. However, these vesicles and the late SCV have reduced acidity, confirming the hypothesis that the SCV interacts with lysosomes and that *Salmonella* actively reduces the lysosomal content/activity of its replicative niche (McGourty et al., 2012). Interestingly, our data strongly suggest that VAMP7-mediated vesicle

fusion with the late SCV promotes SIF formation and *Salmonella* replication within the vacuole. Thus, this confirms that SIF formation is crucial for bacterial replication. In the future it will be important to determine if the bacteria actively regulate the successive cycles of interactions between the SCV and the lysosomal system, and what are the *Salmonella* effectors that could be implicated in this process.

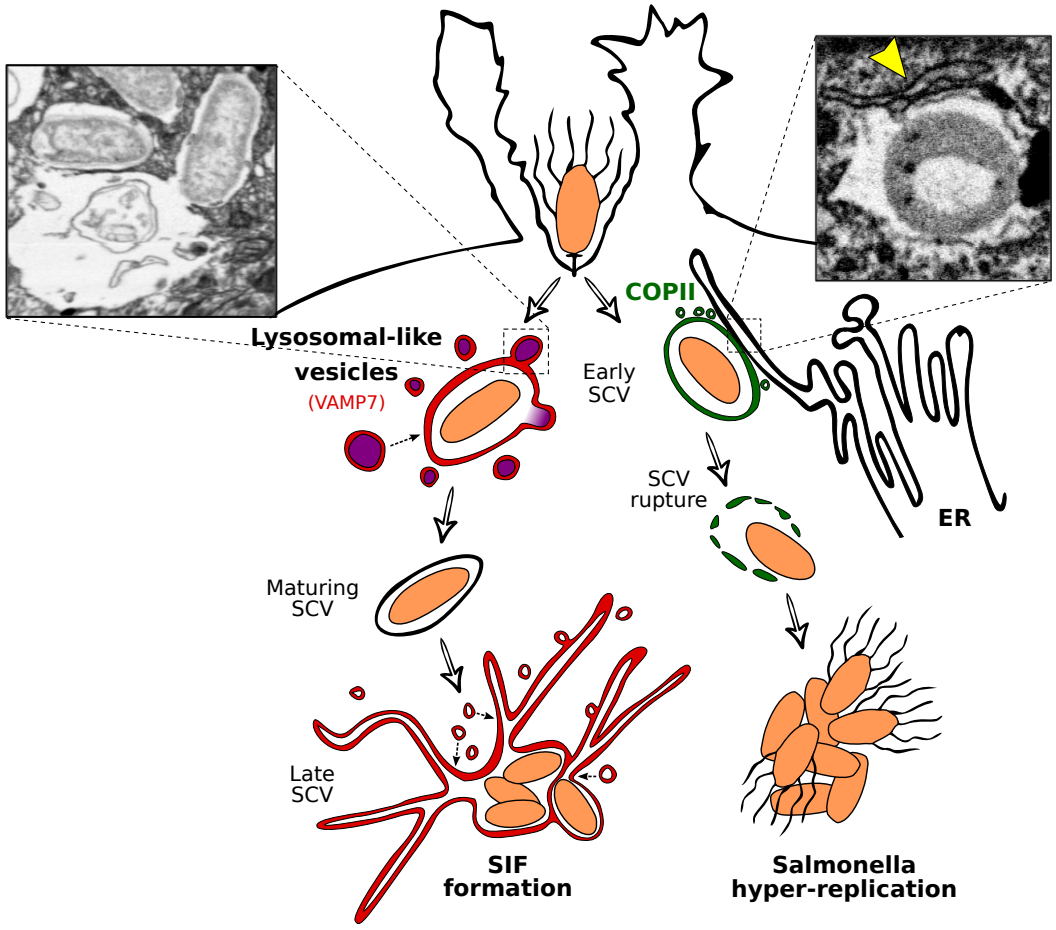

Figure 35 – Model for SCV interaction with the host cell ER or lysosome-like vesicles. The early SCV contacts with the ER, as seen in the FIB/SEM section on the right top corner (yellow arrowhead). COPII complex (green) assembly and accumulation around the early SCV promote vacuolar rupture, *Salmonella* escape into the host cytosol and hyper-replication. The early SCV fuses with acidic VAMP7-poisitive lysosome-like vesicles (red vesicles with purple fill). The ultrastructural detail of vesicle fusion is shown in the FIB/SEM section on the left top corner. The lysosomal content, including VAMP7, is then temporarily depleted from the maturing SCV. At later stages, VAMP7-positive vesicles with decreased acidity (red vesicles) associate again with the late SCV, promoting SIF formation and *Salmonella* replication within the vacuole.

In summary, we presented in this part of the PhD project a novel methodology to determine the protein composition of isolated SCVs. By combining this

approach with three-dimensional light and electron microcopy methods, we demonstrated that interactions between the SCV, at different stages of its maturation, and other host cell compartments, regulate *Salmonella* localization and replication within epithelial cells (***Figure 35***).

Altogether, it is possible to conclude that the combined use of MS-based proteomics of isolated organelles and microscopy-based assays to study bacterial infection are instrumental to understand principles of cell architecture, compartmental organization and trafficking between organelles. These methodologies are also crucial to better understand how invasive bacterial pathogens hijack host cellular processes. Moreover, host-pathogen interactions at a cellular level need to be studied under a perspective that takes into account the spatiotemporal resolution of biological events and the singularity of each individual cell.

REFERENCES

Abrahams, G.L., and Hensel, M. (2006). Manipulating cellular transport and immune responses: dynamic interactions between intracellular Salmonella enterica and its host cells. Cell Microbiol *8*, 728–737.

Agbaje, M., Begum, R.H., Oyekunle, M.A., Ojo, O.E., and Adenubi, O.T. (2011). Evolution of Salmonella nomenclature: a critical note. Folia Microbiol. (Praha) *56*, 497–503.

Agbor, T.A., and McCormick, B.A. (2011). Salmonella effectors: important players modulating host cell function during infection. Cell Microbiol *13*, 1858–1869.

Akhmanova, A., and Hoogenraad, C.C. (2005). Microtubule plus-end-tracking proteins: mechanisms and functions. Curr Opin Cell Biol *17*, 47–54.

Alto, N.M., Shao, F., Lazar, C.S., Brost, R.L., Chua, G., Mattoo, S., McMahon, S.A., Ghosh, P., Hughes, T.R., Boone, C., et al. (2006). Identification of a bacterial type III effector family with G protein mimicry functions. Cell *124*, 133–145.

Amano, M., Nakayama, M., and Kaibuchi, K. (2010). Rho-kinase/ROCK: A key regulator of the cytoskeleton and cell polarity. Cytoskeleton (Hoboken) *67*, 545–554.

Amin, N.D., Zheng, Y.-L., Kesavapany, S., Kanungo, J., Guszczynski, T., Sihag, R.K., Rudrabhatla, P., Albers, W., Grant, P., and Pant, H.C. (2008). Cyclin-dependent kinase 5 phosphorylation of human septin SEPT5 (hCDCrel-1) modulates exocytosis. J. Neurosci. *28*, 3631–3643.

Aoki, K., and Matsuda, M. (2009). Visualization of small GTPase activity with fluorescence resonance energy transfer-based biosensors. Nature Protocols *4*, 1623–1631.

Bajaj, V., Lucas, R.L., Hwang, C., and Lee, C.A. (1996). Co-ordinate regulation of Salmonella typhimurium invasion genes by environmental and regulatory factors is mediated by control of hilA expression. Mol Microbiol *22*, 703–714.

Bakowski, M.A., Braun, V., and Brumell, J.H. (2008). Salmonella-containing vacuoles: directing traffic and nesting to grow. Traffic *9*, 2022–2031.

Bakowski, M.A., Cirulis, J.T., Brown, N.F., Finlay, B.B., and Brumell, J.H. (2007). SopD acts cooperatively with SopB during Salmonella enterica serovar Typhimurium invasion. Cell Microbiol *9*, 2839–2855.

Baum, B., and Kunda, P. (2005). Actin nucleation: spire - actin nucleator in a class of its own. Curr Biol *15*, R305–R308.

Beauregard, K.E., Lee, K.D., Collier, R.J., and Swanson, J.A. (1997). pH-dependent perforation of macrophage phagosomes by listeriolysin O from Listeria monocytogenes. J Exp Med *186*, 1159–1163.

Bergeron, J.J.M., Au, C.E., Desjardins, M., McPherson, P.S., and Nilsson, T. (2010). Cell biology through proteomics--ad astra per alia porci. Trends Cell Biol *20*, 337–345.

Bertin, A., McMurray, M.A., Thai, L., Garcia, G., Votin, V., Grob, P., Allyn, T., Thorner, J., and Nogales, E. (2010). Phosphatidylinositol-4,5-bisphosphate promotes budding yeast septin filament assembly and organization. J. Mol. Biol. *404*, 711–731.

Bierne, H., Miki, H., Innocenti, M., Scita, G., Gertler, F.B., Takenawa, T., and Cossart, P. (2005). WASP-related proteins, Abi1 and Ena/VASP are required for Listeria invasion induced by the Met receptor. J Cell Sci *118*, 1537–1547.

Birmingham, C.L., and Brumell, J.H. (2006). Autophagy recognizes intracellular Salmonella enterica serovar Typhimurium in damaged vacuoles. Autophagy *2*, 156–158.

Birmingham, C.L., Canadien, V., Gouin, E., Troy, E.B., Yoshimori, T., Cossart, P., Higgins, D.E., and Brumell, J.H. (2007). Listeria monocytogenes evades killing by autophagy during colonization of host cells. Autophagy *3*, 442–451.

Birmingham, C.L., Smith, A.C., Bakowski, M.A., Yoshimori, T., and Brumell, J.H. (2006). Autophagy controls Salmonella infection in response to damage to the Salmonella-containing vacuole. J Biol Chem *281*, 11374–11383.

Bishop, A.L., and Hall, A. (2000). Rho GTPases and their effector proteins. Biochem J *348 Pt 2*, 241–255.

Blondeau, F., Ritter, B., Allaire, P.D., Wasiak, S., Girard, M., Hussain, N.K., Angers, A., Legendre-Guillemin, V., Roy, L., Boismenu, D., et al. (2004). Tandem MS analysis of brain clathrin-coated vesicles reveals their critical involvement in synaptic vesicle recycling. Proc Natl Acad Sci USA *101*, 3833–3838.

Bonifacino, J.S., and Rojas, R. (2006). Retrograde transport from endosomes to the trans-Golgi network. Nat Rev Mol Cell Biol *7*, 568–579.

Borgese, N., Francolini, M., and Snapp, E. (2006). Endoplasmic reticulum architecture: structures in flux. Curr Opin Cell Biol *18*, 358–364.

Bos, J.L., Rehmann, H., and Wittinghofer, A. (2007). GEFs and GAPs: critical elements in the control of small G proteins. Cell *129*, 865–877.

Boucrot, E., Henry, T., Borg, J.-P., Gorvel, J.-P., and Méresse, S. (2005). The intracellular fate of Salmonella depends on the recruitment of kinesin. Science *308*, 1174–1178.

Bougnères, L., Girardin, S.E., Weed, S.A., Karginov, A.V., Olivo-Marin, J.-C., Parsons, J.T., Sansonetti, P.J., and Van Nhieu, G.T. (2004). Cortactin and Crk cooperate to trigger actin polymerization during Shigella invasion of epithelial cells. J Cell Biol *166*, 225–235.

Brandizzi, F., and Barlowe, C. (2013). Organization of the ER-Golgi interface for membrane traffic control. Nat Rev Mol Cell Biol *14*, 382–392.

Braun, V., Fraisier, V., Raposo, G., Hurbain, I., Sibarita, J.-B., Chavrier, P., Galli, T., and Niedergang, F. (2004). TI-VAMP/VAMP7 is required for optimal phagocytosis of opsonised particles in macrophages. Embo J *23*, 4166–4176.

Braun, V., Wong, A., Landekic, M., Hong, W.J., Grinstein, S., and Brumell, J.H. (2010). Sorting nexin 3 (SNX3) is a component of a tubular endosomal network induced by Salmonella and involved in maturation of the Salmonella-containing vacuole. Cell Microbiol *12*, 1352–1367.

Brawn, L.C., Hayward, R.D., and Koronakis, V. (2007). Salmonella SPI1 effector SipA persists after entry and cooperates with a SPI2 effector to regulate phagosome maturation and intracellular replication. Cell Host Microbe *1*, 63–75.

Brenner, F.W., Villar, R.G., Angulo, F.J., Tauxe, R., and Swaminathan, B. (2000). Salmonella nomenclature. J. Clin. Microbiol. *38*, 2465–2467.

Breuza, L., Halbeisen, R., Jenö, P., Otte, S., Barlowe, C., Hong, W., and Hauri, H.-P. (2004). Proteomics of endoplasmic reticulum-Golgi intermediate compartment (ERGIC) membranes from brefeldin A-treated HepG2 cells identifies ERGIC-32, a new cycling protein that interacts with human Erv46. J Biol Chem *279*, 47242–47253.

Brieher, W.M., Coughlin, M., and Mitchison, T.J. (2004). Fascin-mediated propulsion of Listeria monocytogenes independent of frequent nucleation by the Arp2/3 complex. J Cell Biol *165*, 233–242.

Bright, N.A., Gratian, M.J., and Luzio, J.P. (2005). Endocytic delivery to lysosomes mediated by concurrent fusion and kissing events in living cells. Curr Biol *15*, 360–365.

Brumell, J.H., Tang, P., Mills, S.D., and Finlay, B.B. (2001). Characterization of Salmonella-induced filaments (Sifs) reveals a delayed interaction between Salmonella-containing vacuoles and late endocytic compartments. Traffic *2*, 643–653.

Brunet, S., Thibault, P., Gagnon, E., Kearney, P., Bergeron, J.J.M., and Desjardins, M. (2003). Organelle proteomics: looking at less to see more. Trends Cell Biol *13*, 629–638.

Bujny, M.V., Ewels, P.A., Humphrey, S., Attar, N., Jepson, M.A., and Cullen, P.J. (2008). Sorting nexin-1 defines an early phase of Salmonella-containing vacuole-remodeling during Salmonella infection. J Cell Sci *121*, 2027–2036.

Campbell-Valois, F.-X., Trost, M., Chemali, M., Dill, B.D., Laplante, A., Duclos, S., Sadeghi, S., Rondeau, C., Morrow, I.C., Bell, C., et al. (2012). Quantitative proteomics reveals that only a subset of the endoplasmic reticulum contributes to the phagosome. Mol Cell Proteomics *11*, M111.016378.

Campellone, K.G., and Welch, M.D. (2010). A nucleator arms race: cellular control of actin assembly. Nat Rev Mol Cell Biol *11*, 237–251.

Cardoso, C.M.P., Jordao, L., and Vieira, O.V. (2010). Rab10 regulates phagosome maturation and its overexpression rescues Mycobacterium-containing phagosomes maturation. Traffic *11*, 221–235.

Carroll, K.S., Hanna, J., Simon, I., Krise, J., Barbero, P., and Pfeffer, S.R. (2001). Role of Rab9 GTPase in facilitating receptor recruitment by TIP47. Science *292*, 1373–1376.

Caudron, F., and Barral, Y. (2009). Septins and the lateral compartmentalization of eukaryotic membranes. Dev Cell *16*, 493–506.

Cebrian, I., Visentin, G., Blanchard, N., Jouve, M., Bobard, A., Moita, C., Enninga, J., Moita, L.F., Amigorena, S., and Savina, A. (2011). Sec22b regulates phagosomal maturation and antigen crosspresentation by dendritic cells. Cell *147*, 1355–1368.

Chakravortty, D., Rohde, M., Jäger, L., Deiwick, J., and Hensel, M. (2005). Formation of a novel surface structure encoded by Salmonella Pathogenicity Island 2. Embo J *24*, 2043–2052.

Chang, L., and Goldman, R.D. (2004). Intermediate filaments mediate cytoskeletal crosstalk. Nat Rev Mol Cell Biol *5*, 601–613.

Chao, J.T., Wong, A.K.O., Tavassoli, S., Young, B.P., Chruscicki, A., Fang, N.N., Howe, L.J., Mayor, T., Foster, L.J., and Loewen, C.J.R. (2014). Polarization of the Endoplasmic Reticulum by ER-Septin Tethering. Cell *158*, 620–632.

Chen, Y.A., and Scheller, R.H. (2001). SNARE-mediated membrane fusion. Nat Rev Mol Cell Biol *2*, 98–106.

Cherfils, J., and Zeghouf, M. (2011). Chronicles of the GTPase switch. Nat. Chem. Biol. *7*, 493–495.

Cherfils, J., and Zeghouf, M. (2013). Regulation of small GTPases by GEFs, GAPs, and GDIs. Physiol. Rev. *93*, 269–309.

Collinet, C., Stöter, M., Bradshaw, C.R., Samusik, N., Rink, J.C., Kenski, D., Habermann, B., Buchholz, F., Henschel, R., Mueller, M.S., et al. (2010). Systems survey of endocytosis by multiparametric image analysis. Nature *464*, 243–249.

Collins, R.F., Schreiber, A.D., Grinstein, S., and Trimble, W.S. (2002). Syntaxins 13 and 7 function at distinct steps during phagocytosis. J Immunol *169*, 3250–3256.

Cossart, P., Boquet, P., Normark, S., and Rappuoli, R. (1996). Cellular microbiology emerging. Science *271*, 315–316.

Cossart, P., and Helenius, A. (2014). Endocytosis of viruses and bacteria. Cold Spring Harb Perspect Biol *6*.

Cossart, P., and Roy, C.R. (2010). Manipulation of host membrane machinery by bacterial pathogens. Curr Opin Cell Biol *22*, 547–554.

Cossart, P., and Sansonetti, P.J. (2004). Bacterial invasion: the paradigms of enteroinvasive pathogens. Science *304*, 242–248.

Cox, J., and Mann, M. (2008). MaxQuant enables high peptide identification rates, individualized p.p.b.-range mass accuracies and proteome-wide protein quantification. Nat Biotechnol *26*, 1367–1372.

Cox, J., and Mann, M. (2011). Quantitative, high-resolution proteomics for data-driven systems biology. Annu. Rev. Biochem. *80*, 273–299.

Cox, J., Neuhauser, N., Michalski, A., Scheltema, R.A., Olsen, J.V., and Mann, M. (2011). Andromeda: a peptide search engine integrated into the MaxQuant environment. J. Proteome Res. *10*, 1794–1805.

Creasey, E.A., and Isberg, R.R. (2012). The protein SdhA maintains the integrity of the Legionella-containing vacuole. Proc Natl Acad Sci USA *109*, 3481–3486.

Creasey, E.A., and Isberg, R.R. (2014). Maintenance of vacuole integrity by bacterial pathogens. Curr Opin Microbiol *17*, 46–52.

Dai, S., Zhang, Y., Weimbs, T., Yaffe, M.B., and Zhou, D. (2007). Bacteria-generated PtdIns(3)P recruits VAMP8 to facilitate phagocytosis. Traffic *8*, 1365–1374.

DE DUVE, C., PRESSMAN, B.C., GIANETTO, R., WATTIAUX, R., and APPELMANS, F. (1955). Tissue fractionation studies. 6. Intracellular distribution patterns of enzymes in rat-liver tissue. Biochem J *60*, 604–617.

Deane, J.E., Abrusci, P., Johnson, S., and Lea, S.M. (2010). Timing is everything: the regulation of type III secretion. Cellular and Molecular Life Sciences : CMLS *67*, 1065–1075.

Del Conte-Zerial, P., Brusch, L., Rink, J.C., Collinet, C., Kalaidzidis, Y., Zerial, M., and Deutsch, A. (2008). Membrane identity and GTPase cascades regulated by toggle and cut-out switches. Mol. Syst. Biol. *4*, 206.

Demali, K.A., Jue, A.L., and Burridge, K. (2006). IpaA targets beta1 integrins and rho to promote actin cytoskeleton rearrangements necessary for Shigella entry. J Biol Chem *281*, 39534–39541.

Desjardins, M., Huber, L.A., Parton, R.G., and Griffiths, G. (1994). Biogenesis of phagolysosomes proceeds through a sequential series of interactions with the endocytic apparatus. J Cell Biol *124*, 677–688.

Diepold, A., and Wagner, S. (2014). Assembly of the bacterial type III secretion machinery. FEMS Microbiol. Rev. *38*, 802–822.

Doherty, G.J., and McMahon, H.T. (2009). Mechanisms of Endocytosis. Annu. Rev. Biochem. *78*, 857–902.

Drecktrah, D., Knodler, L.A., Galbraith, K., and Steele-Mortimer, O. (2005). The Salmonella SPI1 effector SopB stimulates nitric oxide production long after invasion. Cell Microbiol *7*, 105–113.

Drecktrah, D., Knodler, L.A., Howe, D., and Steele-Mortimer, O. (2007). Salmonella trafficking is defined by continuous dynamic interactions with the endolysosomal system. Traffic *8*, 212–225.

Drecktrah, D., Levine-Wilkinson, S., Dam, T., Winfree, S., Knodler, L.A., Schroer, T.A., and Steele-Mortimer, O. (2008). Dynamic behavior of Salmonella-induced membrane tubules in epithelial cells. Traffic *9*, 2117–2129.

Driskell, O.J., Mironov, A., Allan, V.J., and Woodman, P.G. (2007). Dynein is required for receptor sorting and the morphogenesis of early endosomes. Nat Cell Biol *9*, 113–120.

Dupont, N., Lacas-Gervais, S., Bertout, J., Paz, I., Freche, B., Nhieu, G.T.V., van der Goot, F.G., Sansonetti, P.J., and Lafont, F. (2009). Shigella phagocytic vacuolar membrane remnants participate in the cellular response to pathogen invasion and are regulated by autophagy. Cell Host Microbe *6*, 137–149.

Duve, C. (1975). Exploring cells with a centrifuge. Science *189*, 186–194.

Eden, E.R., White, I.J., Tsapara, A., and Futter, C.E. (2010). Membrane contacts between endosomes and ER provide sites for PTP1B-epidermal growth factor receptor interaction. Nat Cell Biol *12*, 267–272.

Egile, C., Loisel, T.P., Laurent, V., Li, R., Pantaloni, D., Sansonetti, P.J., and Carlier, M.F. (1999). Activation of the CDC42 effector N-WASP by the Shigella flexneri IcsA protein promotes actin nucleation by Arp2/3 complex and bacterial actin-based motility. J Cell Biol *146*, 1319–1332.

Ehsani, S., Santos, J.C., Rodrigues, C.D., Henriques, R., Audry, L., Zimmer, C., Sansonetti, P., Tran Van Nhieu, G., and Enninga, J. (2012). Hierarchies of host factor dynamics at the entry site of Shigella flexneri during host cell invasion. Infect Immun.

Eichelberg, K., and Galán, J.E. (1999). Differential regulation of Salmonella typhimurium type III secreted proteins by pathogenicity island 1 (SPI-1)-encoded transcriptional activators InvF and hilA. Infect Immun *67*, 4099–4105.

English, A.R., and Voeltz, G.K. (2013). Endoplasmic Reticulum Structure and Interconnections with Other Organelles. Cold Spring Harb Perspect Biol *5*, a013227–a013227.

Enninga, J., and Rosenshine, I. (2009). Imaging the assembly, structure and activity of type III secretion systems. Cell Microbiol *11*, 1462–1470.

Enninga, J., Mounier, J., Sansonetti, P., and Tran Van Nhieu, G. (2005). Secretion of type III effectors into host cells in real time. Nat Methods *2*, 959–965.

Estey, M.P., Kim, M.S., and Trimble, W.S. (2011). Septins. Curr Biol *21*, R384–R387.

Etienne-Manneville, S., and Hall, A. (2002). Rho GTPases in cell biology. Nature *420*, 629–635.

Fairn, G.D., and Grinstein, S. (2012). How nascent phagosomes mature to become phagolysosomes. Trends Immunol.

Fan, J.-Y., Roth, J., and Zuber, C. (2003). Ultrastructural analysis of transitional endoplasmic reticulum and pre-Golgi intermediates: a highway for cars and trucks. Histochem. Cell Biol. *120*, 455–463.

Ferreira, J.G., Pereira, A.L., and Maiato, H. (2014). Microtubule plus-end tracking proteins and their roles in cell division. Int Rev Cell Mol Biol *309*, 59–140.

Figueira, R., and Holden, D.W. (2012). Functions of the Salmonella pathogenicity island 2 (SPI-2) type III secretion system effectors. Microbiology (Reading, Engl.) *158*, 1147–1161.

Finsel, I., Ragaz, C., Hoffmann, C., Harrison, C.F., Weber, S., van Rahden, V.A., Johannes, L., and Hilbi, H. (2013). The Legionella Effector RidL Inhibits Retrograde Trafficking to Promote Intracellular Replication. Cell Host Microbe *14*, 38–50.

Fletcher, D.A., and Mullins, R.D. (2010). Cell mechanics and the cytoskeleton. Nature *463*, 485–492.

Fredlund, J., and Enninga, J. (2014). Cytoplasmic access by intracellular bacterial pathogens. Trends in Microbiology *22*, 128–137.

Friedman, J.R., and Voeltz, G.K. (2011). The ER in 3D: a multifunctional dynamic membrane network. Trends Cell Biol.

Friedman, J.R., Webster, B.M., Mastronarde, D.N., Verhey, K.J., and Voeltz, G.K. (2010). ER sliding dynamics and ER-mitochondrial contacts occur on acetylated microtubules. J Cell Biol *190*, 363–375.

Fu, Y., and Galán, J.E. (1999). A salmonella protein antagonizes Rac-1 and Cdc42 to mediate host-cell recovery after bacterial invasion. Nature *401*, 293–297.

Fujita, H., Katoh, H., Hasegawa, H., Yasui, H., Aoki, J., Yamaguchi, Y., and Negishi, M. (2000). Molecular decipherment of Rho effector pathways regulating tight-junction permeability. Biochem J *346 Pt 3*, 617–622.

Gagnon, E., Duclos, S., Rondeau, C., Chevet, E., Cameron, P.H., Steele-Mortimer, O., Paiement, J., Bergeron, J.J.M., and Desjardins, M. (2002). Endoplasmic reticulum-mediated phagocytosis is a mechanism of entry into macrophages. Cell *110*, 119–131.

Garcia-del Portillo, F., and Finlay, B.B. (1995). Targeting of Salmonella typhimurium to vesicles containing lysosomal membrane glycoproteins bypasses compartments with mannose 6-phosphate receptors. J Cell Biol *129*, 81–97.

Garin, J., Diez, R., Kieffer, S., Dermine, J.F., Duclos, S., Gagnon, E., Sadoul, R., Rondeau, C., and Desjardins, M. (2001). The phagosome proteome: insight into phagosome functions. J Cell Biol *152*, 165–180.

Gatto, L., Vizcaíno, J.A., Hermjakob, H., Huber, W., and Lilley, K.S. (2010). Organelle proteomics experimental designs and analysis. Proteomics *10*, 3957–3969.

Glick, B.S., and Nakano, A. (2009). Membrane traffic within the Golgi apparatus. Annu Rev Cell Dev Biol *25*, 113–132.

Goebeler, V., Poeter, M., Zeuschner, D., Gerke, V., and Rescher, U. (2008). Annexin A8 regulates late endosome organization and function. Mol Biol Cell *19*, 5267–5278.

Goitre, L., Trapani, E., Trabalzini, L., and Retta, S.F. (2014). The Ras superfamily of small GTPases: the unlocked secrets. Methods Mol Biol *1120*, 1–18.

Goldstein, J.L., Brown, M.S., Anderson, R.G., Russell, D.W., and Schneider, W.J. (1985). Receptor-mediated endocytosis: concepts emerging from the LDL receptor system. Annu. Rev. Cell Biol. *1*, 1–39.

Goley, E.D., and Welch, M.D. (2006). The ARP2/3 complex: an actin nucleator comes of age. Nat Rev Mol Cell Biol *7*, 713–726.

Gouin, E., Egile, C., Dehoux, P., Villiers, V., Adams, J., Gertler, F., Li, R., and Cossart, P. (2004). The RickA protein of Rickettsia conorii activates the Arp2/3 complex. Nature *427*, 457–461.

Gouin, E., Welch, M.D., and Cossart, P. (2005). Actin-based motility of intracellular pathogens. Curr Opin Microbiol *8*, 35–45.

Graham, J.M., and Rickwood, D. (1997). Subcellular Fractionation : A Practical Approach (Oxford University Press, USA).

Graham, J.M. (2002). OptiPrep density gradient solutions for mammalian organelles. ScientificWorldJournal *2*, 1440–1443.

Grant, B.D., and Donaldson, J.G. (2009). Pathways and mechanisms of endocytic recycling. Nat Rev Mol Cell Biol *10*, 597–608.

Gruenberg, J. (2001). The endocytic pathway: a mosaic of domains. Nat Rev Mol Cell Biol *2*, 721–730.

Guermonprez, P., Saveanu, L., Kleijmeer, M., Davoust, J., Van Endert, P., and Amigorena, S. (2003). ER-phagosome fusion defines an MHC class I cross-presentation compartment in dendritic cells. Nature *425*, 397–402.

Guignot, J., and Servin, A.L. (2008). Maintenance of the Salmonella-containing vacuole in the juxtanuclear area: a role for intermediate filaments. Microb. Pathog. *45*, 415–422.

Gupton, S.L., and Gertler, F.B. (2007). Filopodia: the fingers that do the walking. Sci. STKE *2007*, re5.

Haglund, C.M., and Welch, M.D. (2011). Pathogens and polymers: microbe-host interactions illuminate the cytoskeleton. J Cell Biol *195*, 7–17.

Hall, P.A., Jung, K., Hillan, K.J., and Russell, S.E.H. (2005). Expression profiling the human septin gene family. J. Pathol. *206*, 269–278.

Ham, H., Sreelatha, A., and Orth, K. (2011). Manipulation of host membranes by bacterial effectors. Nat Rev Microbiol *9*, 635–646.

Hamon, M.A., Ribet, D., Stavru, F., and Cossart, P. (2012). Listeriolysin O: the Swiss army knife of Listeria. Trends in Microbiology *20*, 360–368.

Handa, Y., Suzuki, M., Ohya, K., Iwai, H., Ishijima, N., Koleske, A.J., Fukui, Y., and Sasakawa, C. (2007). Shigella IpgB1 promotes bacterial entry through the ELMO-Dock180 machinery. Nat Cell Biol *9*, 121–128.

Haraga, A., Ohlson, M.B., and Miller, S.I. (2008). Salmonellae interplay with host cells. Nat Rev Microbiol *6*, 53–66.

Hardt, W.D., Chen, L.M., Schuebel, K.E., Bustelo, X.R., and Galán, J.E. (1998). S. typhimurium encodes an activator of Rho GTPases that induces membrane ruffling and nuclear responses in host cells. Cell *93*, 815–826.

Harrison, R.E., Brumell, J.H., Khandani, A., Bucci, C., Scott, C.C., Jiang, X., Finlay, B.B., and Grinstein, S. (2004). Salmonella impairs RILP recruitment to Rab7 during maturation of invasion vacuoles. Mol Biol Cell *15*, 3146–3154.

Hayer, A., Stoeber, M., Bissig, C., and Helenius, A. (2010a). Biogenesis of caveolae: stepwise assembly of large caveolin and cavin complexes. Traffic *11*, 361–382.

Hayer, A., Stoeber, M., Ritz, D., Engel, S., Meyer, H.H., and Helenius, A. (2010b). Caveolin-1 is ubiquitinated and targeted to intralumenal vesicles in endolysosomes for degradation. J Cell Biol *191*, 615–629.

Hayward, R.D., and Koronakis, V. (1999). Direct nucleation and bundling of actin by the SipC protein of invasive Salmonella. Embo J *18*, 4926–4934.

Hayward, R.D., Cain, R.J., McGhie, E.J., Phillips, N., Garner, M.J., and Koronakis, V. (2005). Cholesterol binding by the bacterial type III translocon is essential for virulence effector delivery into mammalian cells. Mol Microbiol *56*, 590–603.

Hänisch, J., Ehinger, J., Ladwein, M., Rohde, M., Derivery, E., Bosse, T., Steffen, A., Bumann, D., Misselwitz, B., Hardt, W.-D., et al. (2010). Molecular dissection of Salmonella-induced membrane ruffling versus invasion. Cell Microbiol *12*, 84–98.

Hänisch, J., Kölm, R., Wozniczka, M., Bumann, D., Rottner, K., and Stradal, T.E.B. (2011). Activation of a RhoA/myosin II-dependent but Arp2/3 complex-independent pathway facilitates Salmonella invasion. Cell Host Microbe *9*, 273–285.

He, C., and Klionsky, D.J. (2009). Regulation mechanisms and signaling pathways of autophagy. Annu Rev Genet *43*, 67–93.

Heasman, S.J., and Ridley, A.J. (2008). Mammalian Rho GTPases: new insights into their functions from in vivo studies. Nat Rev Mol Cell Biol *9*, 690–701.

Henley, J.R., Krueger, E.W., Oswald, B.J., and McNiven, M.A. (1998). Dynamin-mediated internalization of caveolae. J Cell Biol *141*, 85–99.

Henry, T., Gorvel, J.-P., and Méresse, S. (2006). Molecular motors hijacking by intracellular pathogens. Cell Microbiol *8*, 23–32.

Hernandez, L.D., Hueffer, K., Wenk, M.R., and Galán, J.E. (2004). Salmonella modulates vesicular traffic by altering phosphoinositide metabolism. Science *304*, 1805–1807.

Herrmann, H., Bär, H., Kreplak, L., Strelkov, S.V., and Aebi, U. (2007). Intermediate filaments: from cell architecture to nanomechanics. Nat Rev Mol Cell Biol *8*, 562–573.

High, N., Mounier, J., Prévost, M.C., and Sansonetti, P.J. (1992). IpaB of Shigella flexneri causes entry into epithelial cells and escape from the phagocytic vacuole. Embo J *11*, 1991–1999.

Hilbi, H., and Haas, A. (2012). Secretive bacterial pathogens and the secretory pathway. Traffic *13*, 1187–1197.

Hilbi, H., Hoffmann, C., and Harrison, C.F. (2011). Legionella spp. outdoors: colonization, communication and persistence. Environ Microbiol Rep *3*, 286–296.

Hoffmann, C., Finsel, I., and Hilbi, H. (2013). Pathogen vacuole purification from legionella-infected amoeba and macrophages. Methods Mol Biol *954*, 309–321.

Hoffmann, C., Finsel, I., Otto, A., Pfaffinger, G., Rothmeier, E., Hecker, M., Becher, D., and Hilbi, H. (2014). Functional analysis of novel Rab GTPases identified in the proteome of purified Legionella-containing vacuoles from macrophages. Cell Microbiol *16*, 1034–1052.

Hong, W. (2005). SNAREs and traffic. Biochimica Et Biophysica Acta (BBA) - Molecular Cell Research *1744*, 120–144.

Horgan, C.P., and McCaffrey, M.W. (2011). Rab GTPases and microtubule motors. Biochem. Soc. Trans. *39*, 1202–1206.

Horiuchi, H., Lippé, R., McBride, H.M., Rubino, M., Woodman, P., Stenmark, H., Rybin, V., Wilm, M., Ashman, K., Mann, M., et al. (1997). A novel Rab5 GDP/GTP exchange factor complexed to Rabaptin-5 links nucleotide exchange to effector recruitment and function. Cell *90*, 1149–1159.

Houde, M., Bertholet, S., Gagnon, E., Brunet, S., Goyette, G., Laplante, A., Princiotta, M.F., Thibault, P., Sacks, D., and Desjardins, M. (2003). Phagosomes are competent organelles for antigen cross-presentation. Nature *425*, 402–406.

Huang, Y.-W., Yan, M., Collins, R.F., Diciccio, J.E., Grinstein, S., and Trimble, W.S. (2008). Mammalian septins are required for phagosome formation. Mol Biol Cell *19*, 1717–1726.

Hubber, A., and Roy, C.R. (2010). Modulation of host cell function by Legionella pneumophila type IV effectors. Annu Rev Cell Dev Biol *26*, 261–283.

Humphreys, D., Davidson, A.C., Hume, P.J., Makin, L.E., and Koronakis, V. (2013). Arf6 coordinates actin assembly through the WAVE complex, a mechanism usurped by Salmonella to invade host cells. Proc Natl Acad Sci USA *110*, 16880–16885.

Humphreys, D., Davidson, A., Hume, P.J., and Koronakis, V. (2012). Salmonella Virulence Effector SopE and Host GEF ARNO Cooperate to Recruit and Activate WAVE to Trigger Bacterial Invasion. Cell Host Microbe *11*, 129–139.

Humphries, A.C., and Way, M. (2013). The non-canonical roles of clathrin and actin in pathogen internalization, egress and spread. Nat Rev Microbiol *11*, 551–560.

Huotari, J., and Helenius, A. (2011). Endosome maturation. Embo J *30*, 3481–3500.

Ibarra, J.A., and Steele-Mortimer, O. (2009). Salmonella--the ultimate insider. Salmonella virulence factors that modulate intracellular survival. Cell Microbiol *11*, 1579–1586.

Isberg, R.R., O'Connor, T.J., and Heidtman, M. (2009). The Legionella pneumophila replication vacuole: making a cosy niche inside host cells. Nat Rev Microbiol *7*, 13–24.

Jackson, L.P. (2014). Structure and mechanism of COPI vesicle biogenesis. Curr Opin Cell Biol *29C*, 67–73.

Jaffe, A.B., and Hall, A. (2005). Rho GTPases: biochemistry and biology. Annu Rev Cell Dev Biol *21*, 247–269.

Jahn, R., and Scheller, R.H. (2006). SNAREs--engines for membrane fusion. Nat Rev Mol Cell Biol *7*, 631–643.

Jensen, D., and Schekman, R. (2011). COPII-mediated vesicle formation at a glance. J Cell Sci *124*, 1–4.

Jo, E.-K., Yuk, J.-M., Shin, D.-M., and Sasakawa, C. (2013). Roles of autophagy in elimination of intracellular bacterial pathogens. Front Immunol *4*, 97.

Johannes, L., Parton, R.G., Bassereau, P., and Mayor, S. (2015). Building endocytic pits without clathrin. Nat Rev Mol Cell Biol *16*, 311–321.

Jolly, C., Winfree, S., Hansen, B., and Steele-Mortimer, O. (2013). The Annexin A2/p11 complex is required for efficient invasion of Salmonella Typhimurium in epithelial cells. Cell Microbiol.

Jones, A.T. (2007). Macropinocytosis: searching for an endocytic identity and role in the uptake of cell penetrating peptides. J. Cell. Mol. Med. *11*, 670–684.

Jordan, M.A., and Wilson, L. (2004). Microtubules as a target for anticancer drugs. Nat. Rev. Cancer *4*, 253–265.

Jordens, I., Fernandez-Borja, M., Marsman, M., Dusseljee, S., Janssen, L., Calafat, J., Janssen, H., Wubbolts, R., and Neefjes, J. (2001). The Rab7 effector protein RILP controls lysosomal transport by inducing the recruitment of dynein-dynactin motors. Curr Biol *11*, 1680–1685.

Jovic, M., Sharma, M., Rahajeng, J., and Caplan, S. (2010). The early endosome: a busy sorting station for proteins at the crossroads. Histol. Histopathol. *25*, 99–112.

Kagan, J.C., and Roy, C.R. (2002). Legionella phagosomes intercept vesicular traffic from endoplasmic reticulum exit sites. Nat Cell Biol *4*, 945–954.

Kagan, J.C., Stein, M.-P., Pypaert, M., and Roy, C.R. (2004). Legionella subvert the functions of Rab1 and Sec22b to create a replicative organelle. J Exp Med *199*, 1201–1211.

Kaniuk, N.A., Canadien, V., Bagshaw, R.D., Bakowski, M., Braun, V., Landekic, M., Mitra, S., Huang, J., Heo, W.D., Meyer, T., et al. (2011). Salmonella exploits Arl8B-directed kinesin activity to promote endosome tubulation and cell-to-cell transfer. Cell Microbiol *13*, 1812–1823.

Kim, M.S., Froese, C.D., Estey, M.P., and Trimble, W.S. (2011). SEPT9 occupies the terminal positions in septin octamers and mediates polymerization-dependent functions in abscission. J Cell Biol *195*, 815–826.

Kinoshita, M., Field, C.M., Coughlin, M.L., Straight, A.F., and Mitchison, T.J. (2002). Self- and actin-templated assembly of Mammalian septins. Dev Cell *3*, 791–802.

Klebe, C., Prinz, H., Wittinghofer, A., and Goody, R.S. (1995). The kinetic mechanism of Ran--nucleotide exchange catalyzed by RCC1. Biochemistry *34*, 12543–12552.

Knoblach, B., Keller, B.O., Groenendyk, J., Aldred, S., Zheng, J., Lemire, B.D., Li, L., and Michalak, M. (2003). ERp19 and ERp46, new members of the thioredoxin family of endoplasmic reticulum proteins. Mol Cell Proteomics *2*, 1104–1119.

Knodler, L.A., Nair, V., and Steele-Mortimer, O. (2014). Quantitative assessment of cytosolic Salmonella in epithelial cells. PLoS ONE *9*, e84681.

Knodler, L.A., Vallance, B.A., Celli, J., Winfree, S., Hansen, B., Montero, M., and Steele-Mortimer, O. (2010). Dissemination of invasive Salmonella via bacterial-induced extrusion of mucosal epithelia. Proc Natl Acad Sci USA *107*, 17733–17738.

Koh, A.L.Y., Sun, C.X., Zhu, F., and Glogauer, M. (2005). The role of Rac1 and Rac2 in bacterial killing. Cell. Immunol. *235*, 92–97.

Kotloff, K.L., Winickoff, J.P., Ivanoff, B., Clemens, J.D., Swerdlow, D.L., Sansonetti, P.J., Adak, G.K., and Levine, M.M. (1999). Global burden of Shigella infections: implications for vaccine development and implementation of control strategies. Bull. World Health Organ. *77*, 651–666.

Krieger, V., Liebl, D., Zhang, Y., Rajashekar, R., Chlanda, P., Giesker, K., Chikkaballi, D., and Hensel, M. (2014). Reorganization of the endosomal system in salmonella-infected cells: the ultrastructure of salmonella-induced tubular compartments. PLoS Pathog *10*, e1004374.

Kubori, T., and Galán, J.E. (2003). Temporal regulation of salmonella virulence effector function by proteasome-dependent protein degradation. Cell *115*, 333–342.

Kumar, Y., and Valdivia, R.H. (2009). Leading a sheltered life: intracellular pathogens and maintenance of vacuolar compartments. Cell Host Microbe *5*, 593–601.

Kurokawa, K., Okamoto, M., and Nakano, A. (2014). Contact of cis-Golgi with ER exit sites executes cargo capture and delivery from the ER. Nat Commun *5*, 3653.

Lambert, M.A., and Smith, S.G.J. (2009). The PagN protein mediates invasion via interaction with proteoglycan. FEMS Microbiol. Lett. *297*, 209–216.

Lara-Tejero, M., Kato, J., Wagner, S., Liu, X., and Galán, J.E. (2011). A sorting platform determines the order of protein secretion in bacterial type III systems. Science *331*, 1188–1191.

LaRock, D.L., Chaudhary, A., and Miller, S.I. (2015). Salmonellae interactions with host processes. Nat Rev Microbiol *13*, 191–205.

Lee, B.-Y., Jethwaney, D., Schilling, B., Clemens, D.L., Gibson, B.W., and Horwitz, M.A. (2010). The Mycobacterium bovis bacille Calmette-Guerin phagosome proteome. Mol Cell Proteomics *9*, 32–53.

Legg, J.A., Bompard, G., Dawson, J., Morris, H.L., Andrew, N., Cooper, L., Johnston, S.A., Tramountanis, G., and Machesky, L.M. (2007). N-WASP involvement in dorsal ruffle formation in mouse embryonic fibroblasts. Mol Biol Cell *18*, 678–687.

Lenzen, C., Cool, R.H., Prinz, H., Kuhlmann, J., and Wittinghofer, A. (1998). Kinetic analysis by fluorescence of the interaction between Ras and the catalytic domain of the guanine nucleotide exchange factor Cdc25Mm. Biochemistry *37*, 7420–7430.

Li, Q., Jagannath, C., Rao, P.K., Singh, C.R., and Lostumbo, G. (2010). Analysis of phagosomal proteomes: From latex-bead to bacterial phagosomes. Proteomics *10*, 4098–4116.

Lippé, R., Miaczynska, M., Rybin, V., Runge, A., and Zerial, M. (2001). Functional synergy between Rab5 effector Rabaptin-5 and exchange factor Rabex-5 when physically associated in a complex. Mol Biol Cell *12*, 2219–2228.

Lippincott-Schwartz, J., Yuan, L.C., Bonifacino, J.S., and Klausner, R.D. (1989). Rapid redistribution of Golgi proteins into the ER in cells treated with brefeldin A: evidence for membrane cycling from Golgi to ER. Cell *56*, 801–813.

Liss, V., and Hensel, M. (2015). Take the tube: remodeling of the endosomal system by intracellular Salmonella enterica. Cell Microbiol.

Lord, C., Ferro-Novick, S., and Miller, E.A. (2013). The highly conserved COPII coat complex sorts cargo from the endoplasmic reticulum and targets it to the golgi. Cold Spring Harb Perspect Biol *5*.

Luber, C.A., Cox, J., Lauterbach, H., Fancke, B., Selbach, M., Tschopp, J., Akira, S., Wiegand, M., Hochrein, H., O'Keeffe, M., et al. (2010). Quantitative proteomics reveals subset-specific viral recognition in dendritic cells. Immunity *32*, 279–289.

Luzio, J.P., Gray, S.R., and Bright, N.A. (2010). Endosome-lysosome fusion. Biochem. Soc. Trans. *38*, 1413–1416.

Luzio, J.P., Parkinson, M.D.J., Gray, S.R., and Bright, N.A. (2009). The delivery of endocytosed cargo to lysosomes. Biochem. Soc. Trans. *37*, 1019–1021.

Luzio, J.P., Pryor, P.R., and Bright, N.A. (2007). Lysosomes: fusion and function. Nat Rev Mol Cell Biol *8*, 622–632.

Machacek, M., Hodgson, L., Welch, C., Elliott, H., Pertz, O., Nalbant, P., Abell, A., Johnson, G.L., Hahn, K.M., and Danuser, G. (2009). Coordination of Rho GTPase activities during cell protrusion. Nature *461*, 99–103.

Majowicz, S.E., Musto, J., Scallan, E., Angulo, F.J., Kirk, M., O'Brien, S.J., Jones, T.F., Fazil, A., Hoekstra, R.M., International Collaboration on Enteric Disease 'Burden of Illness' Studies (2010). The global burden of nontyphoidal Salmonella gastroenteritis. Clin. Infect. Dis. *50*, 882–889.

Malik-Kale, P., Jolly, C.E., Lathrop, S., Winfree, S., Luterbach, C., and Steele-Mortimer, O. (2011). Salmonella - at home in the host cell. Front Microbiol *2*, 125.

Malik-Kale, P., Winfree, S., and Steele-Mortimer, O. (2012). The bimodal lifestyle of intracellular salmonella in epithelial cells: replication in the cytosol obscures defects in vacuolar replication. PLoS ONE *7*, e38732.

Mallo, G.V., Espina, M., Smith, A.C., Terebiznik, M.R., Alemán, A., Finlay, B.B., Rameh, L.E., Grinstein, S., and Brumell, J.H. (2008). SopB promotes phosphatidylinositol 3-phosphate formation on Salmonella vacuoles by recruiting Rab5 and Vps34. J Cell Biol *182*, 741–752.

Marelli, M., Smith, J.J., Jung, S., Yi, E., Nesvizhskii, A.I., Christmas, R.H., Saleem, R.A., Tam, Y.Y.C., Fagarasanu, A., Goodlett, D.R., et al. (2004). Quantitative mass spectrometry reveals a role for the GTPase Rho1p in actin organization on the peroxisome membrane. J Cell Biol *167*, 1099–1112.

Marinissen, M.J., and Gutkind, J.S. (2005). Scaffold proteins dictate Rho GTPase-signaling specificity. Trends Biochem Sci *30*, 423–426.

Marquis, H., and Hager, E.J. (2000). pH-regulated activation and release of a bacteria-associated phospholipase C during intracellular infection by Listeria monocytogenes. Mol Microbiol *35*, 289–298.

Marsman, M., Jordens, I., Kuijl, C., Janssen, L., and Neefjes, J. (2004). Dynein-mediated vesicle transport controls intracellular Salmonella replication. Mol Biol Cell *15*, 2954–2964.

Maxfield, F.R., and Yamashiro, D.J. (1987). Endosome acidification and the pathways of receptor-mediated endocytosis. Adv. Exp. Med. Biol. *225*, 189–198.

Mayor, S., and Pagano, R.E. (2007). Pathways of clathrin-independent endocytosis. Nat Rev Mol Cell Biol *8*, 603–612.

McEwan, D.G., Richter, B., Claudi, B., Wigge, C., Wild, P., Farhan, H., McGourty, K., Coxon, F.P., Franz-Wachtel, M., Perdu, B., et al. (2014). PLEKHM1 Regulates Salmonella-Containing Vacuole Biogenesis and Infection. Cell Host Microbe.

McGhie, E.J., Brawn, L.C., Hume, P.J., Humphreys, D., and Koronakis, V. (2009). Salmonella takes control: effector-driven manipulation of the host. Curr Opin Microbiol *12*, 117–124.

McGhie, E.J., Hayward, R.D., and Koronakis, V. (2004). Control of actin turnover by a salmonella invasion protein. Mol. Cell *13*, 497–510.

McGourty, K., Thurston, T.L., Matthews, S.A., Pinaud, L., Mota, L.J., and Holden, D.W. (2012). Salmonella inhibits retrograde trafficking of mannose-6-phosphate receptors and lysosome function. Science *338*, 963–967.

McLauchlan, H., Newell, J., Morrice, N., Osborne, A., West, M., and Smythe, E. (1998). A novel role for Rab5-GDI in ligand sequestration into clathrin-coated pits. Curr Biol *8*, 34–45.

McMahon, K.-A., Zajicek, H., Li, W.-P., Peyton, M.J., Minna, J.D., Hernandez, V.J., Luby-Phelps, K., and Anderson, R.G.W. (2009). SRBC/cavin-3 is a caveolin adapter protein that regulates caveolae function. Embo J *28*, 1001–1015.

Mellman, I., Fuchs, R., and Helenius, A. (1986). Acidification of the endocytic and exocytic pathways. Annu. Rev. Biochem. *55*, 663–700.

Mellouk, N., Weiner, A., Aulner, N., Schmitt, C., Elbaum, M., Shorte, S.L., Danckaert, A., and Enninga, J. (2014). Shigella subverts the host recycling compartment to rupture its vacuole. Cell Host Microbe *16*, 517–530.

Mercer, J., and Helenius, A. (2009). Virus entry by macropinocytosis. Nat Cell Biol *11*, 510–520.

Méresse, S., Unsworth, K.E., Habermann, A., Griffiths, G., Fang, F., Martínez-Lorenzo, M.J., Waterman, S.R., Gorvel, J.P., and Holden, D.W. (2001). Remodelling of the actin cytoskeleton is essential for replication of intravacuolar Salmonella. Cell Microbiol *3*, 567–577.

Mijouin, L., Rosselin, M., Bottreau, E., Pizarro-Cerdá, J., Cossart, P., Velge, P., and Wiedemann, A. (2012). Salmonella enteritidis Rck-mediated invasion requires activation of Rac1, which is dependent on the class I PI 3-kinases-Akt signaling pathway. The FASEB Journal : Official Publication of the Federation of American Societies for Experimental Biology *26*, 1569–1581.

Miller, S.E., Mathiasen, S., Bright, N.A., Pierre, F., Kelly, B.T., Kladt, N., Schauss, A., Merrifield, C.J., Stamou, D., Höning, S., et al. (2015). CALM regulates clathrin-coated vesicle size and maturation by directly sensing and driving membrane curvature. Dev Cell *33*, 163–175.

Mogelsvang, S., Marsh, B.J., Ladinsky, M.S., and Howell, K.E. (2004). Predicting function from structure: 3D structure studies of the mammalian Golgi complex. Traffic *5*, 338–345.

Molloy, M.P., Herbert, B.R., Walsh, B.J., Tyler, M.I., Traini, M., Sanchez, J.C., Hochstrasser, D.F., Williams, K.L., and Gooley, A.A. (1998). Extraction of membrane proteins by differential solubilization for separation using two-dimensional gel electrophoresis. Electrophoresis *19*, 837–844.

Molmeret, M., Bitar, D.M., Han, L., and Kwaik, Y.A. (2004). Disruption of the phagosomal membrane and egress of Legionella pneumophila into the cytoplasm during the last stages of intracellular infection of macrophages and Acanthamoeba polyphaga. Infect Immun *72*, 4040–4051.

Molmeret, M., Santic, M., Asare, R., Carabeo, R.A., and Abu Kwaik, Y. (2007). Rapid escape of the dot/icm mutants of Legionella pneumophila into the cytosol of mammalian and protozoan cells. Infect Immun *75*, 3290–3304.

Morel, E., Parton, R.G., and Gruenberg, J. (2009). Annexin A2-dependent polymerization of actin mediates endosome biogenesis. Dev Cell *16*, 445–457.

Mostowy, S., and Cossart, P. (2009). Cytoskeleton rearrangements during Listeria infection: clathrin and septins as new players in the game. Cell Motil. Cytoskeleton *66*, 816–823.

Mostowy, S., and Cossart, P. (2011). Autophagy and the cytoskeleton: new links revealed by intracellular pathogens. Autophagy *7*, 780–782.

Mostowy, S., and Cossart, P. (2012). Septins: the fourth component of the cytoskeleton. Nat Rev Mol Cell Biol *13*, 183–194.

Mostowy, S., Bonazzi, M., Hamon, M.A., Tham, T.N., Mallet, A., Lelek, M., Gouin, E., Demangel, C., Brosch, R., Zimmer, C., et al. (2010). Entrapment of intracytosolic bacteria by septin cage-like structures. Cell Host Microbe *8*, 433–444.

Mostowy, S., Janel, S., Forestier, C., Roduit, C., Kasas, S., Pizarro-Cerdá, J., Cossart, P., and Lafont, F. (2011). A role for septins in the interaction between the Listeria monocytogenes INVASION PROTEIN InlB and the Met receptor. Biophys. J. *100*, 1949–1959.

Mostowy, S., Nam Tham, T., Danckaert, A., Guadagnini, S., Boisson-Dupuis, S., Pizarro-Cerdá, J., and Cossart, P. (2009). Septins regulate bacterial entry into host cells. PLoS ONE *4*, e4196.

Mota, L.J., Ramsden, A.E., Liu, M., Castle, J.D., and Holden, D.W. (2009). SCAMP3 is a component of the Salmonella-induced tubular network and reveals an interaction between bacterial effectors and post-Golgi trafficking. Cell Microbiol *11*, 1236–1253.

Mounier, J., Popoff, M.R., Enninga, J., Frame, M.C., Sansonetti, P.J., and Van Nhieu, G.T. (2009). The IpaC carboxyterminal effector domain mediates Src-dependent actin polymerization during Shigella invasion of epithelial cells. PLoS Pathog *5*, e1000271.

Myeni, S.K., and Zhou, D. (2010). The C terminus of SipC binds and bundles F-actin to promote Salmonella invasion. J Biol Chem *285*, 13357–13363.

Nagata, K.-I., Kawajiri, A., Matsui, S., Takagishi, M., Shiromizu, T., Saitoh, N., Izawa, I., Kiyono, T., Itoh, T.J., Hotani, H., et al. (2003). Filament formation of MSF-A, a mammalian septin, in human mammary epithelial cells depends on interactions with microtubules. J Biol Chem *278*, 18538–18543.

Nichols, C.D., and Casanova, J.E. (2010). Salmonella-directed recruitment of new membrane to invasion foci via the host exocyst complex. Curr Biol *20*, 1316–1320.

Nielsen, E., Severin, F., Backer, J.M., Hyman, A.A., and Zerial, M. (1999). Rab5 regulates motility of early endosomes on microtubules. Nat Cell Biol *1*, 376–382.

Niu, T.-K., Pfeifer, A.C., Lippincott-Schwartz, J., and Jackson, C.L. (2005). Dynamics of GBF1, a Brefeldin A-sensitive Arf1 exchange factor at the Golgi. Mol Biol Cell *16*, 1213–1222.

NOVIKOFF, A.B., BEAUFAY, H., and DE DUVE, C. (1956). Electron microscopy of lysosomerich fractions from rat liver. J Biophys Biochem Cytol *2*, 179–184.

Nuoffer, C., Davidson, H.W., Matteson, J., Meinkoth, J., and Balch, W.E. (1994). A GDP-bound of rab1 inhibits protein export from the endoplasmic reticulum and transport between Golgi compartments. J Cell Biol *125*, 225–237.

Ogawa, M., Handa, Y., Ashida, H., Suzuki, M., and Sasakawa, C. (2008). The versatility of Shigella effectors. Nat Rev Microbiol *6*, 11–16.

Ogawa, M., Yoshimori, T., Suzuki, T., Sagara, H., Mizushima, N., and Sasakawa, C. (2005). Escape of intracellular Shigella from autophagy. Science *307*, 727–731.

Oh, P., McIntosh, D.P., and Schnitzer, J.E. (1998). Dynamin at the neck of caveolae mediates their budding to form transport vesicles by GTP-driven fission from the plasma membrane of endothelium. J Cell Biol *141*, 101–114.

Oh, Y.K., Alpuche-Aranda, C., Berthiaume, E., Jinks, T., Miller, S.I., and Swanson, J.A. (1996). Rapid and complete fusion of macrophage lysosomes with phagosomes containing Salmonella typhimurium. Infect Immun *64*, 3877–3883.

Ohya, K., Handa, Y., Ogawa, M., Suzuki, M., and Sasakawa, C. (2005). IpgB1 is a novel Shigella effector protein involved in bacterial invasion of host cells. Its activity to promote membrane ruffling via Rac1 and Cdc42 activation. J Biol Chem *280*, 24022–24034.

Ong, S.-E., and Mann, M. (2005). Mass spectrometry-based proteomics turns quantitative. Nat. Chem. Biol. *1*, 252–262.

Orchard, R.C., and Alto, N.M. (2012). Mimicking GEFs: a common theme for bacterial pathogens. Cell Microbiol *14*, 10–18.

Orci, L., Ravazzola, M., Le Coadic, M., Shen, W.-W., Demaurex, N., and Cosson, P. (2009). From the Cover: STIM1-induced precortical and cortical subdomains of the endoplasmic reticulum. Proc Natl Acad Sci USA *106*, 19358–19362.

Palade, G.E. (1982). Problems in intracellular membrane traffic. Ciba Found. Symp. 1–14.

Pan, F., Malmberg, R.L., and Momany, M. (2007). Analysis of septins across kingdoms reveals orthology and new motifs. BMC Evol. Biol. *7*, 103.

Parsot, C. (2009). Shigella type III secretion effectors: how, where, when, for what purposes? Curr Opin Microbiol *12*, 110–116.

Parton, R.G., and Howes, M.T. (2010). Revisiting caveolin trafficking: the end of the caveosome. J Cell Biol *191*, 439–441.

Patel, J.C., and Galán, J.E. (2006). Differential activation and function of Rho GTPases during Salmonella-host cell interactions. J Cell Biol *175*, 453–463.

Paz, I., Sachse, M., Dupont, N., Mounier, J., Cederfur, C., Enninga, J., Leffler, H., Poirier, F., Prevost, M.-C., Lafont, F., et al. (2010). Galectin-3, a marker for vacuole lysis by invasive pathogens. Cell Microbiol *12*, 530–544.

Pertz, O. (2010). Spatio-temporal Rho GTPase signaling - where are we now? J Cell Sci *123*, 1841–1850.

Pertz, O., and Hahn, K.M. (2004). Designing biosensors for Rho family proteins--deciphering the dynamics of Rho family GTPase activation in living cells. J Cell Sci *117*, 1313–1318.

Pflieger, D., Le Caer, J.-P., Lemaire, C., Bernard, B.A., Dujardin, G., and Rossier, J. (2002). Systematic identification of mitochondrial proteins by LC-MS/MS. Anal. Chem. *74*, 2400–2406.

Phalipon, A., and Sansonetti, P.J. (2007). Shigella's ways of manipulating the host intestinal innate and adaptive immune system: a tool box for survival? Immunol Cell Biol *85*, 119–129.

Pizarro-Cerdá, J., Kühbacher, A., and Cossart, P. (2012). Entry of Listeria monocytogenes in mammalian epithelial cells: an updated view. Cold Spring Harb Perspect Med *2*.

Praefcke, G.J.K., and McMahon, H.T. (2004). The dynamin superfamily: universal membrane tubulation and fission molecules? Nat Rev Mol Cell Biol *5*, 133–147.

Pryor, P.R., Mullock, B.M., Bright, N.A., Gray, S.R., and Luzio, J.P. (2000). The role of intraorganellar Ca2+ in late endosome-lysosome heterotypic fusion and in the reformation of lysosomes from hybrid organelles. J Cell Biol *149*, 1053–1062.

Pryor, P.R., Mullock, B.M., Bright, N.A., Lindsay, M.R., Gray, S.R., Richardson, S.C.W., Stewart, A., James, D.E., Piper, R.C., and Luzio, J.P. (2004). Combinatorial SNARE complexes with VAMP7 or VAMP8 define different late endocytic fusion events. EMBO Rep *5*, 590–595.

Py, B.F., Lipinski, M.M., and Yuan, J. (2007). Autophagy limits Listeria monocytogenes intracellular growth in the early phase of primary infection. Autophagy *3*, 117–125.

Qualmann, B., and Kessels, M.M. (2009). New players in actin polymerization--WH2-domain-containing actin nucleators. Trends Cell Biol *19*, 276–285.

Ragaz, C., Pietsch, H., Urwyler, S., Tiaden, A., Weber, S.S., and Hilbi, H. (2008). The Legionella pneumophila phosphatidylinositol-4 phosphate-binding type IV substrate SidC recruits endoplasmic reticulum vesicles to a replication-permissive vacuole. Cell Microbiol *10*, 2416–2433.

Raiborg, C., Wenzel, E.M., and Stenmark, H. (2015). ER-endosome contact sites: molecular compositions and functions. Embo J *34*, 1848–1858.

Ramarao, N., Le Clainche, C., Izard, T., Bourdet-Sicard, R., Ageron, E., Sansonetti, P.J., Carlier, M.-F., and Tran Van Nhieu, G. (2007). Capping of actin filaments by vinculin activated by the Shigella IpaA carboxyl-terminal domain. FEBS Lett. *581*, 853–857.

Ramsden, A.E., Holden, D.W., and Mota, L.J. (2007). Membrane dynamics and spatial distribution of Salmonella-containing vacuoles. Trends in Microbiology *15*, 516–524.

Rao, S.K., Huynh, C., Proux-Gillardeaux, V., Galli, T., and Andrews, N.W. (2004). Identification of SNAREs involved in synaptotagmin VII-regulated lysosomal exocytosis. J Biol Chem *279*, 20471–20479.

Rathman, M., Barker, L.P., and Falkow, S. (1997). The unique trafficking pattern of Salmonella typhimurium-containing phagosomes in murine macrophages is independent of the mechanism of bacterial entry. Infect Immun *65*, 1475–1485.

Ray, K., Bobard, A., Danckaert, A., Paz-Haftel, I., Clair, C., Ehsani, S., Tang, C., Sansonetti, P., Tran, G.V.N., and Enninga, J. (2010). Tracking the dynamic interplay between bacterial and host factors during pathogen-induced vacuole rupture in real time. Cell Microbiol *12*, 545–556.

Ray, K., Marteyn, B., Sansonetti, P.J., and Tang, C.M. (2009). Life on the inside: the intracellular lifestyle of cytosolic bacteria. Nat Rev Microbiol *7*, 333–340.

Richter, S., Geldner, N., Schrader, J., Wolters, H., Stierhof, Y.-D., Rios, G., Koncz, C., Robinson, D.G., and Jürgens, G. (2007). Functional diversification of closely related ARF-GEFs in protein secretion and recycling. Nature *448*, 488–492.

Ridley, A.J. (2001). Rho GTPases and cell migration. J Cell Sci *114*, 2713–2722.

Riederer, M.A., Soldati, T., Shapiro, A.D., Lin, J., and Pfeffer, S.R. (1994). Lysosome biogenesis requires Rab9 function and receptor recycling from endosomes to the trans-Golgi network. J Cell Biol *125*, 573–582.

Roberts, E.A., Chua, J., Kyei, G.B., and Deretic, V. (2006). Higher order Rab programming in phagolysosome biogenesis. J Cell Biol *174*, 923–929.

Robinson, C.G., and Roy, C.R. (2006). Attachment and fusion of endoplasmic reticulum with vacuoles containing Legionella pneumophila. Cell Microbiol *8*, 793–805.

Rocha, N., Kuijl, C., van der Kant, R., Janssen, L., Houben, D., Janssen, H., Zwart, W., and Neefjes, J. (2009). Cholesterol sensor ORP1L contacts the ER protein VAP to control Rab7-RILP-p150 Glued and late endosome positioning. J Cell Biol *185*, 1209–1225.

Rogers, L.D., and Foster, L.J. (2007). The dynamic phagosomal proteome and the contribution of the endoplasmic reticulum. Proc Natl Acad Sci USA *104*, 18520–18525.

Rogers, L.D., and Foster, L.J. (2008). Contributions of proteomics to understanding phagosome maturation. Cell Microbiol *10*, 1405–1412.

Romero, S., Grompone, G., Carayol, N., Mounier, J., Guadagnini, S., Prevost, M.-C., Sansonetti, P.J., and Nhieu, G.T.V. (2011). ATP-mediated Erk1/2 activation stimulates bacterial capture by filopodia, which precedes Shigella invasion of epithelial cells. Cell Host Microbe *9*, 508–519.

Rosselin, M., Virlogeux-Payant, I., Roy, C., Bottreau, E., Sizaret, P.-Y., Mijouin, L., Germon, P., Caron, E., Velge, P., and Wiedemann, A. (2010). Rck of Salmonella enterica, subspecies enterica serovar enteritidis, mediates zipper-like internalization. Cell Res. *20*, 647–664.

Rottner, K., Hänisch, J., and Campellone, K.G. (2010). WASH, WHAMM and JMY: regulation of Arp2/3 complex and beyond. Trends Cell Biol *20*, 650–661.

Rottner, K., Stradal, T.E.B., and Wehland, J. (2005). Bacteria-host-cell interactions at the plasma membrane: stories on actin cytoskeleton subversion. Dev Cell *9*, 3–17.

Rotty, J.D., Wu, C., and Bear, J.E. (2012). New insights into the regulation and cellular functions of the ARP2/3 complex. Nat Rev Mol Cell Biol.

Rowland, A.A., Chitwood, P.J., Phillips, M.J., and Voeltz, G.K. (2014). ER Contact Sites Define the Position and Timing of Endosome Fission. Cell *159*, 1027–1041.

Saarikangas, J., and Barral, Y. (2011). The emerging functions of septins in metazoans. EMBO Rep *12*, 1118–1126.

Sachse, M., Urbé, S., Oorschot, V., Strous, G.J., and Klumperman, J. (2002). Bilayered clathrin coats on endosomal vacuoles are involved in protein sorting toward lysosomes. Mol Biol Cell *13*, 1313–1328.

Sadowski, P.G., Dunkley, T.P.J., Shadforth, I.P., Dupree, P., Bessant, C., Griffin, J.L., and Lilley, K.S. (2006). Quantitative proteomic approach to study subcellular localization of membrane proteins. Nature Protocols *1*, 1778–1789.

Savas, J.N., Stein, B.D., Wu, C.C., and Yates, J.R.I. (2011). Mass spectrometry accelerates membrane protein analysis. Trends Biochem Sci *36*, 388–396.

Schnatwinkel, C., Christoforidis, S., Lindsay, M.R., Uttenweiler-Joseph, S., Wilm, M., Parton, R.G., and Zerial, M. (2004). The Rab5 effector Rabankyrin-5 regulates and coordinates different endocytic mechanisms. PLoS Biol *2*, E261.

Schroeder, N., Henry, T., de Chastellier, C., Zhao, W., Guilhon, A.-A., Gorvel, J.-P., and Méresse, S. (2010). The virulence protein SopD2 regulates membrane dynamics of Salmonella-containing vacuoles. PLoS Pathog *6*, e1001002.

Schroeder, N., Mota, L.J., and Méresse, S. (2011). Salmonella-induced tubular networks. Trends in Microbiology.

Sciaky, N., Presley, J., Smith, C., Zaal, K.J., Cole, N., Moreira, J.E., Terasaki, M., Siggia, E., and Lippincott-Schwartz, J. (1997). Golgi tubule traffic and the effects of brefeldin A visualized in living cells. J Cell Biol *139*, 1137–1155.

Scott, C.C., Cuellar-Mata, P., Matsuo, T., Davidson, H.W., and Grinstein, S. (2002). Role of 3-phosphoinositides in the maturation of Salmonella-containing vacuoles within host cells. J Biol Chem *277*, 12770–12776.

Scott, C.C., Vacca, F., and Gruenberg, J. (2014). Endosome maturation, transport and functions. Semin. Cell Dev. Biol. *31*, 2–10.

Seaman, M.N.J. (2012). The retromer complex - endosomal protein recycling and beyond. J Cell Sci *125*, 4693–4702.

Semerdjieva, S., Shortt, B., Maxwell, E., Singh, S., Fonarev, P., Hansen, J., Schiavo, G., Grant, B.D., and Smythe, E. (2008). Coordinated regulation of AP2 uncoating from clathrin-coated vesicles by rab5 and hRME-6. J Cell Biol *183*, 499–511.

Seto, S., Tsujimura, K., and Koide, Y. (2011). Rab GTPases regulating phagosome maturation are differentially recruited to mycobacterial phagosomes. Traffic *12*, 407–420.

Sharma, S., Quintana, A., Findlay, G.M., Mettlen, M., Baust, B., Jain, M., Nilsson, R., Rao, A., and Hogan, P.G. (2013). An siRNA screen for NFAT activation identifies septins as coordinators of store-operated Ca2+ entry. Nature *499*, 238–242.

Shevchuk, O., Batzilla, C., Hägele, S., Kusch, H., Engelmann, S., Hecker, M., Haas, A., Heuner, K., Glöckner, G., and Steinert, M. (2009). Proteomic analysis of Legionella-containing phagosomes isolated from Dictyostelium. Int. J. Med. Microbiol. *299*, 489–508.

Simeone, R., Bobard, A., Lippmann, J., Bitter, W., Majlessi, L., Brosch, R., and Enninga, J. (2012). Phagosomal rupture by Mycobacterium tuberculosis results in toxicity and host cell death. PLoS Pathog *8*, e1002507.

Singh, R., Jamieson, A., and Cresswell, P. (2008). GILT is a critical host factor for Listeria monocytogenes infection. Nature *455*, 1244–1247.

Sirajuddin, M., Farkasovsky, M., Hauer, F., Kühlmann, D., Macara, I.G., Weyand, M., Stark, H., and Wittinghofer, A. (2007). Structural insight into filament formation by mammalian septins. Nature *449*, 311–315.

Sirajuddin, M., Farkasovsky, M., Zent, E., and Wittinghofer, A. (2009). GTP-induced conformational changes in septins and implications for function. Proc Natl Acad Sci USA *106*, 16592–16597.

Sit, S.-T., and Manser, E. (2011). Rho GTPases and their role in organizing the actin cytoskeleton. J Cell Sci *124*, 679–683.

Sivars, U., Aivazian, D., and Pfeffer, S.R. (2003). Yip3 catalyses the dissociation of endosomal Rab-GDI complexes. Nature *425*, 856–859.

Skoudy, A., Mounier, J., Aruffo, A., Ohayon, H., Gounon, P., Sansonetti, P., and Tran Van Nhieu, G. (2000). CD44 binds to the Shigella IpaB protein and participates in bacterial invasion of epithelial cells. Cell Microbiol *2*, 19–33.

Smith, G.A., Marquis, H., Jones, S., Johnston, N.C., Portnoy, D.A., and Goldfine, H. (1995). The two distinct phospholipases C of Listeria monocytogenes have overlapping roles in escape from a vacuole and cell-to-cell spread. Infect Immun *63*, 4231–4237.

Soppina, V., Rai, A.K., Ramaiya, A.J., Barak, P., and Mallik, R. (2009). Tug-of-war between dissimilar teams of microtubule motors regulates transport and fission of endosomes. Proc Natl Acad Sci USA *106*, 19381–19386.

Spiliotis, E.T. (2010). Regulation of microtubule organization and functions by septin GTPases. Cytoskeleton (Hoboken) *67*, 339–345.

Spiliotis, E.T., Hunt, S.J., Hu, Q., Kinoshita, M., and Nelson, W.J. (2008). Epithelial polarity requires septin coupling of vesicle transport to polyglutamylated microtubules. J Cell Biol *180*, 295–303.

Srikanth, C.V., Mercado-Lubo, R., Hallstrom, K., and McCormick, B.A. (2011). Salmonella effector proteins and host-cell responses. Cellular and Molecular Life Sciences : CMLS.

Stachowiak, J.C., Brodsky, F.M., and Miller, E.A. (2013). A cost-benefit analysis of the physical mechanisms of membrane curvature. Nat Cell Biol *15*, 1019–1027.

Stachowiak, J.C., Schmid, E.M., Ryan, C.J., Ann, H.S., Sasaki, D.Y., Sherman, M.B., Geissler, P.L., Fletcher, D.A., and Hayden, C.C. (2012). Membrane bending by protein-protein crowding. Nat Cell Biol *14*, 944–949.

Steele-Mortimer, O., Méresse, S., Gorvel, J.P., Toh, B.H., and Finlay, B.B. (1999). Biogenesis of Salmonella typhimurium-containing vacuoles in epithelial cells involves interactions with the early endocytic pathway. Cell Microbiol *1*, 33–49.

Steele-Mortimer, O. (2008). The Salmonella-containing vacuole: moving with the times. Curr Opin Microbiol *11*, 38–45.

Stefan, C.J., Manford, A.G., and Emr, S.D. (2013). ER-PM connections: sites of information transfer and inter-organelle communication. Curr Opin Cell Biol *25*, 434–442.

Stender, S., Friebel, A., Linder, S., Rohde, M., Mirold, S., and Hardt, W.D. (2000). Identification of SopE2 from Salmonella typhimurium, a conserved guanine nucleotide exchange factor for Cdc42 of the host cell. Mol Microbiol *36*, 1206–1221.

Stenmark, H., Parton, R.G., Steele-Mortimer, O., Lütcke, A., Gruenberg, J., and Zerial, M. (1994). Inhibition of rab5 GTPase activity stimulates membrane fusion in endocytosis. Embo J *13*, 1287–1296.

Stenmark, H. (2009). Rab GTPases as coordinators of vesicle traffic. Nat Rev Mol Cell Biol *10*, 513–525.

Stevens, J.M., Galyov, E.E., and Stevens, M.P. (2006). Actin-dependent movement of bacterial pathogens. Nat Rev Microbiol *4*, 91–101.

Stockinger, W., Zhang, S.C., Trivedi, V., Jarzylo, L.A., Shieh, E.C., Lane, W.S., Castoreno, AB, and Nohturfft, A. (2006). Differential requirements for actin polymerization, calmodulin, and Ca2+ define distinct stages of lysosome/phagosome targeting. Mol Biol Cell *17*, 1697–1710.

Stuart, L.M., Boulais, J., Charriere, G.M., Hennessy, E.J., Brunet, S., Jutras, I., Goyette, G., Rondeau, C., Letarte, S., Huang, H., et al. (2007). A systems biology analysis of the Drosophila phagosome. Nature *445*, 95–101.

Swaminathan, B., and Gerner-Smidt, P. (2007). The epidemiology of human listeriosis. Microbes Infect *9*, 1236–1243.

Swanson, J.A. (2008). Shaping cups into phagosomes and macropinosomes. Nat Rev Mol Cell Biol *9*, 639–649.

Szul, T., and Sztul, E. (2011). COPII and COPI traffic at the ER-Golgi interface. Physiology (Bethesda) *26*, 348–364.

Takenawa, T., and Suetsugu, S. (2007). The WASP-WAVE protein network: connecting the membrane to the cytoskeleton. Nat Rev Mol Cell Biol *8*, 37–48.

Taylor, S.W., Fahy, E., and Ghosh, S.S. (2003a). Global organellar proteomics. Trends Biotechnol *21*, 82–88.

Taylor, S.W., Fahy, E., Zhang, B., Glenn, G.M., Warnock, D.E., Wiley, S., Murphy, A.N., Gaucher, S.P., Capaldi, R.A., Gibson, B.W., et al. (2003b). Characterization of the human heart mitochondrial proteome. Nat Biotechnol *21*, 281–286.

Taylor, S.W., Warnock, D.E., Glenn, G.M., Zhang, B., Fahy, E., Gaucher, S.P., Capaldi, R.A., Gibson, B.W., and Ghosh, S.S. (2002). An alternative strategy to determine the mitochondrial proteome using sucrose gradient fractionation and 1D PAGE on highly purified human heart mitochondria. J. Proteome Res. *1*, 451–458.

Thurston, T.L.M., Wandel, M.P., Muhlinen, von, N., Foeglein, A., and Randow, F. (2012). Galectin 8 targets damaged vesicles for autophagy to defend cells against bacterial invasion. Nature *482*, 414–418.

Tomasevic, N., Jia, Z., Russell, A., Fujii, T., Hartman, J.J., Clancy, S., Wang, M., Beraud, C., Wood, K.W., and Sakowicz, R. (2007). Differential regulation of WASP and N-WASP by Cdc42, Rac1, Nck, and PI(4,5)P2. Biochemistry *46*, 3494–3502.

Toulmay, A., and Prinz, W.A. (2011). Lipid transfer and signaling at organelle contact sites: the tip of the iceberg. Curr Opin Cell Biol *23*, 458–463.

Touret, N., Paroutis, P., Terebiznik, M., Harrison, R.E., Trombetta, S., Pypaert, M., Chow, A., Jiang, A., Shaw, J., Yip, C., et al. (2005). Quantitative and dynamic assessment of the contribution of the ER to phagosome formation. Cell *123*, 157–170.

Trost, M., English, L., Lemieux, S., Courcelles, M., Desjardins, M., and Thibault, P. (2009). The phagosomal proteome in interferon-gamma-activated macrophages. Immunity *30*, 143–154.

Tsujita, K., Suetsugu, S., Sasaki, N., Furutani, M., Oikawa, T., and Takenawa, T. (2006). Coordination between the actin cytoskeleton and membrane deformation by a novel membrane tubulation domain of PCH proteins is involved in endocytosis. J Cell Biol *172*, 269–279.

Urwyler, S., Nyfeler, Y., Ragaz, C., Lee, H., Mueller, L.N., Aebersold, R., and Hilbi, H. (2009). Proteome analysis of Legionella vacuoles purified by magnetic immunoseparation reveals secretory and endosomal GTPases. Traffic *10*, 76–87.

van der Heijden, J., and Finlay, B.B. (2012). Type III effector-mediated processes in Salmonella infection. Future Microbiol *7*, 685–703.

Vorwerk, S., Krieger, V., Deiwick, J., Hensel, M., and Hansmeier, N. (2015). Proteomes of host cell membranes modified by intracellular activities of Salmonella enterica. Mol Cell Proteomics *14*, 81–92.

Walther, T.C., and Mann, M. (2010). Mass spectrometry-based proteomics in cell biology. J Cell Biol *190*, 491–500.

Wang, Y., Botvinick, E.L., Zhao, Y., Berns, M.W., Usami, S., Tsien, R.Y., and Chien, S. (2005). Visualizing the mechanical activation of Src. Nature *434*, 1040–1045.

Wasiak, S., Legendre-Guillemin, V., Puertollano, R., Blondeau, F., Girard, M., de Heuvel, E., Boismenu, D., Bell, A.W., Bonifacino, J.S., and McPherson, P.S. (2002). Enthoprotin: a novel clathrin-associated protein identified through subcellular proteomics. J Cell Biol *158*, 855–862.

Wasylnka, J.A., Bakowski, M.A., Szeto, J., Ohlson, M.B., Trimble, W.S., Miller, S.I., and Brumell, J.H. (2008). Role for myosin II in regulating positioning of Salmonella-containing vacuoles and intracellular replication. Infect Immun *76*, 2722–2735.

Weber, T., Zemelman, BV, McNew, J.A., Westermann, B., Gmachl, M., Parlati, F., Sollner, T.H., and Rothman, J.E. (1998). SNAREpins: Minimal machinery for membrane fusion. Cell *92*, 759–772.

Wennerberg, K., Rossman, K.L., and Der, C.J. (2005). The Ras superfamily at a glance. J Cell Sci *118*, 843–846.

Wittinghofer, A., Scheffzek, K., and Ahmadian, M.R. (1997). The interaction of Ras with GTPase-activating proteins. FEBS Lett. *410*, 63–67.

Wollert, T., and Hurley, J.H. (2010). Molecular mechanism of multivesicular body biogenesis by ESCRT complexes. Nature *464*, 864–869.

Wu, C.C., Yates, J.R., Neville, M.C., and Howell, K.E. (2000). Proteomic analysis of two functional states of the Golgi complex in mammary epithelial cells. Traffic *1*, 769–782.

Wu, C.C., and Yates, J.R. (2003). The application of mass spectrometry to membrane proteomics. Nat Biotechnol *21*, 262–267.

Xie, G.-X., and Palmer, P.P. (2007). How regulators of G protein signaling achieve selective regulation. J. Mol. Biol. *366*, 349–365.

Xu, L., Shen, X., Bryan, A., Banga, S., Swanson, M.S., and Luo, Z.-Q. (2010). Inhibition of host vacuolar H+-ATPase activity by a Legionella pneumophila effector. PLoS Pathog *6*, e1000822.

Yates, J.R., Gilchrist, A., Howell, K.E., and Bergeron, J.J.M. (2005). Proteomics of organelles and large cellular structures. Nat Rev Mol Cell Biol *6*, 702–714.

Yoshida, S., Hoppe, A.D., Araki, N., and Swanson, J.A. (2009). Sequential signaling in plasma-membrane domains during macropinosome formation in macrophages. J Cell Sci *122*, 3250–3261.

Yoshida, S., Katayama, E., Kuwae, A., Mimuro, H., Suzuki, T., and Sasakawa, C. (2002). Shigella deliver an effector protein to trigger host microtubule destabilization, which promotes Rac1 activity and efficient bacterial internalization. Embo J *21*, 2923–2935.

Zerial, M., and McBride, H. (2001). Rab proteins as membrane organizers. Nat Rev Mol Cell Biol *2*, 107–117.

Zhang, M., Chen, L., Wang, S., and Wang, T. (2009). Rab7: roles in membrane trafficking and disease. Biosci. Rep. *29*, 193–209.

Zhou, D., Mooseker, M.S., and Galán, J.E. (1999a). An invasion-associated Salmonella protein modulates the actin-bundling activity of plastin. Proc Natl Acad Sci USA *96*, 10176–10181.

Zhou, D., Mooseker, M.S., and Galán, J.E. (1999b). Role of the S. typhimurium actin-binding protein SipA in bacterial internalization. Science *283*, 2092–2095.

Zurek, N., Sparks, L., and Voeltz, G. (2011). Reticulon short hairpin transmembrane domains are used to shape ER tubules. Traffic *12*, 28–41.

ANNEXES

A. Annexes

Manuscript 2: ***Table S3*** – Complete list of host proteins enriched in the SCV, at 30 min, 3 h or at both time-points

B. Electronic Annexes on CD

Manuscript 1 – ***Movies S1-S8***

Manuscript 2 – ***Movies S1-S6***

Manuscript 2: ***Table S1 –*** Relative protein abundances at the 30 min SCV comparing to the non-infected control, for the complete list of host proteins identified by proteomics

Manuscript 2: ***Table S2 –*** Relative protein abundances at the 3 h SCV comparing to the non-infected control, for the complete list of host proteins identified by proteomics

Complete thesis manuscript

Complete list of host proteins enriched in the SCV, at 30 min, 3 h or at both time-points.

Proteins enriched only at the 30 min SCV			
Entry	**Entry name**	**Protein names**	**Subcellular location**
P31946	1433B_HUMAN	14-3-3 protein beta/alpha (Protein 1054) (Protein kinase C inhibitor protein 1) (KCIP-1) [Cleaved into: 14-3-3 protein beta/alpha, N-terminally processed]	Cytoplasm. Melanosome.
P62333	PRS10_HUMAN	26S protease regulatory subunit 10B (26S proteasome AAA-ATPase subunit RPT4) (Proteasome 26S subunit ATPase 6) (Proteasome subunit p42)	Cytoplasm. Nucleus.
P23396	RS3_HUMAN	40S ribosomal protein S3	Cytoplasm.
P46782	RS5_HUMAN	40S ribosomal protein S5 [Cleaved into: 40S ribosomal protein S5, N-terminally processed]	
P62081	RS7_HUMAN	40S ribosomal protein S7	Cytoplasm – cytoskeleton – microtubule organizing center – centrosome.
P08865	RSSA_HUMAN	40S ribosomal protein SA (37 kDa laminin receptor precursor) (37LRP) (37/67 kDa laminin receptor) (LRP/LR) (67 kDa laminin receptor) (67LR) (Colon carcinoma laminin-binding protein) (Laminin receptor 1) (LamR) (Laminin-binding protein precursor p40) (LBP/p40) (Multidrug resistance-associated protein MGr1-Ag) (NEM/1CHD4)	Cell membrane. Cytoplasm. Nucleus.
Q96IR7	HPDL_HUMAN	4-hydroxyphenylpyruvate dioxygenase-like protein (EC 1.13.-.-) (Glyoxalase domain-containing protein 1)	
P05387	RLA2_HUMAN	60S acidic ribosomal protein P2 (Renal carcinoma antigen NY-REN-44)	
P26373	RL13_HUMAN	60S ribosomal protein L13 (Breast basic conserved protein 1)	
P40429	RL13A_HUMAN	60S ribosomal protein L13a (23 kDa highly basic protein)	Cytoplasm.
Q02543	RL18A_HUMAN	60S ribosomal protein L18a	
P83731	RL24_HUMAN	60S ribosomal protein L24 (60S ribosomal protein L30)	
Q02878	RL6_HUMAN	60S ribosomal protein L6 (Neoplasm-related protein C140) (Tax-responsive enhancer element-binding protein 107) (TaxREB107)	
P18124	RL7_HUMAN	60S ribosomal protein L7	
P62736	ACTA_HUMAN	Actin, aortic smooth muscle (Alpha-actin-2) (Cell growth-inhibiting gene 46 protein)	Cytoplasm – cytoskeleton.
P61160	ARP2_HUMAN	Actin-related protein 2 (Actin-like protein 2)	Cytoplasm – cytoskeleton. Cell projection.
P00568	KAD1_HUMAN	Adenylate kinase isoenzyme 1 (AK 1) (EC 2.7.4.3) (EC 2.7.4.6) (ATP-AMP transphosphorylase 1) (ATP:AMP phosphotransferase) (Adenylate monophosphate kinase) (Myokinase)	Cytoplasm.
Q9Y679	AUP1_HUMAN	Ancient ubiquitous protein 1	Endoplasmic reticulum membrane; Single-pass type III membrane protein; Cytoplasmic side.
P07355	ANXA2_HUMAN	Annexin A2 (Annexin II) (Annexin-2) (Calpactin I heavy chain) (Calpactin-1 heavy chain) (Chromobindin-8) (Lipocortin II) (Placental anticoagulant protein IV) (PAP-IV) (Protein I) (p36)	Secreted – extracellular space – extracellular matrix – basement membrane. Melanosome.
P25705	ATPA_HUMAN	ATP synthase subunit alpha, mitochondrial	Mitochondrion inner membrane. Cell membrane; Peripheral membrane protein; Extracellular side.
Q08211	DHX9_HUMAN	ATP-dependent RNA helicase A (RHA) (EC 3.6.4.13) (DEAH box protein 9) (Leukophysin) (LKP) (Nuclear DNA helicase II) (NDH II)	Nucleus – nucleolus. Cytoplasm.
Q9Y6D5	BIG2_HUMAN	Brefeldin A-inhibited guanine nucleotide-exchange protein 2 (Brefeldin A-inhibited GEP 2) (ADP-ribosylation factor guanine nucleotide-exchange factor 2)	Cytoplasm. Membrane. Golgi apparatus. Cytoplasm – perinuclear region. Golgi apparatus – trans-Golgi network. Endosome. Cytoplasm – cytoskeleton – microtubule organizing center – centrosome. Cell projection – dendrite. Cytoplasmic vesicle. Cell junction – synapse. Cytoplasm – cytoskeleton.
Q08AD1	CAMP2_HUMAN	Calmodulin-regulated spectrin-associated protein 2 (Calmodulin-regulated spectrin-associated protein 1-like protein 1)	Cytoplasm – cytoskeleton.
O43852	CALU_HUMAN	Calumenin (Crocalbin) (IEF SSP 9302)	Endoplasmic reticulum lumen. Secreted. Melanosome. Sarcoplasmic reticulum lumen.
P31327	CPSM_HUMAN	Carbamoyl-phosphate synthase [ammonia], mitochondrial (EC 6.3.4.16) (Carbamoyl-phosphate synthetase I) (CPSase I)	Mitochondrion. Nucleus – nucleolus.
P07858	CATB_HUMAN	Cathepsin B (EC 3.4.22.1) (APP secretase) (APPS) (Cathepsin B1) [Cleaved into: Cathepsin B light chain; Cathepsin B heavy chain]	Lysosome. Melanosome. Secreted – extracellular space.
Q9UBR2	CATZ_HUMAN	Cathepsin Z (EC 3.4.18.1) (Cathepsin P) (Cathepsin X)	Lysosome.
P11717	MPRI_HUMAN	Cation-independent mannose-6-phosphate receptor (CI Man-6-P receptor) (CI-MPR) (M6PR) (300 kDa mannose 6-phosphate receptor) (MPR 300) (Insulin-like growth factor 2 receptor) (Insulin-like growth factor II receptor) (IGF-II receptor) (M6P/IGF2 receptor) (M6P/IGF2R) (CD antigen CD222)	Lysosome membrane; Single-pass type I membrane protein.
Q00610	CLH1_HUMAN	Clathrin heavy chain 1 (Clathrin heavy chain on chromosome 17) (CLH-17)	Cytoplasmic vesicle membrane; Peripheral membrane protein; Cytoplasmic side. Membrane – coated pit; Peripheral membrane protein; Cytoplasmic side. Melanosome.
P10909	CLUS_HUMAN	Clusterin (Aging-associated gene 4 protein) (Apolipoprotein J) (Apo-J) (Complement cytolysis inhibitor) (CLI) (Complement-associated protein SP-40,40) (Ku70-binding protein 1) (NA1/NA2) (Testosterone-repressed prostate message 2) (TRPM-2) [Cleaved into: Clusterin beta chain (ApoJalpha) (Complement cytolysis inhibitor a chain); Clusterin alpha chain (ApoJbeta) (Complement cytolysis inhibitor b chain)]	Secreted. Nucleus. Cytoplasm. Mitochondrion membrane; Peripheral membrane protein; Cytoplasmic side. Cytoplasm – cytosol. Microsome. Endoplasmic reticulum. Cytoplasmic vesicle – secretory vesicle – chromaffin granule.
Q15021	CND1_HUMAN	Condensin complex subunit 1 (Chromosome condensation-related SMC-associated protein 1) (Chromosome-associated protein D2) (hCAP-D2) (Non-SMC condensin I complex subunit D2) (XCAP-D2 homolog)	Nucleus. Cytoplasm. Chromosome.
P12277	KCRB_HUMAN	Creatine kinase B-type (EC 2.7.3.2) (B-CK) (Creatine kinase B chain)	Cytoplasm.
Q86VP6	CAND1_HUMAN	Cullin-associated NEDD8-dissociated protein 1 (Cullin-associated and neddylation-dissociated protein 1) (TBP-interacting protein of 120 kDa A) (TBP-interacting protein 120A) (p120 CAND1)	Cytoplasm. Nucleus.

P06493	CDK1_HUMAN	Cyclin-dependent kinase 1 (CDK1) (EC 2.7.11.22) (EC 2.7.11.23) (Cell division control protein 2 homolog) (Cell division protein kinase 1) (p34 protein kinase)	Nucleus. Cytoplasm. Mitochondrion. Cytoplasm – cytoskeleton – microtubule organizing center – centrosome.
P24941	CDK2_HUMAN	Cyclin-dependent kinase 2 (EC 2.7.11.22) (Cell division protein kinase 2) (p33 protein kinase)	Cytoplasm – cytoskeleton – microtubule organizing center – centrosome. Nucleus – Cajal body. Cytoplasm. Endosome.
P21291	CSRP1_HUMAN	Cysteine and glycine-rich protein 1 (Cysteine-rich protein 1) (CRP) (CRP1) (Epididymis luminal protein 141) (HEL-141)	Nucleus.
Q14204	DYHC1_HUMAN	Cytoplasmic dynein 1 heavy chain 1 (Cytoplasmic dynein heavy chain 1) (Dynein heavy chain, cytosolic)	Cytoplasm – cytoskeleton.
Q7L576	CYFP1_HUMAN	Cytoplasmic FMR1-interacting protein 1 (Specifically Rac1-associated protein 1) (Sra-1) (p140sra-1)	Cytoplasm – perinuclear region. Cell projection – lamellipodium. Cell projection – ruffle. Cell junction – synapse – synaptosome.
Q96F07	CYFP2_HUMAN	Cytoplasmic FMR1-interacting protein 2 (p53-inducible protein 121)	Cytoplasm. Cytoplasm – perinuclear region. Cell junction – synapse – synaptosome.
Q07065	CKAP4_HUMAN	Cytoskeleton-associated protein 4 (63-kDa cytoskeleton-linking membrane protein) (Climp-63) (p63)	Endoplasmic reticulum membrane; Single-pass type II membrane protein. Cell membrane; Single-pass type II membrane protein. Cytoplasm – cytoskeleton. Cytoplasm – perinuclear region.
Q14008	CKAP5_HUMAN	Cytoskeleton-associated protein 5 (Colonic and hepatic tumor overexpressed gene protein) (Ch-TOG)	Cytoplasm – cytoskeleton – microtubule organizing center – centrosome. Cytoplasm – cytoskeleton – spindle pole.
Q96HY6	DDRGK_HUMAN	DDRGK domain-containing protein 1	Endoplasmic reticulum.
Q14126	DSG2_HUMAN	Desmoglein-2 (Cadherin family member 5) (HDGC)	Cell membrane; Single-pass type I membrane protein. Cell junction – desmosome.
Q9UHL4	DPP2_HUMAN	Dipeptidyl peptidase 2 (EC 3.4.14.2) (Dipeptidyl aminopeptidase II) (Dipeptidyl peptidase 7) (Dipeptidyl peptidase II) (DPP II) (Quiescent cell proline dipeptidase)	Lysosome. Cytoplasmic vesicle. Secreted.
P78527	PRKDC_HUMAN	DNA-dependent protein kinase catalytic subunit (DNA-PK catalytic subunit) (DNA-PKcs) (EC 2.7.11.1) (DNPK1) (p460)	Nucleus. Nucleus – nucleolus.
P25685	DNJB1_HUMAN	DnaJ homolog subfamily B member 1 (DnaJ protein homolog 1) (Heat shock 40 kDa protein 1) (HSP40) (Heat shock protein 40) (Human DnaJ protein 1) (hDj-1)	Cytoplasm. Nucleus. Nucleus – nucleolus.
Q9UBS4	DJB11_HUMAN	DnaJ homolog subfamily B member 11 (APOBEC1-binding protein 2) (ABBP-2) (DnaJ protein homolog 9) (ER-associated DNAJ) (ER-associated Hsp40 co-chaperone) (Endoplasmic reticulum DNA J domain-containing protein 3) (ER-resident protein ERdj3) (ERdj3) (ERj3p) (HEDJ) (Human DnaJ protein 9) (hDj-9) (PWP1-interacting protein 4)	Endoplasmic reticulum lumen.
Q9UDY4	DNJB4_HUMAN	DnaJ homolog subfamily B member 4 (Heat shock 40 kDa protein 1 homolog) (HSP40 homolog) (Heat shock protein 40 homolog) (Human liver DnaJ-like protein)	Cytoplasm. Cell membrane.
O75165	DJC13_HUMAN	DnaJ homolog subfamily C member 13 (Required for receptor-mediated endocytosis 8) (RME-8)	
P04843	RPN1_HUMAN	Dolichyl-diphosphooligosaccharide--protein glycosyltransferase subunit 1 (EC 2.4.99.18) (Dolichyl-diphosphooligosaccharide--protein glycosyltransferase 67 kDa subunit) (Ribophorin I) (RPN-I) (Ribophorin-1)	Endoplasmic reticulum membrane; Single-pass type I membrane protein. Melanosome.
P46977	STT3A_HUMAN	Dolichyl-diphosphooligosaccharide--protein glycosyltransferase subunit STT3A (Oligosaccharyl transferase subunit STT3A) (STT3-A) (EC 2.4.99.18) (B5) (Integral membrane protein 1) (Transmembrane protein TMC)	Endoplasmic reticulum membrane; Multi-pass membrane protein.
Q03001	DYST_HUMAN	Dystonin (230 kDa bullous pemphigoid antigen) (230/240 kDa bullous pemphigoid antigen) (Bullous pemphigoid antigen 1) (BPA) (Bullous pemphigoid antigen) (Dystonia musculorum protein) (Hemidesmosomal plaque protein)	Cytoplasm – cytoskeleton. Cytoplasm – cytoskeleton. Cytoplasm – myofibril – sarcomere – Z line. Cytoplasm – myofibril – sarcomere – H zone. Cytoplasm – cytoskeleton. Cell junction – hemidesmosome. Nucleus. Nucleus envelope. Membrane; Single-pass membrane protein. Endoplasmic reticulum membrane; Single-pass membrane protein. Cytoplasm – cytoskeleton. Membrane; Single-pass membrane protein. Cytoplasm – cytoskeleton. Cell projection – axon. Membrane. Cytoplasm – cytoskeleton. Cytoplasm – cell cortex. Cell membrane; Lipid-anchor.
P30040	ERP29_HUMAN	Endoplasmic reticulum resident protein 29 (ERp29) (Endoplasmic reticulum resident protein 28) (ERp28) (Endoplasmic reticulum resident protein 31) (ERp31)	Endoplasmic reticulum lumen. Melanosome.
P00533	EGFR_HUMAN	Epidermal growth factor receptor (EC 2.7.10.1) (Proto-oncogene c-ErbB-1) (Receptor tyrosine-protein kinase erbB-1)	Cell membrane; Single-pass type I membrane protein. Endoplasmic reticulum membrane; Single-pass type I membrane protein. Golgi apparatus membrane; Single-pass type I membrane protein. Nucleus membrane; Single-pass type I membrane protein. Endosome. Endosome membrane. Nucleus. Secreted.
Q9P0I2	EMC3_HUMAN	ER membrane protein complex subunit 3 (Transmembrane protein 111)	Membrane; Multi-pass membrane protein.
Q04637	IF4G1_HUMAN	Eukaryotic translation initiation factor 4 gamma 1 (eIF-4-gamma 1) (eIF-4G 1) (eIF-4G1) (p220)	
P47756	CAPZB_HUMAN	F-actin-capping protein subunit beta (CapZ beta)	Cytoplasm – cytoskeleton. Cytoplasm – myofibril – sarcomere.

Q96CS3	FAF2_HUMAN	FAS-associated factor 2 (Protein ETEA) (UBX domain-containing protein 3B) (UBX domain-containing protein 8)	Cytoplasm. Lipid droplet. Endoplasmic reticulum.
P49327	FAS_HUMAN	Fatty acid synthase (EC 2.3.1.85) [Includes: [Acyl-carrier-protein] S-acetyltransferase (EC 2.3.1.38); [Acyl-carrier-protein] S-malonyltransferase (EC 2.3.1.39); 3-oxoacyl-[acyl-carrier-protein] synthase (EC 2.3.1.41); 3-oxoacyl-[acyl-carrier-protein] reductase (EC 1.1.1.100); 3-hydroxyacyl-[acyl-carrier-protein] dehydratase (EC 4.2.1.59); Enoyl-[acyl-carrier-protein] reductase (EC 1.3.1.39); Oleoyl-[acyl-carrier-protein] hydrolase (EC 3.1.2.14)]	Cytoplasm. Melanosome.
P04075	ALDOA_HUMAN	Fructose-bisphosphate aldolase A (EC 4.1.2.13) (Lung cancer antigen NY-LU-1) (Muscle-type aldolase)	Cytoplasm – myofibril – sarcomere – I band. Cytoplasm – myofibril – sarcomere – M line.
P17931	LEG3_HUMAN	Galectin-3 (Gal-3) (35 kDa lectin) (Carbohydrate-binding protein 35) (CBP 35) (Galactose-specific lectin 3) (Galactoside-binding protein) (GALBP) (IgE-binding protein) (L-31) (Laminin-binding protein) (Lectin L-29) (Mac-2 antigen)	Cytoplasm. Nucleus. Secreted.
Q9Y2Q3	GSTK1_HUMAN	Glutathione S-transferase kappa 1 (EC 2.5.1.18) (GST 13-13) (GST class-kappa) (GSTK1-1) (hGSTK1) (Glutathione S-transferase subunit 13)	Peroxisome.
P04406	G3P_HUMAN	Glyceraldehyde-3-phosphate dehydrogenase (GAPDH) (EC 1.2.1.12) (Peptidyl-cysteine S-nitrosylase GAPDH) (EC 2.6.99.-)	Cytoplasm – cytosol. Nucleus. Cytoplasm – perinuclear region. Membrane. Cytoplasm – cytoskeleton.
O00461	GOLI4_HUMAN	Golgi integral membrane protein 4 (Golgi integral membrane protein, cis) (GIMPc) (Golgi phosphoprotein 4) (Golgi-localized phosphoprotein of 130 kDa) (Golgi phosphoprotein of 130 kDa)	Golgi apparatus – Golgi stack membrane; Single-pass type II membrane protein. Endosome membrane; Single-pass type II membrane protein.
Q08379	GOGA2_HUMAN	Golgin subfamily A member 2 (130 kDa cis-Golgi matrix protein) (GM130) (GM130 autoantigen) (Golgin-95)	Golgi apparatus – Golgi stack membrane; Peripheral membrane protein.
Q14789	GOGB1_HUMAN	Golgin subfamily B member 1 (372 kDa Golgi complex-associated protein) (GCP372) (Giantin) (Macrogolgin)	Golgi apparatus membrane; Single-pass type I membrane protein.
P04899	GNAI2_HUMAN	Guanine nucleotide-binding protein G(i) subunit alpha-2 (Adenylate cyclase-inhibiting G alpha protein)	Cytoplasm. Cytoplasm – cytoskeleton – microtubule organizing center – centrosome. Cell membrane.
P62873	GBB1_HUMAN	Guanine nucleotide-binding protein G(I)/G(S)/G(T) subunit beta-1 (Transducin beta chain 1)	
P62879	GBB2_HUMAN	Guanine nucleotide-binding protein G(I)/G(S)/G(T) subunit beta-2 (G protein subunit beta-2) (Transducin beta chain 2)	Cytoplasm – perinuclear region.
P29992	GNA11_HUMAN	Guanine nucleotide-binding protein subunit alpha-11 (G alpha-11) (G-protein subunit alpha-11) (Guanine nucleotide-binding protein G(y) subunit alpha)	Cell membrane; Lipid-anchor. Cytoplasm.
P09601	HMOX1_HUMAN	Heme oxygenase 1 (HO-1) (EC 1.14.99.3)	Microsome. Endoplasmic reticulum membrane; Peripheral membrane protein; Cytoplasmic side.
Q99729	ROAA_HUMAN	Heterogeneous nuclear ribonucleoprotein A/B (hnRNP A/B) (APOBEC1-binding protein 1) (ABBP-1)	Nucleus. Cytoplasm.
P61978	HNRPK_HUMAN	Heterogeneous nuclear ribonucleoprotein K (hnRNP K) (Transformation up-regulated nuclear protein) (TUNP)	Cytoplasm. Nucleus – nucleoplasm. Cell projection – podosome.
Q9Y4L1	HYOU1_HUMAN	Hypoxia up-regulated protein 1 (150 kDa oxygen-regulated protein) (ORP-150) (170 kDa glucose-regulated protein) (GRP-170)	Endoplasmic reticulum lumen.
O95373	IPO7_HUMAN	Importin-7 (Imp7) (Ran-binding protein 7) (RanBP7)	Cytoplasm. Nucleus.
Q70UQ0	IKIP_HUMAN	Inhibitor of nuclear factor kappa-B kinase-interacting protein (I kappa-B kinase-interacting protein) (IKBKB-interacting protein) (IKK-interacting protein)	Endoplasmic reticulum membrane; Single-pass membrane protein.
P12268	IMDH2_HUMAN	Inosine-5'-monophosphate dehydrogenase 2 (IMP dehydrogenase 2) (IMPD 2) (IMPDH 2) (EC 1.1.1.205) (IMPDH-II)	Cytoplasm. Nucleus.
P19525	E2AK2_HUMAN	Interferon-induced, double-stranded RNA-activated protein kinase (EC 2.7.11.1) (Eukaryotic translation initiation factor 2-alpha kinase 2) (eIF-2A protein kinase 2) (Interferon-inducible RNA-dependent protein kinase) (P1/eIF-2A protein kinase) (Protein kinase RNA-activated) (PKR) (Tyrosine-protein kinase EIF2AK2) (EC 2.7.10.2) (p68 kinase)	Cytoplasm. Nucleus. Cytoplasm – perinuclear region.
O75569	PRKRA_HUMAN	Interferon-inducible double-stranded RNA-dependent protein kinase activator A (PKR-associated protein X) (PKR-associating protein X) (Protein activator of the interferon-induced protein kinase) (Protein kinase, interferon-inducible double-stranded RNA-dependent activator)	Cytoplasm – perinuclear region. Cytoplasm.
P41252	SYIC_HUMAN	Isoleucine--tRNA ligase, cytoplasmic (EC 6.1.1.5) (Isoleucyl-tRNA synthetase) (IRS) (IleRS)	Cytoplasm.
Q86UP2	KTN1_HUMAN	Kinectin (CG-1 antigen) (Kinesin receptor)	Endoplasmic reticulum membrane; Single-pass type II membrane protein.
P42704	LPPRC_HUMAN	Leucine-rich PPR motif-containing protein, mitochondrial (130 kDa leucine-rich protein) (LRP 130) (GP130)	Mitochondrion. Nucleus – nucleoplasm. Nucleus inner membrane. Nucleus outer membrane.
Q9UIQ6	LCAP_HUMAN	Leucyl-cystinyl aminopeptidase (Cystinyl aminopeptidase) (EC 3.4.11.3) (Insulin-regulated membrane aminopeptidase) (Insulin-responsive aminopeptidase) (IRAP) (Oxytocinase) (OTase) (Placental leucine aminopeptidase) (P-LAP) [Cleaved into: Leucyl-cystinyl aminopeptidase, pregnancy serum form]	Cell membrane; Single-pass type II membrane protein. Secreted.
P11117	PPAL_HUMAN	Lysosomal acid phosphatase (LAP) (EC 3.1.3.2)	Lysosome membrane; Single-pass membrane protein; Lumenal side. Lysosome lumen.
Q9UPN3	MACF1_HUMAN	Microtubule-actin cross-linking factor 1, isoforms 1/2/3/5 (620 kDa actin-binding protein) (ABP620) (Actin cross-linking family protein 7) (Macrophin-1) (Trabeculin-alpha)	Cytoplasm – cytoskeleton. Cytoplasm. Golgi apparatus. Cell membrane. Cell projection – ruffle membrane. Cytoplasm. Golgi apparatus.
P46821	MAP1B_HUMAN	Microtubule-associated protein 1B (MAP-1B) [Cleaved into: MAP1B heavy chain; MAP1 light chain LC1]	Cytoplasm – cytoskeleton. Cytoplasm. Cell junction – synapse. Cell projection – dendritic spine.
Q9Y6C9	MTCH2_HUMAN	Mitochondrial carrier homolog 2 (Met-induced mitochondrial protein)	Mitochondrion inner membrane; Multi-pass membrane protein.
O43684	BUB3_HUMAN	Mitotic checkpoint protein BUB3	Nucleus. Chromosome – centromere – kinetochore.
Q9Y3A3	PHOCN_HUMAN	MOB-like protein phocein (2C4D) (Class II mMOB1) (Mob1 homolog 3) (Mob3) (Mps one binder kinase activator-like 3) (Preimplantation protein 3)	Cytoplasm – perinuclear region. Membrane; Peripheral membrane protein. Golgi apparatus – Golgi stack membrane; Peripheral membrane protein.

Q5VZF2	MBNL2_HUMAN	Muscleblind-like protein 2 (Muscleblind-like protein 1) (Muscleblind-like protein-like) (Muscleblind-like protein-like 39)	Nucleus. Cytoplasm.
O95297	MPZL1_HUMAN	Myelin protein zero-like protein 1 (Protein zero-related)	Membrane; Single-pass type I membrane protein.
Q9NZM1	MYOF_HUMAN	Myoferlin (Fer-1-like protein 3)	Cell membrane; Single-pass type II membrane protein. Nucleus membrane; Single-pass type II membrane protein. Cytoplasmic vesicle membrane; Single-pass type II membrane protein.
Q86SF2	GALT7_HUMAN	N-acetylgalactosaminyltransferase 7 (EC 2.4.1.-) (Polypeptide GalNAc transferase 7) (GalNAc-T7) (pp-GaNTase 7) (Protein-UDP acetylgalactosaminyltransferase 7) (UDP-GalNAc:polypeptide N-acetylgalactosaminyltransferase 7)	Golgi apparatus membrane; Single-pass type II membrane protein.
P32004	L1CAM_HUMAN	Neural cell adhesion molecule L1 (N-CAM-L1) (NCAM-L1) (CD antigen CD171)	Cell membrane; Single-pass type I membrane protein.
Q9Y314	NOSIP_HUMAN	Nitric oxide synthase-interacting protein (eNOS-interacting protein)	Cytoplasm. Nucleus.
Q9UBU9	NXF1_HUMAN	Nuclear RNA export factor 1 (Tip-associated protein) (Tip-associating protein) (mRNA export factor TAP)	Nucleus – nucleoplasm. Nucleus speckle. Cytoplasm.
P50897	PPT1_HUMAN	Palmitoyl-protein thioesterase 1 (PPT-1) (EC 3.1.2.22) (Palmitoyl-protein hydrolase 1)	Lysosome.
P23284	PPIB_HUMAN	Peptidyl-prolyl cis-trans isomerase B (PPIase B) (EC 5.2.1.8) (CYP-S1) (Cyclophilin B) (Rotamase B) (S-cyclophilin) (SCYLP)	Endoplasmic reticulum lumen. Melanosome.
O60437	PEPL_HUMAN	Periplakin (190 kDa paraneoplastic pemphigus antigen) (195 kDa cornified envelope precursor protein)	Cell junction – desmosome. Cytoplasm – cytoskeleton. Cell membrane. Nucleus. Mitochondrion.
Q13162	PRDX4_HUMAN	Peroxiredoxin-4 (EC 1.11.1.15) (Antioxidant enzyme AOE372) (AOE37-2) (Peroxiredoxin IV) (Prx-IV) (Thioredoxin peroxidase AO372) (Thioredoxin-dependent peroxide reductase A0372)	Cytoplasm. Secreted.
P51659	DHB4_HUMAN	Peroxisomal multifunctional enzyme type 2 (MFE-2) (17-beta-hydroxysteroid dehydrogenase 4) (17-beta-HSD 4) (D-bifunctional protein) (DBP) (Multifunctional protein 2) (MPF-2) [Cleaved into: (3R)-hydroxyacyl-CoA dehydrogenase (EC 1.1.1.n12); Enoyl-CoA hydratase 2 (EC 4.2.1.107) (EC 4.2.1.119) (3-alpha,7-alpha,12-alpha-trihydroxy-5-beta-cholest-24-enoyl-CoA hydratase)]	Peroxisome.
Q6Y7W6	PERQ2_HUMAN	PERQ amino acid-rich with GYF domain-containing protein 2 (GRB10-interacting GYF protein 2) (Trinucleotide repeat-containing gene 15 protein)	
P42356	PI4KA_HUMAN	Phosphatidylinositol 4-kinase alpha (PI4-kinase alpha) (PI4K-alpha) (PtdIns-4-kinase alpha) (EC 2.7.1.67)	Cytoplasm. Membrane.
O00592	PODXL_HUMAN	Podocalyxin (GCTM-2 antigen) (Gp200) (Podocalyxin-like protein 1) (PC) (PCLP-1)	Apical cell membrane. Cell projection – lamellipodium. Cell projection – filopodium. Cell projection – ruffle. Cell projection – microvillus. Membrane raft. Membrane; Single-pass type I membrane protein.
Q9UMS4	PRP19_HUMAN	Pre-mRNA-processing factor 19 (Nuclear matrix protein 200) (PRP19/PSO4 homolog) (hPso4) (Senescence evasion factor)	Nucleus. Nucleus – nucleoplasm. Cytoplasm – cytoskeleton – spindle.
Q9UHG3	PCYOX_HUMAN	Prenylcysteine oxidase 1 (EC 1.8.3.5) (Prenylcysteine lyase)	Lysosome.
P20618	PSB1_HUMAN	Proteasome subunit beta type-1 (EC 3.4.25.1) (Macropain subunit C5) (Multicatalytic endopeptidase complex subunit C5) (Proteasome component C5) (Proteasome gamma chain)	Cytoplasm. Nucleus.
O75128	COBL_HUMAN	Protein cordon-bleu	Cell membrane; Peripheral membrane protein; Cytoplasmic side. Cytoplasm – cytoskeleton. Cell projection – ruffle. Cytoplasm.
Q9NSV4	DIAP3_HUMAN	Protein diaphanous homolog 3 (Diaphanous-related formin-3) (DRF3) (MDia2)	Cytoplasm – cytosol.
Q96JJ7	TMX3_HUMAN	Protein disulfide-isomerase TMX3 (EC 5.3.4.1) (Thioredoxin domain-containing protein 10) (Thioredoxin-related transmembrane protein 3)	Endoplasmic reticulum membrane; Single-pass membrane protein.
Q14320	FA50A_HUMAN	Protein FAM50A (Protein HXC-26) (Protein XAP-5)	Nucleus.
Q14331	FRG1_HUMAN	Protein FRG1 (FSHD region gene 1 protein)	Nucleus – Cajal body. Nucleus speckle. Nucleus – nucleolus.
Q969G5	PRDBP_HUMAN	Protein kinase C delta-binding protein (Cavin-3) (Serum deprivation response factor-related gene product that binds to C-kinase) (hSRBC)	
P55735	SEC13_HUMAN	Protein SEC13 homolog (SEC13-like protein 1) (SEC13-related protein)	Cytoplasmic vesicle – COPII-coated vesicle membrane; Peripheral membrane protein; Cytoplasmic side. Endoplasmic reticulum membrane; Peripheral membrane protein; Cytoplasmic side. Nucleus – nuclear pore complex.
Q01105	SET_HUMAN	Protein SET (HLA-DR-associated protein II) (Inhibitor of granzyme A-activated DNase) (IGAAD) (PHAPII) (Phosphatase 2A inhibitor I2PP2A) (I-2PP2A) (Template-activating factor I) (TAF-I)	Cytoplasm – cytosol. Endoplasmic reticulum. Nucleus – nucleoplasm.
O95486	SC24A_HUMAN	Protein transport protein Sec24A (SEC24-related protein A)	Cytoplasm. Cytoplasm – perinuclear region. Endoplasmic reticulum membrane. Golgi apparatus membrane.
P53992	SC24C_HUMAN	Protein transport protein Sec24C (SEC24-related protein C)	Cytoplasm. Cytoplasm – perinuclear region. Endoplasmic reticulum membrane. Golgi apparatus membrane.
O94979	SC31A_HUMAN	Protein transport protein Sec31A (ABP125) (ABP130) (SEC31-like protein 1) (SEC31-related protein A) (Web1-like protein)	Cytoplasm. Cytoplasmic vesicle – COPII-coated vesicle membrane; Peripheral membrane protein; Cytoplasmic side. Endoplasmic reticulum membrane; Peripheral membrane protein.

Q969M3	YIPF5_HUMAN	Protein YIPF5 (Five-pass transmembrane protein localizing in the Golgi apparatus and the endoplasmic reticulum 5) (Smooth muscle cell-associated protein 5) (SMAP-5) (YIP1 family member 5) (YPT-interacting protein 1 A)	Endoplasmic reticulum membrane; Multi-pass membrane protein. Golgi apparatus – Golgi stack membrane; Multi-pass membrane protein. Cytoplasmic vesicle – COPII-coated vesicle.
Q7L2E3	DHX30_HUMAN	Putative ATP-dependent RNA helicase DHX30 (EC 3.6.4.13) (DEAH box protein 30)	Cytoplasm. Mitochondrion. Cytoplasm. Mitochondrion matrix – mitochondrion nucleoid.
P61019	RAB2A_HUMAN	Ras-related protein Rab-2A	Endoplasmic reticulum-Golgi intermediate compartment membrane; Lipid-anchor. Melanosome. Endoplasmic reticulum membrane; Lipid-anchor. Golgi apparatus membrane; Lipid-anchor.
P20338	RAB4A_HUMAN	Ras-related protein Rab-4A	Membrane; Peripheral membrane protein. Cytoplasm.
P20340	RAB6A_HUMAN	Ras-related protein Rab-6A (Rab-6)	Golgi apparatus membrane; Lipid-anchor.
P51149	RAB7A_HUMAN	Ras-related protein Rab-7a	Late endosome. Lysosome. Cytoplasmic vesicle – phagosome. Melanosome. Cytoplasmic vesicle – phagosome membrane; Lipid-anchor; Cytoplasmic side.
P61224	RAP1B_HUMAN	Ras-related protein Rap-1b (GTP-binding protein smg p21B)	Cell membrane. Cytoplasm – cytosol. Cell junction.
Q92900	RENT1_HUMAN	Regulator of nonsense transcripts 1 (EC 3.6.4.-) (ATP-dependent helicase RENT1) (Nonsense mRNA reducing factor 1) (NORF1) (Up-frameshift suppressor 1 homolog) (hUpf1)	Cytoplasm. Cytoplasm – P-body. Nucleus.
Q9NQC3	RTN4_HUMAN	Reticulon-4 (Foocen) (Neurite outgrowth inhibitor) (Nogo protein) (Neuroendocrine-specific protein) (NSP) (Neuroendocrine-specific protein C homolog) (RTN-x) (Reticulon-5)	Endoplasmic reticulum membrane; Multi-pass membrane protein.
Q8TC12	RDH11_HUMAN	Retinol dehydrogenase 11 (EC 1.1.1.300) (Androgen-regulated short-chain dehydrogenase/reductase 1) (HCV core-binding protein HCBP12) (Prostate short-chain dehydrogenase/reductase 1) (Retinal reductase 1) (RalR1)	Endoplasmic reticulum membrane; Single-pass type II membrane protein.
P35637	FUS_HUMAN	RNA-binding protein FUS (75 kDa DNA-pairing protein) (Oncogene FUS) (Oncogene TLS) (POMp75) (Translocated in liposarcoma protein)	Nucleus.
P16615	AT2A2_HUMAN	Sarcoplasmic/endoplasmic reticulum calcium ATPase 2 (SERCA2) (SR Ca(2+)-ATPase 2) (EC 3.6.3.8) (Calcium pump 2) (Calcium-transporting ATPase sarcoplasmic reticulum type, slow twitch skeletal muscle isoform) (Endoplasmic reticulum class 1/2 Ca(2+) ATPase)	Endoplasmic reticulum membrane; Multi-pass membrane protein. Sarcoplasmic reticulum membrane; Multi-pass membrane protein.
Q15019	SEPT2_HUMAN	Septin-2 (Neural precursor cell expressed developmentally down-regulated protein 5) (NEDD-5)	Cytoplasm. Cytoplasm – cytoskeleton. Cytoplasm – cytoskeleton – spindle. Chromosome – centromere – kinetochore. Cleavage furrow. Midbody. Cytoplasm – cell cortex. Cell projection – cilium membrane.
Q07955	SRSF1_HUMAN	Serine/arginine-rich splicing factor 1 (Alternative-splicing factor 1) (ASF-1) (Splicing factor, arginine/serine-rich 1) (pre-mRNA-splicing factor SF2, P33 subunit)	Cytoplasm. Nucleus speckle.
P67775	PP2AA_HUMAN	Serine/threonine-protein phosphatase 2A catalytic subunit alpha isoform (PP2A-alpha) (EC 3.1.3.16) (Replication protein C) (RP-C)	Cytoplasm. Nucleus. Chromosome – centromere. Cytoplasm – cytoskeleton – spindle pole.
O00743	PPP6_HUMAN	Serine/threonine-protein phosphatase 6 catalytic subunit (PP6C) (EC 3.1.3.16) [Cleaved into: Serine/threonine-protein phosphatase 6 catalytic subunit, N-terminally processed]	Cytoplasm.
P62140	PP1B_HUMAN	Serine/threonine-protein phosphatase PP1-beta catalytic subunit (PP-1B) (PPP1CD) (EC 3.1.3.16) (EC 3.1.3.53)	Cytoplasm. Nucleus. Nucleus – nucleoplasm. Nucleus – nucleolus.
Q15165	PON2_HUMAN	Serum paraoxonase/arylesterase 2 (PON 2) (EC 3.1.1.2) (EC 3.1.1.81) (Aromatic esterase 2) (A-esterase 2) (Serum aryldialkylphosphatase 2)	Membrane; Peripheral membrane protein.
Q15005	SPCS2_HUMAN	Signal peptidase complex subunit 2 (EC 3.4.-.-) (Microsomal signal peptidase 25 kDa subunit) (SPase 25 kDa subunit)	Microsome membrane; Multi-pass membrane protein. Endoplasmic reticulum membrane; Multi-pass membrane protein.
Q9Y5M8	SRPRB_HUMAN	Signal recognition particle receptor subunit beta (SR-beta) (Protein APMCF1)	Endoplasmic reticulum membrane; Single-pass membrane protein.
P05023	AT1A1_HUMAN	Sodium/potassium-transporting ATPase subunit alpha-1 (Na(+)/K(+) ATPase alpha-1 subunit) (EC 3.6.3.9) (Sodium pump subunit alpha-1)	Cell membrane; Multi-pass membrane protein. Melanosome.
P54709	AT1B3_HUMAN	Sodium/potassium-transporting ATPase subunit beta-3 (Sodium/potassium-dependent ATPase subunit beta-3) (ATPB-3) (CD antigen CD298)	Cell membrane; Single-pass type II membrane protein. Melanosome.
P17405	ASM_HUMAN	Sphingomyelin phosphodiesterase (EC 3.1.4.12) (Acid sphingomyelinase) (aSMase)	Lysosome.
Q9NTJ3	SMC4_HUMAN	Structural maintenance of chromosomes protein 4 (SMC protein 4) (SMC-4) (Chromosome-associated polypeptide C) (hCAP-C) (XCAP-C homolog)	Nucleus. Cytoplasm. Chromosome.
Q86Y82	STX12_HUMAN	Syntaxin-12	Endosome membrane; Single-pass type IV membrane protein. Golgi apparatus membrane; Single-pass type IV membrane protein. Endomembrane system; Single-pass type IV membrane protein; Cytoplasmic side.

P17987	TCPA_HUMAN	T-complex protein 1 subunit alpha (TCP-1-alpha) (CCT-alpha)	Cytoplasm. Cytoplasm – cytoskeleton – microtubule organizing center – centrosome.
Q99832	TCPH_HUMAN	T-complex protein 1 subunit eta (TCP-1-eta) (CCT-eta) (HIV-1 Nef-interacting protein)	Cytoplasm.
Q9H3N1	TMX1_HUMAN	Thioredoxin-related transmembrane protein 1 (Thioredoxin domain-containing protein 1) (Transmembrane Trx-related protein)	Membrane; Single-pass type I membrane protein. Endoplasmic reticulum membrane; Single-pass type I membrane protein.
Q8IUR0	TPPC5_HUMAN	Trafficking protein particle complex subunit 5	Golgi apparatus – cis-Golgi network. Endoplasmic reticulum.
P29401	TKT_HUMAN	Transketolase (TK) (EC 2.2.1.1)	
A5PLL7	TM189_HUMAN	Transmembrane protein 189	Endoplasmic reticulum membrane; Multi-pass membrane protein.
Q9BTV4	TMM43_HUMAN	Transmembrane protein 43 (Protein LUMA)	Endoplasmic reticulum. Nucleus inner membrane; Multi-pass membrane protein.
P29144	TPP2_HUMAN	Tripeptidyl-peptidase 2 (TPP-2) (EC 3.4.14.10) (Tripeptidyl aminopeptidase) (Tripeptidyl-peptidase II) (TPP-II)	Cytoplasm. Nucleus.
P67936	TPM4_HUMAN	Tropomyosin alpha-4 chain (TM30p1) (Tropomyosin-4)	Cytoplasm – cytoskeleton.
Q12792	TWF1_HUMAN	Twinfilin-1 (Protein A6) (Protein tyrosine kinase 9)	Cytoplasm. Cytoplasm – cytoskeleton.
Q6IBS0	TWF2_HUMAN	Twinfilin-2 (A6-related protein) (hA6RP) (Protein tyrosine kinase 9-like) (Twinfilin-1-like protein)	Cytoplasm – cytoskeleton. Cytoplasm – perinuclear region. Cell projection – stereocilium.
P30530	UFO_HUMAN	Tyrosine-protein kinase receptor UFO (EC 2.7.10.1) (AXL oncogene)	Cell membrane; Single-pass type I membrane protein.
P09661	RU2A_HUMAN	U2 small nuclear ribonucleoprotein A' (U2 snRNP A')	Nucleus.
Q8WVY7	UBCP1_HUMAN	Ubiquitin-like domain-containing CTD phosphatase 1 (EC 3.1.3.16) (Nuclear proteasome inhibitor UBLCP1)	Nucleus.
Q9NYU2	UGGG1_HUMAN	UDP-glucose:glycoprotein glucosyltransferase 1 (UGT1) (hUGT1) (EC 2.4.1.-) (UDP--Glc:glycoprotein glucosyltransferase) (UDP-glucose ceramide glucosyltransferase-like 1)	Endoplasmic reticulum lumen. Endoplasmic reticulum-Golgi intermediate compartment.
Q9NZ01	TECR_HUMAN	Very-long-chain enoyl-CoA reductase (EC 1.3.1.93) (Synaptic glycoprotein SC2) (Trans-2,3-enoyl-CoA reductase) (TER)	Endoplasmic reticulum membrane; Multi-pass membrane protein.
Q9Y3E0	GOT1B_HUMAN	Vesicle transport protein GOT1B (Germ cell tumor 2) (Golgi transport 1 homolog B) (Putative NF-kappa-B-activating protein 470) (hGOT1a)	Golgi apparatus membrane; Multi-pass membrane protein.
Q12981	SEC20_HUMAN	Vesicle transport protein SEC20 (BCL2/adenovirus E1B 19 kDa protein-interacting protein 1) (Transformation-related gene 8 protein) (TRG-8)	Mitochondrion. Endoplasmic reticulum membrane; Single-pass type IV membrane protein.
Q9P0L0	VAPA_HUMAN	Vesicle-associated membrane protein-associated protein A (VAMP-A) (VAMP-associated protein A) (VAP-A) (33 kDa VAMP-associated protein) (VAP-33)	Endoplasmic reticulum membrane; Single-pass type IV membrane protein.
O95292	VAPB_HUMAN	Vesicle-associated membrane protein-associated protein B/C (VAMP-B/VAMP-C) (VAMP-associated protein B/C) (VAP-B/VAP-C)	Endoplasmic reticulum membrane; Single-pass type IV membrane protein.
O75396	SC22B_HUMAN	Vesicle-trafficking protein SEC22b (ER-Golgi SNARE of 24 kDa) (ERS-24) (ERS24) (SEC22 vesicle-trafficking protein homolog B) (SEC22 vesicle-trafficking protein-like 1)	Endoplasmic reticulum membrane; Single-pass type IV membrane protein. Endoplasmic reticulum-Golgi intermediate compartment membrane. Golgi apparatus – cis-Golgi network membrane. Golgi apparatus – trans-Golgi network membrane. Melanosome.
Q12907	LMAN2_HUMAN	Vesicular integral-membrane protein VIP36 (Glycoprotein GP36b) (Lectin mannose-binding 2) (Vesicular integral-membrane protein 36) (VIP36)	Endoplasmic reticulum-Golgi intermediate compartment membrane; Single-pass type I membrane protein. Golgi apparatus membrane; Single-pass membrane protein. Endoplasmic reticulum membrane; Single-pass type I membrane protein.
P18206	VINC_HUMAN	Vinculin (Metavinculin) (MV)	Cytoplasm – cytoskeleton. Cell junction – adherens junction. Cell membrane; Peripheral membrane protein; Cytoplasmic side. Cell junction – focal adhesion.
P45880	VDAC2_HUMAN	Voltage-dependent anion-selective channel protein 2 (VDAC-2) (hVDAC2) (Outer mitochondrial membrane protein porin 2)	Mitochondrion outer membrane.
P21283	VATC1_HUMAN	V-type proton ATPase subunit C 1 (V-ATPase subunit C 1) (Vacuolar proton pump subunit C 1)	
P61421	VA0D1_HUMAN	V-type proton ATPase subunit d 1 (V-ATPase subunit d 1) (32 kDa accessory protein) (V-ATPase 40 kDa accessory protein) (V-ATPase AC39 subunit) (p39) (Vacuolar proton pump subunit d 1)	Membrane; Peripheral membrane protein; Cytoplasmic side.
P61964	WDR5_HUMAN	WD repeat-containing protein 5 (BMP2-induced 3-kb gene protein)	Nucleus.
P12956	XRCC6_HUMAN	X-ray repair cross-complementing protein 6 (EC 3.6.4.-) (EC 4.2.99.-) (5'-deoxyribose-5-phosphate lyase Ku70) (5'-dRP lyase Ku70) (70 kDa subunit of Ku antigen) (ATP-dependent DNA helicase 2 subunit 1) (ATP-dependent DNA helicase II 70 kDa subunit) (CTC box-binding factor 75 kDa subunit) (CTC75) (CTCBF) (DNA repair protein XRCC6) (Lupus Ku autoantigen protein p70) (Ku70) (Thyroid-lupus autoantigen) (TLAA)	Nucleus. Chromosome.
O95159	ZFPL1_HUMAN	Zinc finger protein-like 1 (Zinc finger protein MCG4)	Golgi apparatus – cis-Golgi network membrane; Single-pass membrane protein.
Q15043	S39AE_HUMAN	Zinc transporter ZIP14 (LIV-1 subfamily of ZIP zinc transporter 4) (LZT-Hs4) (Solute carrier family 39 member 14) (Zrt- and Irt-like protein 14) (ZIP-14)	Cell membrane; Multi-pass membrane protein. Cell projection – lamellipodium.

Proteins enriched only at the 3 hour SCV			
Entry	**Entry name**	**Protein names**	**Subcellular location**
Q16401	PSMD5_HUMAN	26S proteasome non-ATPase regulatory subunit 5 (26S protease subunit S5 basic) (26S proteasome subunit S5B)	
P08195	4F2_HUMAN	4F2 cell-surface antigen heavy chain (4F2hc) (4F2 heavy chain antigen) (Lymphocyte activation antigen 4F2 large subunit) (Solute carrier family 3 member 2) (CD antigen CD98)	Apical cell membrane; Single-pass type II membrane protein. Melanosome.
Q96D46	NMD3_HUMAN	60S ribosomal export protein NMD3 (hNMD3)	Cytoplasm. Nucleus – nucleoplasm. Nucleus – nucleolus.
Q8N556	AFAP1_HUMAN	Actin filament-associated protein 1 (110 kDa actin filament-associated protein) (AFAP-110)	Cytoplasm – cytoskeleton.
P30566	PUR8_HUMAN	Adenylosuccinate lyase (ASL) (EC 4.3.2.2) (Adenylosuccinase) (ASase)	
P30520	PURA2_HUMAN	Adenylosuccinate synthetase isozyme 2 (AMPSase 2) (AdSS 2) (EC 6.3.4.4) (Adenylosuccinate synthetase, acidic isozyme) (Adenylosuccinate synthetase, liver isozyme) (L-type adenylosuccinate synthetase) (IMP--aspartate ligase 2)	Cytoplasm.
P12814	ACTN1_HUMAN	Alpha-actinin-1 (Alpha-actinin cytoskeletal isoform) (F-actin cross-linking protein) (Non-muscle alpha-actinin-1)	Cytoplasm – cytoskeleton. Cytoplasm – myofibril – sarcomere – Z line. Cell membrane. Cell junction. Cell projection – ruffle.
P08758	ANXA5_HUMAN	Annexin A5 (Anchorin CII) (Annexin V) (Annexin-5) (Calphobindin I) (CBP-I) (Endonexin II) (Lipocortin V) (Placental anticoagulant protein 4) (PP4) (Placental anticoagulant protein I) (PAP-I) (Thromboplastin inhibitor) (Vascular anticoagulant-alpha) (VAC-alpha)	
P08133	ANXA6_HUMAN	Annexin A6 (67 kDa calelectrin) (Annexin VI) (Annexin-6) (Calphobindin-II) (CPB-II) (Chromobindin-20) (Lipocortin VI) (Protein III) (p68) (p70)	Cytoplasm. Melanosome.
O95782	AP2A1_HUMAN	AP-2 complex subunit alpha-1 (100 kDa coated vesicle protein A) (Adapter-related protein complex 2 subunit alpha-1) (Adaptor protein complex AP-2 subunit alpha-1) (Alpha-adaptin A) (Alpha1-adaptin)	Cell membrane. Membrane – coated pit; Peripheral membrane protein; Cytoplasmic side.
P63010	AP2B1_HUMAN	AP-2 complex subunit beta (AP105B) (Adapter-related protein complex 2 subunit beta) (Adaptor protein complex AP-2 subunit beta) (Beta-2-adaptin) (Beta-adaptin) (Clathrin assembly protein complex 2 beta large chain)	Cell membrane. Membrane – coated pit; Peripheral membrane protein; Cytoplasmic side.
Q12797	ASPH_HUMAN	Aspartyl/asparaginyl beta-hydroxylase (EC 1.14.11.16) (Aspartate beta-hydroxylase) (ASP beta-hydroxylase) (Peptide-aspartate beta-dioxygenase)	Endoplasmic reticulum membrane; Single-pass type II membrane protein.
P53396	ACLY_HUMAN	ATP-citrate synthase (EC 2.3.3.8) (ATP-citrate (pro-S-)-lyase) (ACL) (Citrate cleavage enzyme)	Cytoplasm.
Q92499	DDX1_HUMAN	ATP-dependent RNA helicase DDX1 (EC 3.6.4.13) (DEAD box protein 1) (DEAD box protein retinoblastoma) (DBP-RB)	Nucleus. Cytoplasm. Cytoplasmic granule.
Q9NVP1	DDX18_HUMAN	ATP-dependent RNA helicase DDX18 (EC 3.6.4.13) (DEAD box protein 18) (Myc-regulated DEAD box protein) (MrDb)	Nucleus – nucleolus.
Q9H4G0	E41L1_HUMAN	Band 4.1-like protein 1 (Neuronal protein 4.1) (4.1N)	Cytoplasm – cytoskeleton.
O15155	BET1_HUMAN	BET1 homolog (hBET1) (Golgi vesicular membrane-trafficking protein p18)	Endoplasmic reticulum membrane; Single-pass type IV membrane protein. Golgi apparatus – cis-Golgi network membrane.
P15291	B4GT1_HUMAN	Beta-1,4-galactosyltransferase 1 (Beta-1,4-GalTase 1) (Beta4Gal-T1) (b4Gal-T1) (EC 2.4.1.-) (UDP-Gal:beta-GlcNAc beta-1,4-galactosyltransferase 1) (UDP-galactose:beta-N-acetylglucosamine beta-1,4-galactosyltransferase 1) [Cleaved into: Processed beta-1,4-galactosyltransferase 1] [Includes: Lactose synthase A protein (EC 2.4.1.22); N-acetyllactosamine synthase (EC 2.4.1.90) (Nal synthase); Beta-N-acetylglucosaminylglycopeptide beta-1,4-galactosyltransferase (EC 2.4.1.38); Beta-N-acetylglucosaminyl-glycolipid beta-1,4-galactosyltransferase (EC 2.4.1.-)]	Golgi apparatus – Golgi stack membrane; Single-pass type II membrane protein. Cell membrane; Single-pass type II membrane protein. Cell surface. Golgi apparatus – Golgi stack membrane; Single-pass type II membrane protein. Secreted.
O43252	PAPS1_HUMAN	Bifunctional 3'-phosphoadenosine 5'-phosphosulfate synthase 1 (PAPS synthase 1) (PAPSS 1) (Sulfurylase kinase 1) (SK 1) (SK1) [Includes: Sulfate adenylyltransferase (EC 2.7.7.4) (ATP-sulfurylase) (Sulfate adenylate transferase) (SAT); Adenylyl-sulfate kinase (EC 2.7.1.25) (3'-phosphoadenosine-5'-phosphosulfate synthase) (APS kinase) (Adenosine-5'-phosphosulfate 3'-phosphotransferase) (Adenylylsulfate 3'-phosphotransferase)]	
O95340	PAPS2_HUMAN	Bifunctional 3'-phosphoadenosine 5'-phosphosulfate synthase 2 (PAPS synthase 2) (PAPSS 2) (Sulfurylase kinase 2) (SK 2) (SK2) [Includes: Sulfate adenylyltransferase (EC 2.7.7.4) (ATP-sulfurylase) (Sulfate adenylate transferase) (SAT); Adenylyl-sulfate kinase (EC 2.7.1.25) (3'-phosphoadenosine-5'-phosphosulfate synthase) (APS kinase) (Adenosine-5'-phosphosulfate 3'-phosphotransferase) (Adenylylsulfate 3'-phosphotransferase)]	
P11586	C1TC_HUMAN	C-1-tetrahydrofolate synthase, cytoplasmic (C1-THF synthase) [Cleaved into: C-1-tetrahydrofolate synthase, cytoplasmic, N-terminally processed] [Includes: Methylenetetrahydrofolate dehydrogenase (EC 1.5.1.5); Methenyltetrahydrofolate cyclohydrolase (EC 3.5.4.9); Formyltetrahydrofolate synthetase (EC 6.3.4.3)]	Cytoplasm.
Q05682	CALD1_HUMAN	Caldesmon (CDM)	Cytoplasm – cytoskeleton. Cytoplasm – myofibril.
P14384	CBPM_HUMAN	Carboxypeptidase M (CPM) (EC 3.4.17.12)	Cell membrane; Lipid-anchor – GPI-anchor.

P35221	CTNA1_HUMAN	Catenin alpha-1 (Alpha E-catenin) (Cadherin-associated protein) (Renal carcinoma antigen NY-REN-13)	Cytoplasm – cytoskeleton. Cell junction – adherens junction. Cell membrane; Peripheral membrane protein; Cytoplasmic side. Cell junction. Cell membrane; Peripheral membrane protein; Cytoplasmic side.
O60716	CTND1_HUMAN	Catenin delta-1 (Cadherin-associated Src substrate) (CAS) (p120 catenin) (p120(ctn)) (p120(cas))	Cytoplasm. Nucleus. Cell membrane. Nucleus.
P43121	MUC18_HUMAN	Cell surface glycoprotein MUC18 (Cell surface glycoprotein P1H12) (Melanoma cell adhesion molecule) (Melanoma-associated antigen A32) (Melanoma-associated antigen MUC18) (S-endo 1 endothelial-associated antigen) (CD antigen CD146)	Membrane; Single-pass type I membrane protein.
Q6UVK1	CSPG4_HUMAN	Chondroitin sulfate proteoglycan 4 (Chondroitin sulfate proteoglycan NG2) (Melanoma chondroitin sulfate proteoglycan) (Melanoma-associated chondroitin sulfate proteoglycan)	Apical cell membrane; Single-pass type I membrane protein; Extracellular side. Cell projection – lamellipodium membrane; Single-pass type I membrane protein; Extracellular side.
Q96JG6	CC132_HUMAN	Coiled-coil domain-containing protein 132	
Q99829	CPNE1_HUMAN	Copine-1 (Copine I)	
Q69YN2	C19L1_HUMAN	CWF19-like protein 1	
P49643	PRI2_HUMAN	DNA primase large subunit (EC 2.7.7.-) (DNA primase 58 kDa subunit) (p58)	
Q99543	DNJC2_HUMAN	DnaJ homolog subfamily C member 2 (M-phase phosphoprotein 11) (Zuotin-related factor 1) [Cleaved into: DnaJ homolog subfamily C member 2, N-terminally processed]	Nucleus. Cytoplasm – cytosol.
Q9UJW0	DCTN4_HUMAN	Dynactin subunit 4 (Dyn4) (Dynactin subunit p62)	Cytoplasm – cytoskeleton. Cytoplasm – cytoskeleton – microtubule organizing center – centrosome.
O00429	DNM1L_HUMAN	Dynamin-1-like protein (EC 3.6.5.5) (Dnm1p/Vps1p-like protein) (DVLP) (Dynamin family member proline-rich carboxyl-terminal domain less) (Dymple) (Dynamin-like protein) (Dynamin-like protein 4) (Dynamin-like protein IV) (HdynIV) (Dynamin-related protein 1)	Cytoplasm – cytosol. Golgi apparatus. Endomembrane system; Peripheral membrane protein. Mitochondrion outer membrane; Peripheral membrane protein. Peroxisome. Membrane – clathrin-coated pit. Cytoplasmic vesicle – secretory vesicle – synaptic vesicle.
P50570	DYN2_HUMAN	Dynamin-2 (EC 3.6.5.5)	Cytoplasm. Cytoplasm – cytoskeleton. Cell junction – synapse – postsynaptic cell membrane – postsynaptic density. Cell junction – synapse. Midbody.
Q9H4M9	EHD1_HUMAN	EH domain-containing protein 1 (PAST homolog 1) (hPAST1) (Testilin)	Recycling endosome membrane; Peripheral membrane protein. Early endosome membrane; Peripheral membrane protein. Cell membrane; Peripheral membrane protein; Cytoplasmic side.
Q9NZN4	EHD2_HUMAN	EH domain-containing protein 2 (PAST homolog 2)	Cell membrane; Peripheral membrane protein; Cytoplasmic side. Endosome membrane; Peripheral membrane protein.
Q9UKM7	MA1B1_HUMAN	Endoplasmic reticulum mannosyl-oligosaccharide 1,2-alpha-mannosidase (EC 3.2.1.113) (ER alpha-1,2-mannosidase) (ER mannosidase 1) (ERMan1) (Man9GlcNAc2-specific-processing alpha-mannosidase) (Mannosidase alpha class 1B member 1)	Endoplasmic reticulum membrane; Single-pass type II membrane protein.
Q96JJ3	ELMO2_HUMAN	Engulfment and cell motility protein 2 (Protein ced-12 homolog A) (hCed-12A)	Cytoplasm. Cytoplasm – cytosol. Membrane.
Q14244	MAP7_HUMAN	Ensconsin (Epithelial microtubule-associated protein of 115 kDa) (E-MAP-115) (Microtubule-associated protein 7) (MAP-7)	Cytoplasm – perinuclear region. Basolateral cell membrane. Cytoplasm – cytoskeleton.
P41567	EIF1_HUMAN	Eukaryotic translation initiation factor 1 (eIF1) (A121) (Protein translation factor SUI1 homolog) (Sui1iso1)	
P78344	IF4G2_HUMAN	Eukaryotic translation initiation factor 4 gamma 2 (eIF-4-gamma 2) (eIF-4G 2) (eIF4G 2) (Death-associated protein 5) (DAP-5) (p97)	
Q96KP1	EXOC2_HUMAN	Exocyst complex component 2 (Exocyst complex component Sec5)	
O60645	EXOC3_HUMAN	Exocyst complex component 3 (Exocyst complex component Sec6)	
Q96A65	EXOC4_HUMAN	Exocyst complex component 4 (Exocyst complex component Sec8)	
O00471	EXOC5_HUMAN	Exocyst complex component 5 (Exocyst complex component Sec10) (hSec10)	Cytoplasm.
P15311	EZRI_HUMAN	Ezrin (Cytovillin) (Villin-2) (p81)	Apical cell membrane; Peripheral membrane protein; Cytoplasmic side. Cell projection. Cell projection – microvillus membrane; Peripheral membrane protein; Cytoplasmic side. Cell projection – ruffle membrane; Peripheral membrane protein; Cytoplasmic side. Cytoplasm – cell cortex. Cytoplasm – cytoskeleton.
P09382	LEG1_HUMAN	Galectin-1 (Gal-1) (14 kDa laminin-binding protein) (HLBP14) (14 kDa lectin) (Beta-galactoside-binding lectin L-14-I) (Galaptin) (HBL) (HPL) (Lactose-binding lectin 1) (Lectin galactoside-binding soluble 1) (Putative MAPK-activating protein PM12) (S-Lac lectin 1)	Secreted – extracellular space – extracellular matrix.
P09104	ENOG_HUMAN	Gamma-enolase (EC 4.2.1.11) (2-phospho-D-glycerate hydro-lyase) (Enolase 2) (Neural enolase) (Neuron-specific enolase) (NSE)	Cytoplasm. Cell membrane.
Q9NUQ3	TXLNG_HUMAN	Gamma-taxilin (Environmental lipopolysaccharide-responding gene protein) (Factor inhibiting ATF4-mediated transcription) (FIAT) (Lipopolysaccharide-specific response protein 5)	Nucleus membrane. Cytoplasm – cytosol.
Q9BSJ2	GCP2_HUMAN	Gamma-tubulin complex component 2 (GCP-2) (hGCP2) (Gamma-ring complex protein 103 kDa) (h103p) (hGrip103) (Spindle pole body protein Spc97 homolog) (hSpc97)	Cytoplasm – cytoskeleton – microtubule organizing center – centrosome.
P14314	GLU2B_HUMAN	Glucosidase 2 subunit beta (80K-H protein) (Glucosidase II subunit beta) (Protein kinase C substrate 60.1 kDa protein heavy chain) (PKCSH)	Endoplasmic reticulum.
Q06210	GFPT1_HUMAN	Glutamine--fructose-6-phosphate aminotransferase [isomerizing] 1 (EC 2.6.1.16) (D-fructose-6-phosphate amidotransferase 1) (Glutamine:fructose-6-phosphate amidotransferase 1) (GFAT 1) (GFAT1) (Hexosephosphate aminotransferase 1)	

P13807	GYS1_HUMAN	Glycogen [starch] synthase, muscle (EC 2.4.1.11)	
O00178	GTPB1_HUMAN	GTP-binding protein 1 (G-protein 1) (GP-1) (GP1)	Cytoplasm.
P01834	IGKC_HUMAN	Ig kappa chain C region	
Q14974	IMB1_HUMAN	Importin subunit beta-1 (Importin-90) (Karyopherin subunit beta-1) (Nuclear factor p97) (Pore targeting complex 97 kDa subunit) (PTAC97)	Cytoplasm. Nucleus envelope.
Q13418	ILK_HUMAN	Integrin-linked protein kinase (EC 2.7.11.1) (59 kDa serine/threonine-protein kinase) (ILK-1) (ILK-2) (p59ILK)	Cell junction – focal adhesion. Cell membrane; Peripheral membrane protein; Cytoplasmic side. Cell projection – lamellipodium. Cytoplasm – myofibril – sarcomere.
Q12894	IFRD2_HUMAN	Interferon-related developmental regulator 2 (Protein SKMC15)	
Q07866	KLC1_HUMAN	Kinesin light chain 1 (KLC 1)	Cell projection – growth cone. Cytoplasmic vesicle. Cytoplasm – cytoskeleton.
Q9H0B6	KLC2_HUMAN	Kinesin light chain 2 (KLC 2)	Cytoplasm – cytoskeleton.
Q99661	KIF2C_HUMAN	Kinesin-like protein KIF2C (Kinesin-like protein 6) (Mitotic centromere-associated kinesin) (MCAK)	Cytoplasm – cytoskeleton. Nucleus. Chromosome – centromere. Chromosome – centromere – kinetochore.
Q16850	CP51A_HUMAN	Lanosterol 14-alpha demethylase (LDM) (EC 1.14.13.70) (CYPLI) (Cytochrome P450 51A1) (Cytochrome P450-14DM) (Cytochrome P45014DM) (Cytochrome P450LI) (Sterol 14-alpha demethylase)	Endoplasmic reticulum membrane. Microsome membrane.
Q92615	LAR4B_HUMAN	La-related protein 4B (La ribonucleoprotein domain family member 4B) (La ribonucleoprotein domain family member 5) (La-related protein 5)	Cytoplasm – cytosol.
Q9H089	LSG1_HUMAN	Large subunit GTPase 1 homolog (hLsg1) (EC 3.6.1.-)	Cytoplasm. Endoplasmic reticulum. Nucleus – Cajal body.
O95202	LETM1_HUMAN	LETM1 and EF-hand domain-containing protein 1, mitochondrial (Leucine zipper-EF-hand-containing transmembrane protein 1)	Mitochondrion inner membrane; Single-pass membrane protein.
Q13724	MOGS_HUMAN	Mannosyl-oligosaccharide glucosidase (EC 3.2.1.106) (Processing A-glucosidase I)	Endoplasmic reticulum membrane; Single-pass type II membrane protein.
Q8N6R0	MET13_HUMAN	Methyltransferase-like protein 13 (EC 2.1.1.-)	
Q8IVT2	MISP_HUMAN	Mitotic interactor and substrate of PLK1 (Mitotic spindle positioning protein)	Cell junction – focal adhesion. Cytoplasm – cytoskeleton. Cytoplasm – cell cortex.
Q8NB16	MLKL_HUMAN	Mixed lineage kinase domain-like protein (hMLKL)	Cytoplasm. Cell membrane.
P26038	MOES_HUMAN	Moesin (Membrane-organizing extension spike protein)	Cell membrane; Peripheral membrane protein; Cytoplasmic side. Cytoplasm – cytoskeleton. Apical cell membrane; Peripheral membrane protein; Cytoplasmic side. Cell projection – microvillus membrane; Peripheral membrane protein; Cytoplasmic side.
O00499	BIN1_HUMAN	Myc box-dependent-interacting protein 1 (Amphiphysin II) (Amphiphysin-like protein) (Box-dependent myc-interacting protein 1) (Bridging integrator 1)	Nucleus. Cytoplasm.
P16435	NCPR_HUMAN	NADPH--cytochrome P450 reductase (CPR) (P450R) (EC 1.6.2.4)	Endoplasmic reticulum membrane; Peripheral membrane protein.
P61081	UBC12_HUMAN	NEDD8-conjugating enzyme Ubc12 (EC 6.3.2.-) (NEDD8 carrier protein) (NEDD8 protein ligase) (Ubiquitin-conjugating enzyme E2 M)	
Q8WX92	NELFB_HUMAN	Negative elongation factor B (NELF-B) (Cofactor of BRCA1)	Nucleus.
P55769	NH2L1_HUMAN	NHP2-like protein 1 (High mobility group-like nuclear protein 2 homolog 1) (OTK27) (SNU13 homolog) (hSNU13) (U4/U6.U5 tri-snRNP 15.5 kDa protein) [Cleaved into: NHP2-like protein 1, N-terminally processed]	Nucleus – nucleolus.
P43490	NAMPT_HUMAN	Nicotinamide phosphoribosyltransferase (NAmPRTase) (Nampt) (EC 2.4.2.12) (Pre-B-cell colony-enhancing factor 1) (Pre-B cell-enhancing factor) (Visfatin)	Nucleus. Cytoplasm. Secreted.
P22307	NLTP_HUMAN	Non-specific lipid-transfer protein (NSL-TP) (EC 2.3.1.176) (Propanoyl-CoA C-acyltransferase) (SCP-chi) (SCPX) (Sterol carrier protein 2) (SCP-2) (Sterol carrier protein X) (SCP-X)	Cytoplasm. Mitochondrion. Peroxisome. Mitochondrion.
P80303	NUCB2_HUMAN	Nucleobindin-2 (DNA-binding protein NEFA) (Gastric cancer antigen Zg4) (Prepronesfatin) [Cleaved into: Nesfatin-1]	Golgi apparatus. Membrane; Peripheral membrane protein. Cytoplasm. Secreted. Endoplasmic reticulum. Nucleus envelope. Secreted.
P19338	NUCL_HUMAN	Nucleolin (Protein C23)	Nucleus – nucleolus. Cytoplasm.
O95302	FKBP9_HUMAN	Peptidyl-prolyl cis-trans isomerase FKBP9 (PPIase FKBP9) (EC 5.2.1.8) (63 kDa FK506-binding protein) (63 kDa FKBP) (FKBP-63) (FK506-binding protein 9) (FKBP-9) (Rotamase)	Endoplasmic reticulum.
O14936	CSKP_HUMAN	Peripheral plasma membrane protein CASK (hCASK) (EC 2.7.11.1) (Calcium/calmodulin-dependent serine protein kinase) (Protein lin-2 homolog)	Nucleus. Cytoplasm. Cell membrane; Peripheral membrane protein.
O00541	PESC_HUMAN	Pescadillo homolog	Nucleus – nucleolus. Nucleus – nucleoplasm. Chromosome.
Q9Y446	PKP3_HUMAN	Plakophilin-3	Nucleus. Cell junction – desmosome.
P11940	PABP1_HUMAN	Polyadenylate-binding protein 1 (PABP-1) (Poly(A)-binding protein 1)	Cytoplasm. Nucleus.
Q13310	PABP4_HUMAN	Polyadenylate-binding protein 4 (PABP-4) (Poly(A)-binding protein 4) (Activated-platelet protein 1) (APP-1) (Inducible poly(A)-binding protein) (iPABP)	Cytoplasm.
Q96GQ7	DDX27_HUMAN	Probable ATP-dependent RNA helicase DDX27 (EC 3.6.4.13) (DEAD box protein 27)	Nucleus.
Q02809	PLOD1_HUMAN	Procollagen-lysine,2-oxoglutarate 5-dioxygenase 1 (EC 1.14.11.4) (Lysyl hydroxylase 1) (LH1)	Rough endoplasmic reticulum membrane; Peripheral membrane protein; Lumenal side.
O60568	PLOD3_HUMAN	Procollagen-lysine,2-oxoglutarate 5-dioxygenase 3 (EC 1.14.11.4) (Lysyl hydroxylase 3) (LH3)	Rough endoplasmic reticulum membrane; Peripheral membrane protein; Lumenal side.
O15460	P4HA2_HUMAN	Prolyl 4-hydroxylase subunit alpha-2 (4-PH alpha-2) (EC 1.14.11.2) (Procollagen-proline,2-oxoglutarate-4-dioxygenase subunit alpha-2)	Endoplasmic reticulum lumen.
P13667	PDIA4_HUMAN	Protein disulfide-isomerase A4 (EC 5.3.4.1) (Endoplasmic reticulum resident protein 70) (ER protein 70) (ERp70) (Endoplasmic reticulum resident protein 72) (ER protein 72) (ERp-72) (ERp72)	Endoplasmic reticulum lumen. Melanosome.
Q15084	PDIA6_HUMAN	Protein disulfide-isomerase A6 (EC 5.3.4.1) (Endoplasmic reticulum protein 5) (ER protein 5) (ERp5) (Protein disulfide isomerase P5) (Thioredoxin domain-containing protein 7)	Endoplasmic reticulum lumen. Cell membrane. Melanosome.

Q658Y4	F91A1_HUMAN	Protein FAM91A1	
Q8NCA5	FA98A_HUMAN	Protein FAM98A	
Q9UKS6	PACN3_HUMAN	Protein kinase C and casein kinase substrate in neurons protein 3 (SH3 domain-containing protein 6511)	Cytoplasm. Cell membrane; Peripheral membrane protein; Cytoplasmic side.
Q96M27	PRRC1_HUMAN	Protein PRRC1 (Proline-rich and coiled-coil-containing protein 1)	Golgi apparatus.
Q13123	RED_HUMAN	Protein Red (Cytokine IK) (IK factor) (Protein RER)	Nucleus.
Q15436	SC23A_HUMAN	Protein transport protein Sec23A (SEC23-related protein A)	Smooth endoplasmic reticulum membrane; Peripheral membrane protein. Golgi apparatus membrane; Peripheral membrane protein.
P50336	PPOX_HUMAN	Protoporphyrinogen oxidase (PPO) (EC 1.3.3.4)	Mitochondrion inner membrane; Peripheral membrane protein; Intermembrane side.
P35241	RADI_HUMAN	Radixin	Cell membrane; Peripheral membrane protein; Cytoplasmic side. Cytoplasm – cytoskeleton. Cleavage furrow.
Q9UN86	G3BP2_HUMAN	Ras GTPase-activating protein-binding protein 2 (G3BP-2) (GAP SH3 domain-binding protein 2)	Cytoplasm.
Q68EM7	RHG17_HUMAN	Rho GTPase-activating protein 17 (Rho-type GTPase-activating protein 17) (RhoGAP interacting with CIP4 homologs protein 1) (RICH-1)	Membrane; Peripheral membrane protein. Cytoplasm. Cell junction – tight junction.
P23921	RIR1_HUMAN	Ribonucleoside-diphosphate reductase large subunit (EC 1.17.4.1) (Ribonucleoside-diphosphate reductase subunit M1) (Ribonucleotide reductase large subunit)	Cytoplasm.
Q15418	KS6A1_HUMAN	Ribosomal protein S6 kinase alpha-1 (S6K-alpha-1) (EC 2.7.11.1) (90 kDa ribosomal protein S6 kinase 1) (p90-RSK 1) (p90RSK1) (p90S6K) (MAP kinase-activated protein kinase 1a) (MAPK-activated protein kinase 1a) (MAPKAP kinase 1a) (MAPKAPK-1a) (Ribosomal S6 kinase 1) (RSK-1)	Nucleus. Cytoplasm.
Q9Y265	RUVB1_HUMAN	RuvB-like 1 (EC 3.6.4.12) (49 kDa TATA box-binding protein-interacting protein) (49 kDa TBP-interacting protein) (54 kDa erythrocyte cytosolic protein) (ECP-54) (INO80 complex subunit H) (Nuclear matrix protein 238) (NMP 238) (Pontin 52) (TIP49a) (TIP60-associated protein 54-alpha) (TAP54-alpha)	Nucleus matrix. Nucleus – nucleoplasm. Cytoplasm. Membrane. Cytoplasm – cytoskeleton – microtubule organizing center – centrosome.
Q9Y230	RUVB2_HUMAN	RuvB-like 2 (EC 3.6.4.12) (48 kDa TATA box-binding protein-interacting protein) (48 kDa TBP-interacting protein) (51 kDa erythrocyte cytosolic protein) (ECP-51) (INO80 complex subunit J) (Repressing pontin 52) (Reptin 52) (TIP49b) (TIP60-associated protein 54-beta) (TAP54-beta)	Nucleus matrix. Nucleus – nucleoplasm. Cytoplasm. Membrane.
Q7KZI7	MARK2_HUMAN	Serine/threonine-protein kinase MARK2 (EC 2.7.11.1) (EC 2.7.11.26) (ELKL motif kinase 1) (EMK-1) (MAP/microtubule affinity-regulating kinase 2) (PAR1 homolog) (PAR1 homolog b) (Par-1b) (Par1b)	Cell membrane; Peripheral membrane protein. Cytoplasm. Lateral cell membrane. Cytoplasm – cytoskeleton.
Q96SB4	SRPK1_HUMAN	SRSF protein kinase 1 (EC 2.7.11.1) (SFRS protein kinase 1) (Serine/arginine-rich protein-specific kinase 1) (SR-protein-specific kinase 1)	Cytoplasm. Nucleus. Nucleus matrix. Microsome. Cytoplasm. Nucleus matrix. Microsome.
Q7KZF4	SND1_HUMAN	Staphylococcal nuclease domain-containing protein 1 (100 kDa coactivator) (EBNA2 coactivator p100) (Tudor domain-containing protein 11) (p100 co-activator)	Cytoplasm. Nucleus. Melanosome.
Q6ZRP7	QSOX2_HUMAN	Sulfhydryl oxidase 2 (EC 1.8.3.2) (Neuroblastoma-derived sulfhydryl oxidase) (Quiescin Q6-like protein 1)	Membrane; Single-pass membrane protein. Secreted. Cell membrane; Single-pass membrane protein. Nucleus membrane; Single-pass membrane protein.
P78371	TCPB_HUMAN	T-complex protein 1 subunit beta (TCP-1-beta) (CCT-beta)	Cytoplasm.
P48643	TCPE_HUMAN	T-complex protein 1 subunit epsilon (TCP-1-epsilon) (CCT-epsilon)	Cytoplasm. Cytoplasm – cytoskeleton – microtubule organizing center – centrosome.
P50990	TCPQ_HUMAN	T-complex protein 1 subunit theta (TCP-1-theta) (CCT-theta) (Renal carcinoma antigen NY-REN-15)	Cytoplasm. Cytoplasm – cytoskeleton – microtubule organizing center – centrosome.
P10599	THIO_HUMAN	Thioredoxin (Trx) (ATL-derived factor) (ADF) (Surface-associated sulphydryl protein) (SASP)	Nucleus. Cytoplasm. Secreted.
P23258	TBG1_HUMAN	Tubulin gamma-1 chain (Gamma-1-tubulin) (Gamma-tubulin complex component 1) (GCP-1)	Cytoplasm – cytoskeleton – microtubule organizing center – centrosome.
Q14157	UBP2L_HUMAN	Ubiquitin-associated protein 2-like (Protein NICE-4)	
O60701	UGDH_HUMAN	UDP-glucose 6-dehydrogenase (UDP-Glc dehydrogenase) (UDP-GlcDH) (UDPGDH) (EC 1.1.1.22)	
Q969H8	CS010_HUMAN	UPF0556 protein C19orf10 (Interleukin-25) (IL-25) (Stromal cell-derived growth factor SF20)	Secreted. Endoplasmic reticulum-Golgi intermediate compartment.
P46939	UTRO_HUMAN	Utrophin (Dystrophin-related protein 1) (DRP-1)	Cell junction – synapse – postsynaptic cell membrane; Peripheral membrane protein; Cytoplasmic side. Cytoplasm – cytoskeleton.
Q9UID3	VPS51_HUMAN	Vacuolar protein sorting-associated protein 51 homolog (Another new gene 2 protein) (Protein fat-free homolog)	Golgi apparatus – trans-Golgi network.
Q8N1B4	VPS52_HUMAN	Vacuolar protein sorting-associated protein 52 homolog (SAC2 suppressor of actin mutations 2-like protein)	Golgi apparatus – trans-Golgi network membrane; Peripheral membrane protein. Endosome membrane; Peripheral membrane protein.
Q9Y6W5	WASF2_HUMAN	Wiskott-Aldrich syndrome protein family member 2 (WASP family protein member 2) (Protein WAVE-2) (Verprolin homology domain-containing protein 2)	Cytoplasm – cytoskeleton. Cell projection – lamellipodium.
Q7Z739	YTHD3_HUMAN	YTH domain-containing family protein 3	
Q86UK7	ZN598_HUMAN	Zinc finger protein 598	

Proteins enriched at 30 min and 3 hour SCV

Entry	Entry name	Protein names	Subcellular location
P15880	RS2_HUMAN	40S ribosomal protein S2 (40S ribosomal protein S4) (Protein LLRep3)	
P46781	RS9_HUMAN	40S ribosomal protein S9	Cytoplasm.
Q9BRK5	CAB45_HUMAN	45 kDa calcium-binding protein (Cab45) (Stromal cell-derived factor 4) (SDF-4)	Golgi apparatus lumen. Cytoplasm. Cell projection – bleb.
P05388	RLA0_HUMAN	60S acidic ribosomal protein P0 (60S ribosomal protein L10E)	Nucleus. Cytoplasm.
Q07020	RL18_HUMAN	60S ribosomal protein L18	Cytoplasm.
P62424	RL7A_HUMAN	60S ribosomal protein L7a (PLA-X polypeptide) (Surfeit locus protein 3)	
P32969	RL9_HUMAN	60S ribosomal protein L9	
P11021	GRP78_HUMAN	78 kDa glucose-regulated protein (GRP-78) (Endoplasmic reticulum lumenal Ca(2+)-binding protein grp78) (Heat shock 70 kDa protein 5) (Immunoglobulin heavy chain-binding protein) (BiP)	Endoplasmic reticulum lumen. Melanosome. Cytoplasm.
Q15650	TRIP4_HUMAN	Activating signal cointegrator 1 (ASC-1) (Thyroid receptor-interacting protein 4) (TR-interacting protein 4) (TRIP-4)	Nucleus. Cytoplasm. Cytoplasm – cytoskeleton – microtubule organizing center – centrosome.
P52895	AK1C2_HUMAN	Aldo-keto reductase family 1 member C2 (EC 1.-.-.-) (3-alpha-HSD3) (Chlordecone reductase homolog HAKRD) (Dihydrodiol dehydrogenase 2) (DD-2) (DD2) (Dihydrodiol dehydrogenase/bile acid-binding protein) (DD/BABP) (Trans-1,2-dihydrobenzene-1,2-diol dehydrogenase) (EC 1.3.1.20) (Type III 3-alpha-hydroxysteroid dehydrogenase) (EC 1.1.1.357)	Cytoplasm.
Q8IWZ3	ANKH1_HUMAN	Ankyrin repeat and KH domain-containing protein 1 (HIV-1 Vpr-binding ankyrin repeat protein) (Multiple ankyrin repeats single KH domain) (hMASK)	Cytoplasm.
Q6DD88	ATLA3_HUMAN	Atlastin-3 (EC 3.6.5.-)	Endoplasmic reticulum membrane; Multi-pass membrane protein.
Q7Z478	DHX29_HUMAN	ATP-dependent RNA helicase DHX29 (EC 3.6.4.13) (DEAH box protein 29) (Nucleic acid helicase DDXx)	Cytoplasm.
P27708	PYR1_HUMAN	CAD protein [Includes: Glutamine-dependent carbamoyl-phosphate synthase (EC 6.3.5.5); Aspartate carbamoyltransferase (EC 2.1.3.2); Dihydroorotase (EC 3.5.2.3)]	Cytoplasm. Nucleus.
P27824	CALX_HUMAN	Calnexin (IP90) (Major histocompatibility complex class I antigen-binding protein p88) (p90)	Endoplasmic reticulum membrane; Single-pass type I membrane protein. Endoplasmic reticulum. Melanosome.
Q14444	CAPR1_HUMAN	Caprin-1 (Cell cycle-associated protein 1) (Cytoplasmic activation- and proliferation-associated protein 1) (GPI-anchored membrane protein 1) (GPI-anchored protein p137) (GPI-p137) (p137GPI) (Membrane component chromosome 11 surface marker 1) (RNA granule protein 105)	Cytoplasm – cytosol. Cell projection – dendrite.
O75718	CRTAP_HUMAN	Cartilage-associated protein	Secreted – extracellular space – extracellular matrix.
Q7Z460	CLAP1_HUMAN	CLIP-associating protein 1 (Cytoplasmic linker-associated protein 1) (Multiple asters homolog 1) (Protein Orbit homolog 1) (hOrbit1)	Cytoplasm – cytoskeleton. Cytoplasm – cytoskeleton – microtubule organizing center – centrosome. Chromosome – centromere – kinetochore. Cytoplasm – cytoskeleton – spindle. Golgi apparatus – trans-Golgi network.
Q9Y6G5	COMDA_HUMAN	COMM domain-containing protein 10	
Q9BPX3	CND3_HUMAN	Condensin complex subunit 3 (Chromosome-associated protein G) (Condensin subunit CAP-G) (hCAP-G) (Melanoma antigen NY-MEL-3) (Non-SMC condensin I complex subunit G) (XCAP-G homolog)	Nucleus. Cytoplasm. Chromosome.
O43175	SERA_HUMAN	D-3-phosphoglycerate dehydrogenase (3-PGDH) (EC 1.1.1.95)	
P49792	RBP2_HUMAN	E3 SUMO-protein ligase RanBP2 (EC 6.3.2.-) (358 kDa nucleoporin) (Nuclear pore complex protein Nup358) (Nucleoporin Nup358) (Ran-binding protein 2) (RanBP2) (p270)	Nucleus. Nucleus membrane. Nucleus – nuclear pore complex.
P29692	EF1D_HUMAN	Elongation factor 1-delta (EF-1-delta) (Antigen NY-CO-4)	Nucleus.
P13639	EF2_HUMAN	Elongation factor 2 (EF-2)	Cytoplasm.
Q969X5	ERGI1_HUMAN	Endoplasmic reticulum-Golgi intermediate compartment protein 1 (ER-Golgi intermediate compartment 32 kDa protein) (ERGIC-32)	Endoplasmic reticulum membrane; Multi-pass membrane protein. Endoplasmic reticulum-Golgi intermediate compartment membrane; Multi-pass membrane protein. Golgi apparatus membrane; Multi-pass membrane protein.
P14625	ENPL_HUMAN	Endoplasmin (94 kDa glucose-regulated protein) (GRP-94) (Heat shock protein 90 kDa beta member 1) (Tumor rejection antigen 1) (gp96 homolog)	Endoplasmic reticulum lumen. Melanosome.
Q9BY44	EIF2A_HUMAN	Eukaryotic translation initiation factor 2A (eIF-2A) (65 kDa eukaryotic translation initiation factor 2A) [Cleaved into: Eukaryotic translation initiation factor 2A, N-terminally processed]	
Q9BSJ8	ESYT1_HUMAN	Extended synaptotagmin-1 (E-Syt1) (Membrane-bound C2 domain-containing protein)	Endoplasmic reticulum membrane; Multi-pass membrane protein. Cell membrane; Peripheral membrane protein.
P21333	FLNA_HUMAN	Filamin-A (FLN-A) (Actin-binding protein 280) (ABP-280) (Alpha-filamin) (Endothelial actin-binding protein) (Filamin-1) (Non-muscle filamin)	Cytoplasm – cell cortex. Cytoplasm – cytoskeleton.
O75369	FLNB_HUMAN	Filamin-B (FLN-B) (ABP-278) (ABP-280 homolog) (Actin-binding-like protein) (Beta-filamin) (Filamin homolog 1) (Fh1) (Filamin-3) (Thyroid autoantigen) (Truncated actin-binding protein) (Truncated ABP)	Cytoplasm – cell cortex. Cytoplasm – cytoskeleton. Cytoplasm – myofibril – sarcomere – Z line. Cytoplasm – cytoskeleton.
P06744	G6PI_HUMAN	Glucose-6-phosphate isomerase (GPI) (EC 5.3.1.9) (Autocrine motility factor) (AMF) (Neuroleukin) (NLK) (Phosphoglucose isomerase) (PGI) (Phosphohexose isomerase) (PHI) (Sperm antigen 36) (SA-36)	Cytoplasm. Secreted.
P30419	NMT1_HUMAN	Glycylpeptide N-tetradecanoyltransferase 1 (EC 2.3.1.97) (Myristoyl-CoA:protein N-myristoyltransferase 1) (NMT 1) (Type I N-myristoyltransferase) (Peptide N-myristoyltransferase 1)	Cytoplasm.
P63244	GBLP_HUMAN	Guanine nucleotide-binding protein subunit beta-2-like 1 (Cell proliferation-inducing gene 21 protein) (Guanine nucleotide-binding protein subunit beta-like protein 12.3) (Human lung cancer oncogene 7 protein) (HLC-7) (Receptor for activated C kinase) (Receptor of activated protein kinase C 1) (RACK1) [Cleaved into: Guanine nucleotide-binding protein subunit beta-2-like 1, N-terminally processed]	Cell membrane; Peripheral membrane protein. Cytoplasm. Cytoplasm – perinuclear region. Cytoplasm – cytoskeleton. Nucleus. Perikaryon. Cell projection – dendrite. Cell projection – phagocytic cup.
Q14643	ITPR1_HUMAN	Inositol 1,4,5-trisphosphate receptor type 1 (IP3 receptor isoform 1) (IP3R 1) (InsP3R1) (Type 1 inositol 1,4,5-trisphosphate receptor) (Type 1 InsP3 receptor)	Endoplasmic reticulum membrane; Multi-pass membrane protein.

Q14573	ITPR3_HUMAN	Inositol 1,4,5-trisphosphate receptor type 3 (IP3 receptor isoform 3) (IP3R 3) (InsP3R3) (Type 3 inositol 1,4,5-trisphosphate receptor) (Type 3 InsP3 receptor)	Endoplasmic reticulum membrane; Multi-pass membrane protein.
P33176	KINH_HUMAN	Kinesin-1 heavy chain (Conventional kinesin heavy chain) (Ubiquitous kinesin heavy chain) (UKHC)	Cytoplasm – cytoskeleton.
Q6PKG0	LARP1_HUMAN	La-related protein 1 (La ribonucleoprotein domain family member 1)	Cytoplasm.
Q9UQ13	SHOC2_HUMAN	Leucine-rich repeat protein SHOC-2 (Protein soc-2 homolog) (Protein sur-8 homolog)	Cytoplasm. Nucleus.
Q96AG4	LRC59_HUMAN	Leucine-rich repeat-containing protein 59 (Ribosome-binding protein p34) (p34)	Microsome membrane; Single-pass type II membrane protein. Endoplasmic reticulum membrane; Single-pass type II membrane protein. Nucleus envelope.
P00338	LDHA_HUMAN	L-lactate dehydrogenase A chain (LDH-A) (EC 1.1.1.27) (Cell proliferation-inducing gene 19 protein) (LDH muscle subunit) (LDH-M) (Renal carcinoma antigen NY-REN-59)	Cytoplasm.
O95573	ACSL3_HUMAN	Long-chain-fatty-acid--CoA ligase 3 (EC 6.2.1.3) (Long-chain acyl-CoA synthetase 3) (LACS 3)	Mitochondrion outer membrane; Single-pass type III membrane protein. Peroxisome membrane; Single-pass type III membrane protein. Microsome membrane; Single-pass type III membrane protein. Endoplasmic reticulum membrane; Single-pass type III membrane protein.
Q8NF37	PCAT1_HUMAN	Lysophosphatidylcholine acyltransferase 1 (LPC acyltransferase 1) (LPCAT-1) (LysoPC acyltransferase 1) (EC 2.3.1.23) (1-acylglycerophosphocholine O-acyltransferase) (1-alkylglycerophosphocholine O-acetyltransferase) (EC 2.3.1.67) (Acetyl-CoA:lyso-platelet-activating factor acetyltransferase) (Acetyl-CoA:lyso-PAF acetyltransferase) (Lyso-PAF acetyltransferase) (LysoPAFAT) (Acyltransferase-like 2) (Phosphonoformate immuno-associated protein 3)	Endoplasmic reticulum membrane; Single-pass type II membrane protein. Golgi apparatus membrane; Single-pass type II membrane protein. Lipid droplet.
P27816	MAP4_HUMAN	Microtubule-associated protein 4 (MAP-4)	Cytoplasm – cytoskeleton.
Q15785	TOM34_HUMAN	Mitochondrial import receptor subunit TOM34 (hTom34) (Translocase of outer membrane 34 kDa subunit)	Cytoplasm. Mitochondrion outer membrane; Peripheral membrane protein; Cytoplasmic side.
P35579	MYH9_HUMAN	Myosin-9 (Cellular myosin heavy chain, type A) (Myosin heavy chain 9) (Myosin heavy chain, non-muscle IIa) (Non-muscle myosin heavy chain A) (NMMHC-A) (Non-muscle myosin heavy chain IIa) (NMMHC II-a) (NMMHC-IIA)	Cytoplasm – cytoskeleton. Cytoplasm – cell cortex.
P00387	NB5R3_HUMAN	NADH-cytochrome b5 reductase 3 (B5R) (Cytochrome b5 reductase) (EC 1.6.2.2) (Diaphorase-1) [Cleaved into: NADH-cytochrome b5 reductase 3 membrane-bound form; NADH-cytochrome b5 reductase 3 soluble form]	Endoplasmic reticulum membrane; Lipid-anchor; Cytoplasmic side. Mitochondrion outer membrane; Lipid-anchor; Cytoplasmic side. Cytoplasm.
Q13765	NACA_HUMAN	Nascent polypeptide-associated complex subunit alpha (NAC-alpha) (Alpha-NAC) (allergen Hom s 2)	Cytoplasm. Nucleus.
Q09666	AHNK_HUMAN	Neuroblast differentiation-associated protein AHNAK (Desmoyokin)	Nucleus.
Q14697	GANAB_HUMAN	Neutral alpha-glucosidase AB (EC 3.2.1.84) (Alpha-glucosidase 2) (Glucosidase II subunit alpha)	Endoplasmic reticulum. Golgi apparatus. Melanosome.
Q02818	NUCB1_HUMAN	Nucleobindin-1 (CALNUC)	Golgi apparatus – cis-Golgi network membrane; Peripheral membrane protein; Lumenal side. Cytoplasm.
Q8NFH5	NUP53_HUMAN	Nucleoporin NUP53 (35 kDa nucleoporin) (Mitotic phosphoprotein 44) (MP-44) (Nuclear pore complex protein Nup53) (Nucleoporin Nup35)	Nucleus – nuclear pore complex. Nucleus membrane; Peripheral membrane protein.
Q9NYL4	FKB11_HUMAN	Peptidyl-prolyl cis-trans isomerase FKBP11 (PPIase FKBP11) (EC 5.2.1.8) (19 kDa FK506-binding protein) (19 kDa FKBP) (FKBP-19) (FK506-binding protein 11) (FKBP-11) (Rotamase)	Membrane; Single-pass membrane protein.
Q9Y285	SYFA_HUMAN	Phenylalanine--tRNA ligase alpha subunit (EC 6.1.1.20) (CML33) (Phenylalanyl-tRNA synthetase alpha subunit) (PheRS)	Cytoplasm.
Q13492	PICAL_HUMAN	Phosphatidylinositol-binding clathrin assembly protein (Clathrin assembly lymphoid myeloid leukemia protein)	Membrane – clathrin-coated pit. Golgi apparatus. Cytoplasmic vesicle – clathrin-coated vesicle. Nucleus.
Q15149	PLEC_HUMAN	Plectin (PCN) (PLTN) (Hemidesmosomal protein 1) (HD1) (Plectin-1)	Cytoplasm – cytoskeleton. Cell junction – hemidesmosome.
O15031	PLXB2_HUMAN	Plexin-B2 (MM1)	Cell membrane; Single-pass type I membrane protein.
Q10471	GALT2_HUMAN	Polypeptide N-acetylgalactosaminyltransferase 2 (EC 2.4.1.41) (Polypeptide GalNAc transferase 2) (GalNAc-T2) (pp-GaNTase 2) (Protein-UDP acetylgalactosaminyltransferase 2) (UDP-GalNAc:polypeptide N-acetylgalactosaminyltransferase 2) [Cleaved into: Polypeptide N-acetylgalactosaminyltransferase 2 soluble form]	Golgi apparatus – Golgi stack membrane; Single-pass type II membrane protein. Secreted.
P26599	PTBP1_HUMAN	Polypyrimidine tract-binding protein 1 (PTB) (57 kDa RNA-binding protein PPTB-1) (Heterogeneous nuclear ribonucleoprotein I) (hnRNP I)	Nucleus.
Q9H0S4	DDX47_HUMAN	Probable ATP-dependent RNA helicase DDX47 (EC 3.6.4.13) (DEAD box protein 47)	Nucleus – nucleolus.
Q8NBJ5	GT251_HUMAN	Procollagen galactosyltransferase 1 (EC 2.4.1.50) (Collagen beta(1-O)galactosyltransferase 1) (Glycosyltransferase 25 family member 1) (Hydroxylysine galactosyltransferase 1)	Endoplasmic reticulum lumen.
O00469	PLOD2_HUMAN	Procollagen-lysine,2-oxoglutarate 5-dioxygenase 2 (EC 1.14.11.4) (Lysyl hydroxylase 2) (LH2)	Rough endoplasmic reticulum membrane; Peripheral membrane protein; Lumenal side.
Q53EL6	PDCD4_HUMAN	Programmed cell death protein 4 (Neoplastic transformation inhibitor protein) (Nuclear antigen H731-like) (Protein 197/15a)	Nucleus. Cytoplasm.
P13674	P4HA1_HUMAN	Prolyl 4-hydroxylase subunit alpha-1 (4-PH alpha-1) (EC 1.14.11.2) (Procollagen-proline,2-oxoglutarate-4-dioxygenase subunit alpha-1)	Endoplasmic reticulum lumen.
Q5VYK3	ECM29_HUMAN	Proteasome-associated protein ECM29 homolog (Ecm29)	Endoplasmic reticulum. Endoplasmic reticulum-Golgi intermediate compartment. Endosome. Cytoplasm – cytoskeleton – microtubule organizing center – centrosome. Nucleus. Endosome – multivesicular body. Cytoplasmic vesicle.
Q8IVF2	AHNK2_HUMAN	Protein AHNAK2	Nucleus.
P07237	PDIA1_HUMAN	Protein disulfide-isomerase (PDI) (EC 5.3.4.1) (Cellular thyroid hormone-binding protein) (Prolyl 4-hydroxylase subunit beta) (p55)	Endoplasmic reticulum lumen. Melanosome. Cell membrane; Peripheral membrane protein.
P30101	PDIA3_HUMAN	Protein disulfide-isomerase A3 (EC 5.3.4.1) (58 kDa glucose-regulated protein) (58 kDa microsomal protein) (p58) (Disulfide isomerase ER-60) (Endoplasmic reticulum resident protein 57) (ER protein 57) (ERp57) (Endoplasmic reticulum resident protein 60) (ER protein 60) (ERp60)	Endoplasmic reticulum. Endoplasmic reticulum lumen. Melanosome.

Q15437	SC23B_HUMAN	Protein transport protein Sec23B (SEC23-related protein B)	Golgi apparatus membrane. Endoplasmic reticulum membrane. Endoplasmic reticulum-Golgi intermediate compartment membrane.
O60231	DHX16_HUMAN	Putative pre-mRNA-splicing factor ATP-dependent RNA helicase DHX16 (EC 3.6.4.13) (ATP-dependent RNA helicase #3) (DEAH-box protein 16)	Nucleus.
P14618	KPYM_HUMAN	Pyruvate kinase PKM (EC 2.7.1.40) (Cytosolic thyroid hormone-binding protein) (CTHBP) (Opa-interacting protein 3) (OIP-3) (Pyruvate kinase 2/3) (Pyruvate kinase muscle isozyme) (Thyroid hormone-binding protein 1) (THBP1) (Tumor M2-PK) (p58)	Cytoplasm. Nucleus.
Q13283	G3BP1_HUMAN	Ras GTPase-activating protein-binding protein 1 (G3BP-1) (EC 3.6.4.12) (EC 3.6.4.13) (ATP-dependent DNA helicase VIII) (hDH VIII) (GAP SH3 domain-binding protein 1)	Cytoplasm. Cytoplasm – cytosol. Cytoplasmic granule. Cell membrane. Nucleus.
P46940	IQGA1_HUMAN	Ras GTPase-activating-like protein IQGAP1 (p195)	Cell membrane.
O75116	ROCK2_HUMAN	Rho-associated protein kinase 2 (EC 2.7.11.1) (Rho kinase 2) (Rho-associated, coiled-coil-containing protein kinase 2) (Rho-associated, coiled-coil-containing protein kinase II) (ROCK-II) (p164 ROCK-2)	Cytoplasm. Cell membrane; Peripheral membrane protein. Nucleus. Cytoplasm – cytoskeleton – microtubule organizing center – centrosome.
Q9P0V9	SEP10_HUMAN	Septin-10	Cytoplasm. Cytoplasm – cytoskeleton.
Q9UHD8	SEPT9_HUMAN	Septin-9 (MLL septin-like fusion protein MSF-A) (MLL septin-like fusion protein) (Ovarian/Breast septin) (Ov/Br septin) (Septin D1)	Cytoplasm – cytoskeleton.
Q9H4A3	WNK1_HUMAN	Serine/threonine-protein kinase WNK1 (EC 2.7.11.1) (Erythrocyte 65 kDa protein) (p65) (Kinase deficient protein) (Protein kinase lysine-deficient 1) (Protein kinase with no lysine 1) (hWNK1)	Cytoplasm.
Q13813	SPTN1_HUMAN	Spectrin alpha chain, non-erythrocytic 1 (Alpha-II spectrin) (Fodrin alpha chain) (Spectrin, non-erythroid alpha subunit)	Cytoplasm – cytoskeleton. Cytoplasm – cell cortex.
Q01082	SPTB2_HUMAN	Spectrin beta chain, non-erythrocytic 1 (Beta-II spectrin) (Fodrin beta chain) (Spectrin, non-erythroid beta chain 1)	Cytoplasm – cytoskeleton. Cytoplasm – myofibril – sarcomere – M line. Cell membrane; Peripheral membrane protein; Cytoplasmic side.
O15020	SPTN2_HUMAN	Spectrin beta chain, non-erythrocytic 2 (Beta-III spectrin) (Spinocerebellar ataxia 5 protein)	Cytoplasm – cytoskeleton. Cytoplasm – cell cortex.
Q9UEW8	STK39_HUMAN	STE20/SPS1-related proline-alanine-rich protein kinase (Ste-20-related kinase) (EC 2.7.11.1) (DCHT) (Serine/threonine-protein kinase 39)	Cytoplasm. Nucleus.
O95347	SMC2_HUMAN	Structural maintenance of chromosomes protein 2 (SMC protein 2) (SMC-2) (Chromosome-associated protein E) (hCAP-E) (XCAP-E homolog)	Nucleus. Cytoplasm. Chromosome.
Q12846	STX4_HUMAN	Syntaxin-4 (Renal carcinoma antigen NY-REN-31)	Cell membrane; Single-pass type IV membrane protein.
Q9Y490	TLN1_HUMAN	Talin-1	Cell projection – ruffle membrane; Peripheral membrane protein; Cytoplasmic side. Cytoplasm – cytoskeleton. Cell surface. Cell junction – focal adhesion.
P50991	TCPD_HUMAN	T-complex protein 1 subunit delta (TCP-1-delta) (CCT-delta) (Stimulator of TAR RNA-binding)	Cytoplasm. Melanosome. Cytoplasm – cytoskeleton – microtubule organizing center – centrosome.
P49368	TCPG_HUMAN	T-complex protein 1 subunit gamma (TCP-1-gamma) (CCT-gamma) (hTRiC5)	Cytoplasm.
P40227	TCPZ_HUMAN	T-complex protein 1 subunit zeta (TCP-1-zeta) (Acute morphine dependence-related protein 2) (CCT-zeta-1) (HTR3) (Tcp20)	Cytoplasm.
P04818	TYSY_HUMAN	Thymidylate synthase (TS) (TSase) (EC 2.1.1.45)	Nucleus. Cytoplasm. Mitochondrion. Mitochondrion matrix. Mitochondrion inner membrane.
Q92616	GCN1L_HUMAN	Translational activator GCN1 (HsGCN1) (GCN1-like protein 1)	
Q15631	TSN_HUMAN	Translin (EC 3.1.-.-) (Component 3 of promoter of RISC) (C3PO)	Cytoplasm. Nucleus.
P43307	SSRA_HUMAN	Translocon-associated protein subunit alpha (TRAP-alpha) (Signal sequence receptor subunit alpha) (SSR-alpha)	Endoplasmic reticulum membrane; Single-pass type I membrane protein.
Q9Y3I0	RTCB_HUMAN	tRNA-splicing ligase RtcB homolog (EC 6.5.1.3)	Cytoplasm.
Q5T6F2	UBAP2_HUMAN	Ubiquitin-associated protein 2 (UBAP-2)	
P08670	VIME_HUMAN	Vimentin	Cytoplasm.
Q9H0V9	LMA2L_HUMAN	VIP36-like protein (Lectin mannose-binding 2-like) (LMAN2-like protein)	Endoplasmic reticulum membrane; Single-pass type I membrane protein. Golgi apparatus membrane; Single-pass type I membrane protein.
Q969S3	ZN622_HUMAN	Zinc finger protein 622 (Zinc finger-like protein 9)	Cytoplasm. Nucleus.

Saudade…